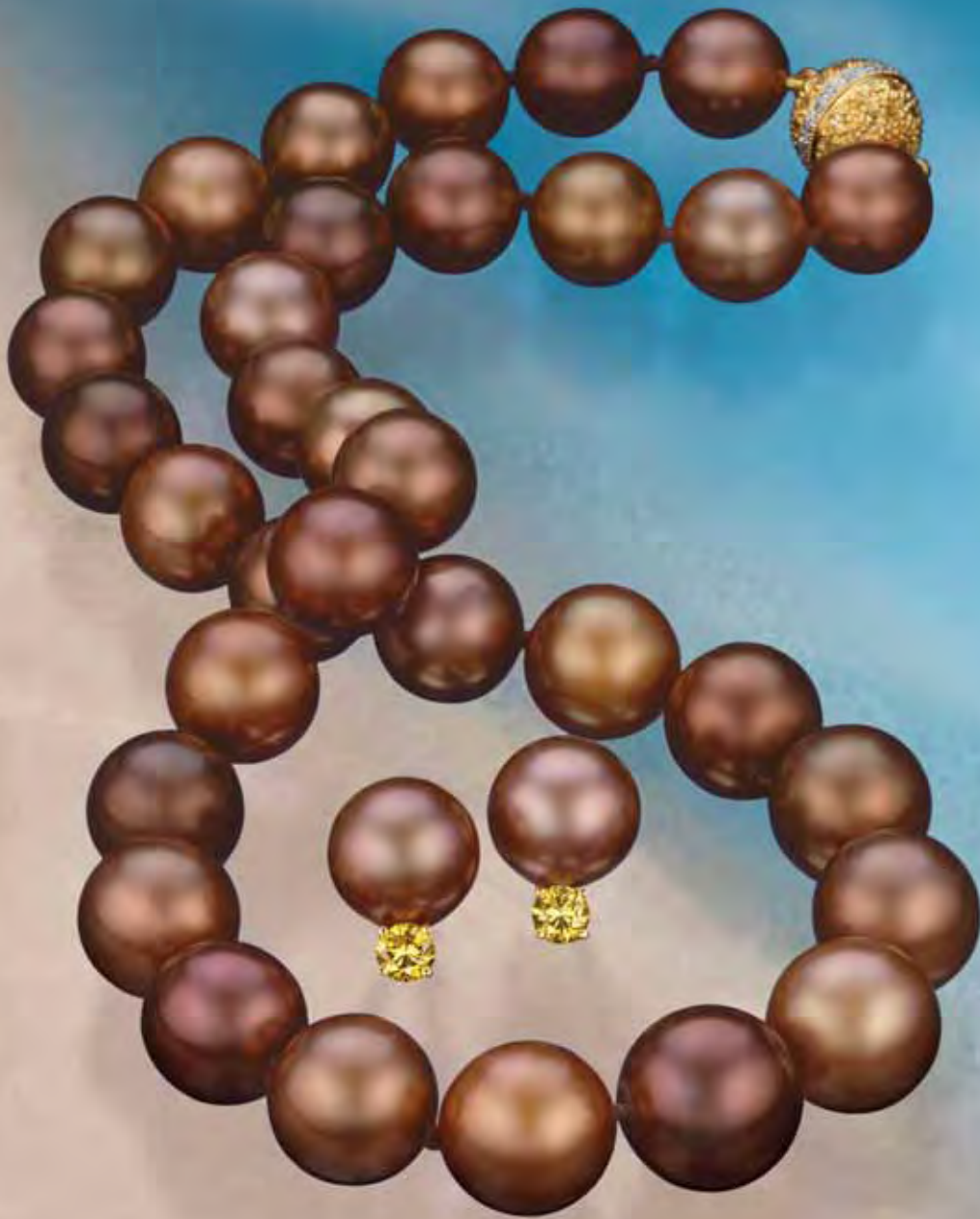


VOLUME XLII

# GEMS & GEMOLOGY

WINTER 2006



*Impact of Graining on Diamond Clarity Grading . . .*

*"Chocolate Pearls" . . . Leopard Opal . . . Rainbow Andradite from Japan*

THE QUARTERLY JOURNAL OF THE GEMOLOGICAL INSTITUTE OF AMERICA



pg. 216



pg. 223

## EDITORIAL

### 205 Remembering G. Robert Crowningshield

*Alice S. Keller*

## FEATURE ARTICLES

### 206 The Impact of Internal Whitish and Reflective Graining on the Clarity Grading of D-to-Z Color Diamonds at the GIA Laboratory

*John M. King, Thomas M. Moses, and Wuyi Wang*

A study of two important types of graining and how GIA determines their impact on a diamond's clarity grade.

### 222 Identification of "Chocolate Pearls" Treated by Ballerina Pearl Co.

*Wuyi Wang, Kenneth Scarratt, Akira Hyatt, Andy Hsi-Tien Shen, and Matthew Hall*

Examines the "chocolate" color treatment process for cultured pearls and techniques for identifying these products.

### 236 Leopard Opal: Play-of-Color Opal in Vesicular Basalt from Zimapán, Hidalgo State, Mexico

*Robert Raymond Coenraads and Alfonso Rosas Zenil*

A look at the origin and properties of this colorful ornamental stone, which is known from only one source.

### 248 The Cause of Iridescence in Rainbow Andradite from Nara, Japan

*Thomas Hainschwang and Franck Notari*

Characterizes this iridescent garnet from Japan and explains the cause of its unusual color phenomenon.

## REGULAR FEATURES

### 260 Lab Notes

Lizards in imitation amber • Large demantoid of exceptional color • A large Fancy white diamond with whitish banding • Prolonged change of color in a pink diamond • Strand of natural nacreous and non-nacreous pearls • Poudretteite • Unusual gem pyroxmangite

### 268 Gem News International

Diamond trading in Sierra Leone • Jewelry repair damages a diamond • Green augelite from Peru • Bicolored beryl from Namibia • Diopside from Afghanistan • California jadeite with copper inclusions • Labradorite from Mexico • Gem news from Mogok, Myanmar • Moonstone from Madagascar • Phenomenal fire opal • "Sunset" quartz from Brazil • Swedish Blue (slag) and Swedish Iron Ore • Tourmaline mining at Nandihizana, Madagascar • Green uvite from Afghanistan • Synthetic corundum "gem rough" in Tanzania • Small treated synthetic pink diamonds • "Chocolate" Tahitian cultured pearls • Treated violetish blue quartz from Brazil • Circular inclusions in a diffusion-treated sapphire • Diffusion-treated synthetic sapphire with unusual fluorescence

### 293 2006 Challenge Winners

### 294 Book Reviews

### 297 Gemological Abstracts

### 309 2006 Index



pg. 260



pg. 269

## EDITORIAL STAFF

### Editor-in-Chief

Alice S. Keller  
akeller@gia.edu

### Managing Editor

Thomas W. Overton  
tom.overton@gia.edu

### Technical Editor

Sally Magaña  
sally.magana@gia.edu

### Consulting Editor

Carol M. Stockton

### Contributing Editor

James E. Shigley

### Editor

Brendan M. Laurs  
The Robert Mouawad Campus  
5345 Armada Drive  
Carlsbad, CA 92008  
(760) 603-4503  
blaurs@gia.edu

### Associate Editor

Stuart Overlin  
soverlin@gia.edu

### Circulation Coordinator

Debbie Ortiz  
(760) 603-4000, ext. 7142  
dortiz@gia.edu

### Editors, Lab Notes

Thomas M. Moses  
Shane F. McClure

### Editor, Gem News International

Brendan M. Laurs

### Editors, Book Reviews

Susan B. Johnson  
Jana E. Miyahira-Smith  
Stuart Overlin

### Editors, Gemological Abstracts

Brendan M. Laurs  
Thomas W. Overton

## PRODUCTION STAFF

### Art Director

Karen Myers

### Production Assistant

Allison DeLong

### Website:

www.gia.edu

## EDITORIAL REVIEW BOARD

Shigeru Akamatsu  
*Tokyo, Japan*

Alan T. Collins  
*London, United Kingdom*

John Emmett  
*Brush Prairie, Washington*

Emmanuel Fritsch  
*Nantes, France*

Henry A. Hänni  
*Basel, Switzerland*

A. J. A. (Bram) Janse  
*Perth, Australia*

Alan Jobbins  
*Caterham, United Kingdom*

Mary L. Johnson  
*San Diego, California*

Anthony R. Kampf  
*Los Angeles, California*

Robert E. Kane  
*Helena, Montana*

Lore Kiefert  
*New York, New York*

Thomas M. Moses  
*New York, New York*

George Rossman  
*Pasadena, California*

Kenneth Scarratt  
*Bangkok, Thailand*

James E. Shigley  
*Carlsbad, California*

Christopher P. Smith  
*New York, New York*

Christopher M. Welbourn  
*Reading, United Kingdom*

## SUBSCRIPTIONS

Subscriptions to addresses in the U.S. are priced as follows: **\$74.95** for one year (4 issues), **\$194.95** for three years (12 issues). Subscriptions sent elsewhere are **\$85.00** for one year, **\$225.00** for three years. Canadian subscribers should add GST.

Special rates are available for GIA alumni and current GIA students. One year: **\$64.95** to addresses in the U.S., **\$75.00** elsewhere; three years: **\$179.95** to addresses in the U.S., **\$210.00** elsewhere. Please have your student or Alumni number ready when ordering. Go to [www.gia.edu](http://www.gia.edu) or contact the Circulation Coordinator.

Single copies of this issue may be purchased for **\$19.00** in the U.S., **\$22.00** elsewhere. Discounts are given for bulk orders of 10 or more of any one issue. A limited number of back issues are also available for purchase. Please address all inquiries regarding subscriptions and single copy or back issue purchases to the Circulation Coordinator (see above) or visit [www.gia.edu](http://www.gia.edu).

To obtain a Japanese translation of *Gems & Gemology*, contact GIA Japan, Okachimachi Cy Bldg., 5-15-14 Ueno, Taitoku, Tokyo 110, Japan. Our Canadian goods and service registration number is 126142892RT.

## MANUSCRIPT SUBMISSIONS

*Gems & Gemology* welcomes the submission of articles on all aspects of the field. Please see the Guidelines for Authors on our Website, or contact the Managing Editor. Letters on articles published in *Gems & Gemology* are also welcome.

Abstracting is permitted with credit to the source. Libraries are permitted to photocopy beyond the limits of U.S. copyright law for private use of patrons. Instructors are permitted to photocopy isolated articles for noncommercial classroom use without fee. Copying of the photographs by any means other than traditional photocopying techniques (Xerox, etc.) is prohibited without the express permission of the photographer (where listed) or author of the article in which the photo appears (where no photographer is listed). For other copying, reprint, or republication permission, please contact the Managing Editor.

*Gems & Gemology* is published quarterly by the Gemological Institute of America, a nonprofit educational organization for the gem and jewelry industry, The Robert Mouawad Campus, 5345 Armada Drive, Carlsbad, CA 92008.

Postmaster: Return undeliverable copies of *Gems & Gemology* to The Robert Mouawad Campus, 5345 Armada Drive, Carlsbad, CA 92008.

Any opinions expressed in signed articles are understood to be the opinions of the authors and not of the publisher.

## ABOUT THE COVER

*Treated-color "chocolate" cultured pearls created from Tahitian cultured pearls have become a popular segment of the pearl market in recent years. The article by Dr. Wuyi Wang and co-authors on pp. 222-235 of this issue examines a selection of "chocolate pearls" treated by Ballerina Pearl Co. in order to determine the basic process used and means of identifying these treated pearls.*

*The "chocolate pearls" in the necklace range from ~12.0 to 13.7 mm; those in the earrings are 12.1 mm (left) and 12.3 mm (right). Jewelry courtesy of Emiko Pearls International; photo by Robert Weldon.*

*Color separations for Gems & Gemology are by Pacific PreMedia, Carlsbad, California.*

*Printing is by Allen Press, Lawrence, Kansas.*

© 2006 Gemological Institute of America All rights reserved. ISSN 0016-626X

# Remembering

## G. ROBERT CROWNINGSHIELD

Gemology lost one of its original pioneers with the passing of G. Robert Crowningshield on November 8 at the age of 87. During a career that spanned six decades, his wide-reaching achievements as a researcher, author, and educator helped shape modern gemology.

Born in Colorado Springs, Colorado, Bob Crowningshield graduated from San Diego State College (now San Diego State University) with a degree in natural science. As an officer in the U.S. Navy from 1942 to 1946, he read books on gems to pass the long hours at sea and even arranged an unscheduled stop in Colombo, the capital of Ceylon (now Sri Lanka) and a bustling trade center for gems. As fate would have it, the owner of the first jewelry store he visited had a son who had graduated from GIA's resident program in Los Angeles in 1939. When the young man told Crowningshield of a school dedicated to the science of gems, his destiny became clear, and he enrolled at GIA once his tour of duty was over.

After graduating from the Institute in 1947, Crowningshield stayed on campus in Los Angeles as an instructor. Two years later, he was sent to New York to help start up GIA's East Coast office, where he worked for more than four decades, rising to the position of vice president.

Crowningshield championed the spectroscope as a tool for gemological research. Pencil in hand, he sketched absorption spectra for every stone he examined. His collection of hand-drawn illustrations, first published in Richard T. Liddicoat's 1962 edition of the *Handbook of Gem Identification*, demonstrated the value of the spectroscope to gemologists. So did a historic discovery that solved the mystery of irradiated yellow diamonds.

One morning in 1956, Crowningshield was viewing the spectrum of a large yellow diamond when he noticed something odd: an absorption line just below the 600 nm mark. He suspected the line was evidence of irradiation, a colorizing treatment that was becoming widespread with the dawn of the atomic age. When his subsequent research confirmed that irradiated yellow diamonds could be identified by the absorption line at around 592 nm, it was a breakthrough the diamond industry had been waiting for.

Crowningshield's career was marked by many other "firsts" and singular contributions to gemology. With Liddicoat, Bert Krashes, and other GIA colleagues, he developed the GIA Diamond Grading System in the early 1950s. He is personally credited with devising GIA's system and nomenclature for fancy-color diamonds. Crowningshield's studies in the early 1960s demonstrated how tissue-nucleated freshwater cultured pearls could be identified through X-radiography. He coauthored one of the first characterizations of tanzanite in a 1968 *Lapidary Journal* article and published the Summer 1971 *G&G* initial report on General Electric's gem-quality synthetic diamonds. His Spring 1983 *G&G* article on orangy pink to pinkish orange "padparadscha" sapphire is regarded as a classic explanation of this gem's color. Crowningshield's final

*G&G* article, from the Summer 1989 issue, was on the first formal grading of the famed Hope diamond.

Many other discoveries were set forth in Crowningshield's long-running *G&G* column, which contained brief notes from the New York lab (and eventually became the journal's present-day Lab Notes section). Between 1957 and 1999, he turned out more than 1,000 observations of interesting and unusual gems. His 1970 note on "milky" graining in diamonds was the first articulation of what has become an important feature in the clarity grading of diamonds, as described in the lead article in this issue.

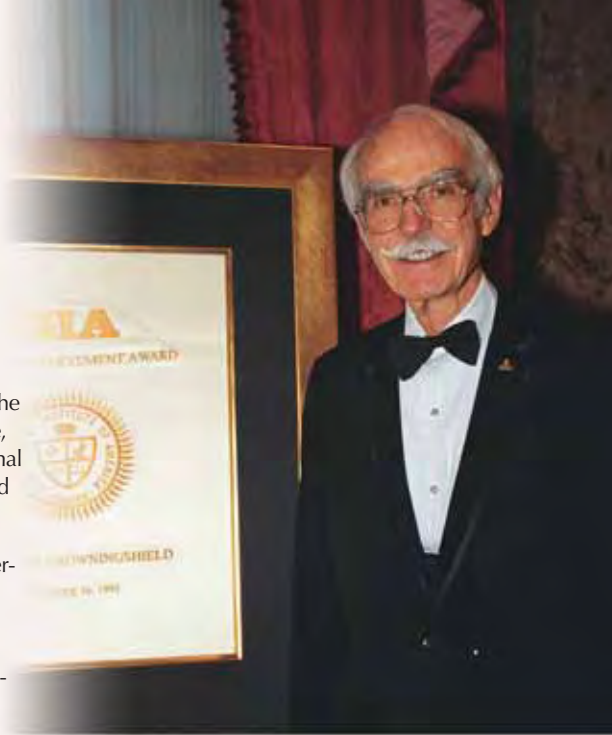
His scientific achievements alone would have earned Bob Crowningshield a place in geological history, but they don't tell the whole story. His reputation for accuracy and integrity played a key role in establishing GIA's diamond grading reports as an industry standard. Crowningshield was also a respected educator who taught scores of jewelers across the United States and presented at all but two American Gem Society (AGS) Conclaves from 1951 to 1993. (A complete review of his career can be found in Thomas Moses and James Shigley's "G. Robert Crowningshield: A Legendary Gemologist," Fall 2003 *G&G*, pp. 184–199.)

After stepping down from his day-to-day role in the New York office, Crowningshield remained in Manhattan's Upper West Side. He still paid visits to the laboratory and continued to inspire the Institute's next generation of gemologists. In retirement, he was honored with *Modern Jeweler's* Lifetime Achievement Award in 1995 and the AGS Lifetime Achievement Award in 2003. GIA established the G. Robert Crowningshield Research Fund in 2003 to advance his vision of safeguarding the integrity of gems through knowledge.

To this editor, Bob Crowningshield was a friend, a teacher, and a remarkable fountain of knowledge. I was frequently amazed at his ability to recount the properties of stones he had seen decades before. A brilliant writer and researcher, a kind and patient colleague, Bob Crowningshield will be missed—and well remembered—by the legions of people he influenced.



Alice S. Keller  
Editor-in-Chief



# THE IMPACT OF INTERNAL WHITISH AND REFLECTIVE GRAINING ON THE CLARITY GRADING OF D-TO-Z COLOR DIAMONDS AT THE GIA LABORATORY

John M. King, Thomas M. Moses, and Wuyi Wang

Unlike many other characteristics that affect the clarity grade of a diamond, determination of the impact of “whitish” graining and “reflective” graining requires analysis that goes beyond visibility at 10× magnification. The importance of this determination is further underscored by the fact that such graining often is the only characteristic present in large, high-clarity, high-color diamonds. This article reviews the history of reporting on such graining by the GIA Laboratory, considers the causes of the different types of graining most commonly encountered, and examines the methodology and critical assessment GIA graders use to determine the impact of such graining on the clarity grade of a diamond.

One of the most misunderstood features in diamond clarity grading is the impact of graining, especially internal “whitish” or “reflective” graining (see, e.g., figure 1). R. E. Kane’s 1980 *Gems & Gemology* article, “The Elusive Nature of Graining in Gem Quality Diamonds,” gave the reader an overview of the causes of graining, illustrated the range of appearances associated with it, and generally outlined its relationship to clarity grading at the GIA Laboratory (see also Kane, 1982). The present article looks at this subject 25 years—and literally millions of diamonds—later.

For the purposes of diamond grading, *graining* refers to optical discontinuities that are observable with a 10× loupe or a standard gemological microscope. The overall transparency of a diamond can be affected by these discontinuities to varying extent. While fractures and cleavages are also discontinuities, an important difference is that with graining no open space (i.e., air/diamond interface) is present. Whitish graining can be classified into banded, tatami, and overall haziness, whereas

reflective graining typically consists of internal reflective planes.

Many of the forms graining takes (e.g., surface lines or colored bands) are readily observed, and their relationship to clarity can be understood with standard diamond grading conditions and criteria (i.e., ease of visibility at 10× magnification and location). But whitish graining and reflective graining are often more difficult to distinguish and relate to clarity, since their visibility is influenced more by optical factors such as the type of lighting and the angles of observation in relation to the lighting.

---

Note: The photomicrographs provided in this article represent a static view of a graining feature, and are often taken from a viewing angle in which the feature is most obvious. It is important to remember that one factor in determining graining’s impact on a clarity grade is the effect of subtle movement of the diamond during observation. While the feature illustrated in the image may appear obvious, the determination mentioned in the caption reflects Laboratory awareness of all the factors that influence the clarity grade.

See end of article for About the Authors and Acknowledgments.

GEMS & GEMOLOGY, Vol. 42, No. 4, pp. 206–220.

© 2006 Gemological Institute of America



*Figure 1. The 30+ ct pear shape and 18 ct oval shown here are representative of the large colorless to near-colorless diamonds in which whitish graining may affect the clarity. This effect is often misunderstood due to the elusive nature of such graining. The photomicrograph illustrates a classic example of the cottony banding encountered in whitish graining that will have an impact on the clarity grade. Photo © Harold & Erica Van Pelt; photomicrograph by Vincent Cracco, magnified 21×.*

Also, because such graining is a natural part of the diamond structure, many trade members do not believe it should be a clarity characteristic. However, undeniably there are varying degrees of visibility associated with whitish and reflective graining, which has resulted in considerable debate over the impact it should have on the clarity grade (Nir Livnat, pers. comm., 2006).

Other challenges to understanding the impact of such graining on the clarity grade relate in part to the fact that a more complex decision-making process is required to assess whitish or reflective graining than is usually required with most other internal features. This process must take into account the ability not only to discern the feature at 10× magnification, but also to determine its form (i.e., lines, planes, broad areas), texture (i.e., cottony, sheen-like, hazy), and the angle(s) at which it is visible.

In the early years of diamond grading at GIA, the complexity of assessing whitish graining was complicated by the fact that this characteristic was encountered only infrequently at the laboratory. In recent years it has been further complicated (and its importance enhanced) by other factors. For one, in our experience whitish graining is most commonly

encountered in large (e.g., over 4 ct) diamonds. Most of these large diamonds are type II (a diamond type that is relatively free of nitrogen) and often absent of solid inclusions (see, e.g., Moses and Wang, 2006). Another factor is that the complex interaction of light with a diamond's cut when viewed in the face-up position may restrict the observation of this often subtle, visually elusive feature to the pavilion, where such graining can impact the most critical clarity determination of Flawless/Internally Flawless (FL/IF) versus VVS<sub>1</sub> (figure 2). This reinforces the importance of consistent interpretation of this feature, given the potential impact on the value of the diamond.

While reflective graining (figure 3) is observed more often in smaller, type I diamonds and frequently in association with other inclusions, its assessment requires many of the considerations—and complex decision making—described above for whitish graining. Therefore, this article will focus on assessing the appearances and grading of whitish graining in particular, with specific reference to reflective graining where appropriate.

Following an overview of GIA's history of reporting on graining (particularly whitish), we will



Figure 2. Illustrated here are two appearances associated with whitish graining that affects the clarity grade. These diamonds had no other internal features visible at 10× and the graining was only seen through the pavilion, which resulted in a clarity grade of VVS<sub>1</sub>. Photomicrographs by Vincent Cracco; magnified 21× (left) and 15× (right).

summarize the causes of whitish and reflective graining and then describe the system GIA uses to determine the effect of such graining on a diamond's clarity grade.

### HISTORY OF REPORTING AND CLARITY GRADING WHITISH GRAINING AT GIA

The evolution of grading whitish graining is an interesting case study of how diamond grading has developed since its early days. As with many areas of study, in diamond grading the collection of data over time allows the observers to make refinements and clarify the methods used to make assessments. This section presents an overview of the developing awareness of this feature and changes in reporting through the years.

While GIA has issued diamond grading reports since the mid-1950s, it was only in the late 1960s and the 1970s that requests for its grading services began to grow. With the investment craze of the late 1970s—when purchases of goods such as diamonds, silver, and gold were promoted as a hedge against inflation—demand for “certificate” goods rose dramatically. This resulted in huge increases in report production and staffing at GIA. Even though the boom had become a bust by the end of 1980, the trade was now using grading reports routinely in diamond transactions. In fact, laboratory records show that GIA graded more diamonds in the decade of the 1980s than in the previous 25 years of diamond grading combined.

Consequently, early reporting on diamonds with whitish graining was generalized, with broad categories for the appearances and descriptions used. Several years elapsed before senior graders had examined enough diamonds with graining to enable them to review and refine the grading criteria related to this feature. A review of reports and personal notes written by celebrated gemologist G. Robert Crowningshield during the late 1960s and

early 1970s indicates that it was not until this period that diamonds with low diaphaneity were seen in the laboratory. The Spring 1970 issue of *Gems & Gemology* (p. 157) provides insight into the developing awareness of this distinctive appearance when Crowningshield reported the following on examining a “milky” diamond:

We were reminded of certain important diamonds we have graded recently that were just slightly misty but in which no zones nor parallel bands could be seen and no particles whatever, even under highest magnification. Two such stones were top color and free of any imperfections otherwise. It was acknowledged that the slightly lower transparency did affect the value, but we have been at a loss how to arrive at a meaningful grade. It is possible that these stones represent a new source of gem diamonds. If so, we must arrive at an acceptable grade for them so as to be fair to the diamonds and to potential customers.

The following year, Crowningshield (1971a) speculated that these “grained stones” might be from Russia. However, diamantaire Louis Glick (pers. comm., 2006) recently confirmed that he and others had purchased and manufactured similar diamonds in the late 1960s and early 1970s that originated from Sierra Leone. As more of these diamonds were submitted to the laboratory, it became clear that this feature often occurred in larger diamonds high on the D-to-Z color grading scale. It also became apparent that this “misty” appearance was being seen in diamonds from many sources. Recognizing that the loss of transparency affected value, as mentioned above, the laboratory began to systematically report on readily observed graining during the early 1970s. The earliest reporting took the form of a comment. For example, in June 1970 an important 13+ ct, D-color diamond with sufficient graining to impact its transparency was graded



Figure 3. Reflective graining is seen here as: left, an obvious reflective plane; right, linear “fingers” extending along a plane that is more transparent than the “fingers.” With no other inclusions noted, both diamonds would receive a clarity grade of VVS<sub>1</sub>, since the graining was only visible through the pavilion. Photomicrographs by Mitchell Moore and Vincent Cracco.

IF with an asterisk following the clarity grade. The corresponding comment stated: “Near transparent due to unusual internal texture.”

This approach continued throughout much of the early 1970s: Diamonds that exhibited graining but had no other inclusions received clarity grades of FL or IF together with a comment regarding their reduced transparency. Changes in the wording of the comment indicated the continued evolution in thinking as more diamonds with graining were seen. For example, comments from the early 1970s often described the appearance without noting an impact on clarity grade. The comment noted above for the 13+ ct diamond from 1970 is one such example, and a 1973 comment for a 5+ ct pear-shaped diamond stated: “Nothing generally regarded as a flaw or imperfection observed, however whitish internal graining is present.” Less-descriptive comments were seen later in 1973, such as the simple “Graining is present” noted on the report for a 2 ct marquise brilliant graded IF.

Although early in the 1970s Crowningshield (1971b) described an example where he felt the graining affected the clarity grade, it took much of the decade for the laboratory staff to reach a level of certainty as to when the appearance of whitish graining could diminish clarity as much as fractures or solid inclusions. A 1977 report on a 4+ ct marquise brilliant noted a clarity grade of VVS<sub>1</sub> and included a comment stating: “Based on extensive whitish graining.” A 6+ ct pear shape was also graded VVS<sub>1</sub> with a comment noting: “Based on parallel whitish graining not shown [on the report diagram].” By the late 1970s, not only was the degree of other internal graining that did not affect the clarity grade (referred to as transparent graining) noted on the report (see below), but clarity grades lower than VVS<sub>1</sub> were also assigned for whitish graining when the effect was severe.

During the 1980s, whitish graining was routinely treated like other clarity characteristics and

graded on its visibility at 10× magnification with the microscope and loupe. On occasion, the grading decision was based on visibility with the unaided eye. At that time, the methodology used to assess graining (i.e., angle at which the stone was observed, distance and angle of the feature in relation to the light source, and degree of visibility) was still broadly defined in the grading process. The use of such broadly applied methods resulted in a greater range of interpretation of this feature and, therefore, finer and more limited areas of graining that could potentially affect the clarity grade. Such assessments were quite different from those made in the first half of the previous decade, when large areas of graining did not affect the clarity grade *per se*.

This evolution in the assessment of graining resulted in perceived inconsistencies in reporting when diamonds of similar appearance, graded at different times over a period of many months or years, were seen together. While the laboratory instituted a number of policies internally to ensure more consistent performance, the lack of external communication on the subject left the trade in doubt about the grading policy. In looking back over 50 years of reporting and grading graining at the GIA Laboratory, we can summarize the related policies as follows, in chronological order:

- 1950s through the late 1960s—Whitish graining was not considered a clarity characteristic and was not noted on the report. With no other inclusions present, a diamond would be graded FL/IF. Observed graining was sometimes noted for “in-house” identification.
- Early 1970s—Whitish graining was usually not considered a clarity characteristic, but the reduced diaphaneity was acknowledged through a report comment. A diamond could receive a

---

grade of FL/IF and yet have one of a number of different report comments noting the presence of graining.

- Mid-1970s to about 1980—Whitish graining was routinely considered a clarity characteristic. If it was easily seen at 10× magnification, with no other internal features visible, the appropriate clarity grade was assigned with a comment noting that it was based on whitish graining. If transparent graining was present, the diamond was assigned a FL or IF clarity grade, with an additional report comment noting the degree of graining (i.e., *significant*, *moderate*, or *slight*). Other types of graining (e.g., reflective or colored bands) were plotted on the report diagram and noted in the key to symbols.
- About 1980 to the mid-1980s—Whitish graining was considered a clarity characteristic and noted in a report comment when it affected the clarity grade. During this period, *all* diamonds were given an assessment for transparent graining (*significant*, *moderate*, *slight*, or *nil*), and the degree of observed graining that did not affect clarity was given its *own entry line* on all reports. We continued to plot other types of graining that affected the clarity grade on report diagrams.
- Late 1980s to the early 1990s—Whitish graining was considered a clarity characteristic and noted in a report comment when it affected the clarity grade. However, graining that was not severe (i.e., that did not impact the clarity grade) was again indicated on in-house records only (for identification)—unless it was significant, in which case it was still reported in a comment. Other types of graining that affected clarity were plotted on the report diagram.
- Mid-1990s to the present—Whitish graining continues to be considered a clarity characteristic and, when severe enough to affect the clarity grade, is noted in a report comment (“The clarity grade is based on internal graining that is not shown [on the report diagram]”). Any other type of graining that affects the clarity grade is no longer plotted on the report diagram but appears as a report comment, with the same wording as for whitish graining. Significant transparent, colorless graining (that does not affect the clarity grade) continues to be recorded in a report comment, with

the current terminology being “Transparent internal graining is present.” For all graining observed, whether or not it affects the clarity grade, the precise type and its degree are noted internally for identification purposes.

## OVERVIEW OF THE CAUSES OF WHITISH AND REFLECTIVE GRAINING

An “ideal” or “perfect” diamond is composed solely of carbon, and all the carbon atoms are packed in a cubic structure that is repeated continuously throughout the crystal. Physical properties, including optical characteristics, are uniformly distributed in such a diamond. However, virtually all diamond crystals contain discontinuities in this regular pattern of carbon atoms. For example, plastic deformation is a common feature in natural diamonds. When stress is applied to a diamond above a certain temperature, the crystal lattice is distorted along specific planes. This causes a disruption in the regularity of the crystal lattice that is known as a dislocation, and these dislocations remain after the stress is released (Wilks and Wilks, 1991). The presence of impurities (i.e., other elements, such as nitrogen or boron) will also disturb the packing of carbon atoms in the diamond lattice. In addition, some carbon atoms may not be positioned correctly within the lattice structure.

The dislocation of carbon atoms is the predominant cause of graining features in diamond; such dislocations can be introduced either during or after the diamond has formed (Wilks and Wilks, 1991). When these lattice defects or dislocations occur with sufficient density to change the stone’s refractive index or other physical properties, they may create optical disturbances strong enough to be observed with 10× magnification that may have a negative impact on the overall transparency of a faceted diamond. This section focuses on the causes of whitish and reflective graining. For a brief overview of the causes of some other types of graining that are commonly encountered during diamond grading at the Laboratory, see box A.

**Banded or Tatami Whitish Graining.** Some whitish graining appears as straight or wave-like lines or bands in an otherwise “clean” diamond (figure 4, left). Sometimes a group of nearly parallel lines or bands may occur together. These lines are more visible when the stone is examined in a specific orientation, and will disappear when the stone is rotated.

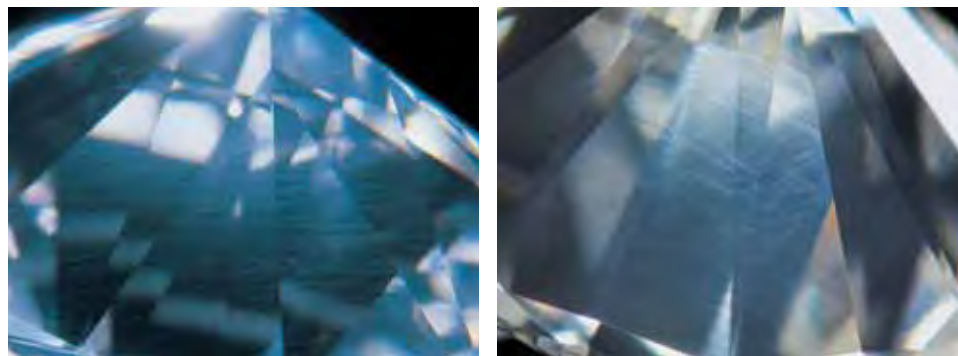


Figure 4. One form of whitish graining appears as wave-like linear bands observed over a wide area of the diamond (left). Whitish “tatami” graining is seen when bands develop in two directions (right). Photomicrographs by Vincent Cracco; magnified 12× (left) and 15× (right).

One notable feature of these lines is their whitish or silky appearance when examined with a microscope and darkfield illumination; another is their dominant development in one direction.

When these whitish lines or bands are well developed in two major directions, a cross-hatched or “tatami” pattern is produced (figure 4, right; Lang, 1967; Moses et al., 1999). In extreme cases, the graining is so intense and widespread that the observer has the sensation of looking through a screen (i.e., the “crisp” appearance is diminished; see, e.g., Moses and Wang, 2006).

Dislocations in the diamond lattice are the main cause of banded or tatami graining. Lattice distortion affects many physical properties, such as refractive index. Instead of light following its typical path through the diamond, in the distorted region it is refracted or diffused due to the difference in R. I. between that region and the surrounding lattice

Figure 5. When examined with crossed polarizers, the graining planes in figure 4 (right) are delineated by the high-order interference colors associated with dislocations in the diamond lattice. Photomicrograph by W. Wang; magnified 27×.



(Fontanella et al., 1977; Balzaretto and da Jornada, 1996). As a result, when examined with crossed polarizers, high-order interference colors may be observed along the graining planes (figure 5).

**Hazy Whitish Graining.** Cloud-like inclusions in diamond typically are composed of numerous tiny microscopic crystals and occur in the cubic growth sector (Shah and Lang, 1963; Fritsch and Scarratt, 1993). When these inclusions are too small to be recognized as individual pinpoint-like crystals with standard microscopic examination, they collectively appear as an overall haziness (figure 6) due to the scattering of light. Such haziness may occur in a very small region, but it typically is seen throughout most of the stone; on rare occasions, it may occur as bands (see Jang-Green, 2006). Because this overall haziness appears to be related to the growth structure (and the individual pinpoints cannot be resolved at the 10× magnification used for clarity grading), in gemology it is usually considered a form of whitish graining.

**Reflective Graining.** Plastic deformation often generates a number of closely spaced parallel planes in some types of diamonds (usually type IaA with high concentrations of nitrogen). It is widely believed that the areas on both sides of the plane slid slightly relative to one another, creating the so-called slip bands (Wilks and Wilks, 1991; Fritsch et al., 2006). Occasionally, the damage to the diamond lattice along slip planes is intense within a very narrow region. When these slip bands are viewed with reflected light in a specific orientation, they may appear as reflective graining (again, see figure 3). As noted above, there are fundamental differences between reflective graining and a fracture or cleavage, since the former involves no air/diamond interface and typically will be observed only in a specific orientation.

Although understanding the cause and resultant

## BOX A: OTHER TYPES OF GRAINING SEEN IN D-TO-Z DIAMONDS

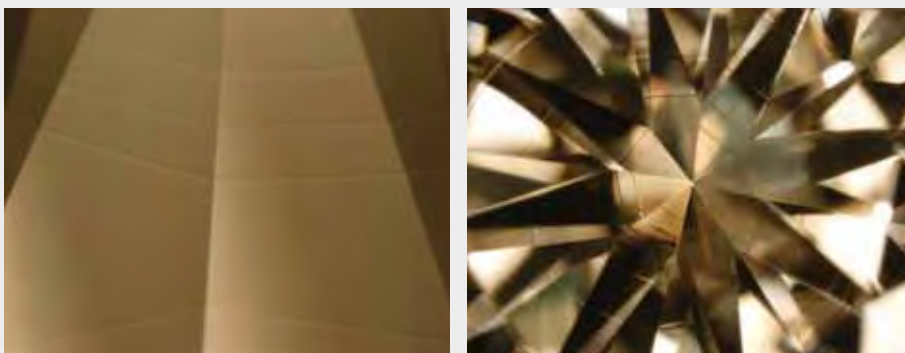


Figure A-1. Occasionally surface grain lines (left) “ring” the diamond and, when the same stone is viewed table up, create a “spider-like” web appearance due to reflections (right). If they are extensive and obvious in the face-up position, these surface grain lines can affect clarity (here, VVS<sub>1</sub>). Photomicrographs by W. Wang; magnified 60× (left) and 30× (right).

In addition to whitish and reflective graining, two other types of graining are commonly encountered in D-to-Z diamonds during the grading process: surface graining and colorless transparent internal graining. These either relate to, or may be confused with, internal reflective graining. The following provides a brief description of their typical appearances and causes, as well as a summary of how each may affect the clarity grade.

**Surface Graining.** As mentioned in the main text, plastic deformation is the likely cause of reflective graining. The parallel planar features (slip bands) generated in this process may appear to be completely internal or to originate from the surface of the diamond where discernable lines are seen (i.e., surface grain lines; see figure A-1). In some cases, these slip bands are only visible on the surface, where they are most easily seen with reflected light. They may not be evident internally if the optical disturbance was quite limited and not severe enough to appear as reflective planes. Nevertheless, if extensive, they may affect the clarity grade.

Another common cause of surface graining is a change in crystallographic orientation (i.e., twinning). For example, a macle is a twinned diamond crystal with a flattened morphology caused by a 180° rotation in the crystal orientation. Since diamond hardness is dependent on crystallographic orientation (e.g., the {111} direction is much harder than the {110} direction), the plane of the twinned crystal may be visible on the surface as a grain line after faceting. This line is brought out during the polishing process, when a shallow step is created at the twin boundary due to the differences in hardness across the twin plane.

Surface graining can also relate to growth sectors

that formed differentially during the crystallization of the diamond. Different growth sectors in a single-crystal diamond may have significant differences in impurity concentration (e.g., nitrogen), resulting in observable optical discontinuities at the growth sector boundaries due to slight differences in R.I. The planes may (see below) or may not be visible internally, depending on the degree of associated optical disturbance. Variations in impurity concentrations between various growth sectors will also affect their hardness. Diamond with a high concentration of nitrogen (up to several hundred parts per million) is distinctly softer than pure diamond (Field, 1979; Yan et al., 2004). Surface graining formed in this way follows diamond

Figure A-2. Surface grain lines may be caused by variations in impurity concentrations (and thus hardness) among different growth sectors. Photomicrograph by W. Wang; magnified 70×.





Figure A-3. Grain lines may be caused by the expansion of inclusions during transport of the diamond to the earth's surface. The extent of grain lines is typically proportional to the size of the inclusion (minute on the left as denoted by the arrow, and larger on the right). Photomicrographs by W. Wang, magnified 100× (left) and 70× (right).

growth zones, usually as straight and distinct lines. For example, the fine graining in figure A-2 exhibited a nearly hexagonal outline on the table facet.

Graining formed due to twinning or variations in growth sectors is normally not extensive and often appears subtle. In clarity grading, a diamond with no other clarity characteristics except surface graining cannot receive a grade of Flawless, but a grade of Internally Flawless is possible. Extensive, numerous surface grain lines can affect the clarity grade of an otherwise Internally Flawless diamond, and may result in grades of VVS or lower depending on the visibility of the graining when the diamond is examined face up.

**Colorless Transparent Internal Graining.** As mentioned in the main text (see "Nature"), graining that appears as bright lines (showing no internal plane) that fade with slight movement of the diamond is often confused with reflective graining. These areas of graining are usually transparent and rarely affect clarity. Two mechanisms are commonly associated with transparent graining.

One cause is the expansion of inclusions. During transport to the earth's surface, differential expansion occurs between a solid inclusion and the host diamond in response to decreasing pressure and temperature. The volume of the diamond (and thus the space the inclusion occupies) changes very little, but some mineral inclusions will expand significantly (Schrauder and Navon, 1993; Sobolev et al., 2000). This expansion exerts stress and may create a local lattice distortion in the surrounding diamond. Occasionally, graining with a wave-like appearance may be seen surrounding a small mineral inclusion. These lines are usually developed in a specific orientation, starting at the inclusion. Transparent grain lines formed in this way are relatively short and proportional to the size of the inclusions (figure A-3). Microscopic observation with crossed polarizers typi-

cally shows very high-order interference colors due to the internal strain surrounding such inclusions (see, e.g., Lu et al., 2001).

A second cause of colorless, transparent internal graining is octahedral growth zoning, which is typically referred to in a diamond as "cubic graining" due to its square or rectangular outline corresponding to an octahedral growth sector (figure A-4; see Wilks and Wilks, 1991; Sunagawa, 2006). This type of graining is caused by variations in impurity concentrations in different growth sectors, as described above. The graining is created by optical differences at the boundaries of these growth zones. Like graining caused by the expansion of inclusions, this type of graining is occasionally confused with reflective graining since it will appear bright in some positions.

Figure A-4. Transparent internal graining that follows a diamond's octahedral growth sector typically has a square or rectangular outline. This type of graining typically fades in and out of view as the diamond is moved; it is not common for such graining to impact the clarity grade. Photomicrograph by W. Wang, magnified 40×.





*Figure 6. A whitish overall haziness believed to be the result of submicroscopic inclusions is also referred to as whitish graining in gemology. It appears to be related to the growth structure of the diamond. The transparency of this 5.68 ct diamond was noticeably affected when viewed face-up, which would result in a grade in the SI range even if no other inclusions were present. Photo by Vincent Cracco.*

appearance of whitish and reflective graining in a diamond helps the grader identify its presence, the greater challenge is assessing the degree to which such graining affects the clarity grade. Following is the protocol used in the GIA Laboratory to observe graining and determine whether it influences the clarity grade—and, if so, to what degree.

### **THE GIA SYSTEM FOR GRADING WHITISH AND REFLECTIVE GRAINING**

The most important aspect of grading whitish and reflective graining is the initial determination as to whether the graining has any impact on the clarity

of the diamond. Again, it is important to remember that visibility at 10× magnification is not the only determining factor, as illustrated by many of the examples provided below. Once it has been established that a graining feature has an impact, the other criteria for determining a diamond's clarity grade also come into play (i.e., visibility from the crown or pavilion, and ease of visibility—subtle, noticeable, or obvious with the loupe, or readily seen with the unaided eye).

As with other aspects of grading, a controlled observation environment and assessment methodology are critical for consistent results. In fact, any determination requiring visual observation also requires strict control of the lighting, viewing environment, and spatial relationship of the observer to the object.

**Light Source and Viewing Environment.** The ability to observe graining is strongly impacted by optical effects. Therefore, the control of lighting for both the surrounding environment and that used for examination of the diamond is critical. In the GIA Laboratory, observations are made in a room with subdued fluorescent ceiling lights that limit surface reflection and optimize the natural light/dark contrasts observed in the diamond. Windows are shaded to control external lighting. Initially, features are located and identified with a GIA Instruments microscope. The microscope's well light source (used to create the darkfield illumination seen through the microscope oculars) consists of one 25 watt halogen bulb. Halogen bulbs have output in the long-wave ultraviolet region of the spectrum which, on rare occasions, could cause confusion between haziness caused by graining and the "oily" disruption in transparency that can be observed in very strongly fluorescent diamonds. In the instances where graining is questioned in very strongly fluorescent diamonds, a UV filter is placed over the microscope well. The filter prevents the light source's UV component from exciting fluorescence in the diamond, so any noticeable haziness observed in the microscope is considered the effect of graining. Once features are located and identified at 10× magnification in the microscope, the final grade is determined using a fully corrected 10× loupe and the microscope's overhead light source: two 4-watt, 6-inch-long (15 cm) fluorescent bulbs with a color temperature of approximately 6500 K (the cover for the overhead light source also filters UV). Fluorescent lights are

readily available worldwide and are a diamond industry standard. It has long been the position of the GIA Laboratory that in serving the interests of the industry we must use practical equipment that can be duplicated by the trade. For this reason, we make our final clarity grade determination using fluorescent lights.

**Viewing Geometry.** Both whitish graining and reflective graining are often elusive, and subtle changes in the viewing angle between the observer and the diamond can result in these features fading in and out of visibility. For initial assessments in the microscope, we have noted that different graders may reach different conclusions when near a clarity-grade boundary depending on the relationship of the stone holder and angle of the diamond to the observer (i.e., whether they place the holder on the right or left side of the microscope, as is usually determined by whether they are right- or left-handed) or when the distance from the diamond to the light source in the microscope well differs. These potential conflicts are minimized through the use of the loupe and overhead light in the final determination. The diamond is held in a stone holder or tweezers approximately 2–3 inches (5–8 cm) below the microscope's fluorescent overhead light source and from equal to the front edge of the light to 2 inches (5 cm) in front of it (figure 7). This position creates a dark field for determining the contrast between areas of graining and the rest of the diamond. In our experience, it is helpful to have a black background behind the light and the stone whenever a diamond is being examined with a loupe. This practice, which creates a consistent background and uncluttered visual field behind the diamond, is useful for evaluating graining as well.

Because the observation of whitish or reflective graining may be fleeting, the diamond must be examined through a range of motion. If the characteristic fades from view with little movement, it is not likely to affect the clarity grade. The images in figure 8 illustrate the way an internal grain line can be obscure and then appear obvious and then obscure again through a subtle range of motion. In this instance, the graining feature faded from view with very slight movement, so it did not affect the clarity grade. Also important is the angle at which the graining is seen relative to a facet. Graining observed at an extreme angle to a facet (figure 9) is less likely to impact clarity than one seen perpendicular to the facet.



*Figure 7. A consistent observation methodology is critical to assess the effect of graining on clarity. The final determination is made with a loupe as the diamond is held under the microscope's overhead light source—approximately 2–3 inches (5–8 cm) below the light source and in an area between the front edge of the lamp casing to approximately 2 inches beyond that edge. A black background is placed behind the light and the stone to keep the visual field clear and create a dark field for viewing. Photo by Valerie Power.*

**Clarity Factors.** As the student of diamond grading knows, determination of a clarity grade requires consideration of five factors: size, nature, number, relief, and location. All of these factors also enter into the process of assigning a clarity grade with respect to graining. While they are discussed separately here, they are weighed together for the final determination. As mentioned previously, for whitish and reflective graining, the critical first decision in this process is whether or not the observed graining is a clarity characteristic. Once that has been established, the same standard guidelines used for other internal features are applied to establish the clarity grade. Our experience has been, with whitish graining in particular, that the distinction between FL/IF and VVS is the most common and certainly the most important clarity determination. It is much more unusual to encounter diamonds with extensive whitish graining that would result in their being graded below VVS<sub>2</sub>. In the following discussion, the grades indicated assume that there are no additional internal features that would affect the clarity of the diamond.



Figure 8. These three photos illustrate the way some graining fades in and out of view when the diamond is moved through a range of motion. The photo on the left shows, through the pavilion, a very subtle area of graining that, when moved slightly (center) becomes quite obvious. Yet, with little continued movement (right) it disappears. In instances such as this, the graining would not affect the clarity grade. Photomicrographs by Vincent Cracco; magnified 21 $\times$ .

**Size.** Whitish or reflective graining is less likely to have an effect on the clarity grade if it is observed in only a small area within a single facet (figure 10), especially if it is seen only through a pavilion facet. With such limited whitish or reflective graining, a

Figure 9. Some graining is visible only at extreme angles to the facet through which it is viewed, such as that seen on the far right in this 10+ ct pear-shaped diamond. In instances such as this where the graining is in a limited area and only observed at an extreme angle, it does not impact the clarity grade. Photomicrograph by Vincent Cracco; magnified 10 $\times$ .



diamond may still be graded FL/IF. Conversely, when whitish or reflective graining is observed readily through the pavilion, a VVS<sub>1</sub> grade will result (with even lower grades issued for such graining visible through the crown or table, as discussed under “Location” below).

**Nature.** Whitish graining that forms in distinct cottony or sheen-like bands will affect clarity when it is readily visible with the loupe through a subtle range of motion. When whitish graining is not well defined (figure 11) and does not noticeably diminish transparency, it is still possible that the stone will receive a grade of FL/IF. With regard to reflective graining, distinct internal reflective planes will affect the clarity grade (figure 12, left). However, isolated bright lines—with no internal planes visible—will not readily affect clarity, and the diamond could receive a FL/IF grade (figure 12, right, and box A).

A noticeable overall haziness (again, see figure 6) will also impact the stone’s transparency and thus its clarity grade. If such graining is visible only through the pavilion or is subtle face-up, typically a VVS grade will apply (figure 13, left). Noticeable haziness observed through the crown of the diamond will likely result in a clarity grade of VS (figure 13, center). Obvious and eye-visible haziness in grades in the SI range (figure 13, right). At the laboratory, reference diamonds exhibiting a gradation of haziness are used to help determine the boundary at which clarity is affected.

**Number.** As is the case with pinpoint inclusions, a diamond may have numerous whitish bands or

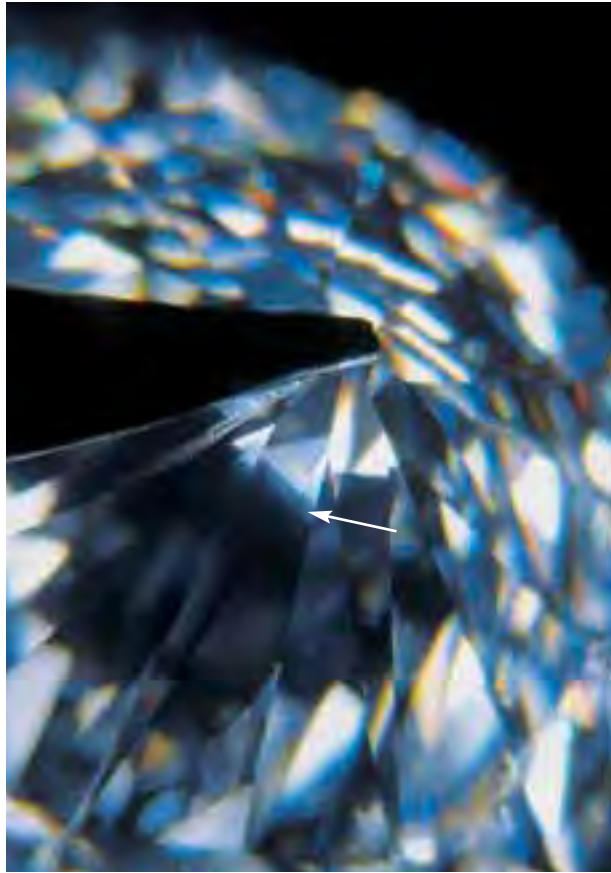


Figure 10. When graining is seen in limited areas, such as that evident near the culet in this diamond, it is not likely to affect the clarity grade. Photomicrograph by Vincent Cracco; magnified 10 $\times$ .

reflective grain lines and still receive a clarity grade as high as VVS<sub>1</sub> if the bands or lines are only observed through the pavilion. However, the higher the quantity of grain lines observed through the crown, the more likely it is that the clarity grade will decrease accordingly. Often, the extent of the area over which bands or lines occur (i.e., “size” versus “number”) is more relevant than the quantity of lines.



Figure 11. One type of whitish graining that usually affects the clarity grade is banding (i.e., alternating cottony or sheen-like lines or bands with dark areas between, as in figures 1 and 2). Whitish graining that has a more amorphous appearance, as illustrated here, and does not diminish transparency when observed through a range of motion, would not affect the clarity grade. Photomicrograph by Vincent Cracco; magnified 12 $\times$ .

*Relief.* In the clarity grading of solid inclusions, *relief* refers to how readily a feature stands out from the surrounding diamond. For graining, relief is complex because, as mentioned above, it is not only a matter of visibility at 10 $\times$  magnification, but it is also a question of the form and texture it takes. Because of this, the contrast exhibited by the graining is very important. Similar to the examples given in “Nature” above, a sheen-like area of graining that does not appear to band (figure 14, left) or affect transparency face-up may not affect the clarity grade, whereas the same characteristic seen with alternating dark bands would likely lower the grade (figure 14, right), because the contrast of grain lines with dark bands results in the greater visibility of the feature. If this feature is visible with the loupe through the pavilion only, the highest grade possible would

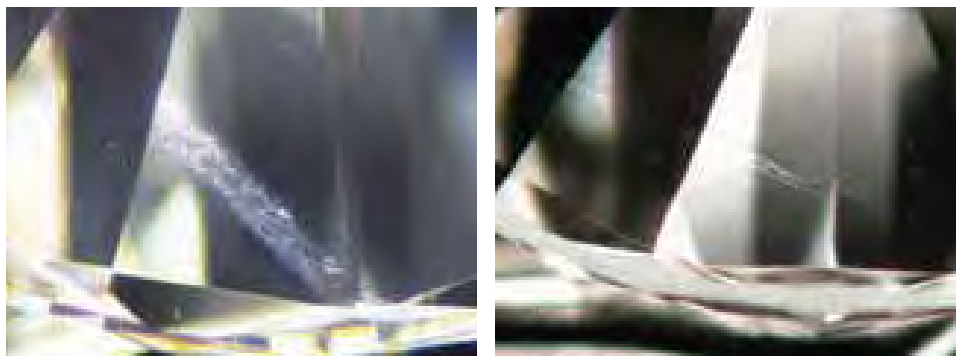


Figure 12. An obvious reflective internal plane (left) reduces the clarity grade of an otherwise clean diamond to VVS<sub>1</sub> if only seen through the pavilion. Bright lines with no internal planar depth (right) typically would not affect the clarity grade, as they usually fade with subtle movement. Photomicrographs by Vincent Cracco (left, 25 $\times$ ) and Mitchell Moore (right, 20 $\times$ ).



Figure 13. As overall haziness becomes more noticeable in the face-up position, the clarity grade is lowered accordingly. The 3+ ct round brilliant-cut diamond on the left has subtle haziness, which is responsible for the VVS clarity grade. More noticeable is the haziness in the 3+ ct cushion cut in the center, which resulted in a VS clarity grade. The haziness in the half-carat round brilliant on the right was so pronounced that it was graded in the SI range. Photos by Yuan Chan.

likely be VVS<sub>1</sub>. When visible through the crown of the diamond, location and size will result in a grade of VVS<sub>2</sub> or lower.

As noted above and illustrated in figure 8, range of motion is important in assessing relief as well. A readily observed grain line that fades out with very subtle movement is less likely to impact clarity than one that remains visible when moved through a greater range.

With regard to relief, it is important to mention one other type of graining that is noted on laboratory reports. Transparent, colorless graining that has an overall rain-like or silvery appearance (figure 15) when the diamond is viewed face-up (without diminishing transparency or forming bands) usually does not affect clarity but, as mentioned earlier, is reported in the comments section as “Transparent internal graining is present.”

*Location.* Location is very important in determining the impact of whitish or reflective graining on the clarity grade of the diamond. Again as noted

above, when such graining is observed through the crown, it will likely have a greater impact (i.e., resulting in a lower grade) than graining observed through the pavilion only, and an even lower grade will be given if the graining is seen in the table area. Location will take precedence over size (extent) as well. For example, long lines or bands covering large areas of numerous facets will likely be graded VVS<sub>1</sub> if they are only visible from the pavilion. As part of “location,” the angle of observation is considered as well. Consequently, a very limited area of graining observed at an extreme angle through the crown or pavilion may not impact the clarity grade (again, see figure 9).

## SUMMARY

The GIA Laboratory strives to report consistently on all aspects of diamond grading. This article outlines the history and development of reporting on a feature that may significantly impact the clarity grade of some of the largest, highest-quality dia-

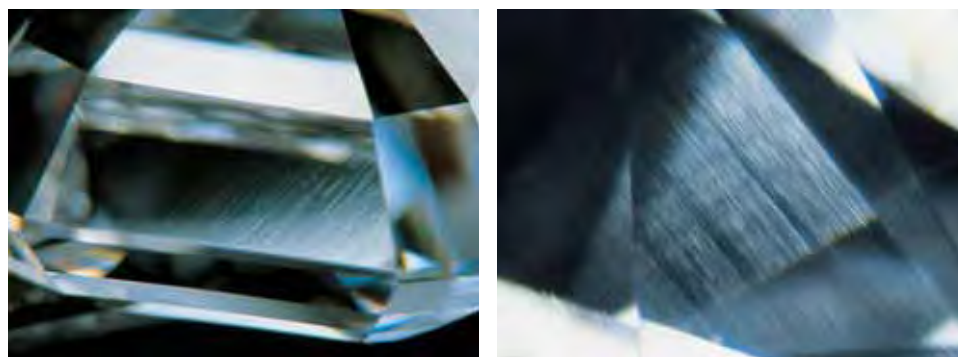


Figure 14. Overall uninterrupted sheen-like graining (left) that does not affect overall transparency when observed through a range of motion may not impact the clarity grade. The contrast seen within bands of graining (right) is more likely to affect the grade given. Photomicrographs by Vincent Cracco; magnified 15× (left) and 47× (right).



*Figure 15. Occasionally graining is observed that exhibits an overall rain-like appearance and is noticeable face up through a range of motion. While such graining does not diminish transparency, as seen in this 10+ ct diamond (left), its obvious visual disruption to the appearance of the diamond (above) results in a report comment noting “Transparent internal graining is present.” Photos by Vincent Cracco; photomicrograph magnified 30x.*

monds encountered. The process of assessing the effect of graining on a clarity grade involves all the classic factors of size, nature, number, relief, and location. However, it also requires consideration of important additional factors, including an understanding of the elusive nature of graining, its visibility under standard grading procedures, its form and texture, and the angle at which it is observed.

In the early years of diamond grading at GIA, staff members saw relatively few diamonds with whitish graining in particular. As a result, such diamonds were categorized broadly, typically with

a note describing the presence of certain appearance factors indicative of such graining. As more diamonds with graining were seen, the need grew for refined criteria. Currently, diamonds that show whitish or reflective graining as bands, lines, or planes in extended areas through a range of motion could receive a clarity grade lower than FL/IF regardless of the absence of fractures or solid inclusions. Consistent with all other aspects of assigning a clarity grade, such a characteristic visible only through the pavilion will typically result in a VVS grade. If it is visible through the crown or table, correspondingly lower grades are assigned based on greater quantity and visibility.

#### ABOUT THE AUTHORS

*Mr. King (jking@gia.edu) is technical director, Mr. Moses is senior vice president, and Dr. Wang is research scientist at the GIA Laboratory in New York.*

#### ACKNOWLEDGMENTS

*The authors would like to express their longstanding respect and admiration for the initial observations and discussions on this topic by the late G. Robert Crowningshield, who for many years was vice president of the GIA Laboratory in New York.*

*In addition, the authors thank the following colleagues from the GIA Laboratory in Carlsbad for their contributions: Bruce Lanzl, director, West Coast Grading Operations; Phillip Yantzer, director, West Coast Grading Laboratory; and Kelly Yantzer, manager, Systems Quality Management. Also, Ron Geurts, Research and Development manager at GIA Belgium, kindly provided insights on grading methods and causes of graining. Ivy Cutler, staff gemologist at the GIA Laboratory in New York, kindly helped with the data search of the historical records.*

## REFERENCES

- Balzaretti N.M., da Jornada J.A.H. (1996) Pressure dependence of the refractive index of diamond, cubic silicon carbide and cubic boron nitride. *Solid State Communications*, Vol. 99, No. 12, pp. 943–948.
- Crowningshield G.R. (1970) Developments and highlights at GIA's lab in New York. *Gems & Gemology*, Vol. 13, No. 5, pp. 156–157.
- Crowningshield G.R. (1971a) Developments and highlights at GIA's lab in New York. *Gems & Gemology*, Vol. 13, No. 9, pp. 286–287.
- Crowningshield G.R. (1971b) Developments and highlights at GIA's lab in New York. *Gems & Gemology*, Vol. 13, No. 11, pp. 344–345.
- Field J.E. (1979) *The Properties of Diamond*. Academic Press, London.
- Fontanella J., Johnston R.L., Colwell J.H., Andeen C. (1977) Temperature and pressure variation of the refractive index of diamond. *Applied Optics*, Vol. 16, No. 11, pp. 2949–2951.
- Fritsch E., Scarratt K. (1993) Gemmological properties of type Ia diamonds with unusually high hydrogen content. *Journal of Gemmology*, Vol. 23, pp. 451–460.
- Fritsch E., Rondeau B., Notari F. (2006) Cleavage resistance of plastically deformed natural diamonds revealed by dissolved planar features. *Diamond and Related Materials*, Vol. 15, pp. 1310–1313.
- Jang-Green H. (2006) Lab Notes: A natural Fancy white diamond with whitish banding. *Gems & Gemology*, Vol. 42, No. 4, pp. 262–263.
- Kane R.E. (1980) The elusive nature of graining in gem quality diamonds. *Gems & Gemology*, Vol. 16, No. 9, pp. 294–314.
- Kane R.E. (1982) Graining in diamond. In D.M. Eash, Ed., *International Gemological Symposium Proceedings 1982*. Gemological Institute of America, Santa Monica, CA, pp. 219–235.
- Lang A.R. (1967) Causes of birefringence in diamond. *Nature*, Vol. 213, pp. 248–251.
- Lu T., Shigley J.E., Koivula J.I., Reinitz I.M. (2001) Observation of etch channels in several natural diamonds. *Diamond and Related Materials*, Vol. 10, No. 1, pp. 68–75.
- Moses T.M., Shigley J.E., McClure S.F., Koivula J.I., Van Daele M. (1999) Observations on GE-processed diamonds: A photographic record. *Gems & Gemology*, Vol. 35, No. 3, pp. 14–22.
- Moses T.M., Wang W. (2006) Diamond with clarity affected by intense graining. *Gems & Gemology*, Vol. 42, No. 2, pp. 162–163.
- Schrauder M., Navon O. (1993) Solid carbon dioxide in a natural diamond. *Nature*, Vol. 365, pp. 42–44.
- Shah C.J., Lang A.R. (1963) An unusual distribution of precipitates in a diamond. *Mineralogical Magazine*, Vol. 33, pp. 594–599.
- Sobolev N.V., Fursenko B.A., Goryainov S.V., Shu J., Hemley R.J., Mao H.-K., Boyd F.R. (2000) Fossilized high pressure from the earth's deep interior: The coesite-in-diamond barometer. *Proceedings of the National Academy of Sciences*, Vol. 97, No. 22, pp. 11875–11879.
- Sunagawa I. (2006) *Crystal Growth, Morphology and Perfection*. Cambridge University Press, Cambridge, England.
- Wilks J., Wilks E.M. (1991) *Properties and Applications of Diamond*. Butterworth-Heinemann, Oxford, England.
- Yan C.S., Mao H.K., Li W., Qian J., Zhao Y., Hemley R.J. (2004) Ultrahard diamond single crystals from chemical vapor deposition. *Physica Status Solidi (A)*, Vol. 201, No. 4, pp. R25–R27.

**Twenty-Five Years  
at Your Fingertips**

Twenty-five years of GEMS & GEMOLOGY means a lot of valuable research. Fortunately, we've got it all—articles, lab notes, gem news, editorials, and book reviews—indexed in this one handy volume. It's an invaluable tool for the serious gemologist, for the far-from-invaluable price of just \$14.95. (\$19.95 internationally) **FREE shipping!**

**Order Yours Today!**

To order, visit [www.gia.edu/gemsandgemology](http://www.gia.edu/gemsandgemology) and click on *Ordering and Renewals*. Call 800-421-7250 ext. 7142 within the U.S., or 760-603-4000 ext. 7142.

Now Available!



The best of

**GEMS & GEMOLOGY®**

on two of the most important subjects  
in the diamond world today—**Over 70 years**  
of compiled research.

# GEMS & GEMOLOGY® IN REVIEW

## SYNTHETIC DIAMONDS

- More than 30 years of cutting-edge synthetic diamond research by leading gemological researchers and producers—50 separate entries comprising more than 300 pages of material
- Editorial commentary by Dr. James Shigley of GIA Research
- PLUS! Includes two wall charts in a sturdy bound-in pouch: the Separation of Synthetic and Natural Diamonds, and Characteristics of HPHT-Grown Synthetic Diamonds

**\$49.95** plus shipping

## COLORED DIAMONDS

- 317 pages of award-winning articles and exceptional color photography
- Editorial commentary by colored diamond color-grading expert John King, technical director of the GIA Laboratory
- PLUS! The *GIA Colored Diamonds Color Reference Charts* booklet explains and illustrates GIA color grades and descriptions for the most common fancy colors, including yellow, pink, blue, and yellow-green

**\$59.95** plus shipping

**Order Yours Today!**

Visit [www.gia.edu/gemsandgemology](http://www.gia.edu/gemsandgemology)

and click on Ordering and Renewals.

Or call 800-421-7250, ext. 7142

(outside the U.S. and Canada,  
760-603-4000, ext. 7142).



# IDENTIFICATION OF “CHOCOLATE PEARLS” TREATED BY BALLERINA PEARL CO.

Wuyi Wang, Kenneth Scarratt, Akira Hyatt, Andy Hsi-Tien Shen, and Matthew Hall

Treated cultured pearls with a “chocolate” coloration have entered the market from several sources. Gemological, spectroscopic, and chemical analyses were performed on both untreated and treated cultured pearls to provide a better understanding of the “chocolate” treatment process that is used by one company (Ballerina Pearl Co.) and to determine how these products can be identified. It is likely that the organic components in black cultured pearls were bleached to create the brown coloration; no foreign coloring agent was detected. Cultured pearls treated by this method can be identified based on their unusual coloration, characteristic fluorescence, UV-Vis-NIR reflectance and Raman spectra, and trace-element composition.

To achieve an attractive and consistent color appearance, cultured pearls are frequently treated by bleaching, dyeing (such as with silver nitrate), or exposure to radiation. A “new” color for cultured pearls was introduced to the market in 2000 (figure 1; see, e.g., “U.S. gem labs...,” 2004; Zachovay, 2005; “GIA identifies...,” 2006; Strack, 2006; “Study shows...,” 2006). The induced brown color reportedly results from the bleaching of “black” Tahitian cultured pearls. These are now known in the trade as “chocolate pearls” and have become quite popular (Sanchez, 2004). They are available from several sources, including Ballerina Pearl Co. in New York and Shanghai Gems SA in Geneva (“Better techniques,” 2006). The companies treating these cultured pearls assert that no color is added during treatment (Sanchez, 2004). However, it is unlikely that all the “chocolate pearls” marketed today have been treated using the same technique.

To better understand the treatment process being used by one company (Ballerina Pearl Co.) and how these new products can be identified, we analyzed the gemological, chemical, and spectroscopic properties of several of these “chocolate pearls” as well as silver-dyed Tahitian cultured pearls and untreated gray and brown Tahitian cultured pearls. In addition,

we asked Ballerina Pearl Co. to treat four Tahitian cultured pearls specifically for this study.

## MATERIALS AND METHODS

A total of 196 cultured pearls weighing 3.75–21.40 ct (9.5–19.7 mm in diameter) were selected for this study (see, e.g., figure 2; a representative list is given in table 1). These included 29 natural-color Tahitian cultured pearls (NCTCP) from GIA’s collection that were obtained directly from pearl farmers. Of these, 19 were dominated by gray coloration and the other 10 by brown coloration. These samples have been in GIA’s collection for at least five years, and the laboratory confirmed that they were natural color. The “chocolate” cultured pearls (CCP; 160 samples) and silver [Ag]-dyed Tahitian cultured pearls (DTCP; three samples) were supplied by Ballerina Pearl Co. and its distributor Emiko Pearl International. We cut through the nacre of two CCPs (Bal-12 and Bal-13) to examine color variation with depth.

---

See end of article for About the Authors and Acknowledgments.  
GEMS & GEMOLOGY, Vol. 42, No. 4, pp. 222–235.  
© 2006 Gemological Institute of America



*Figure 1. Samples of intense brown “chocolate pearls” are shown in this necklace (12.0–13.7 mm) and ring (12.9 mm) that Ballerina Pearl Co. has produced from Tahitian black cultured pearls with their proprietary treatment process. Natural-color Tahitian cultured pearls with dominant brown coloration are rare. Courtesy of Emiko Pearls International; photo by Robert Weldon.*

Details of the treatment remain proprietary, but Ballerina Pearl Co. did disclose that two steps are involved (A. Auerbach, pers. comm., 2006). At our request, Ballerina Pearl Co. subjected four representative undrilled NCTCPs (samples Bal-02, Bal-16, Bal-18, Bal-19) to their two-step treatment process to induce the “chocolate” color. We examined three of them after each of the two steps; sample Bal-02 was only examined after the final step.

The color of all samples was described in accordance with the GIA pearl classification system (Gemological Institute of America, 2000). Visual features were observed using a standard gemological microscope. Reactions to UV radiation were checked in a darkened room with conventional 4-watt long-wave (366 nm) and short-wave (254 nm) lamps.

Infrared reflectance spectra were recorded for 46 samples (all 29 NCTCPs, 10 CCPs of varying colors, three DTCPs, and the four NCTCPs studied before and after treatment). The spectra were collected in the mid-infrared region ( $6000\text{--}400\text{ cm}^{-1}$ ;  $1.0\text{ cm}^{-1}$

resolution) at room temperature with a Thermo-Nicolet Nexus 670 Fourier-transform infrared (FTIR) spectrometer equipped with a KBr beam splitter and MCT-B detector. Instead of using the destructive KBr pellet method, we employed a diffuse reflectance technique that focuses the incident infrared beam on the sample’s surface. Diffused light traveling through the outermost layer provides information about the absorption characteristics of that sample. A total of 512 scans (per spectrum) were collected to improve the signal-to-noise ratio.

Reflectance spectra in the UV-Vis-NIR range of 190–850 nm were collected on 98 samples (all 29 NCTCPs, 62 CCPs of varying colors, three DTCPs, and the four samples examined before and after treatment) using a PerkinElmer Lambda 950 spectrometer at room temperature (step interval = 0.25 nm; slit = 2.0 nm). A black metal disk with a center hole of ~6.0 mm in diameter was used to select a specific area of each cultured pearl for analysis while securing the sample against the light integration sphere.

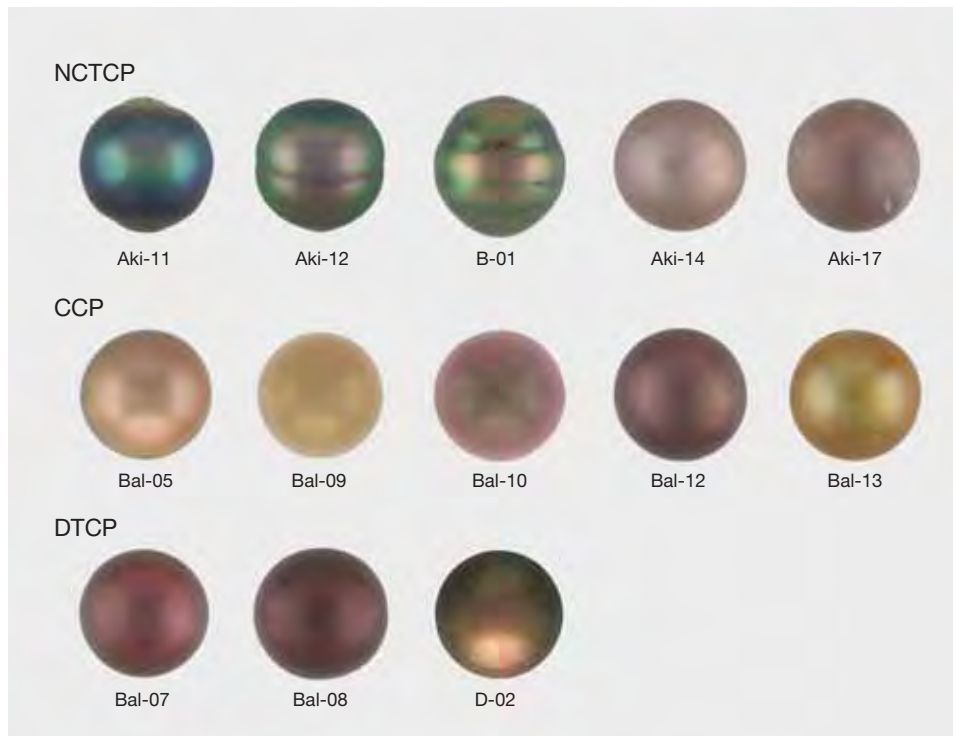


Figure 2. Shown here are some of the cultured pearls (9.05–13.47 mm in diameter) examined as part of this study (top row, natural color; middle row, treated “chocolate” color; bottom row, silver nitrate dyed). Photos by Jessica Arditi and Jian Xin (Jae) Liao.

Raman and photoluminescence spectra of 37 samples (19 NCTCPs of both gray and brown colors, 11 CCPs of varying colors, three DTCPs, and the four samples examined before and after treatment) were recorded at room temperature using a Renishaw inVia Raman microspectrometer that was equipped with an Ar-ion laser operating at two excitation wavelengths (488.0 and 514.5 nm) and a He-Nd laser with 632.8 nm excitation. We calibrated the instrument using the Raman shift of a single-crystal silicon reference. Initial laser power was adjusted for maximum signal intensity while avoiding oversaturation. Up to 10 scans per spectrum were collected to improve the signal-to-noise ratio.

Chemical composition was determined qualitatively with a Thermo-Noran Spectrace QuanX energy-dispersive X-ray fluorescence (EDXRF) spectrometer, and quantitatively using a Thermo X Series inductively coupled plasma-mass spectrometer (ICP-MS) combined with a New Wave UP213 laser ablation system for sampling. We analyzed 47 samples (all 29 NCTCPs, 11 CCPs of varying colors, three DTCPs, and the four samples examined before and after treatment) using EDXRF, and 70 cultured pearls (27 NCTCPs, 38 CCPs, two DTCPs, and three samples examined before and after treatment) using LA-ICP-MS. For EDXRF analysis, all X-ray filter options (none, cellulose, Al, thin Pd, medium Pd, thick Pd, thin Cu, and thick Cu) were applied indi-

vidually with accelerating voltages of 8, 10, 12, 20, 20, 28, 50, and 50 kV, respectively. A collimator of 3.5 mm diameter was used. Beam current was automatically controlled to maintain a 50% dead time in data collection. Live time for data accumulation was 100 seconds. All spectra were collected at ~0.01 Pascal. For the LA-ICP-MS analysis, a laser beam with a wavelength of 213 nm was rastered across the pearl surface along a 1–2 mm line (figure 3). The

Figure 3. This scanning electron microscope image of a NCTCP (Aki-01) shows the platelet structure of the nacre and the effects of the laser penetration into the nacre during LA-ICP-MS analysis. A minute depression with a length of ~1 mm, width of 40  $\mu\text{m}$ , and depth of ~20  $\mu\text{m}$  was created during the analysis.

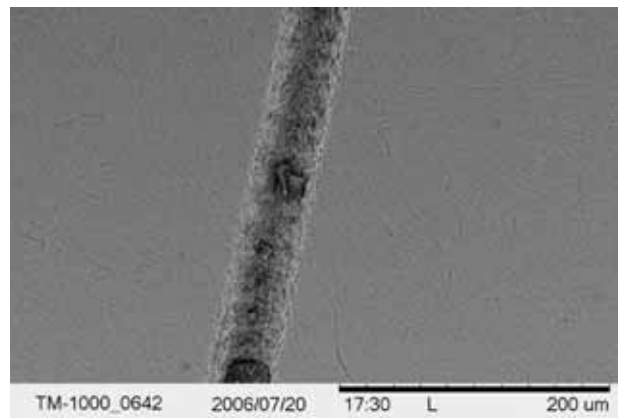


**TABLE 1.** Representative samples of natural-color Tahitian, “chocolate,” and silver-dyed Tahitian cultured pearls examined for this study.

Sample no.	Color	Luster	Surface (extent of spotting)	Size (mm)	Fluorescence to UV radiation	
					Long-wave	Short-wave
<b>Natural-Color Tahitian Cultured Pearls (NCTCPs)</b>						
Aki-01	Greenish gray	High	Heavy	~10.11–10.39	Weak greenish yellow	Weak greenish yellow
Aki-02	Black	High	Moderate	~10.66–14.14	Very weak orange	Very weak greenish yellow
Aki-03	Gray and greenish gray	Medium	Light	~12.29–19.74	Weak orange	Very weak greenish yellow
Aki-04	Dark greenish gray (with rosé)	High	Heavy	~11.62–13.01	Very weak orange	Very weak greenish yellow
Aki-05	Greenish gray	Medium	Moderate	~13.54–17.46	Very weak orange	Very weak greenish yellow
Aki-06	Dark greenish gray (with orient)	High	Light	~11.10–16.37	Very weak yellow	Very weak greenish yellow
Aki-07	Dark greenish gray (with rosé)	High	Moderate	~10.41–12.48	Inert	Inert
Aki-08	Dark greenish gray (with rosé and orient)	High	Heavy	~11.22–13.49	Very weak yellow	Very weak greenish yellow
Aki-09	Dark greenish gray (with rosé)	High	Moderate	~10.90–11.80	Very weak orange	Very weak greenish yellow
Aki-10	Dark greenish gray	Medium	Heavy	~12.56–14.96	Very weak orange	Very weak greenish yellow
Aki-11	Dark violetish gray	High	Heavy	~9.50–9.56	Inert	Inert
Aki-12	Greenish gray (with rosé)	High	Moderate	~9.05–9.52	Very weak yellow	Very weak greenish yellow
Aki-13	Orangy brown and dark gray	Medium	Moderate	~13.9	Weak greenish yellow	Very weak greenish yellow
Aki-14	Orangy brown	Medium	Heavy	~11.7	Weak yellow	Very weak greenish yellow
Aki-15	Pinkish brown	Medium	Heavy	~11.8	Weak yellow	Very weak greenish yellow
Aki-16	Orangy brown	Medium	Heavy	~12.8	weak orange	Very weak greenish yellow
Aki-17	Pinkish brown	Medium	Heavy	~10.4	Very weak yellow	Very weak greenish yellow
Aki-18	Pinkish brown	Low	Heavy	~12.2	Very weak orange	Inert
Aki-19	Dark brown	High	Moderate	~9.9	Very weak orange	Inert
Aki-20	Dark greenish gray (with rosé)	High	Moderate	~10.0	Very weak yellow	Inert
Aki-21	Orangy brown	Low	Heavy	~11.4	Weak orange	Very weak yellow
Aki-22	Dark brown	Low	Heavy	~10.6	Very weak orange	Inert
Aki-23	Orangy brown	Medium	Heavy	~10.9	Weak orange	Very weak greenish yellow
<b>“Chocolate” Cultured Pearls (CCPs)</b>						
Bal-03	Yellowish brown	High	Light	~11.99–12.05	na <sup>a</sup>	na
Bal-12	Dark brown	Medium	Moderate	~10.0	Very weak reddish orange	Inert
Bal-13	Yellow-brown	Medium	Moderate	~10.8	Moderate reddish orange	Very weak orange
Bal-14	Pink-brown	Medium	Light	~14.0	Moderate reddish orange	Weak orange
Bal-56	Orange-brown	High	na	~12.3	Moderate reddish orange	Weak greenish yellow
Bal-57	Orange-brown	High	na	~12.1	Moderate reddish orange	Weak greenish yellow
Bal-58	Orange-brown	High	na	~11.8	Moderate reddish orange	Weak greenish yellow
Bal-59	Orange-brown	High	na	~12.1	Moderate reddish orange	Weak greenish yellow
Bal-60	Orange-brown	High	na	~12.6	Moderate reddish orange	Weak greenish yellow
Bal-61	Orange-brown (with rosé)	High	na	~12.3	Moderate reddish orange	Weak greenish yellow
Bal-62	Orange-brown (with rosé)	High	na	~11.7	Moderate reddish orange	Weak greenish yellow
Bal-63	Orange-brown	High	na	~12.0	Moderate reddish orange	Weak greenish yellow
Bal-64	Orange-brown	High	na	~12.3	Moderate reddish orange	Weak greenish yellow
Bal-65	Orangy brown	High	na	~13.7	Moderate reddish orange	Moderate greenish yellow
Bal-66	Orange-brown (with rosé)	High	na	~12.2	Moderate greenish yellow	Moderate greenish yellow
Bal-67	Orange-brown (with rosé)	High	na	~12.0	Moderate reddish orange	Weak greenish yellow
Bal-68	Orange-brown	High	na	~12.9	Moderate reddish orange	Weak greenish yellow
Bal-69	Orange-brown	High	na	~12.1	Weak reddish orange	Inert
Bal-70	Dark brown	High	na	~12.2	Weak reddish orange	Inert
Bal-71	Orangy brown	High	na	~12.9	Moderate reddish orange	Weak greenish yellow
<b>Dyed Tahitian Cultured Pearls (DTCPs)</b>						
Bal-07	Dark brownish pink	Medium	Moderate	~10.0–10.5	Inert	Inert
Bal-08	Dark pink-brown	Medium	Moderate	~10.0–10.5	Inert	Inert

<sup>a</sup>na = not analyzed.



Figure 4. The induced dark brown color was distributed evenly in the nacre of CCP sample Bal-12 (left, 10.0 mm), which was cut to a depth of ~1 mm. In CCP sample Bal-13 (right, 10.8 mm), yellow-brown color was distributed evenly through most of the outer layer of the nacre (~1.5 mm thick). The same hue, though lighter, was observed in the interface region between the nacre and the nucleus. Photo by Jian Xin (Jae) Liao.

laser rastered across the line only once and the ablation depth was about 20  $\mu\text{m}$  at this condition, which ensured that the composition of only the outermost layer of the nacre was measured.

## RESULTS

**Gemological Observations.** Most of the “black” NCTCPs showed greenish gray to dark greenish gray coloration, which was sometimes inhomogeneous (again, see figure 2). Overtones of violet, blue, yellow, green, and “rosé” were common. Ten of the

NCTCPs showed distinct orangy or pinkish brown colors. Good-quality specimens (~70% of samples in this study) typically showed medium-to-high luster.

The CCPs were dominated by a brown coloration, although some also exhibited yellowish, greenish, pinkish, or orangy hues (again, see figure 2). The tone of the brown color varied significantly among samples, from light to very dark. Orient was usually not observed. Similar to the NCTCPs, the CCPs showed medium to high luster. The three DTCP samples exhibited dark brown coloration with clear pink overtones and medium luster.

When the nacre in one dark brown “chocolate pearl” (Bal-12) was cut to a depth of ~1 mm (figure 4, left), we observed that the dark brown color was distributed evenly with depth. However, in the yellow-brown CCP (Bal-13) that was cut ~1.5 mm through the nacre layer into the nucleus (figure 4, right), the hue was distributed evenly throughout most of the outer nacre, but showed lighter tone at the nucleus interface.

Most of the gray NCTCPs fluoresced very weak orange, yellow, or greenish yellow to long-wave UV radiation, and very weak greenish yellow to short-wave UV. The brown NCTCPs displayed very similar reactions. However, the blemishes seen on the surface of most of the brown cultured pearls exhibited strong greenish yellow fluorescence; this was rarely observed in the gray NCTCPs. Of the 160 CCPs tested, the vast majority (157) displayed weak (~60%) to moderate (~40%) chalky reddish orange fluorescence to long-wave UV. This fluorescence

TABLE 2. Gemological features of four samples before and after “chocolate” treatment by Ballerina Pearl Co.

Feature	Bal-02		Bal-16			Bal-18			Bal-19		
	Untreated	Treated	Untreated	Preparatory treated	Treated	Untreated	Preparatory treated	Treated	Untreated	Preparatory treated	Treated
Color	Greenish gray	Greenish brown	Dark brown	Dark brown	Dark brown	Dark greenish gray (with rosé)	Green brown (with rosé)	Orangy brown (with rosé)	Dark greenish gray (with rosé)	Orange-brown	Orangy brown (with rosé)
Luster	Medium	Medium	Medium	Medium	High	Medium	High	High	High	High	High
Surface (extent of spotting)	Light	Light	Heavy	Heavy	Heavy	Moderate	Moderate	Moderate	Moderate	Moderate	Moderate
Size (mm)	~11.41–11.73		~10.22–10.34			~10.65–10.81			~10.95–11.26		
Weight (ct)	10.65	10.64	7.74	7.72	7.71	8.44	8.42	8.40	9.74	9.70	9.69
Fluorescence											
To long-wave UV	Very weak orange	Moderate greenish yellow	Very weak yellow	Very weak reddish orange	Very weak reddish orange	Very weak yellow	Very weak reddish orange	Moderate reddish orange	Very weak yellow	Very weak reddish orange	Moderate reddish orange
To short-wave UV	Very weak greenish yellow	Weak greenish yellow	Inert	Inert	Inert	Very weak greenish yellow	Inert	Very weak greenish yellow	Very weak greenish yellow	Very weak orangy red	Very weak greenish yellow

was not observed in the NCTCPs, and only three CCPs displayed weak-to-moderate greenish yellow or yellow fluorescence to long-wave UV. When exposed to short-wave UV radiation, 156 CCPs showed weak-to-moderate greenish yellow fluorescence (in four, the reaction was inert). No clear correlation between the intensity of fluorescence and the tone of brown color was observed. The three DTCP samples showed no reaction to either long- or short-wave UV.

The variations in major gemological features exhibited by the four cultured pearls treated by Ballerina Pearl Co. for this study are summarized in table 2. Distinct changes in color were induced in the three gray samples (Bal-02, Bal-18, and Bal-19) by the preparatory process, and the brown color was further enhanced in the second step of treatment (figure 5). The hue of dark brown Bal-16 remained basically unchanged, although the tone was reduced, resulting in a more “chocolate” appearance. After treatment, these “chocolate pearls” lost a slight amount of weight (0.1–0.5%) but the blemishes appeared the same. A slight improvement in luster was observed in two of the four specimens (Bal-16 and Bal-18). A notable difference between samples was observed in their long-wave UV fluorescence. In three samples (Bal-16, Bal-18, and Bal-19), it changed from very weak yellow to distinct reddish orange, with an intensity varying from very weak to moderate. In sample Bal-02, it changed from very weak orange to moderate greenish yellow.

**Infrared Reflectance Spectroscopy.** The NCTCPs displayed consistent absorption features in the mid-infrared region. These features included strong absorption bands at 1514–1506 and 878  $\text{cm}^{-1}$  and weak-to-moderate bands at 1780, ~1084, 713, and 700  $\text{cm}^{-1}$  (figure 6). The gray and brown NCTCPs showed identical features, which are generally consistent with the mineral aragonite (again, see figure 6), in particular with the occurrence of the peak at 1084  $\text{cm}^{-1}$ . However, the peak at 878  $\text{cm}^{-1}$  for the NCTCPs is very different from the 860  $\text{cm}^{-1}$  peak in aragonite, and occurs at nearly the same position as seen in calcite. As expected, no absorption peaks related to organic components were detected from the NCTCPs. Infrared reflectance yielded nearly identical absorption features for the CCPs and DTCPs as for the NCTCPs (figure 7). The four NCTCPs treated for this study showed no detectable variation in their mid-infrared reflectance spectra after the treatment.

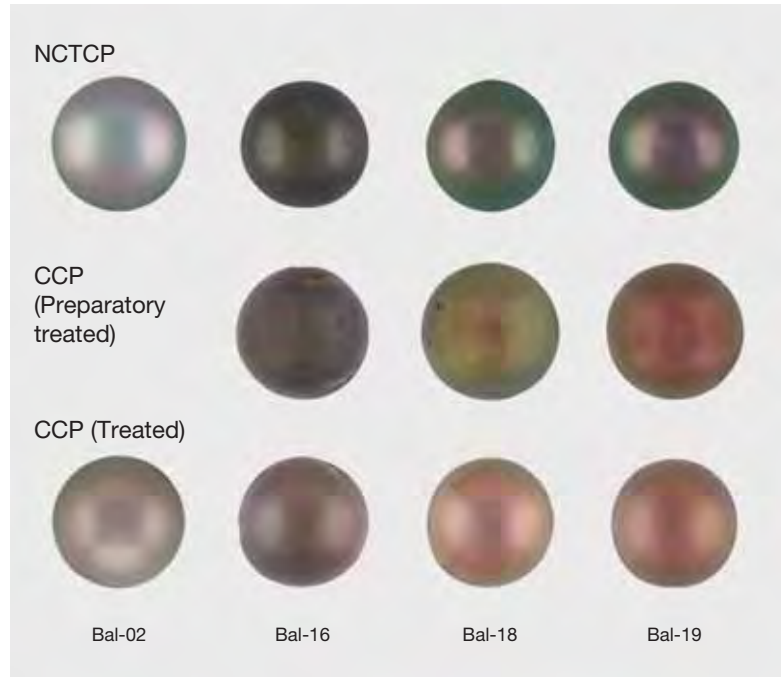
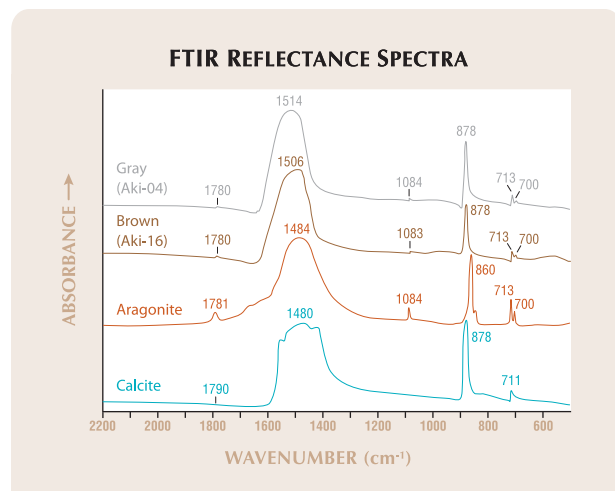


Figure 5. These four Tahitian cultured pearls (top; 10.22–11.73 mm in diameter) were treated by the Ballerina Pearl Co. in a two-stage process to produce “chocolate pearls.” An intense brown color was created in the preparatory treatment (middle) and then enhanced in the final step (bottom). Photos by Jessica Ardit and Jian Xin (Jae) Liao.

Figure 6. The mid-infrared reflectance spectra of the NCTCPs are similar to the spectrum of aragonite, in particular with the occurrence of a peak at 1084  $\text{cm}^{-1}$ . However, the peak at 878  $\text{cm}^{-1}$  for the NCTCPs is much higher in position than the 860  $\text{cm}^{-1}$  peak in aragonite, and occurs at nearly the same position as seen in calcite. Gray and brown NCTCPs examined for this study displayed identical absorption features.



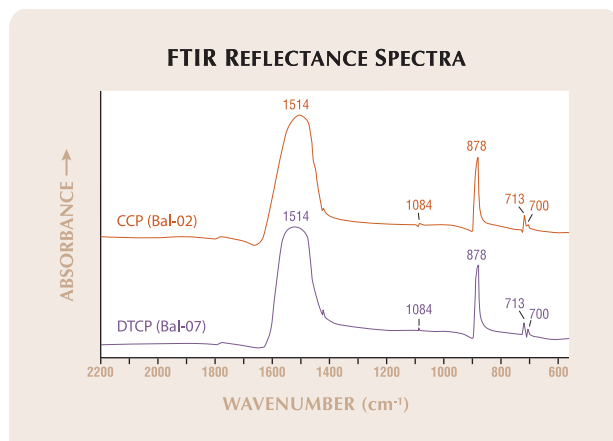


Figure 7. The mid-infrared absorption spectra of the CCPs and DTCPs were nearly identical to those of the NCTCPs in figure 6.

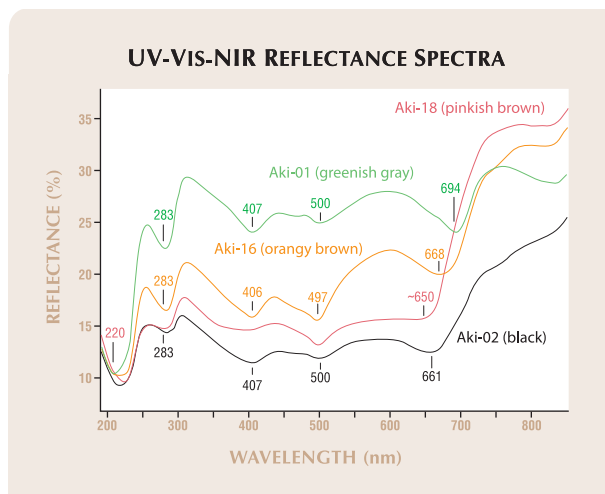


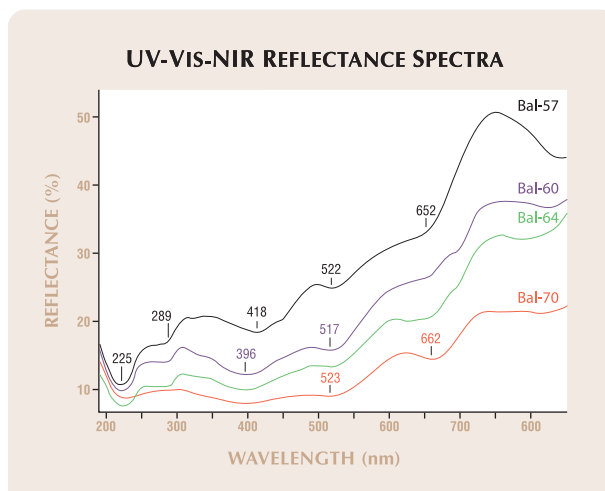
Figure 8. The UV-Vis-NIR reflectance spectra of the NCTCPs of various colors displayed a series of strong absorption bands, as well as a nearly flat baseline.

**UV-Vis-NIR Reflectance Spectroscopy.** Broad absorption bands centered at ~220, 283, ~407, 497–500, and ~650–694 nm occurred consistently in the NCTCPs (figure 8), though the height of the spectral baselines varied greatly. (In general, the darker a cultured pearl is, the lower its UV-Vis-NIR spectral baseline will be.) There was considerable variability among the NCTCP samples in both position and shape of the band at ~650–694 nm. The center of this band shifted as much as ~44 nm. In many of the brown NCTCPs, this band occurred as a shoulder (e.g., Aki-18 in figure 8), and was less distinct than bands recorded from gray NCTCPs. Notably, the baselines of the reflectance spectra were nearly horizontal for all the NCTCPs (both gray and brown), which means that the percentage of light reflectance at ~320 nm is very close to that at ~600 nm. (These two wavelength regions are relatively unaffected by absorption bands and, therefore, provide good reference points to judge the baseline.)

In the CCPs, the absorption bands described above were weaker in intensity or barely present. They also shifted slightly in position (figure 9). The band at 497–500 nm in the NCTCPs shifted consistently to higher wavelengths (510–529 nm) in the CCPs. The four “chocolate pearls” in figure 9 displayed similar brown colors, but the reflectance spectral baseline was inversely proportional to the tone of the brown color; that is, the baseline decreased as the tone increased. The baselines of all these spectra increased in general absorption toward lower wavelengths (higher energy); the reflectance percentage at ~320 nm was much lower than at ~600 nm. In the DTCPs, the spectral variations

were even more dramatic. Only the peaks at ~220 and ~283–285 nm (and a weak absorption at ~700 nm in sample Bal-07) were clearly defined (figure 10). All other peaks observed in the NCTCPs and CCPs were generally less distinct (e.g., those located at 415 and 515 nm) or absent in the DTCPs. Instead, a broad absorption band ranging from ~320 to ~700

Figure 9. In contrast to the spectra shown in figure 8, the UV-Vis-NIR reflectance spectra of the CCPs exhibited baselines that increased in general absorption toward the low-wavelength (high-energy) side. The absorption bands (due to organic components) are less distinct, and some have shifted position, compared to those observed in the NCTCPs. Bal-57, Bal-60, and Bal-64 are orange-brown; Bal-70 is dark brown.



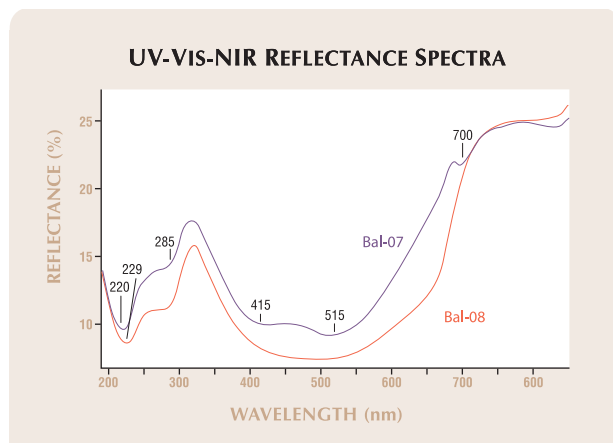


Figure 10. The UV-Vis-NIR reflectance spectra of these two DTCPs are very different from those of the NCTCPs and the CCPs. The spectra are dominated by a broad absorption band that ranges from ~320 to ~700 nm and is centered at ~500 nm.

nm and centered at ~500 nm was recorded. In contrast to the NCTCPs and CCPs, the reflectance percentage at ~320 nm in the DTCPs was much higher than at ~600 nm (again, see figure 10).

Clear variations in reflectance features before and after treatment were recorded in the four NCTCPs that were “chocolate” treated for this study (figure 11). The nearly flat baseline before treatment increased in general absorption toward the low-wavelength (high-energy) side of the spectrum, and the four absorption bands at 283, ~407, 497–500, and ~650–694 nm became broader and weaker and, consequently, less distinct. In addition, the band at ~407 nm shifted to 402–403 nm, the band at 497–500 nm moved 8–18 nm to higher wavelengths, and the band at ~650–694 nm shifted 10–14 nm to lower wavelengths. It should be pointed out that the ~407 nm band observed in figure 8 could occur as low as 403 nm in some NCTCPs (e.g., figure 11). After treatment, the reflectance percentage decreased dramatically in the region of 250–560 nm in three samples (Bal-02, Bal-18, and Bal-19), but this effect was less evident when the starting material was very dark in color (Bal-16).

**Raman and Photoluminescence Spectroscopy.** When excited by 488, 514, and 633 nm lasers, all the cultured pearls showed strong photoluminescence. Broad emission bands centered at ~620, 650, and 725–750 nm were observed (figure 12). Sharp Raman scattering peaks from carbonate components of the nacre overlaid these strong photoluminescence bands. Consistent luminescence features

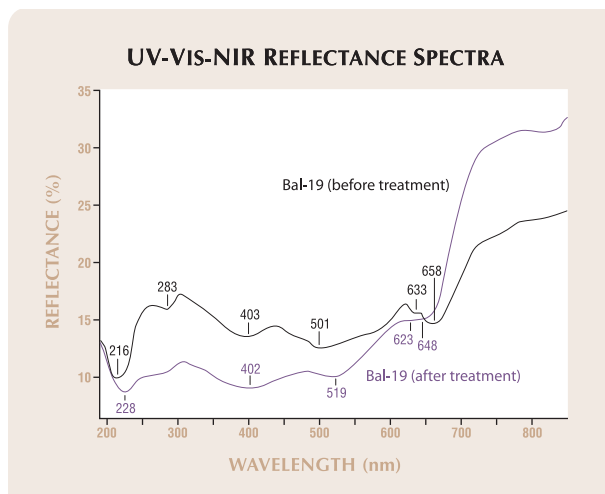
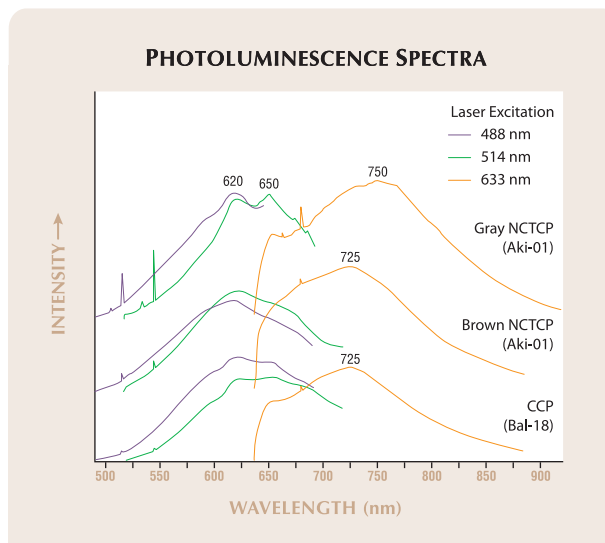


Figure 11. After treatment, the baseline of the UV-Vis-NIR reflectance spectrum of sample Bal-19 increased in general absorption toward the low-wavelength (high-energy) side; this appears to be a useful feature for identifying this type of “chocolate pearl.” Also, absorption bands associated with organic components became less distinct.

were observed in the spectra of the gray NCTCPs (12 samples), as well as in the spectra of those dominated by brown (seven samples). There were some subtle differences in the spectra of the gray and brown NCTCPs. Emission bands at 620 and 650

Figure 12. Strong photoluminescence was observed in both the NCTCPs and CCPs, with broad emission bands centered at ~620, 650, and 725–750 nm. The sharp peaks overlying those photoluminescence bands are caused by Raman scattering from carbonate components of the nacre. The spectra are shifted vertically for clarity.



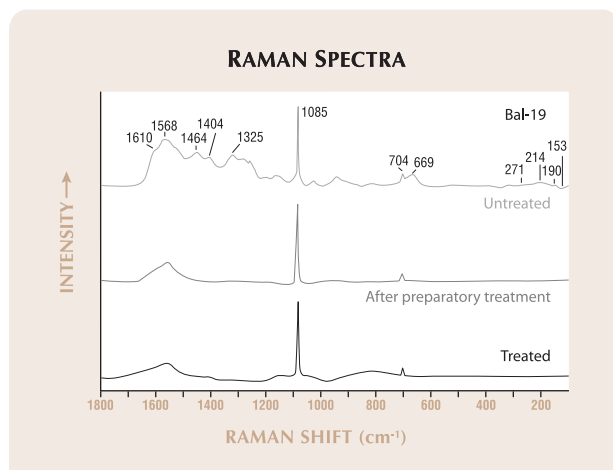


Figure 13. The Raman spectra of NCTCP Bal-19 changed considerably with the “chocolate” treatment, as the intensity of absorption due to organic components decreased significantly after the initial stage. These spectra were collected using 488 nm laser excitation and were normalized to the intensity of the Raman peak for aragonite at 1085  $\text{cm}^{-1}$ . The spectra are shifted vertically for clarity.

nm in the brown NCTCPs were comparatively less distinct than in the gray NCTCPs. In addition, a band centered at  $\sim 725$  nm in the gray NCTCPs occurred at  $\sim 725$  nm in the brown NCTCPs. The brown NCTCPs showed photoluminescence features very similar to those of the 11 CCPs (again, see figure 12) and three DTCPs analyzed in this study (not shown in figure 12). When normalized to the intensity of the Raman scattering peak at 1085  $\text{cm}^{-1}$  associated with the carbonate component of cultured pearls, the photoluminescence intensity of the CCPs was generally stronger than that of the NCTCPs. The weakest photoluminescence was observed in the DTCPs.

In the NCTCP samples, a strong peak at 1085  $\text{cm}^{-1}$ , a moderate peak at 704  $\text{cm}^{-1}$ , and weak peaks in the region of 300–100  $\text{cm}^{-1}$  (271, 214, 190, 153, and 143  $\text{cm}^{-1}$ ) were observed in the Raman spectra of all samples when using 488 and 514 nm laser excitations (figure 13). Several broad bands were observed in the region of 1700–1300  $\text{cm}^{-1}$ , with centers at approximately 1610, 1568, 1464, 1404, and 1325  $\text{cm}^{-1}$ . A weak and broad peak also occurred at  $\sim 669$   $\text{cm}^{-1}$ . When 633 nm laser excitation was applied, the peak at 704  $\text{cm}^{-1}$  resolved into a doublet at 701 and 705  $\text{cm}^{-1}$ , and peaks in the region of 300–100  $\text{cm}^{-1}$  became less distinct. The broad bands in the 1700–1300  $\text{cm}^{-1}$  region and the peak at  $\sim 669$   $\text{cm}^{-1}$  also were present in the Raman spectra with 633 nm laser excitation.

In the four cultured pearls treated for this study, the intensity of the Raman peaks described above decreased significantly after the first stage of treatment: Most peaks were nearly absent below 1500  $\text{cm}^{-1}$ , with the notable exceptions of the 1085 and 704  $\text{cm}^{-1}$  peaks. Completion of the treatment depressed the peaks even further (again, see figure 13).

We also examined the full width at half maximum (FWHM) of the 1085  $\text{cm}^{-1}$  peak in our samples from spectra collected using 514 nm laser excitation. In general, FWHM values were similar for all three sample categories: 5.4–7.8  $\text{cm}^{-1}$  for the NCTCPs, 5.9–8.7  $\text{cm}^{-1}$  for the CCPs, and 6.2–8.2  $\text{cm}^{-1}$  for the DTCPs.

**Chemical Analysis.** In addition to the major element Ca, EDXRF analysis also detected a strong Sr signal in the nacre of all the cultured pearls tested. The only notable difference between the three groups of samples was that a strong Ag signal was recorded in the dyed cultured pearls. No other elements were observed with EDXRF.

Many trace elements were detected in the nacre of the cultured pearls with LA-ICP-MS, largely due to its much higher sensitivity (table 3). In the NCTCPs, relatively high concentrations of Na (5100–8200 ppm), Sr (1080–2320 ppm), K (66–410 ppm), Mg (66–274 ppm), and P (5.0–24.1 ppm) were detected. Traces of Li (0.33–0.58 ppm), B (12–24 ppm), Cr (1.5–4.5 ppm), Mn (up to 3.8 ppm), Zn (up to 18.7 ppm), Cd (up to 8.9 ppm), Ba (up to 2.9 ppm), Pb (up to 1.8 ppm), and Ag (0.01–1.8 ppm) were also detected. Other elements (again, see table 3) either were not detected or were near the detection limits for this instrument.

The composition of the CCPs was very similar to that of the NCTCPs. Concentrations of almost all elements fell in very similar ranges. One exception was the significantly lower concentration of K (average 47 ppm) in the CCPs compared to the NCTCPs (average 197 ppm). Another clear difference was the higher Pb concentrations in the CCPs (average 12.7 ppm) than in the NCTCPs (average 0.5 ppm). In before/after experiments, K concentrations in two samples (Bal-18 and Bal-19) decreased significantly after treatment. However, the opposite results were recorded in sample Aki-16. No significant variations in Pb were measured in the samples before and after treatment (table 3). In the DTCPs, elevated concentrations of Ag (1800–1870 ppm) and slightly enriched Sm (0.24–0.29 ppm); NCTCPs and CCPs had con-

**TABLE 3.** Representative composition of natural-color and “chocolate” treated Tahitian cultured pearls determined by LA-ICP-MS (ppm by weight).<sup>a</sup>

Sample no.	Li	B	Na	Mg	P	K	Cr	Mn	Zn	As	Sr	Ag	Cd	Ba	Pb
<b>Natural-Color Tahitian Cultured Pearls (NCTCPs)</b>															
Aki-04	0.42	18.55	6526	68.39	9.41	197.8	3.71	0.48	3.84	0.85	1181	0.12	0.05	0.71	0.52
Aki-05	0.44	18.57	6057	83.19	20.18	183.1	3.96	0.64	8.34	1.08	1240	0.02	0.15	2.80	0.45
Aki-06	0.36	13.79	5798	77.28	24.08	227.4	3.86	0.56	1.12	0.87	1081	0.01	0.04	0.30	0.17
Aki-07	0.37	16.93	6181	146.8	8.12	260.9	3.89	0.36	2.33	0.36	1203	0.04	8.92	0.38	1.24
Aki-08	0.35	15.61	5600	114.1	7.65	162.7	4.02	0.10	4.05	0.62	1778	0.06	0.14	0.44	0.36
Aki-14	0.35	13.83	5113	242.8	8.48	281.4	3.63	nd <sup>b</sup>	7.53	0.51	1845	0.13	1.02	0.81	0.24
Aki-15	0.45	15.83	5879	136.0	11.51	142.2	4.20	0.29	4.45	0.61	1891	0.16	0.03	0.82	0.35
Aki-16	0.34	15.88	5653	178.6	9.39	164.4	3.34	1.21	5.91	0.43	1932	0.16	0.21	0.62	0.34
Aki-17	0.35	16.31	6463	104.1	9.39	247.8	4.09	0.27	5.72	0.33	1581	0.20	0.09	0.52	0.41
Aki-18	0.46	13.02	7281	196.2	nd	314.9	2.64	0.44	5.83	0.53	1292	0.09	0.64	0.64	0.49
<b>“Chocolate” Cultured Pearls (CCPs)</b>															
Bal-24	0.35	13.78	5464	135.9	8.55	61.54	1.06	2.20	3.32	nd	1415	0.49	0.05	0.43	13.29
Bal-27	0.31	14.18	6487	115.9	13.13	44.30	4.45	6.93	3.64	0.02	1196	0.40	0.02	0.44	13.91
Bal-30	0.40	18.64	6762	82.51	10.51	58.85	4.88	1.19	5.47	nd	1473	0.19	nd	0.49	8.54
Bal-33	0.26	11.30	5487	175.5	8.51	15.14	3.61	1.00	1.77	nd	1095	0.06	0.03	0.50	11.03
Bal-36	0.26	11.01	5546	114.1	6.27	36.16	3.12	1.28	2.45	0.07	1283	0.15	0.02	0.22	8.20
Bal-37	0.31	13.18	6932	171.6	nd	21.88	5.17	1.31	6.01	0.35	1444	0.30	nd	0.60	16.02
Bal-40	0.34	8.75	5667	143.8	3.35	39.10	3.13	0.92	8.85	0.10	1514	0.20	0.00	0.92	22.25
Bal-43	0.36	14.30	5760	105.7	10.60	20.65	2.88	1.07	11.48	0.38	1106	0.27	0.00	0.38	19.62
Bal-46	0.44	14.19	6599	184.8	4.98	54.11	3.50	1.86	2.92	nd	1584	0.13	0.02	0.32	4.88
Bal-49	0.39	17.00	6177	119.8	15.85	55.89	3.39	2.66	15.99	0.00	1272	0.32	0.03	0.73	25.99
<b>Dyed Tahitian Cultured Pearls (DTCs)</b>															
Bal-07	0.46	20.11	7720	104.2	10.34	85.79	3.60	0.72	4.22	0.32	1571	1800	0.22	2.66	0.17
Bal-08	0.51	19.11	7947	123.6	9.16	86.66	3.26	0.21	6.12	0.17	1188	1870	0.07	0.51	0.18
<b>NCTCPs Before and After Treatment</b>															
Bal-16	0.45	15.66	6387	142.5	5.60	74.45	3.23	2.67	16.56	nd	1970	0.11	0.13	1.09	0.26
Bal-16 (1st)	0.46	13.35	5724	179.0	nd	45.68	3.52	2.00	2.00	0.17	2223	0.12	0.02	0.68	0.37
Bal-16 (2nd)	0.73	11.93	6009	165.2	9.03	146.1	0.10	2.90	1.81	0.16	2458	0.04	0.06	0.76	0.31
Bal-18	0.37	13.88	6335	158.5	15.08	139.6	3.36	0.76	6.37	0.02	1723	0.03	0.08	3.14	0.45
Bal-18 (1st)	0.37	13.62	5867	164.9	nd	54.06	2.69	0.39	3.07	nd	1890	0.06	0.07	0.64	0.45
Bal-18 (2nd)	0.49	16.96	5874	195.4	19.84	59.45	0.07	0.93	1.47	0.06	1908	0.02	0.00	0.62	0.36
Bal-19	0.46	17.32	6694	139.2	8.50	118.6	3.70	1.20	4.79	0.03	1455	0.01	0.06	0.34	0.31
Bal-19 (1st)	0.38	15.88	5570	137.3	nd	30.11	3.49	1.39	1.53	0.06	1433	0.04	0.03	0.67	0.26
Bal-19 (2nd)	0.50	17.12	5739	158.1	17.03	92.36	0.03	1.92	0.70	0.10	1464	0.01	nd	0.18	0.19

<sup>a</sup> Laser ablation parameters: 40 μm spot diameter, 30% (0.007 mJ) laser energy, 10 Hz repetition rate, and a 20 μm/s raster rate. NIST SRM 610 and 612 glass reference materials (Pearce et al., 1996) were used as external standards for calibration. The content of calcium throughout the nacre of all cultured pearls is nearly constant (~50 wt.% CaO), so this was employed as an internal standard in the data reduction for all samples. The following isotopes were monitored to determine elemental concentrations: <sup>7</sup>Li, <sup>9</sup>Be, <sup>11</sup>B, <sup>23</sup>Na, <sup>24</sup>Mg, <sup>31</sup>P, <sup>39</sup>K, <sup>43</sup>Ca, <sup>44</sup>Ca, <sup>45</sup>Sc, <sup>51</sup>V, <sup>52</sup>Cr, <sup>55</sup>Mn, <sup>56</sup>Fe, <sup>59</sup>Co, <sup>60</sup>Ni, <sup>65</sup>Cu, <sup>66</sup>Zn, <sup>71</sup>Ga, <sup>72</sup>Ge, <sup>75</sup>As, <sup>82</sup>Se, <sup>85</sup>Rb, <sup>88</sup>Sr, <sup>89</sup>Y, <sup>90</sup>Zr, <sup>93</sup>Nb, <sup>95</sup>Mo, <sup>107</sup>Ag, <sup>111</sup>Cd, <sup>115</sup>In, <sup>118</sup>Sn, <sup>121</sup>Sb, <sup>133</sup>Cs, <sup>137</sup>Ba, <sup>139</sup>La, <sup>140</sup>Ce, <sup>141</sup>Pr, <sup>146</sup>Nd, <sup>147</sup>Sm, <sup>153</sup>Eu, <sup>157</sup>Gd, <sup>159</sup>Tb, <sup>163</sup>Dy, <sup>165</sup>Ho, <sup>166</sup>Er, <sup>169</sup>Tm, <sup>172</sup>Yb, <sup>175</sup>Lu, <sup>178</sup>Hf, <sup>181</sup>Ta, <sup>182</sup>W, <sup>185</sup>Re, <sup>197</sup>Au, <sup>205</sup>Tl, <sup>208</sup>Pb, <sup>209</sup>Bi, <sup>232</sup>Th, and <sup>238</sup>U. Those isotopes marked in boldface roman type were not included in this table, as their concentrations were either below or near the instrumental detection limits.

<sup>b</sup> nd = not detected.

centrations up to 0.05 ppm) were measured, while concentrations of other elements remained similar to those recorded for the untreated samples.

## DISCUSSION

Pearl nacre consists of overlapping platelets of crystalline calcium carbonate (CaCO<sub>3</sub>) in the form of aragonite, with the principal crystal axes of these platy crystals oriented at right angles to the surface. Various organic components occur between the aragonite platelets, producing a range of pearl colors (e.g., Kiefert et al., 2004; Strack, 2006).

Raman spectroscopy is a very effective technique for mineral identification, and in general Raman peaks are much sharper than overly strong photoluminescence bands. In aragonite, the most intense Raman peak occurs near 1085 cm<sup>-1</sup>. Also in aragonite, a doublet may be observed at ~705 and ~701 cm<sup>-1</sup>, whereas in calcite, the other common polymorph of CaCO<sub>3</sub>, only a single band at ~711 cm<sup>-1</sup> occurs (Urmos et al., 1991). Raman spectroscopic analysis of the untreated and treated Tahitian cultured pearls confirmed that aragonite is the only carbonate mineral component present in our samples (figure 13). As expected, no evidence for

calcite (i.e.,  $711\text{ cm}^{-1}$  peak) was observed in the Raman spectra of the natural-color, “chocolate” treated, or dyed Tahitian cultured pearls.

Other Raman features are attributed to various types of organic components, such as conchiolin and porphyrin (Goebel and Dirlam, 1989; Liu, 2003; Huang, 2006). The intensities of these organic component bands varied significantly among the NCTCPs, but they clearly increased with the tone of the cultured pearl colors (not shown in figure 13). After the first stage of treatment, the intensity of Raman peaks due to organic components decreased, especially below  $1500\text{ cm}^{-1}$ ; the peaks were even weaker after the treatment was completed (again, see figure 13).

For the most part, the Raman peak intensities of aragonite in the CCPs were comparable to those of the natural-color samples (figure 13). While many CCPs showed relatively weak organic peaks in the region of  $1700\text{--}1300\text{ cm}^{-1}$ , a few samples like Bal-03 showed strong peaks (not shown). The weaker Raman scattering peaks for organic components in most of the CCPs, and the decreased intensity of these peaks in the four NCTCPs treated for this study, strongly indicate that the treatment mainly involves modifying the organic components between aragonite platelets (see figure 3).

In the DTCPs, we could not detect organic-related components and other Raman peak intensities were much weaker than in the NCTCPs and CCPs. Furthermore, the dyed cultured pearls did not show Raman peaks in the region  $300\text{--}100\text{ cm}^{-1}$ , but they did have a broad band centered at  $\sim 141\text{ cm}^{-1}$ . A Raman band at  $240\text{ cm}^{-1}$  previously reported in dyed cultured pearls by Kiefert et al. (2001) was observed in one sample (Bal-08), with 633 nm laser excitation only.

Infrared reflectance spectroscopy showed more complicated results. Most absorption features were consistent with aragonite, in particular the occurrence of the  $1084\text{ cm}^{-1}$  peak, which is unique to aragonite. However, the  $878\text{ cm}^{-1}$  band, which was consistently observed in all the untreated Tahitian cultured pearls, matched the peak position of calcite well. In aragonite, the same peak usually occurs at higher wavenumbers than  $860\text{ cm}^{-1}$  (Weir and Lippincott, 1961; Adler and Kerr, 1962; Frech et al., 1980). We believe this peak is not related to calcite (as shown by the lack of calcite in the Raman spectra), so the cause of this relatively strong absorption at  $878\text{ cm}^{-1}$  remains unclear. Our spectroscopic analysis revealed nearly identical Raman and infrared

absorption features (figures 6, 7, and 13) for the aragonite peaks in both the untreated and “chocolate” Tahitian cultured pearls, indicating that the aragonite platelets in Tahitian cultured pearls remained basically unchanged during the “chocolate” treatment.

The vast majority of the NCTCPs showed weak yellow, orange, or greenish yellow fluorescence to long-wave UV. In contrast, the CCPs typically displayed characteristic reddish orange fluorescence. This difference in fluorescence was confirmed by the four cultured pearls processed for this study. The causes of the variation in fluorescence color are not clear; this may be attributed to modification of organic components or defects in the constitutional aragonite.

The dyeing of pearls with silver salts to turn them black has been practiced for many decades. First, the pearls are immersed in a silver nitrate solution ( $\text{AgNO}_3$ ) for a period of time in a dark environment, and then they are exposed to a strong light source or are treated with hydrogen sulfate. The Ag-dyeing process leads to the deposition of AgO as extremely fine particles (Strack, 2006). These particles both strongly absorb visible light (inducing the dark brown coloration) and effectively block fluorescence, which is why no fluorescence could be detected in the DTCPs.

A relatively flat baseline in the UV-Vis-NIR reflectance spectra of the NCTCPs—with broad absorption bands at  $\sim 407$ ,  $497\text{--}500$ , and  $650\text{--}694\text{ nm}$ —is consistent with the observed gray or brown colorations (again, see figure 8). The absorption band at  $\sim 283\text{ nm}$  is derived from protein contained in conchiolin, a common feature of all cultured pearls (see, e.g., Iwahashi and Akamatsu, 1994). The absorption bands at  $\sim 407$  and  $497\text{--}500\text{ nm}$  are derived from porphyrin pigment. The  $\sim 407\text{ nm}$  absorption is called the “Solet band,” which is common to all porphyrins (see, e.g., Iwahashi and Akamatsu, 1994). Depending on the fine structure of the porphyrin, this band can occur anywhere from  $390$  to  $425\text{ nm}$  (Britton, 1983). The  $\sim 650\text{--}694\text{ nm}$  absorption band is derived from black pigment in cultured pearls. In addition, there are spectroscopic variations among geographic sources of “black” cultured pearls. For example, the  $661\text{--}694\text{ nm}$  band, which we observed consistently in our Tahitian cultured pearls, was not reported in Mexican cultured pearls (Kiefert et al., 2004), even though they showed very similar coloration. The presence of these bands provides a good indication for substantial quantities of organic components.

Our analysis of a large number of CCPs revealed that the baseline of their UV-Vis-NIR reflectance spectra consistently increased in general absorption toward lower wavelengths (higher energies; figure 9). This absorption increased over the whole region of visible light, resulting in the intense brown coloration. A decrease in intensity (or virtual absence) of these three absorption bands in the 300–700 nm region after treatment, as observed in the CCPs and the four cultured pearls treated for this study (figures 9 and 11), also indicates that the organic components are dramatically modified. Observation of such modified spectra provide good evidence for bleaching during the treatment.

Pearl formation is mainly a process of deposition of aragonite by mollusks. Tahitian cultured pearls, like all of the samples in this study, form in seawater, which contains minor or trace amounts of various elements. Since the geochemical properties of strontium are very similar to those of calcium, it is common for pearls to contain relatively high amounts of Sr (see table 3). Seawater also contains significant amounts of sodium and potassium; their presence in the cultured pearls was well reflected in the compositions we measured with LA-ICP-MS. However, little information is available regarding the incorporation of Na and K in pearls. While Na and K may partially enter the aragonite lattice, these elements also may be enriched at the interfaces between aragonite platelets. It is interesting to note that the untreated NCTCPs also contained traces of Ag (up to 1.8 ppm by LA-ICP-MS analysis, but not detectable by EDXRF). However, much higher concentrations of Ag are needed to induce any observable coloration, as in the Ag-dyed cultured pearls.

LA-ICP-MS analysis of NCTCPs and CCPs (table 3) revealed that both groups had very similar compositions, except for less potassium and relatively higher concentrations of lead in the CCPs. A decrease in K concentration was correlated with some samples treated in this study (table 3), but contradictory results were also observed. In addition, the samples analyzed before and after treatment did not show any detectable variation in Pb concentrations. When not locked into a crystal lattice, K can be a very mobile element (Albarede and Hofmann, 2003). The lower abundance of K in the CCPs strongly indicated that most of the K in the NCTCPs is located at the interfaces between aragonite platelets and can be partially removed in the treatment. Nevertheless, the differences in K and Pb concentrations between NCTCPs

and CCPs were not confirmed in the before/after treatments. The causes for these inconsistencies are not clear. On the basis of these data and observations, it is reasonable to believe that color changes caused by the “chocolate” treatment are mainly related to the reorganization of organic pigments that are present between the aragonite platelets, without the introduction of a foreign coloring agent. The chemical data suggest that the treatment did not add any chemical elements and, therefore, is fundamentally different from the Ag-dyeing treatment.

## IDENTIFICATION

Identification of Ballerina-treated “chocolate” cultured pearls requires a combination of gemological observation, spectroscopic analysis, and trace-element composition. Natural-color cultured pearls rarely show intense brown coloration without a distinct orient or rosé overtone (Scarratt, 1984). Suspicion should be raised for samples that show pronounced “chocolate” coloration.

Most (157 of 160 samples) of the Ballerina CCPs we studied showed a weak-to-moderate reddish orange fluorescence to long-wave UV radiation. The remaining three samples showed greenish yellow fluorescence to long-wave UV, which is similar to the reaction of many untreated Tahitian cultured pearls. Consequently, reddish orange fluorescence to long-wave UV is a useful indication of treatment, but caution must be exercised since there are exceptions. While DTCPs and CCPs can have a similar color appearance, DTCPs are usually inert to both long- and short-wave UV radiation.

Spectroscopic and chemical analyses supply information that is essential for identification. The high concentrations of Ag in dyed cultured pearls can be detected easily with either EDXRF or LA-ICP-MS. Relatively low concentrations of K and elevated contents of Pb, combined with a concentration of Ag consistent with NCTCPs (i.e., <2 ppm) may provide indications of this type of “chocolate” treatment. UV-Vis-NIR reflectance spectroscopy is also very useful due to the systematic differences between NCTCPs, CCPs, and DTCPs. An important feature of the reflectance spectra of brown NCTCPs is that the baseline is nearly flat, similar to that seen with gray NCTCPs. However, the baselines of all the CCPs we examined always increased in general absorption toward the low-wavelength (high-energy) side of the spectra. Untreated cultured pearls from Mexico and South America may show a

similar reaction to long-wave UV as CCPs (Kiefert et al., 2004); however, we may expect quite different reflectance spectra in the UV-Vis-NIR range. In addition, very weak or no absorptions at ~407, 497–500, and 650–694 nm provide good evidence of bleaching treatment. Strong photoluminescence with peaks at ~620 nm and ~725 nm relative to Raman peaks from aragonite is a good indication of bleaching treatment, but it is not conclusive.

## CONCLUSION

In addition to the well-known Ag-dyeing method, brown “chocolate”-colored cultured pearls can be produced using a newly developed bleaching treatment. This method is able to turn black cultured pearls from Tahiti (and very likely other sources) with less attractive or non-uniform colors into those with uniform and pleasing brown colors, and potentially increase their market value. No chemical evidence of foreign coloring agents was detected following Ballerina’s bleaching process. Treated brown cultured pearls, either bleached or dyed, can be identified based on a combination of their gemological properties, chemical composition, and spectroscopic features.

It is important to note that treated cultured pearls with similar “chocolate” colors are also present in the market from sources other than Ballerina Pearl Co. (figure 14). Since the treatment process is proprietary, and the starting materials may come from various sources, there is no guarantee that “chocolate pearls” from other companies will show analogous results.



Figure 14. The “chocolate pearls” now in the marketplace are being produced by a number of different companies. These attractive cultured pearls range from 11.0 to 15.7 mm. Courtesy of Emiko Pearls International; photo by Robert Weldon.

### ABOUT THE AUTHORS

Dr. Wang (wuyi.wang@gia.edu) is a research scientist, Ms. Hyatt is a staff gemologist, and Mr. Hall is manager of analytical research services, at the GIA Laboratory, New York. Mr. Scarratt is director of GIA Research (Thailand) in Bangkok. Dr. Shen is a research scientist at the GIA Laboratory, Carlsbad.

### ACKNOWLEDGMENTS

The authors are grateful to Abe Auerbach of the Ballerina Pearl Co. in New York, as well as Emiko Pearls International in

Seattle, for supplying treated cultured pearl samples for examination. Special thanks to Tom Moses of the GIA Laboratory (New York) for many fruitful discussions and Dr. Christopher Breeding of the GIA Laboratory (Carlsbad) for help in this study. The authors are also grateful to Shigeru Akamatsu of Mikimoto & Co. (Tokyo), Dr. Henry Hänni of the SSEF Swiss Gemmological Laboratory (Basel), and Dr. Lore Kiefert of the AGTA Gemological Testing Center (New York) for their constructive comments and suggestions, which helped improve this article significantly.

## REFERENCES

- Adler H.H., Kerr P.F. (1962) Infrared study of aragonite and calcite. *American Mineralogist*, Vol. 47, pp. 700–717.
- Albarede F., Hofmann A.W. (2003) *Geochemistry: An Introduction*. Cambridge University Press, Cambridge.
- Better techniques improve brown pearls (2006) *Jewellery News Asia*, No. 262, p. 60.
- Britton G. (1983) *The Biochemistry of Natural Pigments*. Cambridge University Press, Cambridge.
- Frech R., Wang E.C., Bates J.B. (1980) The IR and Raman spectra of CaCO<sub>3</sub> (aragonite). *Spectrochimica Acta*, Vol. 36A, pp. 915–919.
- Gemological Institute of America (2000) GIA Pearl Grading Color Reference Charts. Carlsbad, CA.
- GIA identifies three types of brown pearls (2006) *Jewellery News Asia*, No. 265, p. 80.
- Goebel M., Dirlam D.M. (1989) Polynesian black pearls. *Gems & Gemology*, Vol. 25, No. 3, pp.130–148.
- Huang Y.L. (2006) Visible absorption spectrum representation of Tahitian black pearls and treated pearls. *Journal of Gems and Gemmology*, Vol. 8, No. 1, pp. 5–8.
- Iwahashi Y., Akamatsu S. (1994) Porphyrin pigment in black-lip pearls and its application to pearl identification. *Fisheries Science*, Vol. 60, No. 1, pp. 69–71.
- Kiefert L., Hänni H.A., Ostertag T. (2001) Raman spectroscopic applications to gemmology. In I.R. Lewis and H.G.M. Edwards, Eds., *Handbook of Raman Spectroscopy*, Marcel Dekker, New York, pp. 469–489.
- Kiefert L., Moreno D.M., Arizmendi E., Hänni H.A., Elen S. (2004) Cultured pearls from the Gulf of California, Mexico. *Gems & Gemology*, Vol. 40, No. 1, pp. 26–39.
- Liu W.D. (2003) Characteristics of Tahitian black pearls and their application in identification. *Journal of Gems and Gemmology*, Vol. 5, No. 1, pp. 1–4.
- Pearce N.J.G., Perkins W.T., Westgate J.A., Gorton M.P., Jackson S.E., Neal C.R., Chenery S.P. (1996) Application of new and published major and trace elements data for NIST SRM 610 and NIST SRM 612 glass reference materials. *Geostandards Newsletter*, Vol. 20, No. 2, pp. 115–144.
- Sanchez L. (2004) Trade raises questions about chocolate pearls. *Jewellery News Asia*, No. 241, pp. 160, 162.
- Strack E. (2006) *Pearls*. Ruhle-Diebener-Verlag, Baden-Baden, Germany.
- Study shows chocolate pearls are “stained” (2006) *Jewellery News Asia*, No. 265, p. 78.
- Urmos J., Sharma S.K., Mackenzie F.T. (1991) Characterization of some biogenic carbonates with Raman spectroscopy. *American Mineralogist*, Vol. 76, No. 3–4, pp. 641–646.
- U.S. gem labs seek to uncover the process behind brown pearls (2004) *Jewellery News Asia*, No. 241, p. 162.
- Weir C.E., Lippincott E.R. (1961) Infrared studies of aragonite, calcite, and vaterite type structure in the borates, carbonates, and nitrates. *Journal of Research of the National Bureau of Standards A. Physics and Chemistry*, Vol. 65, pp. 173–183.
- Zachovay M. (2005) Gem News International: “Chocolate” Tahitian cultured pearls. *Gems & Gemology*, Vol. 41, No. 2, pp. 183–184.

## Thank You Reviewers

GEMS & GEMOLOGY requires that all articles undergo a peer review process in which each manuscript is evaluated by at least three experts in the field. This process is vital to the accuracy and readability of the published article, but it is also time consuming for the reviewer. Because members of our Editorial Review Board cannot have expertise in every area, we sometimes call on other experts to share their intellect and insight. In addition to the members of our Editorial Review Board, we extend a heartfelt thanks to the following individuals who reviewed manuscripts for *G&G* in 2006.

Mr. Charles Carmona  
Dr. Richard Grigg  
Mr. Matthew Hall  
Mr. Hertz Hasenfeld  
Dr. Frank Hawthorne

Mr. John King  
Ms. Elise Misorowski  
Dr. Andrew Rankin  
Dr. Ilene Reinitz  
Dr. Karl Schmetzer

Dr. Dietmar Schwarz  
Mr. George Solario  
Dr. Jennifer Stone-Sundberg  
Dr. Wuyi Wang

# LEOPARD OPAL: PLAY-OF-COLOR OPAL IN VESICULAR BASALT FROM ZIMAPÁN, HIDALGO STATE, MEXICO

Robert Raymond Coenraads and Alfonso Rosas Zenil

“Leopard opal” consists of vesicular basalt impregnated with play-of-color opal, and is known only from Zimapán, Hidalgo State, Mexico. The formation of this ornamental stone was made possible by an abundance of silica derived from the chemical breakdown of overlying volcanic ash layers, the permeability of the underlying basalt, and the presence of pores in the basalt of an aesthetically pleasing size. The even distribution and small size of the opal-filled vesicles makes the rock attractive when cut or carved and polished. Veinlets and irregular masses of play-of-color opal showing various bodycolors (red, white, and colorless to pale blue) have also been deposited along joints and fractures within the basalt flow. This opal deposit, which may have been worked in pre-Columbian times, has been explored only by a number of small test pits in recent years, and significant potential remains for its future development.

One of the authors (ARZ) spent much of his youth as a *gambusino*, or prospector, exploring remote areas of the Mexican countryside on horseback. In 1965, while investigating some bushes where a fox was hiding, he noticed flashes of color in a lump of vesicular basalt that proved to contain opal. Further prospecting led to the discovery of the deposit itself higher on the hillside. However, it is possible he had only rediscovered it, as an old shallow trench suggested that the deposit could have been worked for opal much earlier, perhaps by pre-Columbian inhabitants of the region. (There are no records of opal having been found in this area by the Spaniards, nor are the authors aware of any recent opal mining other than that of ARZ.) Shortly thereafter (in 1965), ARZ staked the mining claims that are known today as Gemma and Desiré.

Because of the striking spotted appearance of the opal against its black basaltic host, this unique material became known as “Leopard opal.” Word spread, and soon the material attracted the attention of an American, Foster Conton, who visited the prospect and returned to the U.S. with a 6 kg sample given to him by ARZ. He gave the specimen to Albert Eugene

Upton, who after months of research and study decided to have the stone carved into an art piece that would have historical significance for Mexico: a likeness of Cuauhtémoc, the last emperor of the Aztecs (figure 1). Artisan Rafael Tapia of Taxco, Mexico, was commissioned to undertake the carving, which took seven months to complete and had a final weight of 3.375 kg. The silver headdress and mounting were made by Alejandro Gómez. The complete statue stands approximately 48 cm high and weighs a total of 8.2 kg (E. Littig, pers. comm., 1999). Photos of this carving were published in *Lapidary Journal* (Leipner, 1969), which also advertised rough and cabochon-cut pieces of “black matrix opal” from this deposit. In 1970, Mr. Upton donated the carving to Sacred Heart College (now Newman University), in Wichita, Kansas. Apart from some samples cut and polished locally in Mexico or by foreign lapidaries over the years (e.g., figure 2), and an

---

See end of article for About the Authors and Acknowledgments.  
GEMS & GEMOLOGY, Vol. 42, No. 4, pp. 236–246.  
© 2006 Gemological Institute of America



*Figure 1. Leopard opal, vesicular basalt impregnated with play-of-color opal, can be polished into cabochons for use in jewelry or employed as a carving material. This bust (3.375 kg) shows the likeness of Cuauhtémoc, the last emperor of the Aztecs. The carving is by Rafael Tapia, and the silver work is by Alejandro Gómez; it is part of the Newman University collection in Wichita, Kansas. Photo by Charles Rasico, courtesy of Newman University.*

appearance of the material at the 1996 Tucson gem shows (Johnson and Koivula, 1996), there has been little public exposure of Leopard opal, and the deposit has lain in relative obscurity for the last several years.

This is the only known opal deposit in the Zimapán area. The historical significance and geologic setting of the site, as well as the small-scale mining activities carried on there, have not been

described previously in the literature. To date it has been explored only by a number of small test pits, but the authors believe significant potential remains for its future development.

**A History of Mexican Opal.** Long before its rediscovery in modern times, opal was mined and appreciated as a gem material by the pre-Columbian

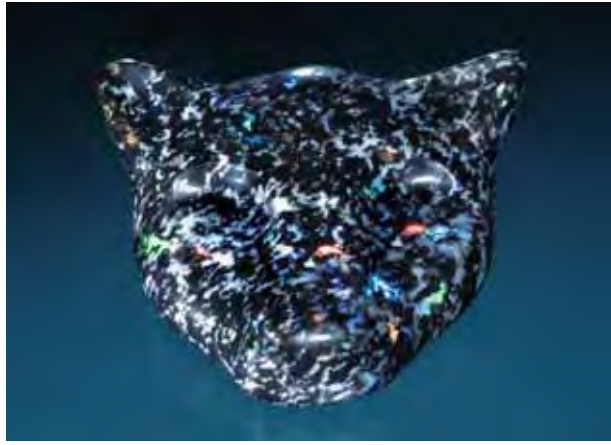


Figure 2. This pre-classical-style jaguar head ( $44.76 \times 42.45 \times 11.30$  mm) carved from Leopard opal was fashioned by Kevin Lane Smith of Tucson, Arizona. Photo by Maha Calderon.

peoples of Mexico and Central America. There are two terms in Nahuatl, the Aztec language, that are used to describe opal: *quetza litzle pyolitli*, meaning “stone which changes color in movement” (or “bird of paradise stone”) and *huitzitziltepatl*, “stone like a bird of a thousand colors” (or “hummingbird

stone”). Some of these Mexican opals were taken to Europe and the present United States by the Spaniards in the early 16th century (White, 1998). The Spanish monarchy, however, had more of an interest in finding Mexican gold, and opal is not mentioned on the invoices of precious objects sent by the Spanish *conquistador* Hernán Cortés to Charles V of Spain during this period (Leechman, 1961).

Eventually, many of the pre-Columbian opal mines were closed and their locations lost. It is interesting to note that Zimapán is indicated as the source of many old opal specimens in museums around the world (see, e.g., Leechman, 1961; Heylmun, 1984b). One such example is a ring containing a “fire opal of Zimapán” (Ball, 1931) worn by Antonio Eusebio de Cubero in a 17th century portrait by Diego Velázquez.

In the mid-1800s, the opal deposits in the state of Querétaro were rediscovered (see, e.g., Koivula et al., 1983). Numerous small open-cut mines began operating in the district (Heylmun, 1983a), and the capital, Querétaro City, became Mexico’s most important cutting and polishing center (Webster,

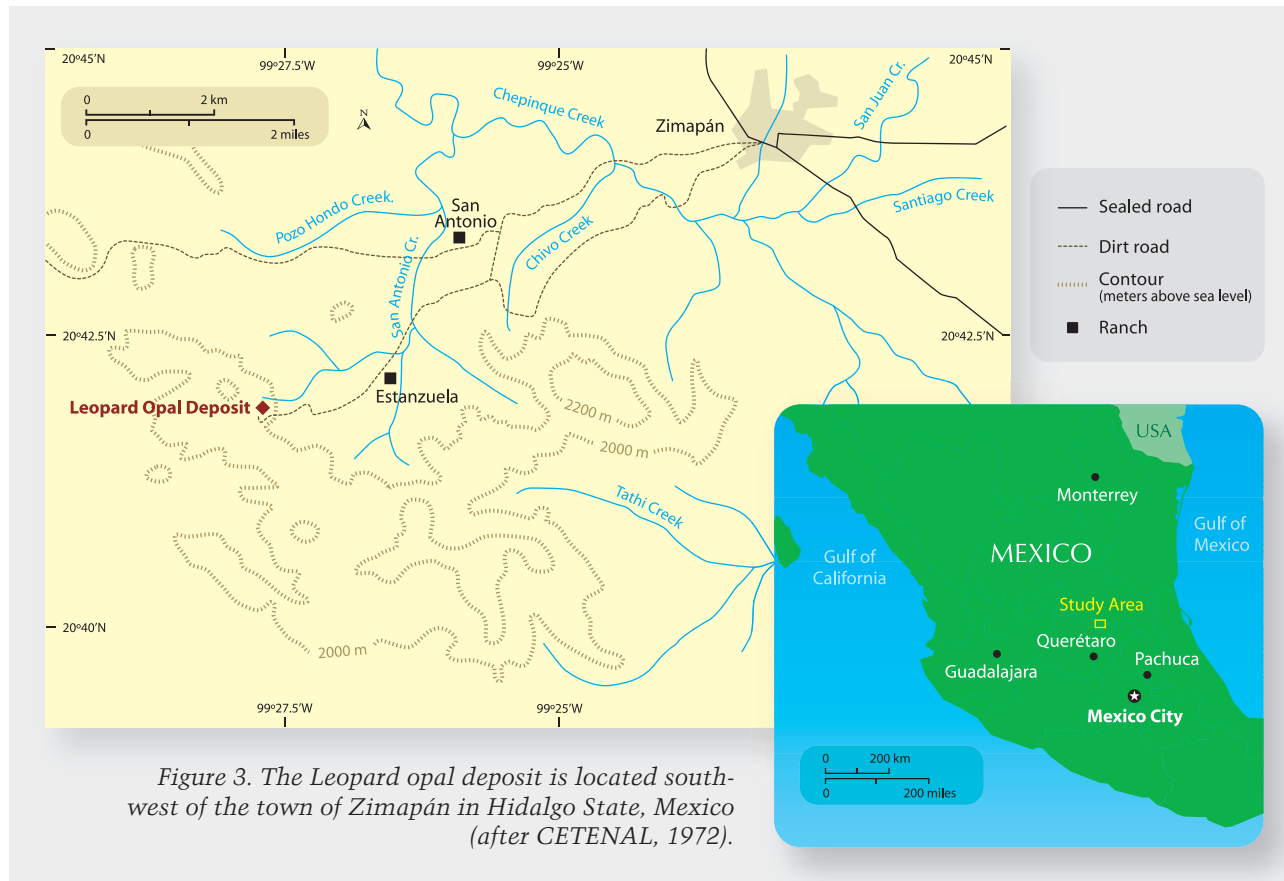


Figure 3. The Leopard opal deposit is located southwest of the town of Zimapán in Hidalgo State, Mexico (after CETENAL, 1972).

1983). The region has made Mexico famous for its fire opal, an orange-red (fiery) opal that often displays play-of-color. Most Mexican fire opal is open-pit mined from hard pink-to-red Cenozoic rhyolite using labor-intensive hand methods (see, e.g., Mallory, 1969a,b; Zeitner, 1979).

In the last 150 years, opal has been found throughout Mexico's Central Volcanic Belt (Heylman, 1984a) in the states of Querétaro, Hidalgo, Guanajuato, San Luis Potosí, Guerrero, Michoacán, Jalisco, and Nayarit. Detailed locality maps and descriptions of the mines were published in a series of articles by Heylman (1983a,b,c). The wide variety of opal types found in Mexico and their local nomenclature are described by Heylman (1984a).

Other Mexican opals, in addition to fire opals, show play-of-color, and some of these are legendary among early Mexican production. The Aztec Sun God opal, a  $36 \times 34 \times 15$  mm, 94.78 ct stone, is believed to originate from Mexico; it has a transparent pale blue bodycolor and displays blue, green, yellow, and red play-of-color (White, 1998). This opal is carved into an image of the sun with a human face. Another notable opal, *El Águila Azteca* (The Aztec Eagle), was discovered in an excavation in Mexico City around 1863 and is believed to have been part of the treasures of the Aztec ruler Moctezuma II (1502–1520). This 32 ct eagle's head was said to "exhibit an infinite series of prismatic colors from a pale lavender to deep ruby red" (White, 1998, p. 46); its present whereabouts are unknown.

## LOCATION

The Leopard opal deposit is located 14 km southwest of the town of Zimapán in Hidalgo State at  $20^{\circ}41.8' \text{ N}$ ,  $99^{\circ}27.7' \text{ W}$  (figure 3). The site is not open to the public, and permission to visit must be obtained from the second author (ARZ). The mine is accessed by a rough dirt track that winds its way to the base of *La Piedra Grande* (The Big Rock, or *Tandhé* in the local Otomhé language), a peak that forms part of a NW-SE trending range. The last kilometer of the track must be negotiated using a 4-wheel drive vehicle or on foot. The mine is located at an elevation of about 2000 m, at a break in slope caused by a change in rock type (figures 4 and 5). A number of small pits and trenches that have produced opal-bearing material may be seen here lying in a trend that follows the geologic contact (figure 6).



Figure 4. The Leopard opal workings are located at 2000 m on a ridge that projects eastward from the side of the peak known as La Piedra Grande or Tandhé (right, background). The workings (yellow arrow) are located along the contact between the softer white tuffs and breccias above and the harder dark vesicular basalts below. The road leading to the mine can be seen as a light line on the darker unit. Photo by R. Coenraads.

## GEOLOGIC SETTING

The geology of the region around Zimapán was described by Carrillo and Suter (1982). The opal deposit is hosted by a sequence of undifferentiated Tertiary-Quaternary age volcanic rocks. On the northeastern slopes of the range (again, see figures 4 and 5), the lower portion of the sequence consists of intercalated lava flows, the most dominant being a massive red-brown quartz porphyry that is clearly visible in the field as a cliff-forming unit. Above these lava flows, and extending to the top of the range, is a series of light-colored units ranging from fine ash-fall tuffs and breccias to layers of pyroclastic blocks (solid rocks blown out of an erupting volcano) up to 50 cm across. The entire volcanic sequence has been tilted about  $20^{\circ}$  southwest and has been offset locally by faulting.

At the mine site, a discontinuous unit of vesicular basalt is found along the contact between the lava flows and overlying pyroclastic layers (again, see figure 5). Vesicular basalt forms when water vapor and gases such as carbon dioxide cannot escape quickly enough from the cooling lava, thus leaving open cavities, or vesicles. The basalt erupted as a lava flow that probably filled a small valley. The vesicles are typically stretched into cylindrical shapes, formed as the hardening (but still plastic) lava continued to flow downhill. There are more

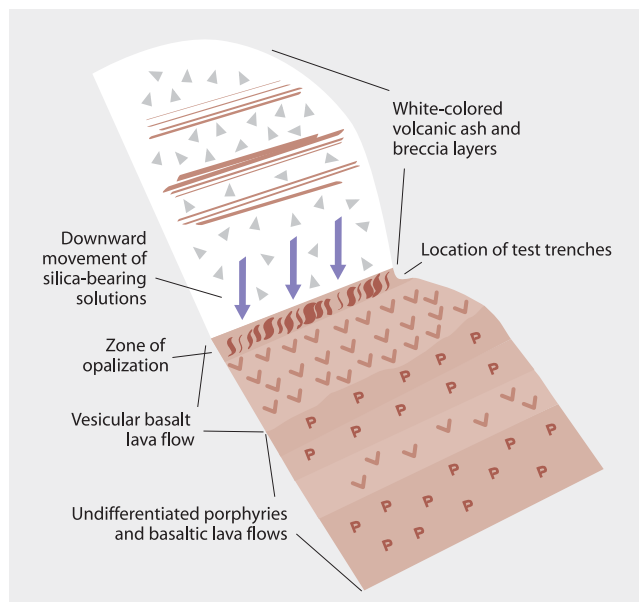


Figure 5. The zone of opalization occurs within the top few meters of a vesicular basalt that is overlain by ash and breccia layers, as seen in the cross-section on the left. The entire sequence dips about 20° southwest. In the photo on the right, looking across the valley to the north of the exploration area, the contact between the well-bedded, whitish volcanic tuffs and breccias, and the underlying darker, featureless basalts is clearly visible. The bedding and the contact are folded and displaced by faulting (visible as diagonal lines). Photo by R. Coenraads.

gas bubbles toward the top of the lava flow because the gases that slowly rose through the still-molten interior remained trapped below the hardened upper skin. Here, the vesicles are sufficiently numerous that the rock has become quite porous and permeable to groundwater. The basalt was, in turn, overlain by ash-fall tuff and breccia units deposited during a series of explosive volcanic eruptions. The ash-fall units are also very porous, and the feldspar and silica glass-rich portions have largely weathered to clay. The presence of abundant cryptocrystalline silica films coating the surfaces of faults and fractures in the lower units suggests that the reaction associated with this weathering process liberated significant quantities of silica, which migrated downward and precipitated into any available open space.

The elongated vesicles or gas cavities in the basalt are filled with transparent colorless opal to semi-opaque opal of various bodycolors ranging from white to pink or pale blue. In some hand specimens, the different bodycolors appear to run in parallel bands or patches (figure 7). The opal displays play-of-color ranging from red to violet.

Together with the vesicle-filling opal, two distinct generations of play-of-color opal are also found filling fractures in the basalt. These are a translucent reddish orange opal (figure 8) typical of the fire opal for which Mexico is renowned, and a

colorless, transparent to pale blue translucent variety similar to the opal found in the basalt vesicles.

## EXPLORATION AND MINING

Since 1965, occasional activities by one of the authors (ARZ) and his family have left several small shallow exploration and mining pits spread out along the geologic contact for a distance of several hundred meters. The section of the old trench found by ARZ, and thought by the authors to be pre-Columbian workings (again, see figure 6, right), also follows the contact. The excavations by ARZ show that opal has permeated the top of the basalt flow, but with a patchy and discontinuous distribution parallel to the contact. Exposures in the pit shown in figure 6, left, reveal that the concentration of opal in vesicles and along fractures is highest at the upper surface of the basalt, which is in direct contact with the overlying tuffs. The concentration of opal falls off rapidly within several meters. At greater distances from the contact, the basalt vesicles are empty. Approximately 1,500 kg of Leopard opal have been removed from these excavations using simple hand-mining techniques, and almost all of this production has been sold in the U.S. The 6 kg piece used for the Cuauhtémoc carving (again, see figure 1) is the largest found to date. Most pieces recovered weigh less than 1 kg.

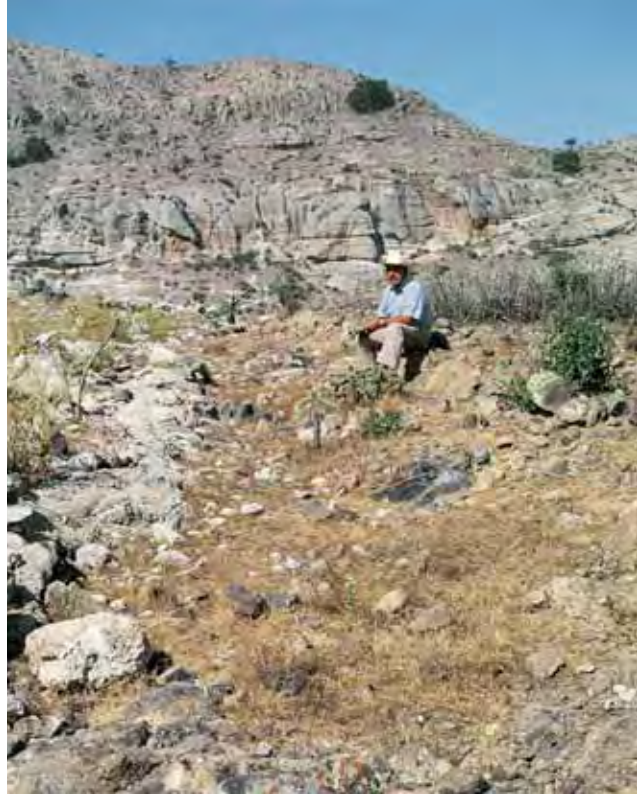


Figure 6. At left, one of a series of mining pits and trenches is located along the contact between the white tuffs and the vesicular basalt. The top of the black basalt lava flow has been exposed, with the hollows and depressions of its surface still filled by white tuff. The opal is concentrated in the vesicles and fractures in the top of this basalt flow. In the photo on the right, the surface expression of the contact between the white tuff (left) and the darker basalt (right) is clearly visible, and a shallow depression can be seen running along the contact. This trench may represent pre-Columbian workings of this opal deposit, as the types of opal recovered here are consistent with those used in pre-Columbian pieces. Photos by R. Coenraads.

The fire opal and pale blue opal is found in thin veins (again, see figure 8) crisscrossing the deposit. The veins thicken in places up to about 2 cm, but the opal tends to fragment into small pieces when dug out. Most is milky and sun-damaged, but it recovers its original appearance and play-of-color when wet. To date, there has been no exploration for this vein opal at depth, where unweathered material may exist. It is possible that this was the type of opal being sought in the pre-Columbian workings, as it closely matches descriptions of the above-mentioned historic pieces, and it is the only known locality of such material in the Zimapán area.

More extensive exploration and deeper mining of the geologic contact in the vicinity of the earlier workings could yield good quantities of opal. The geologic contact also needs to be followed along strike, beyond the known area of opal occurrence, where it may have the potential to produce similar opal-bearing material on adjacent hillsides.

Figure 7. This sample of vesicular basalt (15 cm) was collected near the contact of the lava flow and overlying tuffs and breccias. Most of the vesicles in this sample are filled with transparent-to-translucent opal, and a distinct zonation in opal bodycolor is visible. Photo by R. Coenraads.



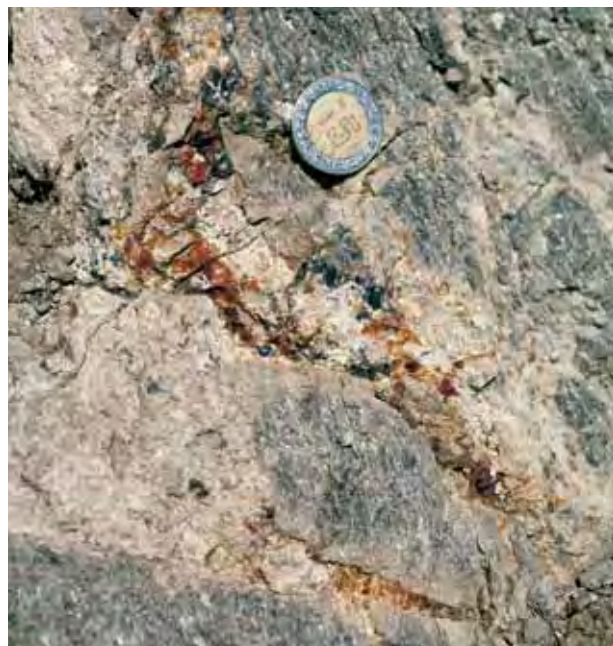


Figure 8. Translucent opal displaying an orange-red bodycolor (fire opal) fills cracks and fractures in the vesicular basalt near the contact. The opal appears to have deposited at the narrowing ends of fractures; some of it shows play-of-color. A Mexican coin (2.5 cm) is provided for scale. Photo by R. Coenraads.

Figure 9. Samples of opal from Zimapán used for this study include a 205 ct polished sample (top), a 100 ct polished sample (center), and a 6.87 ct cabochon (center left) of Leopard opal; 9 g of fire opal (bottom right); and 5 g of colorless to pale blue opal (bottom left). Photo by R. Coenraads.



## MATERIALS AND METHODS

About 2 kg of Leopard opal and chips of opal from the veins were collected by the authors for study. The material, shown in figure 9, includes 9 g of reddish orange fire opal, 5 g of colorless to pale blue opal, and a 6.87 ct cabochon from the personal collection of ARZ. Prior to gemological testing, flat faces were polished on several of the vein opal chips, and two pieces of the rough Leopard opal were ground smooth and polished on one side, yielding final weights of 205 ct and 100 ct. These two Leopard opal samples were prepared according to the guidelines recommended for this porous material (Leipner, 1969). The material was soaked in water prior to slabbing, sawn using a water-soluble mixture (i.e., not oil), and was polished with darker polishes rather than light-colored polishes that are difficult to remove from the pores. Excessive wheel speed and pressure were avoided, as these can generate heat that might damage the opal. The 6.87 ct cabochon showed minor undercutting of the opal spots, since opal, with a Mohs hardness of slightly less than 6, is softer than the feldspar of the basalt matrix, which has a hardness of 6–6.5. Specimens with a more careful sample preparation showed no variation in surface relief.

All samples were examined with a 45× binocular microscope and viewed in a darkened room with a Raytech short- and long-wave UV lamp. Spot refractive index (R.I.) readings were conducted using a Topcon refractometer, and specific gravity (S.G.) was determined for opal pieces without matrix using an Oertling R42 hydrostatic balance. A standard thin section (0.03 mm) of the Leopard opal was cut at New South Wales University in Sydney for study with a polarizing petrologic microscope.

Small pieces of fire opal and colorless “crystal” opal from veins within the Leopard opal deposit, both exhibiting good play-of-color, were crushed for X-ray diffraction (XRD) analysis at the Australian Museum laboratory in Sydney, and the results were compared to standard scans by Diffraction Technology, Canberra, Australia. Other samples from the veins were etched in hydrofluoric acid vapor for times varying between 90 seconds and several minutes to reveal their internal structure, gold coated, and then imaged using the scanning electron microscope (SEM) at the University of Technology, Sydney.

## RESULTS

In hand specimens, the black basalt takes a high polish, thereby providing a good background for the

“leopard spots” of play-of-color opal. The loupe and binocular microscope provide conclusive identification of the material. In figure 10, the 205 ct sample shows a distinct elongation and orientation of its opal-filled vesicles, and also a marked opal bodycolor or zonation from blue to white, similar to that visible in some of the rough hand specimens (again, see figure 7). Figure 11 shows several views of the vesicles of the 100 ct sample; these are filled with transparent opal displaying play-of-color domains that are continuous over several vesicles. Detailed examination (figure 11, center) revealed that the vesicles are highly irregular in shape. Although some have remained empty (see the bottom right corner of the photo), most appear connected to one another by channels along which the silica-bearing fluids could migrate. The inside walls of the vesicles are white, which suggests that a thin coating of another mineral was deposited before the vesicles were filled with opal (again, see figure 11). At higher magnification (figure 11, right), long thin colorless feldspar crystals are visible in the dark basalt matrix.

The thin section (figure 12) revealed that the basalt in this specimen is unweathered and consists of abundant microscopic (0.1–0.2 mm) euhedral

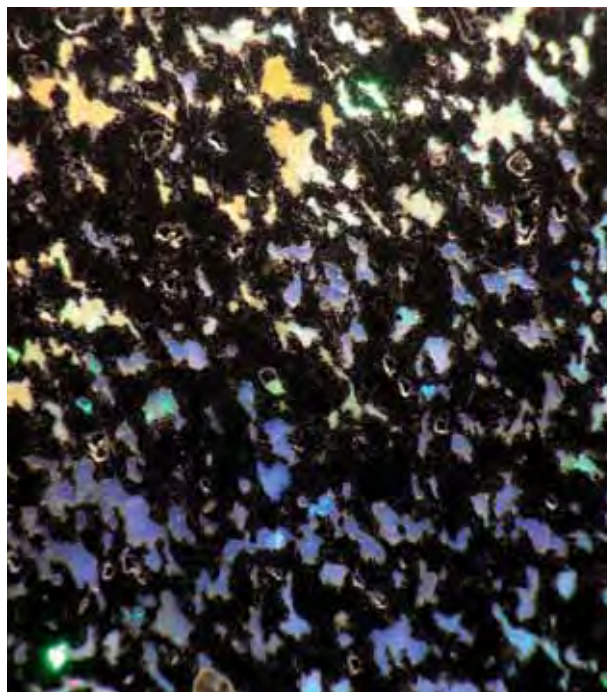
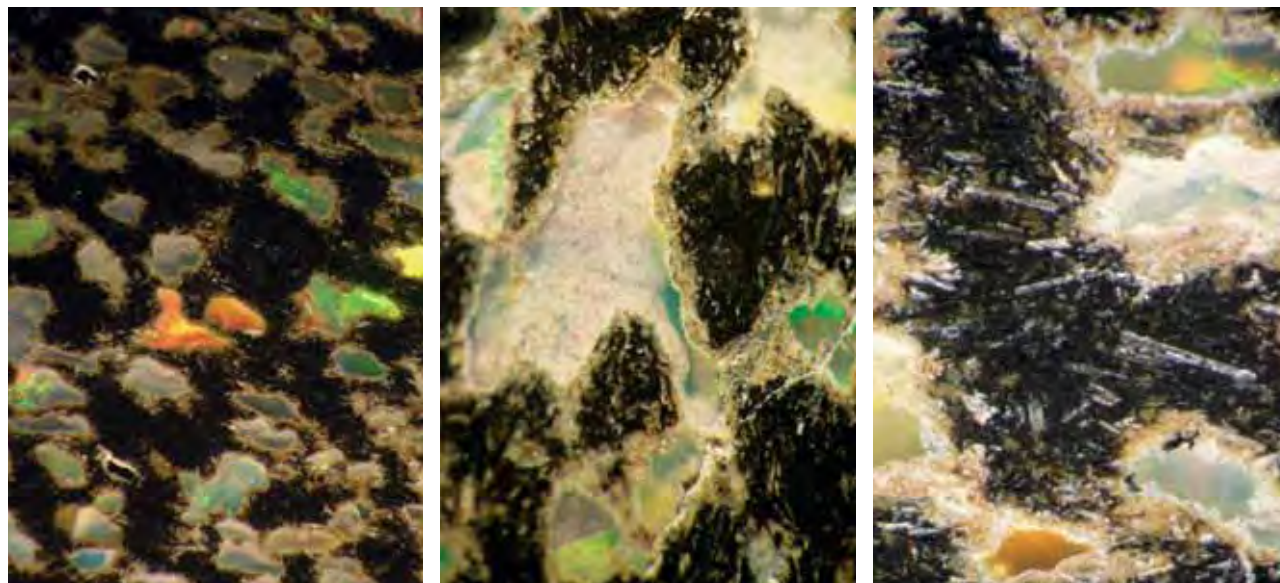


Figure 10. This detail from the 205 ct polished sample in figure 9 displays oriented (bottom right to top left) irregularly shaped vesicles filled with opal that varies in bodycolor from blue (bottom) to yellow, pink, and white (top). Photo by Graham Henry; field of view is 18 mm high.

Figure 11. In this series of photomicrographs, the 100 ct polished sample in figure 9 also shows oriented vesicles filled with colorless opal displaying play-of-color. A domain displaying red play-of-color continues over two vesicles (left). At higher magnification (center), this sample shows an irregular-shaped vesicle that illustrates the interconnected channelways through which the silica-bearing fluids originally migrated. At right, the basalt host reveals numerous elongated transparent feldspar crystals oriented parallel to the direction of elongation of the vesicles. These would have been parallel to the original flow. Photomicrographs by Graham Henry; height of field of view is 11 mm (left), 4 mm (center), 3 mm (right).



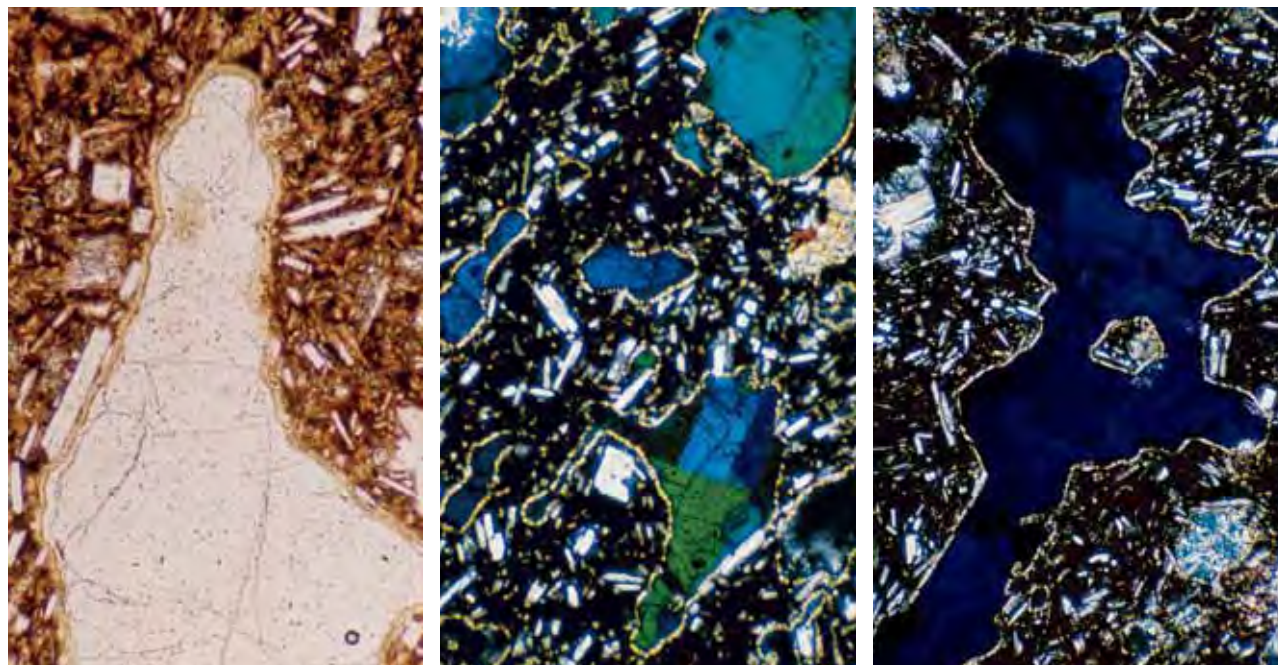


Figure 12. This thin section shows details of the opal-filled vesicular cavities within the basalt. At left, in plane-polarized (normal) light, the opal in the cavities appears colorless. A thin yellowish line (appearing white in hand specimens) is visible around the opal in each cavity. This unknown fibrous mineral lined the inside of the vesicles prior to deposition of the opal. The basalt is comprised of abundant well-formed rectangular crystals of white feldspar together with minor opaque minerals (black grains) in a brown glassy groundmass. At center, the thin section of Leopard opal is viewed between crossed polarizers. The elongated feldspar crystals show a preferred orientation approximately parallel to the lava flow direction, and the opal displays blue and green diffraction colors. In some cases, the opal diffraction color is consistent across several vesicles, while in others several opal domain boundaries lie within a single cavity. At right, the homogenous blue color indicates that the opal precipitated as a single domain of ordered spheres across the large irregularly shaped vesicle. Photomicrographs by R. Coenraads; height of field of view is 0.9 mm (left), 2.2 mm (center and right).

feldspar crystals; these are oriented more-or-less parallel to the direction of the original lava flow (figure 12, center). The vesicles vary in size up to ~1–3 mm, and are also elongated in the direction of flow (again, see figure 12, center). When viewed between crossed polarizers, some of the opal in the vesicles remained dark upon rotation through 360°, as would be expected from an amorphous material, while some displayed diffraction colors (figure 12, center and right). Such colors are typical in thin sections of opal showing play-of-color (R. Flossman, pers. comm., 1999) because of the pseudo-crystalline nature of the material caused by the regular arrangement of its silica spheres. Consistent colors are often visible over several adjacent vesicles, indicating that the orderly deposition and arrangement of silica spheres proceeded unimpeded within the framework of the host basalt.

Viewing Leopard opal with UV radiation highlights the inhomogeneous nature of the material. The basalt matrix is inert to UV, while the opal

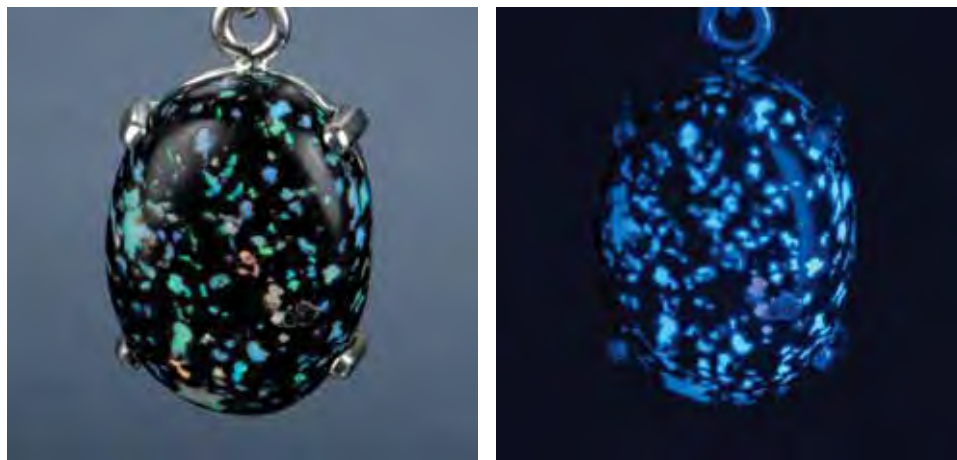
stands out as bluish white spots (stronger under long-wave than short-wave UV) against the black background (figure 13).

Determinations of S.G. and R.I. are not meaningful for Leopard opal, since they will invariably reflect a mixture of basalt, opal, and porosity (for example, the 6.87 ct cabochon showed a 4% weight gain when left in water overnight). The S.G. range of small pieces of opal without matrix was 2.05–2.15. A spot R.I. of ~1.46 was obtained from pieces of opal with polished faces, which is consistent with prior tests (Johnson and Koivula, 1996).

The XRD scans for the reddish orange and colorless opal showed them both to be opal-CT, that is, having a disordered cristobalite-like structure with varying degrees of tridymite stacking (Elzea and Rice, 1996).

Etching of the opal for SEM imaging proved to be more difficult than expected, implying that etch rates for both the spheres and their matrix are more uniform than those seen in most other opal. We were

Figure 13. When this 6.87 ct cabochon (left, under normal lighting) is exposed to long-wave UV radiation (right), the basalt matrix is inert, while the opal stands out as bluish white spots (stronger under long-wave than short-wave UV) against the black background. Photos by Robert Weldon.



therefore unable to use the SEM to discern the internal structure responsible for the opal's play-of color.

## DISCUSSION

Opal-CT is typical of volcanic opal from Mexico (Smallwood, 2000; Fritsch et al., 2002), and this identification indicates that the Zimapán opal formed at reasonably low temperatures, probably between 100°C (Elzea et al., 1994) and 190°C (Rondeau et al., 2004). According to Elzea et al. (1994), it may have precipitated originally at even lower temperatures (~45°C; Rondeau et al., 2004) as opal-A (i.e., with an amorphous pattern) from silica-rich solutions due to water interacting with silica-rich volcanic ash and tuff, and then converted to opal-CT during heating associated with regional tectonic uplift. There appear to have been at least two phases of opal deposition, as indicated by the presence of opal of two distinct bodycolors in the veins. As the orange-red bodycolor of fire opal is caused by iron-rich nanoinclusions (Fritsch et al., 2002), some of the silica-bearing fluids undoubtedly were iron-bearing.

The simultaneous occurrence of a number of factors, all critical to the formation of opal showing play-of-color in a vesicular basalt, highlights the rarity of this Mexican Leopard opal and the low likelihood of finding a similar deposit elsewhere:

1. **Availability of silica.** It is reasonable to assume that the silica-bearing solutions responsible for the deposition of the opal in the vesicles and fractures within the basalt flows percolated downward from the immediately overlying felsic tuffs and breccias.
2. **Permeability of the vesicular basalt and porosity with an advantageous size.** Permeability is

essential for the silica-bearing solutions to penetrate the basalt and reach most of the open spaces. The size of the vesicles is also important, since the abundant, but small, vesicles and their uniform distribution, are necessary for an appealing product. Fractures in the basalt have allowed accumulations of pale blue opal and fire opal that are also of interest.

3. **Environmental factors.** These would have favored the formation of opal instead of cryptocrystalline silica, and also favored formation of play-of-color opal over common opal (potch). The silica-bearing waters would need to be introduced over a sufficiently long period of time and at relatively low temperatures to lead to the precipitation of opal-CT (Elzea et al., 1994). We can assume that the deposit has not been subject to a significant heating event, which would have led to recrystallization of the opal into a more common cryptocrystalline silica product.

## CONCLUSION

Significant potential for Leopard opal exists within the upper portion (top few meters) of the vesicular basalt flow, adjacent to the contact with the overlying tuffs and breccias. There is also potential for the recovery of play-of-color opal and fire opal from cracks and fractures in the upper surface of the basalt. Apart from the shallow trenches that may represent pre-Columbian workings and the small exploration pits opened up by one of the authors (ARZ), the Zimapán deposit of Leopard opal has not been developed and few in the gemological community are aware of the potential of this material. At least several hundred meters of contact exposed on the hillside remain unexplored.

#### ABOUT THE AUTHORS

Dr. Coenraads (coenraads01@optusnet.com.au) is a consulting geologist, geophysicist, and gemologist based in Sydney, Australia, as well as a lecturer for the Gemmological Association of Australia (GAA). Mr. Rosas Zenil is the owner of Calizas y Carbonatos Rossin S.A. de C.V., a limestone mine and crushing plant located in Zimapán.

**ACKNOWLEDGMENTS:** The authors are grateful to consulting geologist Angel Ramón Zuñiga Arista (Lerma, Mexico), who provided geologic and topographic maps; Rad Flossman (New South Wales University, Sydney), who prepared the thin section; Ross Pogson (Australian Museum, Sydney) for carrying out the XRD scans; and

Anthony Smallwood (University of Technology, Sydney) for the SEM study. Dr. Edward Littig, Kelly Snedden, and Charles Rasico (Newman University, Wichita, Kansas) are thanked for their assistance in obtaining the photo of the Aztec warrior statue. The authors are also grateful to John Koivula (AGTA Gemological Testing Center, Carlsbad) for the photo of the leopard head carving; Dr. Graham Henry (GAA, Sydney) for assistance with specimen photography; Kenneth Shannon (Corriente Resources Inc., Vancouver) for marketing information; and Dr. Emmanuel Fritsch and the late Dr. Alfred Levinson for their review of this manuscript. RRC would also like to thank the Cabrera family for their warm hospitality and assistance during visits to Mexico. This study was funded by Worldmin N.L.

#### REFERENCES

- Ball S.H. (1931) Historical notes on gem mining. *Economic Geology*, Vol. 26, No. 7, pp. 681–738.
- Carrillo-Martínez M., Suter M. (1982) Tectónica de los alrededores de Zimapán, Hidalgo y Querétaro [Tectonics around Zimapán, Hidalgo, and Querétaro]. In M. Alcayde and Z. De Cserna, Eds., *Libro Guía de la Excursión Geológica a la Región de Zimapán y Áreas Circundantes, Estados de Hidalgo y Querétaro [Guidebook of the Geologic Excursion to the Zimapán region and Surrounding Areas, Hidalgo and Querétaro States]*, Geological Society of Mexico, Sixth National Geologic Convention, Mexico City, pp. 1–20.
- Comisión de Estudios del Territorio Nacional [CETENAL] (1972) Topographic map sheet, 1st ed., Tecozautla F-14-C-68 HGO.QRO, 1:50,000 scale, Mexico City.
- Elzea J.M., Odom I.E., Miles W.J. (1994) Distinguishing well ordered opal-CT and opal-C from high temperature cristobalite by X-ray diffraction. *Analytica Chimica Acta*, Vol. 286, pp. 107–116.
- Elzea J.M., Rice S.B. (1996) TEM and X-ray diffraction evidence for cristobalite and tridymite stacking sequences in opal. *Clays and Clay Minerals*, Vol. 44, No. 4, pp. 492–500.
- Fritsch E., Ostrooumov M., Rondeau B., Barreau A., Albertini D., Marie A.-M., Lasnier B., Wery J. (2002) Mexican gem opals: Nano- and micro-structure, origin of color, comparison with other common opals of gemmological significance. *Australian Gemmologist*, Vol. 21, No. 6, pp. 230–233.
- Heylman E.B. (1983a) Map of the Queretaro opal mines, Mexico. *Lapidary Journal*, Vol. 37, No. 2, pp. 344–345.
- Heylman E.B. (1983b) Opal localities in west central Mexico. *Lapidary Journal*, Vol. 37, No. 4, pp. 598–602.
- Heylman E.B. (1983c) Four opal localities in Mexico. *Lapidary Journal*, Vol. 37, No. 6, pp. 880–882.
- Heylman E.B. (1984a) Varieties of Mexican opal. *Lapidary Journal*, Vol. 38, No. 5, pp. 746–747.
- Heylman E.B. (1984b) Zimapan opal: Are the mines lost? *Lapidary Journal*, Vol. 38, No. 6, p. 794.
- Johnson M.L., Koivula J.I., Eds. (1996) Gem News: “Leopard opal” from Mexico. *Gems & Gemology*, Vol. 32, No. 1, pp. 54–55.
- Koivula J.I., Fryer C., Keller P.C. (1983) Opal from Querétaro, Mexico: Occurrence and inclusions. *Gems & Gemology*, Vol. 19, No. 2, pp. 87–96.
- Leechman F. (1961) *The Opal Book*. Lansdowne Press, Sydney.
- Leipner H.N., Ed. (1969) About our cover: Cuauhtemoc, last Aztec Emperor. *Lapidary Journal*, Vol. 23, No. 2, pp. 299, 340.
- Mallory L.D. (1969a) Opal mining in western Mexico, part 1. *Lapidary Journal*, Vol. 23, No. 3, pp. 420–428.
- Mallory L.D. (1969b) Opal mining in western Mexico, part 2. *Lapidary Journal*, Vol. 23, No. 4, pp. 570–579.
- Rondeau B., Fritsch E., Guiraud M., Renac C. (2004) Opals from Slovakia (“Hungarian” opals): A re-assessment of the conditions of formation. *European Journal of Mineralogy*, Vol. 16, No. 5, pp. 789–799.
- Smallwood A. (2000) A preliminary investigation of precious opal by laser Raman spectroscopy. *Australian Gemmologist*, Vol. 20, No. 9, pp. 363–366.
- Webster R. (1983) Opal from Mexico. In *Gems, Their Sources, Description and Identification*, revised by B.W. Anderson, 4th ed., Butterworth, London, p. 234.
- White J.S. (1998) Hope’s wonderful opal. *Lapidary Journal*, Vol. 52, No. 5, pp. 44–46, 59.
- Zeitner J.C. (1979) The opal of Queretaro. *Lapidary Journal*, Vol. 33, No. 4, pp. 868–880.

For regular updates from the world of **GEMS & GEMOLOGY**, visit our website at:

[www.gja.edu/gemsandgemology](http://www.gja.edu/gemsandgemology)

# LAMINATED REFERENCE CHARTS

The information you **need...** at a glance!  
Perfect for home or office use.



- HPHT-Grown Synthetic Diamonds
- World Gem Localities
- Gem Treatments
- GIA Diamond Cut Grading System
- Pink Diamond Color Chart
- Recognizing Be-Diffused Rubies & Sapphires

Also available:

- Separation of Natural & Synthetic Diamonds
- Identification of Filled Diamonds

**Only \$14.00** domestic

**\$18.00** international



**GEMS & GEMOLOGY®**

**Order Yours Today!**

Visit [www.gia.edu/gemsandgemology](http://www.gia.edu/gemsandgemology)  
then click on **Ordering and Renewals** to order.

Or call **800-421-7250, ext. 7142**  
(outside the U.S., **760-603-4000, ext. 7142**).

**Buy two or more and SAVE!**

Get additional charts for \$12 each on domestic  
deliveries or \$15 each on international deliveries.

For California deliveries, please add appropriate sales tax.  
For Canada deliveries, add 6% GST.

**FREE shipping! While supplies last.**

# THE CAUSE OF IRIDESCENCE IN RAINBOW ANDRADITE FROM NARA, JAPAN

Thomas Hainschwang and Franck Notari

“Rainbow” andradite from Nara, Japan, occurs as relatively small orangy brown crystals that show attractive iridescence in almost the entire range of the spectrum. The material is nearly pure andradite, as determined by its chemical composition and Vis-NIR and specular reflectance FTIR spectra. Microscopy revealed that two different types of lamellar structures appear to be responsible for the iridescent colors. These lamellar structures cause predominantly thin-film interference and most likely diffraction of light. The terms *interference* and *diffraction* are explained and correlated to the structure and iridescence observed in these garnets.

Garnets with optical phenomena are not commonly encountered, although several types are known, including color-change, star, cat’s-eye, and, rarely, iridescent garnets. Color-change garnets are usually pyrope-spessartine, while star garnets are generally almandine or pyrope-almandine. Iridescence in garnet is known only in andradite and grossular-andradite (also called “grandite”).

These iridescent garnets are mainly known from Sonora, Mexico (see Koivula, 1987; Koivula and Kammerling, 1988; Badar and Akizuki, 1997; Boehm, 2006). They were initially described several decades ago from a locality in Nevada (Ingerson and Barksdale, 1943); the same authors mentioned similar andradites from Japan (Kamihoki, Yamaguchi Prefecture, Chugoku Region, Honshu Island). Iridescent garnet from Japan’s Nara Prefecture (figure 1) was discovered in 2004, and the material has been described by Shimobayashi et al. (2005). More recently, iridescent andradite was found in New Mexico (Burger, 2005). The purpose of this article is to describe the new iridescent garnet from Japan and to attempt a detailed explanation of the color phenomenon observed in this attractive material.

## LOCATION, GEOLOGY, MINING, AND PRODUCTION

“Rainbow” andradite from Nara Prefecture was first recovered in early 2004 by several groups of mineral collectors near the old Kouse magnetite mine at Tenkawa in the Yoshino area (Y. Sakon, pers. comm., 2005). This region lies approximately 60 km southeast of Osaka, and is about 400 km east of the Kamihoki locality described by Ingerson and Barksdale (1943; figure 2). Rocks in this area form part of the regional metamorphic Chichibu belt, which lies just south of the Sanbagawa belt (Takeuchi, 1996).

The first garnets recovered were not of high quality, but in September 2004 a local mineral collector (J. Sugimori) found an outcrop containing gem-quality andradite (i.e., strongly iridescent and relatively “clean” material). Over the next four months, he used hand tools to follow the vein to

---

See end of article for About the Authors and Acknowledgments.  
GEMS & GEMOLOGY, Vol. 42, No. 4, pp. 248–258.  
© 2006 Gemological Institute of America

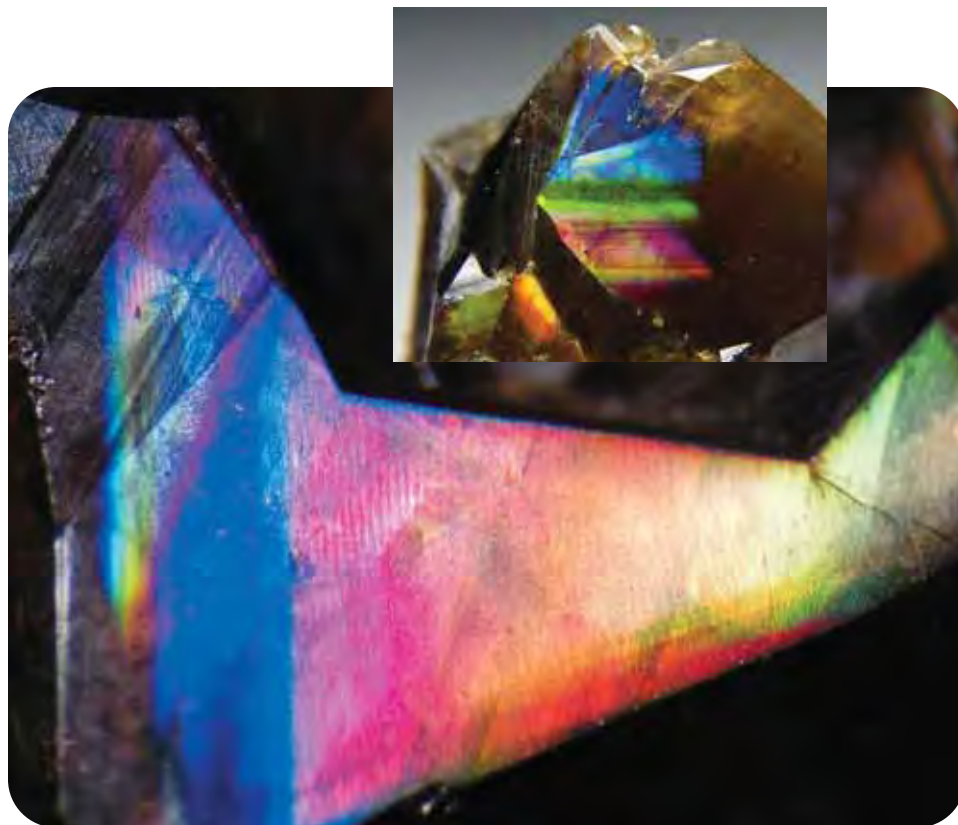


Figure 1. A new source of Rainbow andradite from Nara, Japan, has produced samples with spectacular iridescence, as seen in these unpolished specimens. The crystal face on the left (photomicrograph by T. Hainschwang) is magnified 20 $\times$ , and the crystal in the inset is 1.7 cm wide (photo by Ms. Bee).

a depth of 5 m. Well-formed crystals showing spectacular iridescence (again, see figure 1) have been sold through the Internet and mineral dealers in Japan. Several hundred kilograms of this Rainbow andradite were recovered, and a small proportion of it was gem quality. Some cabochons have been cut, and rare faceted examples also exist (figure 3). In August 2005, local authorities from Tenkawa village prohibited additional garnet recovery from the area to curtail a mining rush (Y. Sakon, pers. comm., 2005).

## MATERIALS AND METHODS

To characterize this material, and better understand the cause of the phenomenon, we examined 60 iridescent garnets from Nara that we obtained from Japanese gem and mineral dealers involved with mining there: a 2.19 ct freeform cabochon (again, see figure 3), three rough samples with polished faces (4.84, 6.12, and 8.03 ct), and 56 rough samples (0.25–3.60 g). For comparison, we examined one partially polished Rainbow garnet of 18.82 ct from Sonora, Mexico.

All samples were examined with a gemological microscope, using reflected and transmitted light, to study their iridescence and microstructure. The

luminescence of all the samples was observed using a standard long- and short-wave ultraviolet (UV) lamp (365 and 254 nm, respectively). We determined refractive index and specific gravity (by hydrostatic weighing) for three of the Nara samples.

We used a JEOL 4800 scanning electron microscope (SEM) equipped with an energy-dispersive X-ray (EDX) spectrometer to obtain images in backscattered electron (BSE) mode and semiquantitative chemical point analyses of one 6.22 ct Nara sample. The sample was prepared as a cuboid, with one face polished parallel to a dodecahedral face and four faces polished perpendicular to dodecahedra, in order to resolve the structure of the material; the dodecahedral face remained unpolished. The beam voltage was 15 kV, with a beam current varying from 10 to 200 pA, depending on the magnification used.

The trace-element composition of five larger (8.40–15.87 ct) Nara crystals was investigated with a Thermo Noran QuanX energy-dispersive X-ray fluorescence (EDXRF) system with a Si detector cooled by a Peltier battery. The EDXRF spectra were recorded with acquisition times of 300–1000 seconds, under vacuum to limit the presence of argon, and with sample rotation to avoid diffraction artifacts.



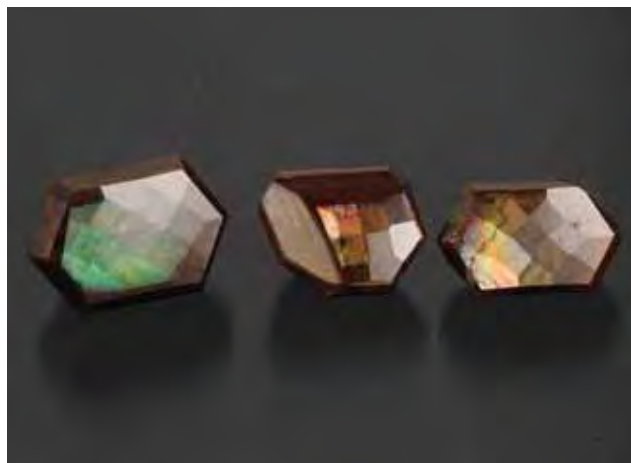
Figure 2. Rainbow andradite from Nara Prefecture was first recovered in early 2004 from the Tenkawa area, located approximately 60 km southeast of Osaka. This deposit is about 400 km east of Japan's original source for this garnet, near Kamihoki.

The infrared spectra of five Nara samples exhibiting smooth crystal faces were recorded at 4  $\text{cm}^{-1}$  resolution with a PerkinElmer Spectrum BXII FTIR spectrometer equipped with a Deuterated Tri-Glycine Sulfate (DTGS) detector. A PerkinElmer

fixed angle specular reflectance accessory was used for specular reflectance spectra.

We recorded visible–near infrared (Vis-NIR) absorption spectra in the 400–1000 nm range for three highly transparent samples and a small trans-

Figure 3. Both cabochon-cut and faceted Rainbow andradite have been produced, typically in freeform shapes. The cabochon on the left weighs 2.19 ct (photo by T. Hainschwang) and the faceted stones on the right are 6.43–11.39 ct (gift of Keiko Suehiro, GIA Collection nos. 36136–36138; photo by C. D. Mengason).



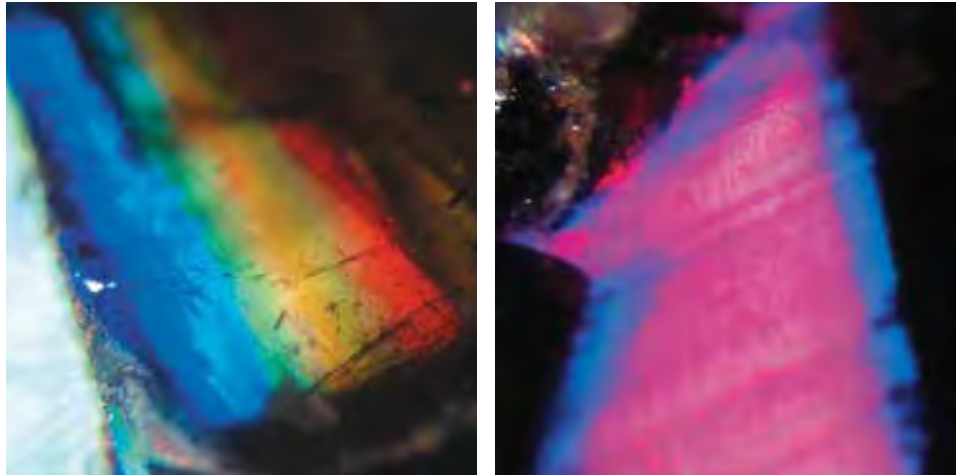


Figure 4. Very colorful and strong iridescence, varying from a range of spectral colors (left) to broad flashes of a single color (right), can be seen in the andradite as the viewing angle changes. Colors such as these were seen on faces oblique to {110}. Photomicrographs by T. Hainschwang; magnified 40× (left) and 60× (right).

parent chip (in order to resolve the 440 nm band), using a custom-made SAS2000 system equipped with an Ocean Optics SD2000 dual-channel spectrometer with a resolution of 1.5 nm. A 2048-element linear silicon CCD detector was employed.

## RESULTS

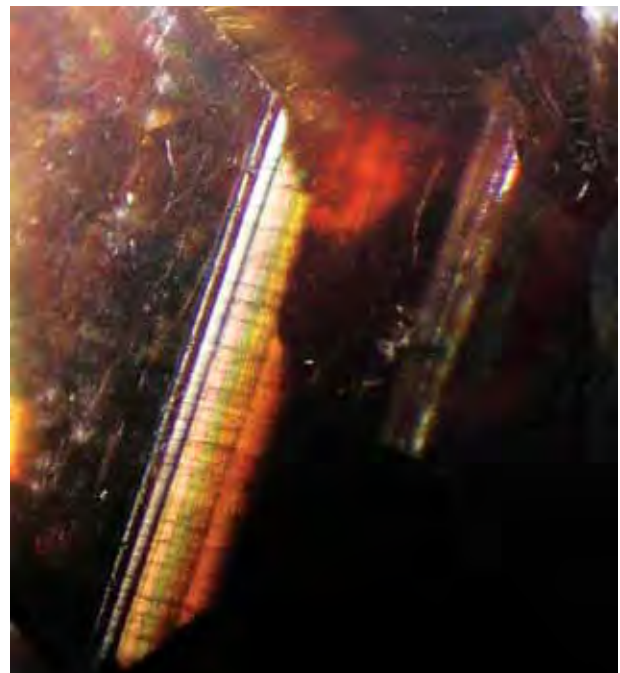
**Standard Gemological Testing.** All of the Nara garnets had an orangy brown bodycolor, but they exhibited a variety of iridescent colors. Depending on the viewing orientation and the particular crystal face, the phenomenon varied from a single color to a range of colors that shifted as the face was moved (see, e.g., figure 4). Some samples also exhibited “white” flashes that appeared to result from several overlapping colors due to the combined interference from multiple layers.

Microscopic examination indicated the presence of a rather complex lamellar (thin-layered) structure (figure 5). Observation of well-formed dodecahedral crystals demonstrated that the iridescence-causing lamellae were most probably oriented parallel to the dodecahedral {110} faces. Thus, six sets of lamellae were present in these garnets, each parallel to two {110} faces. These lamellae caused broad flashes of one or two nonspectral colors (usually “golden,” pinkish red, and blue-green) visible on the {110} faces, always of a relatively weak intensity (figure 6). (“Nonspectral” colors are combinations of spectral colors, which can be seen as a continuous spectral distribution or a combination of primary colors; most colors are nonspectral mixtures.) Brighter and more varied colors were seen on faces oblique to the {110} faces (again, see figures 1 and 4). These irregular striated faces were apparently formed by intergrowth, dis-

tortion, and possibly twinning. According to Shimobayashi et al. (2005), the {211} trapezohedral faces are also present on some of the Nara garnets, but we did not see them on our samples. The iridescent colors were not only observed on the surface of the garnets, but they were also seen deep within the more transparent stones.

Besides the lamellar structure parallel to {110}, we also observed an irregular, wavy, step-like

Figure 5. A complex lamellar structure was apparent in the garnets. Thin-film lamellae oriented parallel to the dodecahedral {110} faces formed the predominant microstructure of the bright, colorful parallel bands. Photomicrograph by T. Hainschwang; magnified 10×.



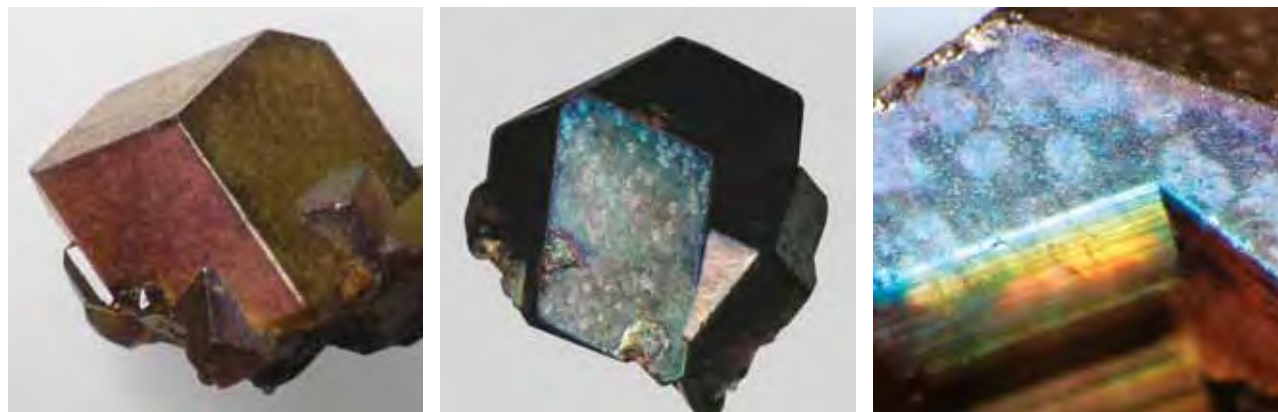


Figure 6. Weak iridescence created broad flashes of nonspectral colors on the dodecahedral {110} faces of the Nara andradites. The colors included “golden” and pinkish red (left, 6.44 ct), greenish blue (center, 9.16 ct), and less commonly bluish purple (right, magnified 15×). The photo on the right also shows (at bottom) the intense lamellar iridescence that is oblique to the dodecahedral face. Photos by T. Hainschwang.

lamellar structure on the dodecahedral faces (figure 7), which was more distinct on practically all faces inclined to the dodecahedra. These two types of lamellar structure are apparently unrelated growth phenomena. Shimobayashi et al. (2005) measured a spacing of ~10–20  $\mu\text{m}$  in the wavy structure; however, they did not assign any phenomenon to these lamellae. In contrast, our microscopic observations suggested that this lamellar structure *does* play a role in the iridescence, even though the lamellae are relatively widely spaced, clearly above the spacing of 100–1000 nm required for a thin-film interference phenomenon (Hirayama et al., 2000). On certain faces, crossed iridescent colors could be seen that appeared to be caused by both the narrow lamellae and the widely spaced wavy lamellae (figure 8). We believe that the moiré-like pattern caused by these crossed iridescent colors is also the result of an interference effect: The crossed grids

cause interference and therefore appear distorted.

The refractive index of these garnets was above the limit of the refractometer (>1.81), as expected for andradite. The specific gravity varied slightly from 3.79 to 3.82. As expected for iron-bearing garnets, the samples were inert to short- and long-wave UV radiation.

**EDXRF Chemical Analysis.** The EDXRF data confirmed that these samples were basically the calcium-iron garnet andradite. Traces of Al and Mn were detected, which most likely indicated very small grossular and spessartine components.

**SEM-BSE Imaging and EDX Chemical Analysis.** The SEM analysis was performed on a face polished perpendicular to {110}. BSE imaging (figure 9) revealed a structure consisting of fine lamellae (with different chemical compositions) parallel to

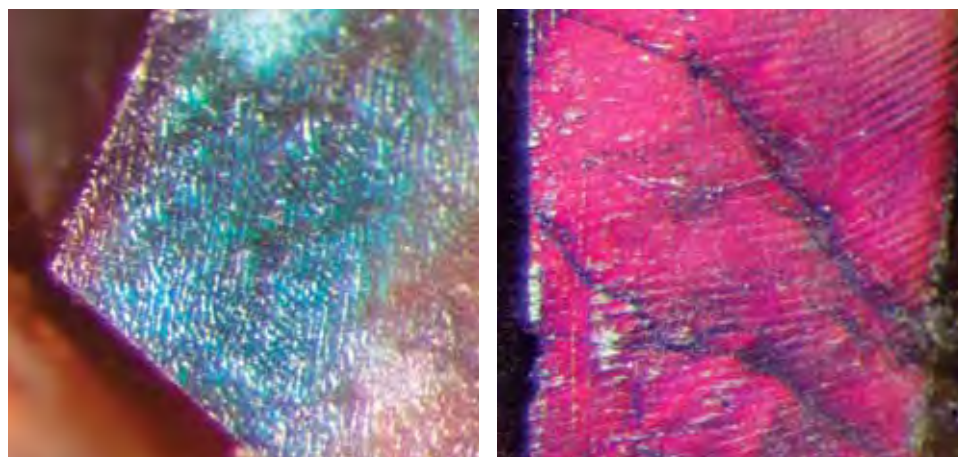


Figure 7. In addition to the fine lamellar structures parallel to {110}, coarser-scale, wavy, step-like structures were seen on practically all faces inclined to the dodecahedra. They appear to produce iridescence colors through a diffraction effect. Photomicrographs by T. Hainschwang; magnified 30× (left) and 45× (right).

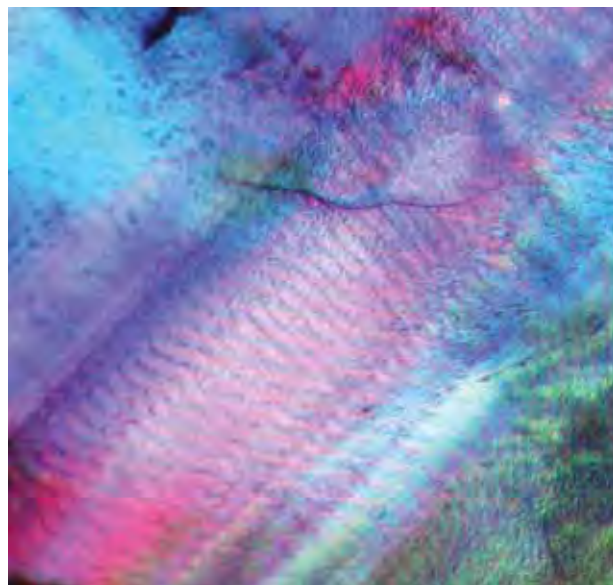
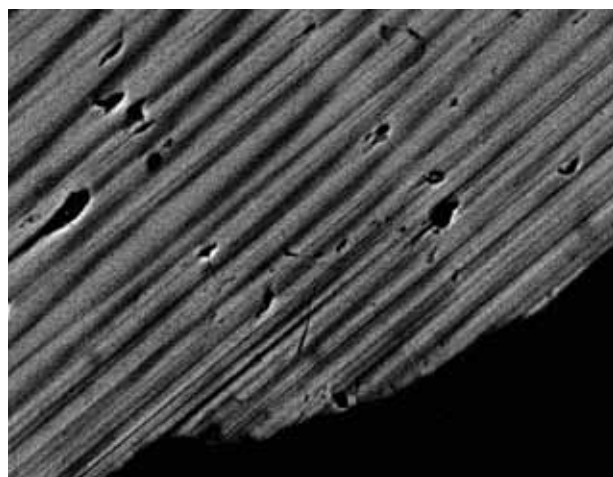


Figure 8. On some of the faces, a moiré pattern was visible, which was apparently related to the wavy structure seen on most of the faces of these garnets. The example shown here has overlapping bright pink to blue to greenish blue iridescence on a face that is oblique to a dodecahedral face. Photomicrograph by T. Hainschwang; magnified 25 $\times$ .

the {110} face. In the BSE image, darker zones are of lower mean atomic number and lighter zones are of higher mean atomic number.

The lamellae were of varying thicknesses, rang-

Figure 9. In this backscattered electron (BSE) image of the fine lamellae parallel to {110}, the brighter zones (with a higher mean atomic number) correspond to pure andradite, while the darker zones (with a lower mean atomic number) are andradite with a grossular component. BSE image width  $\sim 80 \mu\text{m}$ .



ing from about 100 nm to approximately 10  $\mu\text{m}$ ; they appeared to average 100–1000 nm (0.1–1  $\mu\text{m}$ ). This range is in good agreement with that determined by Shimobayashi et al. (2005).

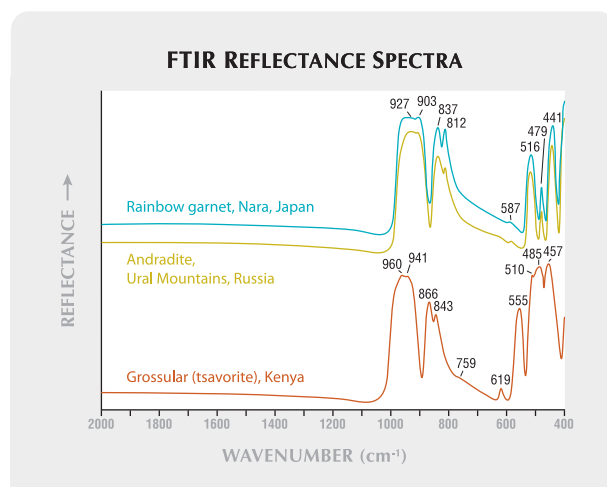
The semiquantitative EDX chemical point analyses performed on darker and lighter lamellae indicated higher aluminum and lower iron in the darker (lower mean atomic number) zones, whereas the lighter (higher mean atomic number) zones were richer in iron and poorer in aluminum. The darker zones on the BSE image contained about 1–1.5% less iron than the brighter zones and about the same or more aluminum. Thus, the brighter lamellae were nearly pure andradite ( $\text{Ca}_3\text{Fe}_2[\text{SiO}_4]_3$ ), and the darker ones were andradite with a slightly elevated grossular ( $\text{Ca}_3\text{Al}_2[\text{SiO}_4]_3$ ) component.

The minute spessartine component (i.e., manganese) detected by EDXRF analysis was not identified by the SEM-EDX technique, since the concentration was below the detection limit of the instrument.

**FTIR Spectroscopy.** The specular reflectance FTIR spectra indicated that the samples were almost pure andradite (commonly a perfect match with our reference spectrum; see figure 10).

**Vis-NIR Spectroscopy.** Vis-NIR spectroscopy (figure 11) showed a typical andradite spectrum, with

Figure 10. A comparison of the specular reflectance FTIR spectra of the Japanese Rainbow garnet with andradite (demantoid) from Russia and grossular (tsavorite) from Kenya indicates that the Japanese material is almost pure andradite.



a distinct absorption at 440 nm and a very broad band centered in the near-infrared range at 860 nm, both assigned to Fe<sup>3+</sup> (Manning, 1967). In thicker specimens, the 440 nm absorption could not be resolved due to complete absorption starting at about 450 nm. In addition, a very weak band at 480 nm was detected.

## DISCUSSION

The Nara locality in Japan represents the second discovery of a commercial source for attractive iridescent garnets after Sonora, Mexico. However, the Japanese material appears very different from the Mexican garnets, which have a more greenish bodycolor and show lamellar stripe-like iridescence, sometimes causing a star (figure 12). The Japanese garnets may resemble some brown opals such as those from Ethiopia (e.g., figure 13), and the iridescence is similar to that of high-quality labradorite from Finland.

The iridescence in this Japanese Rainbow andradite is caused by their lamellar structure: alternating microscopic layers of slightly different composition and varying width. Some layers are nearly pure andradite, while the others are andradite with a grossular component. The spacing of the layers, as revealed by SEM-BSE imaging, is suitable for thin-film interference of visible light, and diffraction-related interference may occur when light hits the edges of these layers. (See box A for a more detailed discussion of diffraction and interference,

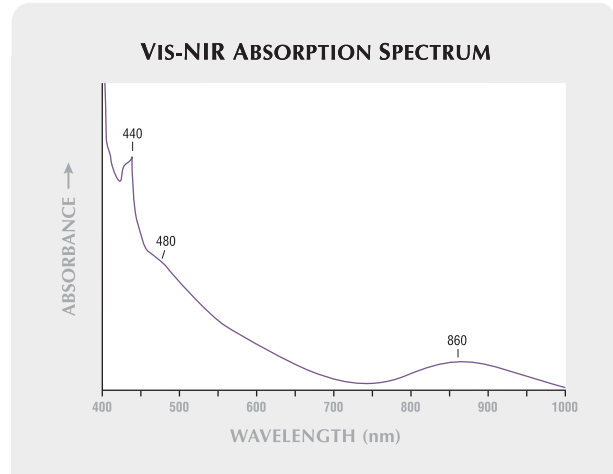


Figure 11. The Vis-NIR spectrum of a small transparent chip of Rainbow andradite is characterized by Fe<sup>3+</sup>-related absorptions at 440 and 860 nm, plus a weak broad band at 480 nm. The Fe<sup>3+</sup>-related absorptions are encountered in all andradite.

and the distinctions between them.) The chemical differences detected in adjacent layers and the associated differences in R.I., combined with this finely layered structure, clearly point toward multilayer thin-film interference as the main cause of the colorful iridescence.

Both diffraction grating and multilayer interference structures are present when the garnets are viewed at oblique angles to the dodecahedral faces. This explains why the most intense iridescent colors can be observed on faces oblique to {110}. The much weaker and less colorful iridescence visible

Figure 12. Iridescent Mexican “grandite” (grossular-andradite) garnets have a different appearance from the Japanese material. The 18.82 ct Mexican garnet shown on the left has a distinct four-rayed star. Its layer-like iridescence (right, magnified 30×) is quite distinct from that of the Japanese Rainbow andradite. Photos by T. Hainschwang.

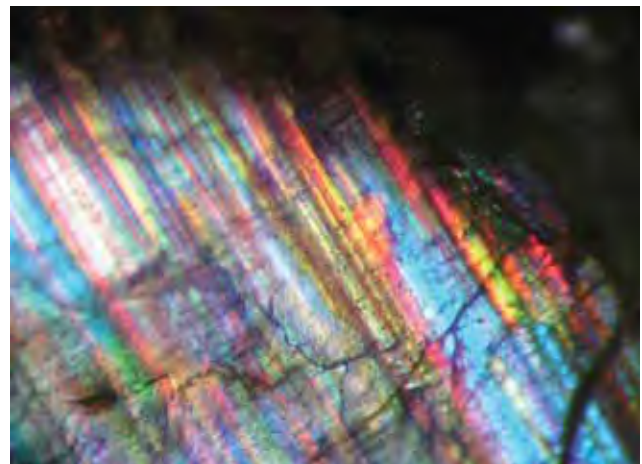




Figure 13. In some cases, the Japanese Rainbow andradite (left) resembles brown opal from Ethiopia (right). The 6.43 ct andradite is a gift of Keiko Suehiro, GIA Collection no. 36137 (photo by C. D. Mengason). The 41.2 g Ethiopian opal nodule is GIA Collection no. 36538 (photo by Robert Weldon).

on {110} faces (figure 6) can be explained by a simple thin-film interference effect.

The other, rather wavy step-like structure visible on almost all faces is likely *not* responsible for any color dispersion due to thin-film interference, because its spacing is much greater than the wavelength of visible light. However, some weaker iridescent colors, which overlap the dominant iridescent colors (figure 7), appear to be caused by a diffraction effect from this structure. This may be explained by comparison to a planar diffraction grating, which will disperse visible light even with a spacing of 20 gratings/mm (a spacing of 50  $\mu\text{m}$ ; see, e.g., Newport Corp., 2006). The wavy lamellae, with their step-like surface, could act like a planar diffraction grating having between 50 and 100 gratings/mm. Similar effects can be seen with the low groove density (less than 87 grooves/mm) present in the shells of most mollusks; Liu et al. (1999) related these grooves to weak iridescence caused by diffraction. Indeed the more widely spaced, wavy, step-like lamellar structure in the garnets is very reminiscent of the step-like structure seen in the nacreous aragonite layer of shell (Liu et al., 1999; Fengming et al., 2004).

However, shell iridescence has also been described as a mixed-layer interference and diffraction phenomenon (Tan et al., 2004), and as a thin-film interference phenomenon (Fritsch and Rossman, 1988). A similar structure consisting of both straight lamellae parallel to {110} and wavy lamellae has been described in iridescent garnets from the Adelaide mining district, Nevada, by Akizuki et al. (1984). The same authors described the lack of this wavy structure in iridescent garnets from Kamihoki, Japan.

Further evidence for a combination of fine lamellae and a wavy lamellar (diffraction grating) structure as the cause of iridescence in these gar-

nets is provided by the moiré pattern visible on many of the faces (again, see figure 8). Moiré patterns are caused by interference due to the superposition of two similarly spaced fine patterns, such as grids; interference on these grids results in their distorted appearance, as seen in the two intersecting sets of iridescent color lamellae in figure 8. In these garnets, we have a total of six sets of straight, narrow multilayer structures (each of them following two of the 12 {110} faces) plus the larger, wavy lamellar structure that does not relate to the dodecahedral faces. Thus, on faces oblique to a simple {110} face, several of these structures and their associated color patterns will overlap and cause very colorful iridescence.

Combinations of multilayer interference and lamellar diffraction grating structures have been credited with causing the bright blue iridescence seen in *Morpho didius* butterflies (Vukusic et al., 1999; Iwase et al., 2004) and, together with scattering, for the bright green iridescence in *Papilio blumei* butterflies (Tada et al., 1999). In *Morpho didius* butterflies, the iridescence-causing structure consists of overlapping tiles on which Christmas tree-like microstructures can be seen; these structures cause multilayer interference in one direction, and diffraction in an orientation approximately perpendicular to the layer-like structure due to its "roughness."

## CONCLUSIONS

First discovered at this locality in 2004, andradite from Nara, Japan, shows an attractive iridescence that is probably caused by a combination of a narrowly spaced lamellar structure following the rhombic dodecahedron {110} and another wavy, widely spaced, step-like lamellar structure (not parallel to the {110} faces) that is visible on almost

## BOX A: IRIDESCENCE, INTERFERENCE, AND DIFFRACTION

Traditionally, the term *iridescence* has been used in gemology to describe only thin-film interference in specific phenomenal gems, such as iris agate, Ammolite, and pearls (see e.g., Fritsch and Rossman, 1988). Today, *iridescence* is frequently used to describe *any* diffraction and/or thin-film interference-related color phenomena. This is likely because interference and diffraction in minerals are closely related phenomena that often occur together, and it can be very difficult to distinguish them without a detailed analysis of the near-surface structure (Vukusic et al., 1999; Iwase et al., 2004).

The main difference between diffraction and thin-film interference is the interference-causing path of the light rays. In diffraction, light waves pass through a grating—or, in the case of garnet, reflect from a patterned, edged surface—and interact with one another. The spacing of these edges needs to be regular and narrow, but not necessarily on the order of the wavelength of visible light; in diffraction gratings, a spacing as low as 20 grooves/mm is sometimes used to create diffraction-related interference and thus disperse the white light into its spectral colors (Newport Corp., 2006). In multilayer films, both reflected and refracted light waves from each boundary between the layers interact with one another, and the interference may be observed if the film thickness is within the range of visible light (Hirayama et al., 2000). Some details on the two mechanisms are summarized below; an in-depth discussion of the theory, mathematics, and physics of diffraction and interference can be found, for example, in Born and Wolf (1999).

The effects caused by the coherent addition of wave amplitudes are known as “interference effects” (Born and Wolf, 1999). When two (or more) waves with equal amplitudes are **in phase** (i.e., crest meets crest and trough meets trough), then the waves enhance each other, and the resulting wave is the sum of their amplitudes; this is called *constructive interference*. If the waves are **out of phase** (i.e., crest meets trough), then the waves cancel each other out completely; this is *destructive interference* (see, e.g., Mathieu et al., 1991).

*Thin-film interference* of visible light occurs when light interacts with a lamellar material consisting of fine layers that have different refractive indices. These layers can be of any state: gaseous, liquid, solid, or even “empty” (vacuum). For example, a soap bubble shows iridescence due to the thin-film interference between the outside-air/soap and soap/inside-air interfaces. The width of the layers must be approximately the same as the wavelength of light, that is, somewhere between 0.1 and 1  $\mu\text{m}$ . When light passes through such a material, it is refracted, and then parts of it are reflected off each layer. The reflected waves are partially or completely in phase or out of phase, thus creating constructive or destructive interference. An example of simple double-layer interference of a “white” light source is shown in figure A-1. The figure has been simplified because the interference of “white” light is quite complicated, since it is composed of all wavelengths

from the UV to the NIR, and each wavelength is refracted differently when entering (and at every boundary with) a thin film.

*Diffraction* is caused by the bending, spreading, and subsequent overlapping of a wavefront when passing through a tiny opening or openings in an otherwise opaque obstacle (e.g., the slits in a diffraction grating) or at boundaries and edges (figure A-2). The light passing through the opening(s) or reflecting off a patterned, edged surface may experience destructive and constructive interference, thus creating dark and bright fringes, respectively, when the openings or edges of the lamellae are small enough (see, e.g., Mathieu et al., 1991). The slit width or pattern spacing needs to be small but not necessarily on the order of the wavelength of light (see, e.g., Liu et al., 1999; Newport Corp., 2006). Experiments performed by one of the authors (TH) with translucent curtain fabric with thread thickness  $\pm 0.08$  mm (80,000 nm) and spacing of 0.25 mm (250,000 nm) between both the horizontal and vertical threads confirm that such a relatively large grid will cause a very distinct diffraction pattern and light dispersion. With a diffraction grating, the effect functions as follows: A large number of identical, equally spaced slits (hence the occasional use of the term *multiple-slit interference*) or lamellae edges will cause many positions of entirely destructive interference fringes between intense constructive interference fringes. A planar diffraction grating used for visible light has a groove density of about 20 to 1800 grooves per mm. A number of different theories exist to explain diffraction; for more details see Born and Wolf (1999).

It is important to note that these effects are not limited to visible light. *Bragg diffraction*, also called *Bragg interference*, is the term for the scattering and interference effect that occurs when X-rays interact with a crystal lattice.

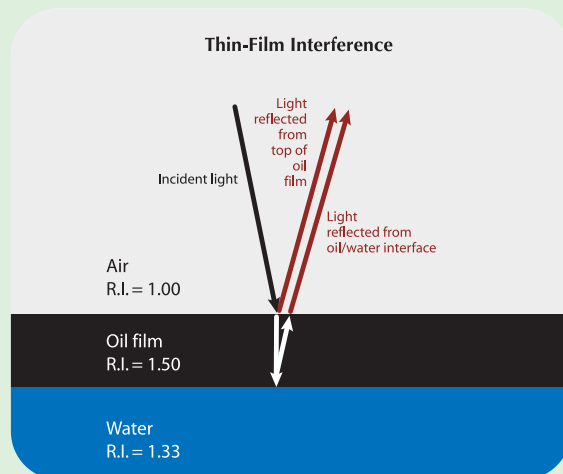


Figure A-1. This diagram shows thin-film interference of monochromatic light from a simple double-film consisting of a layer of oil floating on water.

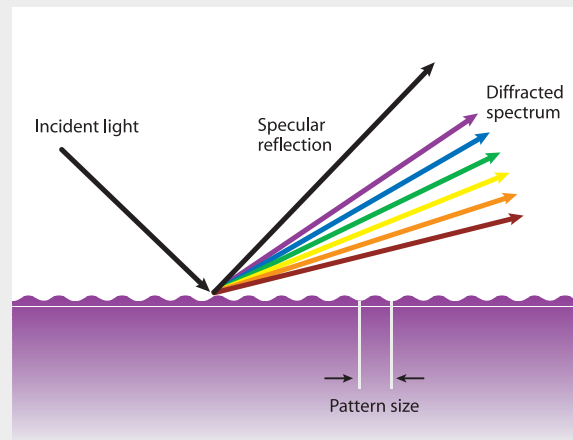
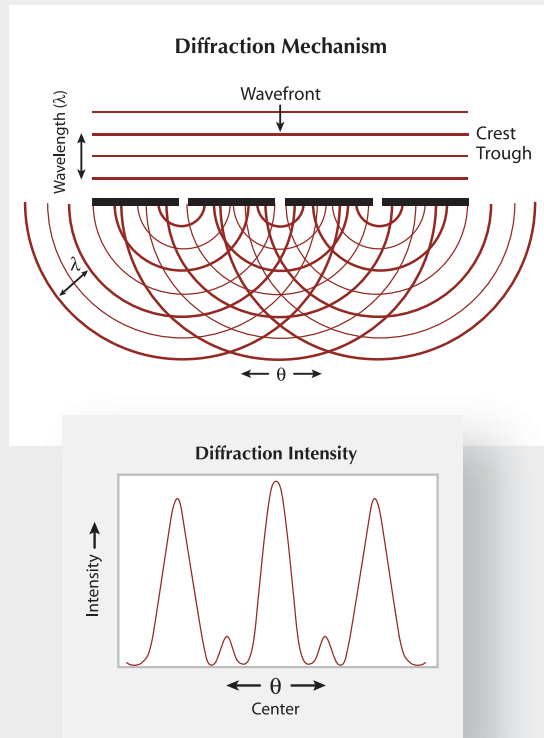


Figure A-2. The effect of wave interference caused by diffraction on multiple slits is shown here (top left) along with the associated approximate diffraction intensity (bottom left). The waves are bent and spread (diffracted) on passing through the slits, and the resulting waves interfere with one another. Although shown here at a single wavelength, the diffraction of white light would project a rainbow pattern. Diffraction created by the reflection of white light off a patterned surface also can show a rainbow pattern (top right).

German physicist Max von Laue suggested in 1912 that molecules in crystalline substances could be used as diffraction gratings. He found that X-rays were reflected and scattered from the individual atoms distributed in equally spaced lattice planes and that the reflected and scattered waves would constructively and destructively interfere to create X-ray diffraction patterns (see, e.g., Diehl and Herres, 2004). Based on Laue's findings, English physicists W. H. Bragg and his son W. L. Bragg explained why the cleavage faces of crystals appear to reflect X-ray beams at certain angles of incidence. The Bragg equation describes at what angles X-rays will be most efficiently diffracted by a crystal when the X-ray wavelength and atomic distance are known (Diehl and Herres, 2004).

Both Bragg's law and diffraction can be used to explain play-of-color in opal, where light beams are diffracted from opposite sides of very small, regularly arranged spheres with diameters of 150–400 nm (Fritsch and Rossman, 1988; Townsend, 2001). Bragg's law can also be applied to the theory of diffraction gratings. The atoms of a crystalline substance and the spheres in opal are very often represented as *layers* to explain the Bragg law of diffraction, since they are equally and regularly spaced. Such diagrams are unfortunately confusing, since they often appear identical to figures explaining thin-film interference phenomena. Again, it must be emphasized that diffraction does not take place on the layers themselves, but rather on individual atoms or spheres.

In gem materials, "pure" diffraction-related interference of light likely is limited to opals showing play-of-color, since the opal structure behaves much like a crystalline structure consisting of tiny atoms: The size of the atoms (approximately equal to X-ray wavelengths) allows diffraction of X-rays, while the size of the opal spheres (approximately equal to the wavelength of visible light) allows diffraction of visible light.

The effect of a multilayer substance such as "spectrolite" feldspar (labradorite) on light has been described as a diffraction effect by certain authors (e.g., Fritsch and Rossman, 1988) and these authors also limited the term *thin-film interference* to a simple double-film (as in iris quartz) such as shown in figure A-1. In the opinion of the present authors, double-layer and multilayer effects both represent thin-film interference phenomena, with the multilayers being more complex than the simple double-layers (see Hirayama et al., 2000).

Therefore, we conclude that the phenomenon of iridescence in gem materials is always an interference phenomenon; the only difference is whether the interference is caused by thin-film interference or by diffraction. Thus, there are gems with iridescence caused purely by thin-film interference (e.g., iris quartz); others with diffraction-related interference (e.g., diffraction of visible light in opal); and still others where dominant thin-film interference combined with some diffraction occurs, as in the Japanese Rainbow andradite described in this article.

all faces. The iridescence on the {110} faces likely is caused by thin-film interference from the straight lamellae, which have a separation of 100–1000 nm. The wavy lamellae, with a spacing of 40  $\mu\text{m}$ , cannot produce iridescence by thin-film interference, and therefore possibly act similar to a diffraction grating. The combination of these two optical effects creates the striking iridescence observed in this Rainbow andradite, which can rival the phenomenal colors of the finest “spectrolite” feldspar (labradorite) from Finland. In some cases, these stones may resemble brown opals from Ethiopia. Due to the prohibition of further garnet recovery by the local authorities from Tenkawa village, the material is slowly becoming scarce in the market but samples can still be seen,

especially on the Internet. Future availability of this attractive garnet will thus solely depend on the local authorities in Japan.

#### ABOUT THE AUTHORS

At the time this article was prepared, Mr. Hainschwang ([thainschwang@yahoo.com](mailto:thainschwang@yahoo.com)) was research gemologist, and Mr. Notari was research manager, at GIA GemTechLab in Geneva, Switzerland.

ACKNOWLEDGMENTS: The authors are grateful to Dr. Emmanuel Fritsch (Institut des Matériaux Jean Rouxel, Nantes, France) for SEM analysis and fruitful discussions, and to Yuichi Sakon (Hokkaido, Japan) for supplying photos and information on the mining and geology of the garnet deposit.

## REFERENCES

- Akizuki M., Nakai H., Suzuki T. (1984) Origin of iridescence in grandite garnet. *American Mineralogist*, Vol. 69, pp. 896–901.
- Bader M.A., Akizuki M. (1997) Iridescent andradite garnet from the Sierra Madre Mountains, Sonora, Mexico. *Neues Jahrbuch für Mineralogie, Monatshefte*, Vol. 12, pp. 529–539.
- Boehm E. (2006) Gem News International: Update on iridescent andradite from Mexico. *Gems & Gemology*, Vol. 42, No. 2, pp. 170–171.
- Born M., Wolf E. (1999) *Principles of Optics: Electromagnetic Theory of Propagation, Interference and Diffraction of Light*, 7th ed. Cambridge University Press, Cambridge, UK, 952 pp.
- Burger F. (2005) Gems in the parking lot. *Lapidary Journal*, Vol. 59, No. 2, pp. 80–82.
- Diehl R., Herres N. (2004) X-ray fingerprinting routine for cut diamonds. *Gems & Gemology*, Vol. 40, No. 1, pp. 40–57.
- Fengming H., Zonghui C., Hua T., Ying Z., Ziqi Z., Mingxing Y. (2004) The microstructure of the shell and cultured blister pearls of *Pteira penguin* from Sanya, Hainan, China. *Journal of Gemmology*, Vol. 29, No. 1, pp. 37–47.
- Fritsch E., Rossman G.R. (1988) An update on color in gems. Part 3: Colors caused by band gaps and physical phenomena. *Gems & Gemology*, Vol. 24, No. 2, pp. 81–102.
- Hirayama H., Kaneda K., Yamashita H., Monden Y. (2000) An accurate illumination model for objects coated with multilayer films. In A. de Sousa and J. Torres, Eds., *Eurographics 2000 Short Presentations*, Interlaken, Switzerland, August 20–25, pp. 145–150.
- Ingerson E., Barksdale J.D. (1943) Iridescent garnet from the Adelaide mining district, Nevada. *American Mineralogist*, Vol. 28, No. 5, pp. 303–312.
- Iwase E., Matsumoto K., Shimoyama I. (2004) The structural-color based on the mechanism of butterfly wing coloring for wide viewing angle reflective display. 17th IEEE International Conference on Micro Electro Mechanical Systems (MEMS '04), Maastricht, The Netherlands, Jan. 25–29, [www.leopard.t.u-tokyo.ac.jp/PDF/iwase3.pdf](http://www.leopard.t.u-tokyo.ac.jp/PDF/iwase3.pdf) [date accessed: 01/05/06].
- Koivula J.I., Ed. (1987) Gem News: Iridescent andradite garnets. *Gems & Gemology*, Vol. 23, No. 3, pp. 173–174.
- Koivula J.I., Kammerling R.C., Eds. (1988) Gem News: More on Mexican andradite. *Gems & Gemology*, Vol. 24, No. 3, pp. 120–121.
- Liu Y., Shigley J.E., Hurwit K.N. (1999) Iridescent color of a shell of the mollusk *Pinctada margaritifera* caused by diffraction. *Optics Express*, Vol. 4, No. 5, pp. 177–182.
- Manning P.G. (1967) The optical absorption spectra of some andradite and the identification of the  ${}^6\text{A}_1 \rightarrow {}^4\text{A}_1$   ${}^4\text{E}(\text{G})$  transition in octahedrally bonded  $\text{Fe}^{3+}$ . *Canadian Journal of Earth Sciences*, Vol. 4, pp. 1039–1047.
- Mathieu J.P., Kastler A., Fleury P. (1991) *Dictionnaire de Physique*, 3rd ed. Masson et Eyrolles, Paris.
- Newport Corp. (2006) Diffraction gratings. [www.newport.com/Diffraction%20Gratings/1/productmain.aspx](http://www.newport.com/Diffraction%20Gratings/1/productmain.aspx) [date accessed: 12/12/05].
- Shimobayashi N., Miyake A., Seto Y. (2005) Rainbow garnet from Tenkawa village in Nara. *Gemmology*, Vol. 36, No. 435, pp. 4–7 [in Japanese with English insert].
- Tada H., Mann S.E., Miaoulis I.N., Wong P.Y. (1999) Effects of a butterfly scale microstructure on the iridescent color observed at different angles. *Optics Express*, Vol. 5, No. 4, pp. 87–92.
- Takeuchi M. (1996) Geology of the Sanbagawa, Chichibu and Shimanto belts in the Kii Peninsula; Yoshino area in Nara Prefecture and Kushidagawa area in Mie Prefecture. *Chishitsu Chosajo Geppo*, Vol. 47, No. 4, pp. 223–244 [in Japanese].
- Tan T.L., Wong D., Lee P. (2004) Iridescence of a shell of mollusk *Haliotis glabra*. *Optics Express*, Vol. 12, No. 20, pp. 4847–4854.
- Townsend I. J. (2001) The geology of Australian opal deposits. *Australian Gemmologist*, Vol. 21, pp. 34–37.
- Vukusic P., Sambles J.R., Lawrence C.R., Wootton R.J. (1999) Quantified interference and diffraction in single *Morpho* butterfly scales. *Proceedings of the Royal Society B*, Vol. 266, pp. 1403–1411.

### Spring 1999

The Identification of Zachery-Treated Turquoise  
Russian Hydrothermal Synthetic Rubies and Sapphires  
The Separation of Natural from Synthetic Colorless Sapphire

### Summer 1999

On the Identification of Emerald Filling Substances  
Sapphire and Garnet from Kalalani, Tanzania  
Russian Synthetic Ametrine

### Fall 1999—Special Issue

Special Symposium Proceedings Issue, including:  
Observations on GE-Processed Diamonds,  
Abstracts of Featured Speakers, Panel  
Sessions, War Rooms, and Poster Sessions

### Winter 1999

Classifying Emerald Clarity Enhancement at the GIA  
Gem Trade Laboratory

Clues to the Process Used by General Electric to Enhance  
the GE POL Diamonds

Diopside Needles as Inclusions in Demantoid Garnet from Russia  
Garnets from Madagascar with a Color Change of  
Blue-Green to Purple

### Spring 2000

Burmese Jade  
Lapis Lazuli from Chile  
Spectroscopic Evidence of GE POL Diamonds  
Chromium-Bearing Taaffeites

### Summer 2000

Characteristics of Nuclei in Chinese Freshwater Cultured Pearls  
Afghan Ruby and Sapphire  
Yellow to Green HPHT-Treated Diamonds  
New Lasering Technique for Diamond  
New Oved Filling Material for Diamonds

### Fall 2000

GE POL Diamonds: Before and After  
Sapphires from Northern Madagascar  
Pre-Columbian Gems from Antigua  
Gem-Quality Hatiyne from Germany

### Winter 2000—Special Issue

Gem Localities of the 1990s  
Enhancement and Detection in the 1990s  
Synthetics in the 1990s  
Technological Developments in the 1990s  
Jewelry of the 1990s

### Spring 2001

Ammolite from Southern Alberta, Canada  
Discovery and Mining of the Argyle Diamond Deposit, Australia  
Hydrothermal Synthetic Red Beryl

### Summer 2001

The Current Status of Chinese Freshwater Cultured Pearls  
Characteristics of Natural-Color and Heat-Treated  
“Golden” South Sea Cultured Pearls  
A New Method for Imitating Asterism

### Fall 2001

Modeling the Appearance of the Round Brilliant  
Cut Diamond: Fire  
Pyrope from the Dora Maira Massif, Italy  
Jeremejevitte: A Gemological Update

### Winter 2001

An Update on “Paraíba” Tourmaline from Brazil  
Spessartine Garnet from San Diego County, California  
Pink to Pinkish Orange Malaya Garnets from  
Bekily, Madagascar  
“Voices of the Earth”: Transcending the Traditional in  
Lapidary Arts

### Spring 2002—Special Issue

The Ultimate Gemologist: Richard T. Liddicoat  
Portable Instruments and Tips on Practical Gemology in the Field  
Liddicoatite Tourmaline from Madagascar  
Star of the South: A Historic 128 ct Diamond

### Summer 2002

Characterization and Grading of Natural-Color Pink Diamonds  
New Chromium- and Vanadium-Bearing Garnets from  
Tranoroa, Madagascar  
Update on the Identification of Treated “Golden” South  
Sea Cultured Pearls

### Fall 2002

Diamonds in Canada  
“Diffusion Ruby” Proves to Be Synthetic Ruby Overgrowth  
on Natural Corundum

### Winter 2002

Chart of Commercially Available Gem Treatments  
Gemesis Laboratory-Created Diamonds  
Legal Protection for Proprietary Diamond Cuts  
Rhodizite-Londonite from the Antsongombato Pegmatite,  
Central Madagascar

### Spring 2003

Photomicrography for Gemologists  
Poudretteite: A Rare Gem from Mogok  
Grandidierite from Sri Lanka

### Summer 2003

Beryllium Diffusion of Ruby and Sapphire  
Seven Rare Gem Diamonds

### Fall 2003

G. Robert Crowningshield: A Legendary Gemologist  
Cause of Color in Black Diamonds from Siberia  
Obtaining U.S. Copyright Registration for the Elara Diamond

### Winter 2003

Gem-Quality CVD Synthetic Diamonds  
Pezzottaite from Madagascar: A New Gem  
Red Beryl from Utah: Review and Update

### Spring 2004

Identification of CVD-Grown Synthetic Diamonds  
Cultured Pearls from Gulf of California, Mexico  
X-Ray Fingerprinting Routine for Cut Diamonds

### Summer 2004

Gem Treatment Disclosure and U.S. Law  
Lab-Grown Colored Diamonds from Chatham  
The 3543 cm<sup>-1</sup> Band in Amethyst Identification

### Fall 2004

Grading Cut Quality of Round Brilliant Diamonds  
Amethyst from Four Peaks, Arizona

### Winter 2004

Creation of a Suite of Peridot Jewelry: From the Himalayas  
to Fifth Avenue  
An Updated Chart on HPHT-Grown Synthetic Diamonds  
A New Method for Detecting Beryllium Diffusion—  
Treated Sapphires (LIBS)

### Spring 2005

Treated-Color Pink-to-Red Diamonds from Lucent Diamonds Inc.  
A Gemological Study of a Collection of Chameleon Diamonds  
Coated Pink Diamond: A Cautionary Tale

### Summer 2005

Characterization and Grading of Natural-Color Yellow Diamonds  
Emeralds from the Kafubu Area, Zambia  
Mt. Mica: A Renaissance in Maine's Gem  
Tourmaline Production

### Fall 2005

A Review of the Political and Economic Forces Shaping  
Today's Diamond Industry  
Experimental CVD Synthetic Diamonds from LIMHP-  
CNRS, France  
Inclusions in Transparent Gem Rhodonite from  
Broken Hill, New South Wales, Australia

### Winter 2005

A Gemological Pioneer: Dr. Edward J. Gübelin  
Characterization of the New Malossi Hydrothermal  
Synthetic Emerald

# 70 PLUS Years of GEMS & GEMOLOGY The Quarterly Journal That Lasts A Lifetime



Fall 2003



Winter 2003



Fall 2005



Winter 2005



Spring 2003



Summer 2003



Spring 2005



Summer 2005



Fall 2002



Winter 2002



Fall 2004



Winter 2004



Spring 2002/Special Issue



Summer 2002



Spring 2004



Summer 2004

## Order Your BACK ISSUES Today!

E-Mail: [gandg@gia.edu](mailto:gandg@gia.edu) or visit [www.gia.edu](http://www.gia.edu)

Call Toll Free 800-421-7250 ext. 7142

or 760-603-4000 ext. 7142

Fax: 760-603-4595 or Write: G&G Subscriptions, P.O. Box 9022,

Carlsbad, CA 92018-9022 USA

	U.S.	Canada	International
Single Issues	\$ 12 ea.	\$ 15 ea.	\$ 18 ea.
Complete Volumes*			
1991–2005	\$ 40 ea.	\$ 48 ea.	\$ 60 ea.
Three-year set	\$ 115 ea.	\$ 135 ea.	\$ 170 ea.
Five-year set	\$ 190 ea.	\$ 220 ea.	\$ 280 ea.

\*10% discount for GIA Alumni and active GIA students.

Some issues from 1981–1998 are also available. Please call or visit our website for details on these and the 2006 issues as they are published.

Limited Quantities Available.

2006

# LAB NOTES

## EDITORS

Thomas M. Moses  
Shane F. McClure  
GIA Laboratory

### Lizards in IMITATION AMBER

As the saying goes, “When it rains, it pours.” In this case, it’s pouring lizards. Recently, not one but two items resembling lizards trapped in amber were submitted to the West Coast laboratory for identification reports (figure 1). Although we occasionally see specimens with insects or animals enclosed in amber or amber imitations (i.e., plastic or copal), it is unusual to have two such pieces submitted within days of each other. Having both samples in the laboratory at the same time offered a special opportunity to examine the similarities and differences between two potentially rare specimens.

The first sample ( $58.14 \times 35.75 \times 24.41$  mm; figure 1, left) contained a

badly decomposed lizard with a broken tail and one foot missing. Microscopic examination between crossed polarizers revealed a narrow strain zone surrounding the lizard’s body. Gas bubbles and bits of fiber were also present, but these were inconclusive for determining whether the host material was amber, copal, or plastic. A spot refractive index (R.I.) reading of 1.55 was obtained—a bit high for amber, but still inconclusive. The fluorescence was chalky greenish yellow to both long- and short-wave ultraviolet (UV) radiation, which was also not conclusive. The hydrostatic specific gravity (S.G.) was  $\sim 1.18$ . For confirmation, the piece was placed in a saturated saline solution (S.G. = 1.13). It was observed to sink at a rate that was consistent

with an S.G. of  $\sim 1.18$ – $1.20$ . However, since the presence of the lizard would affect the S.G. of the specimen, further testing was necessary.

The separation of amber from plastic or copal is gemologically challenging, because the easiest and most reliable tests are destructive. Therefore, we decided first to analyze the sample with our Raman system using excitation from a 785 nm diode laser. The 785 nm laser is useful because it eliminates many problems related to sample fluorescence. The resulting Raman spectrum (figure 2) indicated that the specimen was neither amber nor copal, but rather a polystyrene plastic. All the gemological properties reported above were consistent with polystyrene. After consultation with

*Figure 1. These two specimens proved to be imitations of amber with lizards enclosed. On the left, the lizard was encased in polystyrene; the sample on the right was an assembled piece consisting of a copal base, a plastic top, and a lizard molded between them.*



the client, we tested a small area with a hot point: The acrid odor confirmed our identification.

The second sample (74.5 × 31.9 × 25.32 mm; figure 1, right) was more easily identified than the first. The lizard was in much better condition, having undergone markedly less decomposition. Using magnification and reflected light, we saw a separation plane between the part of the sample below the lizard and the part above, clearly indicating that the specimen had been assembled. Microscopic observation also revealed numerous gas bubbles concentrated along this separation plane. The base of the specimen contained clouds, fractures, and various particles, whereas the upper portion showed a wide strain pattern, flow lines, and gas bubbles around the lizard's body. The R.I. was 1.54 for the lower portion and 1.57 for the upper part. Both halves showed chalky greenish yellow to yellow UV fluorescence, but the lower half showed slightly stronger fluorescence when exposed to long-wave UV.

When the second sample was immersed in the saturated saline solution, it floated with the base up, suggesting an S.G. of ~1.10 for that portion—enough to flip the piece over, but not to sink it. The base had been left rough and pitted, providing a surface on which to conduct hot point and acetone tests where small blemishes would not be noticeable. When the pitted surface was exposed to heat, the odor was resinous and consistent with either amber or copal. Application of acetone to a small area of the base softened the material and left the area slightly etched, a reaction consistent with copal (amber would not be affected). Both the top and bot-

*Editor's note: All items are written by staff members of the GIA Laboratory, East Coast (New York City) and West Coast (Carlsbad, California).*

GEMS & GEMOLOGY, Vol. 42, No. 4, pp. 260–267  
© 2006 Gemological Institute of America

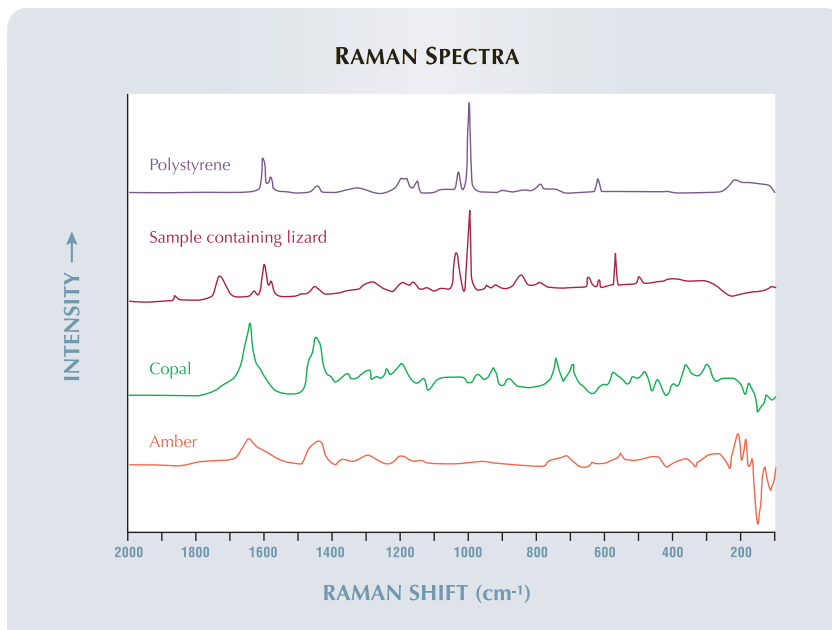


Figure 2. Raman spectroscopy (785 nm excitation) was effective in identifying the material encasing the lizard in figure 1 (left) as polystyrene. Note, however, that the spectra of amber and copal are too similar for this technique to conclusively separate those two materials.

tom parts were analyzed using the 785 nm Raman system for comparison to the first sample. The spectrum for the lower half of the piece indicated amber or copal, whereas the spectrum from the upper half did not match amber, copal, or polystyrene. The R.I., S.G., Raman spectrum, and microscopic features were consistent with a plastic top, but not with polystyrene specifically. Thus, our final conclusion was that this second piece was an assembled specimen consisting of a copal base, a plastic top, and a lizard molded between.

These two items illustrate some of the means and materials that can be used to create imitations of creatures preserved in amber (see the Winter 2005 Gem News International, pp. 361–362, for yet another example). These circumstances also illustrate the ongoing quest of gemological laboratories to develop new and effective nondestructive testing methods to supplement or replace traditional destructive tests.

Kimberly Rockwell

### Large DEMANTOID of Exceptional Color

Recently, the East Coast laboratory received the 5.82 ct transparent green round-brilliant-cut stone in figure 3 for identification. Standard gemological properties (R.I. = OTL, singly

Figure 3. This 5.82 ct demantoid garnet is notable for its exceptional color and size, as well as its unusual pattern of inclusions.





Figure 4. The demantoid in figure 3 contained striking inclusions composed of randomly oriented curved fibers encircled by small, bright, disc-like features. Magnified 50 $\times$ .

refractive, moderate dispersion, S.G. = 3.84, and chrome lines and a 470 nm cutoff seen with the desk-model spectroscopy) identified the gem as a demantoid garnet.

The classic Russian demantoids are famous for their easily observed "horsetail" inclusions—golden yellow curved needles radiating from a point like the tail of a horse. These needles were originally believed to be the asbestiform amphibole byssolite but more recently have been identified as chrysotile (see W. R. Phillips and A. S. Talantsev, "Russian demantoid, czar of the garnet family," Summer 1996 *Gems & Gemology*, pp. 100–111; M. O'Donoghue, *Gems*, Butterworth-Heinemann, Oxford, England, 2006, p. 209). Microscopic examination of this stone revealed needles in a random orientation, as has been observed in some demantoids from a few of the newer Russian localities. Also present were bright disc-like inclusions along the curved needles (figure 4), which gave the

inclusion scene an exotic appearance.

The combination of the stone's relatively large size and strong color saturation was also unusual, as most fine demantoids are less than one carat or, if larger, often have more yellow in the bodycolor. The owner of the stone, Isaac Aharoni of Isaac Aharoni Inc., New York, reported that he purchased it in Russia. This was the second large demantoid garnet we have seen recently, as we also identified a 3.20 ct demantoid for Mr. Aharoni.

Wendi M. Mayerson

## DIAMOND

### Unusually Large Fancy White Diamond with Whitish Banding

Diamonds occasionally contain submicroscopic inclusions, which usually induce a brownish or grayish color appearance and can have a negative impact on clarity. In rare cases, these tiny inclusions can produce a translu-

cent milky "white" color by scattering light that passes through the stone (see E. Fritsch and K. Scarratt, "Gemmological properties of type Ia diamonds with an unusually high hydrogen content," *Journal of Gemmology*, Vol. 23, No. 8, 1993, pp. 451–460; Summer 2000 Lab Notes, p. 156; and the article by J. M. King et al. on pp. 206–220 of this issue). Such was the case with the unusually large (30.87 ct) diamond in figure 5, which was recently examined by the East Coast laboratory.

This Fancy white pear modified brilliant measured 27.96  $\times$  15.91  $\times$  11.53 mm and was submitted for a Colored Diamond Identification and Origin Report. The diamond fluoresced strong blue to long-wave UV radiation and moderate-to-strong blue to short-wave UV. When the short-wave UV lamp was turned off, it phosphoresced weak blue for more than 30 seconds. No absorption lines were visible with a desk-model spectroscope, and the absorption spectrum in the mid-infrared region revealed that it was a nearly pure type IaB diamond with a very high concentration of nitrogen. These properties, except for the unusual phosphorescence, are typical for type IaB Fancy white diamonds (again, see the Summer 2000 Lab Note). Strong absorption peaks were also present at 3105 and 1405  $\text{cm}^{-1}$ , caused by structurally bonded hydrogen, a common feature of cloud-bearing diamonds (again, see Fritsch and Scarratt, 1993).

In addition to its size, an unusual feature of this diamond was the occurrence of straight whitish banding observed throughout the entire stone (figure 6). In the overwhelming majority of instances, whitish graininess caused by submicroscopic inclusions is part of the growth structure and results in a homogenous, milky appearance. The strong banding of the submicroscopic inclusions, which is undoubtedly the cause of the white coloration, is something we have only rarely observed in other type IaB Fancy white diamonds (see Spring



Figure 5. The color of this 30.87 ct Fancy white diamond is due to milky bands of submicroscopic inclusions. Also present are numerous partially graphitized stress fractures.



Figure 6. The submicroscopic inclusions in the diamond in figure 5 are concentrated in bands, something that is rarely seen in Fancy white diamonds. Magnified 15 $\times$ .

1992 Gem News, p. 58). Also visible internally were many rounded crystals, surrounded by partially graphitized stress fractures (again, see figures 5 and 6). However, it is the large size and the unusual color and banding throughout the stone that make this diamond special.

*HyeJin Jang-Green*

### Prolonged Change of Color in Pink Diamond

Change of color in diamonds occurs most frequently in “chameleon” diamonds, which are predominantly greenish yellow to yellowish green in ambient conditions but change to predominantly brownish or orangy yellow after gentle heating or prolonged storage in the dark. In rare instances, however, some diamonds have been known to change color temporarily when cryogenically cooled or exposed to ultraviolet radiation.

The East Coast laboratory recently received a 0.84 ct pink diamond for color grading. As is typical of type Ia pink diamonds, it exhibited obvious pink graining and moderate green transmission luminescence when

viewed with magnification. It fluoresced strong blue to long-wave UV radiation and weaker blue to short-wave UV. The exposure to UV radiation resulted in an obvious change in apparent color from Fancy Deep pink to Fancy Deep orangy pink (figure 7; we were not able to determine whether the change resulted from long- or short-wave UV).

Although the lab has reported on a few similar stones in recent years (see Summer 2002 Lab Notes, pp. 165–166; Winter 2005 Lab Notes, pp. 342–344), the color change has always been temporary, with the diamond reverting to its stable color in a matter of a few seconds to a few hours in normal lighting. Thus, we were surprised to see that this particular diamond retained its orangy pink color for approximately two weeks.

Mindful of the time constraints on lab report services, we attempted to accelerate the return of the pink stable color state. Gentle heating with an alcohol flame, the technique typically used to induce a color change in chameleon diamonds, had no apparent effect. We then cooled the diamond by immersing it in liquid nitrogen, which produced a minimal color shift toward pink. Repeated immersions—or perhaps simply the passage of time—eventually restored the original deep pink color.

Figure 7. The 0.84 ct Fancy Deep pink diamond on the left changed to Fancy Deep orangy pink after exposure to UV radiation (right). Unlike similar diamonds seen by the lab in the past, this change of color persisted for about two weeks.



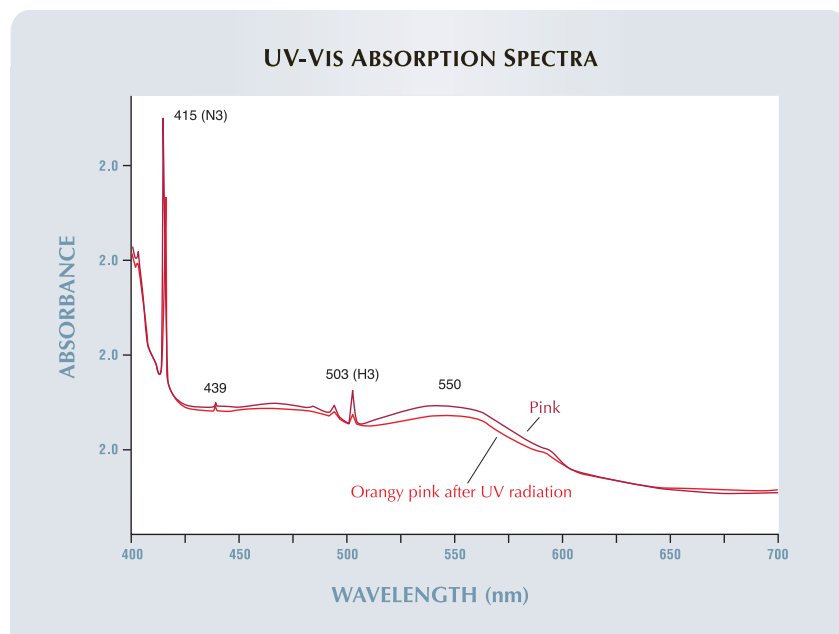


Figure 8. UV-Vis spectroscopy performed on the diamond in figure 7 in both stable and unstable color states showed a decrease in the 550 nm band that is responsible for the pink color of natural pink diamonds.

UV-visible spectroscopy performed during both color states showed the broad band at 550 nm that is typically responsible for natural pink color (figure 8; also see the Winter 2005 Lab Note). Exposure to UV radiation caused a decrease in the intensity of this band, resulting in a transmission window in the orange region and an apparent orangy pink color in the diamond. However, we were not able to determine why the orangy pink color had such a prolonged duration.

It was later suggested by the client that moderate heating of this diamond might result in a shift toward purple, as it had “turned purple” during recutting. Under nonlaboratory conditions in the client’s office and with the client’s assistance, we were able to heat the diamond using an electric coil hot plate. Although an accurate fancy-color grade could not be established without using the lab’s standard viewing environment and procedures, we were indeed able to dis-

cern a shift toward purplish pink. This change of color, however, lasted only a few minutes. Advanced

testing was not possible off site, so we could not obtain comparable UV-Vis spectral data.

Although change of color in diamond as a result of exposure to UV radiation is not a new phenomenon, this stone’s two-week sustained change is particularly noteworthy.

*Siau Fung Yeung and Wuyi Wang*

### Strand of Natural Nacreous and Non-nacreous PEARLS

The East Coast laboratory recently received for identification a graduated strand of 105 round to near-round colored pearls ranging from 2.35 to 5.90 mm (figure 9). From their worn condition, all appeared to be fairly old.

Most of the pearls in the strand were non-nacreous and a variegated brown (often modified by orange, red, or purple) in color. These pearls were somewhat worn, and a number of them had a dried-out appearance; some were cracked or even broken. As explained in a Fall 2005 Gem News International entry (p. 267),

Figure 9. This unusual strand proved to be comprised of non-nacreous pen shell and clam pearls, as well as natural saltwater pearls.





Figure 10. With 90× magnification, the columnar crystalline growth structure of one of the pen shell pearls is visible on this broken surface.

such deterioration is typical of the non-nacreous pearls from pen shell mollusks. The surfaces of these pearls also showed an unusual interlocking crystalline pattern similar to that seen on the non-nacreous pen shell products (E. Strack, *Pearls*, Ruhle-Diebner-Verlag, Stuttgart, Germany, 2006).

Spaced between the brown non-nacreous pearls were eight other porcelaneous pearls ranging from white to yellowish orange and pink, which exhibited varying degrees of color saturation and flame structure. Based on their distinctive structure, these appeared to be giant clam pearls from *Tridacna gigas*.

Finally, there were six white-to-“cream” colored nacreous pearls. These pearls exhibited good luster, various overtone colors, and a platelet-layered nacre structure, all characteristics consistent with natural saltwater pearls.

An X-radiograph revealed natural growth structures in all the pearls. The pen shell pearls displayed a columnar crystalline growth structure, which was also visible with magnification where one was broken

(figure 10), while the clam pearls and nacreous pearls revealed either no visible structure or a layered concentric growth structure typical of those pearl types.

Exposure to long-wave UV radiation produced varied reactions. The pen shell pearls displayed fluorescence ranging from weak-to-strong chalky red and orangy red. The clam pearls displayed moderate pink and yellow fluorescence with some chalkiness as well. The nacreous pearls displayed no fluorescence when exposed to X-rays. Each of these reactions was consistent with the apparent pearl type.

It is quite uncommon to see a strand composed of a combination of natural nacreous and non-nacreous pearls from three different types of mollusks, and this proved an interesting identification exercise.

Akira Hyatt

*[Editors' note: Though past G&G and GIA Laboratory style has been to place quotation marks around the word pearl when referring to non-nacreous pearls, the decision has been made to discontinue this practice.]*

Figure 11. This 3.90 ct poudretteite (9.45 × 10.04 × 6.58 mm) is the first ever submitted to the GIA lab (face-up, left). Eye-visible orange-yellow epigenetic staining is present in both “fingerprints” and needle-like growth/etch tubes (pavilion up, right).



## POUDRETTEITE

The East Coast laboratory received a 3.90 ct transparent light purplish pink pear mixed cut for identification (figure 11). Standard gemological properties showed it to be a doubly refractive uniaxial gemstone with refractive indices of 1.515–1.535 and a hydrostatic S.G. of 2.50. Microscopic examination revealed needle-like growth/etch tubes of varying thickness, many with orange-yellow epigenetic staining; some “fingerprints” showed similar staining (figure 11, right). A two-phase (liquid-gas) inclusion was also present. The stone showed moderate pinkish purple and blue-green pleochroism. It was inert to long-wave UV radiation, but showed a very weak yellow reaction to short-wave. These properties were not a match to any gemstone found in the GIA Lab Manual, so we turned to more advanced testing. Raman spectroscopy confirmed that the stone was a faceted example of the mineral poudretteite.

Discovered in the mid-1960s, but not recognized as a new mineral by the International Mineralogical Association until 1986 (C. P. Smith et al., “Poudretteite: A rare gem species from the Mogok Valley,” Spring 2003 *Gems*

*Gemology*, pp. 24–31), poudretteite is extremely rare. The first seven crystals, named after the family who owned and operated the quarry in Mont Saint-Hilaire, Quebec, where they were found, were quite small—the longest measured just 5 mm. A comprehensive study of a 3.00 ct poudretteite purchased in Myanmar's Mogok Valley in 2000 was published in the Spring 2003 *Gems & Gemology* (again, see Smith et al.). The properties of the stone we examined were consistent with those described by Smith et al. This is the first poudretteite submitted to the GIA Laboratory for an identification report.

Wendi M. Mayerson

### Unusual Gem PYROXMANGITE

Pyroxmangite is another gem material for which basic gemological techniques are inadequate to assign a specific identification. It is difficult to distinguish from other similar minerals, in particular rhodonite, without advanced techniques. Pyroxmangite usually forms in metamorphosed manganese ore deposits and other manganese-rich rocks and minerals. It is found in Japan, Broken Hill, New South Wales, Australia; Minas Gerais, Brazil; and Colorado, among other localities. It is usually closely associated with rhodonite (J. W. Anthony et al., *Handbook of Mineralogy*, Vol. 2, Mineral Data Publishing, Tucson, Arizona, 2003). Because it is typically massive and polycrystalline, and it may be intergrown with rhodonite, facet-quality material is rare.

The East Coast laboratory recently received one faceted specimen, a transparent red 0.68 ct modified lozenge step cut measuring  $6.53 \times 4.87 \times 3.07$  mm (figure 12). It had refractive indices ranging from 1.728 to 1.743, with strong purplish red to strong orangy red pleochroism and an S.G. of 3.71. Examination with a microscope using up to  $60\times$  magnification revealed large two-phase inclusions and whitish tubules containing a dark gray to black material. Two directions



Figure 12. This 0.68 ct modified lozenge step cut proved to be a rare faceted example of pyroxmangite.

of cleavage were visible at the surface along with a few cavities, and the stone took only a moderate polish. With a desk-model spectroscope, we observed a strong band at 410–420 nm, a sharp line at 503 nm, and a broad band at 540–560 nm, indicative of a high manganese content.

We were able to measure the refractive indices and specific gravity with enough precision to narrow the

possible identification to either pyroxmangite or rhodonite (table 1). Unfortunately, chemical and spectroscopic analyses are not useful in separating these two minerals, because their chemical compositions and spectral characteristics are so similar. Both belong to a group of minerals called  $(\text{Ca},\text{Mn})\text{SiO}_3$  pyroxenoids. These pyroxenoids (which include rhodonite, ferrosilite III, wollastonite, busamite, and the pyroxmangite-pyroxferroite series) are part of a larger group of minerals called chain silicates, because their basic structure comprises chains of silica tetrahedra  $(\text{SiO}_4)$ . Differing amounts of Ca, Mn, Mg, and Fe result in different minerals with slightly different chain lengths, and these slight variations in crystal structure allow the separation of pyroxmangite from rhodonite using a technique developed in the early 20th century, powder X-ray diffraction (XRD) analysis.

Powder X-ray diffraction can distinguish two minerals with very similar crystal structures by determining

TABLE 1. Properties of rhodonite and pyroxmangite.<sup>a</sup>

Property	Rhodonite	Pyroxmangite
Formula	$(\text{Mn},\text{Fe},\text{Mg},\text{Ca})\text{SiO}_3$	$\text{MnSiO}_3^b$
Refractive indices		
$\alpha$	1.711–1.734	1.728–1.748
$\beta$	1.716–1.739	1.730–1.742
$\gamma$	1.724–1.748	1.746–1.758
Optic character	Biaxial positive	Biaxial positive
Color	Pink, red, gray, yellow	Pink, red
Pleochroism	Yellowish red, pinkish red, pale yellowish red	Moderate red, purplish red, orangy red
Specific gravity	3.57–3.76	3.61–3.80
No. of $\text{SiO}_4$ per unit cell	5	7
XRD pattern		
Spacing in Å (Intensity)	2.772 (100) 2.980 (65) 2.924 (65) 3.14 (30) 3.34 (25) 3.10 (25) 2.651 (18)	2.967 (100) 2.188 (45) 4.73 (35) 2.630 (35) 1.422 (30) 3.47 (25) 3.04 (25)

<sup>a</sup>From J. W. Anthony et al., *Handbook of Mineralogy*, Vol. 2, Mineral Data Publishing, Tucson, Arizona, 2003). Note: Because pyroxmangite cannot be separated from rhodonite using gemological properties alone, X-ray diffraction analysis was used to compare the crystal structure of each mineral.

<sup>b</sup>Pyroxmangite frequently also contains iron, because it forms a series with pyroxferroite  $(\text{Fe},\text{Mn},\text{Ca})\text{SiO}_3$ .

the spacing and angles between the atomic planes of the crystal structure. For analysis, a very small amount of material is scraped from the girdle of a faceted stone or the base of a cabochon. X-rays are transmitted through this powdered sample, and some of the X-rays are diffracted by the crystal structure to cast a characteristic pattern of arcs on photographic film or digital imaging equipment. The pattern for an unknown sample is then compared with a library of patterns of known materials.

Comparing the XRD pattern of the submitted stone with reference patterns of pyroxmangite (with a seven-silica tetrahedral chain) and rhodonite (with a five-silica tetrahedral chain) indicated that the submitted stone had a crystal structure with a seven-silica tetrahedral chain and atomic spacing consistent with pyroxmangite (table 1).

This rare faceted pyroxmangite is a prime example of a gem that requires advanced techniques in conjunction with good gemological

testing to distinguish it from other similar minerals.

*Carolyn van der Bogert  
and Dino DeGhionno*

**PHOTO CREDITS**

*C. D. Mengason—1; Elizabeth Schrader—3, 9, and 11; Wendi Mayerson—4; Jessica Arditi—5, 7, and 12; HyeJin Jang-Green and Siau Fung Yeung—6; Akira Hyatt—10.*

The  
Dr. Edward J. Gübelin  
**MOST VALUABLE  
ARTICLE  
AWARD**

Simply tell us which three 2006  
articles you found most valuable, and  
you could win a three-year subscription to

**GEMS & GEMOLOGY.**  
PLUS FREE copies of

**GEMS & GEMOLOGY.  
IN REVIEW**  
COLORED DIAMONDS  
&  
SYNTHETIC DIAMONDS

**Vote now  
and WIN!**  
A total value  
of over **\$300!**

Mark the articles in order of preference on the ballot card between  
pages 266 & 267. Then mail the card to arrive **no later than March  
12, 2007** and it will be entered in a drawing for the grand prize.



#### EDITOR

Brendan M. Laurs (blaurs@gia.edu)

#### CONTRIBUTING EDITORS

Emmanuel Fritsch, *IMN, University of Nantes, France* (fritsch@cnrs-immn.fr)

Henry A. Hänni, *SSEF, Basel, Switzerland* (gemlab@ssef.ch)

Franck Notari, *Geneva, Switzerland* (franck.notari@bluewin.ch)

Kenneth V. G. Scarratt, *GIA Research, Bangkok, Thailand* (ken.scarratt@gia.edu)

## DIAMONDS

**Update on Diamond Trading in Sierra Leone.** During the decade-long civil war in Sierra Leone, the Revolutionary United Front (RUF) rebel army committed widespread atrocities against innocent civilians, drawing global condemnation by governments, human rights groups, and concerned citizens. The RUF was partially funded by the country's diamond resources, bringing the issue of conflict diamonds in Sierra Leone to world attention in the late 1990s. Meanwhile, similar diamond-funded conflicts were being waged in other African nations, such as

Angola and the Democratic Republic of Congo. This situation led to the Kimberley Process for certifying diamonds from mine to market, which was implemented in 2002. With the signing of the Lomé Peace Agreement between the Sierra Leone government and the RUF earlier that year, peace has returned to the country.

In August 2006, GIA Education instructor Ric Taylor traveled through the Sierra Leone diamond mining areas of Koidu, Tongo, Kenema, and Bo, some of which were once controlled by the rebels. He saw no evidence of continuing conflict, and residents and journalists in these areas confirmed that there is no desire to return to war. In the town of Koidu (figure 1), in the diamond mining district of Kono in eastern Sierra Leone, one can still see the bare walls of buildings that were looted and burned, but many others have been rebuilt and have roofs of corrugated metal or plastic sheeting. There are several large new mosques that were built with donations from Pakistan.

Once a thriving town, Koidu is still struggling to return to normal. Today, it houses an office of the Integrated Diamond Management Program (IDMP), formerly the Peace Diamond Alliance, a group organized by the U.S. Agency for International Development (USAID) in 2002 to end the role of diamonds in funding the Sierra Leone

*Figure 1. The town of Koidu, in the Kono district of eastern Sierra Leone, was at the center of the county's protracted conflict because of the area's diamond resources. Today, the residents are working to rebuild the town and the local economy. Photo by R. Taylor.*



*Editor's note: The initials at the end of each item identify the editor or contributing editor who provided it. Full names and affiliations are given for other contributors.*

*Interested contributors should send information and illustrations to Brendan Laurs at blaurs@gia.edu (e-mail), 760-603-4595 (fax), or GIA, The Robert Mouawad Campus, 5345 Armada Drive, Carlsbad, CA 92008. Original photos can be returned after consideration or publication.*

GEMS & GEMOLOGY, Vol. 42, No. 4, pp. 268–292

© 2006 Gemological Institute of America



*Figure 2. These students at the Integrated Diamond Management Program's school in Koidu are taught to grade rough diamonds by shape, clarity, color, and size. This is part of several efforts to help the miners receive fair value for their diamonds. Photo by R. Taylor.*



*Figure 3. Most diamond mining in Sierra Leone exploits alluvial deposits. Here, diamond-bearing gravels are screened by independent miners. Photo by R. Taylor.*

conflict. According to Dr. Sahr Tongu, the head of the Koidu office, the name was changed because the organization's original purpose of ending the trade in conflict diamonds in Sierra Leone was achieved. Now, the IDMP works to develop the diamond industry for the benefit of Sierra Leone's people. The organization operates a school in Koidu that trains students to grade rough diamonds (figure 2). In a two-week course, students learn to grade diamonds by shape, clarity, color, and size. Determining value, however, is much more difficult than grading, and requires at least three to five years of experience.

Fortunately, Sierra Leone's Ministry of Mineral Resources provides a valuation service for miners in Koidu, which helps them receive fair prices for their diamonds.

While most of Sierra Leone's production comes from alluvial deposits (figure 3), diamonds are also being recovered from three small kimberlite pipes in the Kono district. The major producer is Koidu Holdings, which mines the No. 1 Pipe at Koidu by open-pit methods (figure 4). Development of the mine began in 2002, with the first production in January 2004. Approximately 20,000 tonnes of kimberlite are processed each month, yielding 6,000–10,000

*Figure 4. In 2002, Koidu Holdings began mining this kimberlite in Sierra Leone (No. 1 Pipe), which today produces several thousand carats of diamonds every month. Photo by R. Taylor.*



carats, depending on grade variations within the pipe. The largest rough diamond recovered to date weighed 84 ct.

According to the Sierra Leone government's Gold and Diamond Department, there has been an increase in the annual legal export of diamonds since 2000. Official figures for 2001 were approximately 222,520 carats; by 2004, reported exports had increased to nearly 691,760 carats (figures for 2005 dropped slightly to 668,700 carats). Interestingly, the value per carat has risen dramatically. In 2001, the overall value was \$116.94/ct; by 2005 it reached \$212.26/ct. According to Frank Karefa-Smart, diamond business advisor to the IDMP, this improvement in value and total exports is due to the fact that higher-quality diamonds that were once smuggled out of the country are now exported legally.

The possession of rough diamonds is strictly controlled, and three different types of licenses are required for their handling. A mining license allows miners to dig for diamonds but not to buy them from other miners. A dealer's license is for those who buy from the miners, but it is not sufficient to export the stones; this requires an export license, which costs Sierra Leoneans US\$40,000 a year. Foreigners who purchase diamonds in Sierra Leone can export them using a local exporter's license for a fee of about 1.5% of the government-declared value.

Diamonds are evaluated for export at the Gold and Diamond Department, which assesses a 3% export tax (based on the value of the rough diamonds on the international market). The stones are then packaged and the paperwork completed according to the Kimberley Process.

Peace has been restored in Sierra Leone, and the Kimberley Process seems to have been effective in bringing Sierra Leone's diamonds into legal channels. However, further development at the mining level is an important next step in maximizing the economic benefit for the people who need it most.

Ric Taylor (rtaylor@gia.edu)  
GIA Education, Carlsbad

**Jewelry repair damages a diamond.** The SSEF Swiss Gemmological Institute recently received a mounted yellow pear-shaped diamond with a small chip on the crown (figure 5) and an associated black inclusion that was visible with a gemmological microscope. It was accompanied by a grading report that did not mention the chip or inclusion, and stated the clarity as VS<sub>1</sub>. The inconsistency of this clarity grade with such an obvious chip/inclusion suggested that these features were created after the diamond was graded. The chip was about 1.0 × 0.5 × 0.3 mm and had the appearance of a cleaved depression. An SEM image (figure 6) showed a stepped crater, with the black spot at its deepest point. The client asked us to identify the black inclusion and determine the cause of the apparent damage. This was the first time we had encountered such a feature.

Chemical analysis performed during the SEM investigation (using a detector for light elements) showed that only carbon was present in the black inclusion, and a

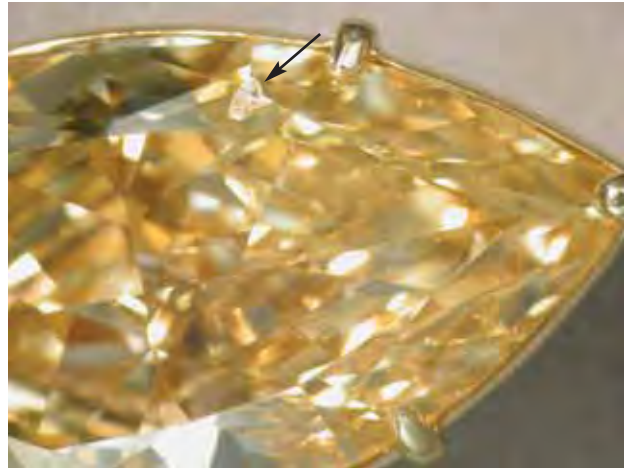
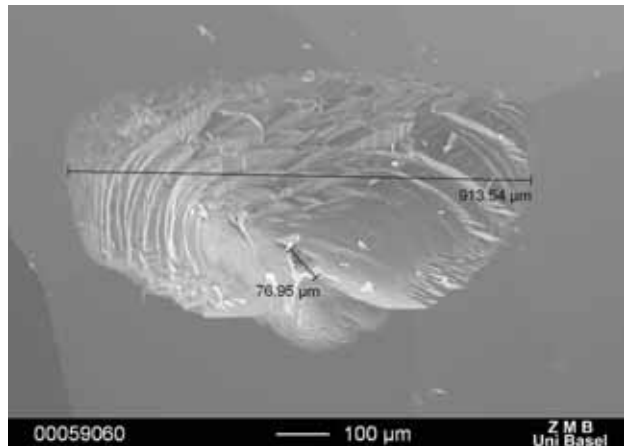


Figure 5. The chip (see arrow) on the crown of this yellow pear-shaped diamond appears to have been created by a misdirected shot from a laser soldering gun. A prong in the setting showed evidence of recent repair by laser soldering. A dark spot at the bottom of the pit was identified as graphite. Photo by H. A. Hänni; © SSEF.

Raman spectrum confirmed the presence of graphite. The association of graphite with such a crater could be explained by a pinpoint source of intense heat, causing a transformation from diamond to graphite. This would have resulted in a volume increase of ~1.6× (the density of diamond being 3.52 g/cm<sup>3</sup> vs. 2.16 g/cm<sup>3</sup> for graphite), creating sufficient expansion to cause the chip.

Careful observation of the setting revealed that one of the prongs on the pendant had recently been repaired by laser soldering. An accidental shot from a laser soldering

Figure 6. This SEM image of the chip in figure 5 shows the stepped shape of the crater walls and a small depression at the base of the pit corresponding to graphite. A phase transformation from diamond to graphite produced by the intense heat of a laser soldering gun would cause a sudden volume expansion, creating the chip. Image © SSEF/ZMB.



gun would have enough energy to cause the phase transition from diamond to graphite. This case shows that great care must be taken to avoid accidentally damaging a gemstone with a laser soldering gun.

HAH

## COLORED STONES AND ORGANIC MATERIALS

**Green augelite from Peru.** Augelite, monoclinic  $\text{Al}_2(\text{PO}_4)(\text{OH})_3$ , is a very rare collector's stone. Until now, the best specimens—yellow-green crystals up to 2 cm—came from Rapid Creek, Yukon Territory, Canada, where they formed within fractures in shales. And the only facetable material was from an historic andalusite deposit at the Champion mine, Mono County, California, which was worked during the 1920s and '30s. This site produced colorless crystals typically to 1 cm (exceptionally up to 2.5 cm), but faceted stones usually weighed a maximum of ~1 ct and were quite rare; the largest one known to this contributor is 4.00 ct (Patricia Gray, pers. comm., 2006).

However, a new source of gem-quality augelite appeared in early 2006, when druses of well-formed light green crystals up to 2 cm (exceptionally up to 5 cm) were discovered in a quartz vein at the small Ortega mine in Ancash Department, northern Peru (see T. P. Moore, "What's New in the Mineral World?" June 30 and October 27, 2006 updates at [www.minrec.org/whatsnew.asp](http://www.minrec.org/whatsnew.asp)). Reportedly, two brothers from Lima had reopened an abandoned mine in search of quartz crystals with Japan-law twinning. They were surprised to find very fine augelite at the deposit.

The augelite crystals (e.g., figure 7) are usually milky, and only small areas near the surface are facetable. The green color is inhomogeneous, so to get the best color the rough must be carefully oriented for cutting. The faceting process is also complicated by two cleavages (perfect in the {110} direction, good in the  $\{\bar{2}10\}$  direction). Gemological properties were measured on three cut stones (0.20–1.19 ct): R.I.— $n_\alpha=1.575$ ,  $n_\beta=1.576$ , and  $n_\gamma=1.590$ ; birefringence—0.015; and fluorescence—light yellow to short-wave and inert to long-wave UV radiation. In addition, three crystals were used to measure hydrostatic S.G. values of 2.69–2.70; the Mohs hardness was determined as 5.5. These properties are comparable to those reported for augelite by M. O'Donoghue (*Gems*, 6th ed., Butterworth-Heinemann, Oxford, England, 2006, p. 385). The largest cut stone seen by this contributor was 1.19 ct, but larger stones should be produced in the future.

Jaroslav Hyrsl ([hyrsl@kuryr.cz](mailto:hyrsl@kuryr.cz))  
Prague, Czech Republic

**Bicolored beryl from the Erongo Mountains, Namibia.** In mid-2006, Jo-Hannes Brunner (Pangolin Trading, Windhoek, Namibia) informed us about a new find of bicolored beryl from Namibia's Erongo Mountains. This area is famous for producing fine specimens of aquamarine, black tourmaline, jeremejevite, and other minerals (see the



Figure 7. A former quartz mine in northern Peru has produced some fine specimens of augelite; the faceted stones weigh 1.19 ct (left) and 0.94 ct (right). Photo by J. Hyrsl.

Fall 2002 GNI section, pp. 264–265 and 266–268; B. Cairncross and U. Barhmann, "Famous mineral localities: The Erongo Mountains, Namibia," *Mineralogical Record*, Vol. 37, No. 5, 2006, pp. 361–470). Only a small amount of the bicolored beryl was recovered, in early 2006, and a few stones have been cut and set into jewelry (figures 8 and 9).

Mr. Brunner donated several pieces of rough and one cut bicolored beryl to GIA for examination. The cut stone (13.68 ct; again, see figure 8) was examined by one of us (KR) and showed the following properties: color—bicolored light greenish blue and yellowish green, with a sharp demarcation between the two colors; R.I.—1.562–1.569 for the blue portion and 1.577–1.584 for the green portion; birefringence—0.007 (both colors); hydrostatic S.G.—2.68; fluo-

Figure 8. This bicolored beryl (13.68 ct) was cut from material recovered in early 2006 from the Erongo Mountains in Namibia. Gift of Jo-Hannes Brunner; GIA Collection no. 36705. Photo by Robert Weldon.





Figure 9. This necklace is set with two bicolored beryls (38 ct total weight) from the Erongo Mountains. Courtesy of Gudrun Bellwinkel, African Art Jewellers, Swakopmund, Namibia.

rescence—green portion = inert, and blue portion = inert to short-wave and very weak green to long-wave UV radiation. A weak line at 427 nm was seen in both color portions with the desk-model spectroscope. These properties are consistent with those reported for aquamarine by M. O'Donoghue (*Gems*, 6th ed., Butterworth-Heinemann, Oxford, England, 2006, pp. 162–164), except that the refractive index values in that publication are slightly higher (1.572–1.590) than those recorded for the blue portion of

Figure 10. This bicolored beryl (2.9 cm tall) from the Erongo Mountains shows bluish green and brownish orange coloration. Juergen Tron collection; photo © Jeff Scovil.



this sample. Microscopic examination revealed numerous fractures and two-phase (fluid-gas) inclusions in the blue part of the stone. The green portion was more heavily included and showed parallel growth structures, opaque inclusions, and densely spaced clusters of growth tubes.

In addition to the light greenish blue and yellowish green colors described here, the bicolored beryl may also be composed of bluish green and brownish orange portions (see figure 10 and the photo on p. 393 of Cairncross and Barhmann, 2006).

Kimberly Rockwell ([krockwell@gia.edu](mailto:krockwell@gia.edu))  
GIA Laboratory, Carlsbad

BML

**Diopside from Afghanistan.** “Olive” green and “chrome” green diopside reportedly from Badakhshan, Afghanistan, were brought to our attention by Farooq Hashmi (Intimate Gems, Jamaica, New York), who obtained the gem-quality rough while on a buying trip to Peshawar in January 2006. The two diopside varieties come from separate deposits that have been worked on an irregular basis for at least two years.

Mr. Hashmi obtained 3–4 kg of the “olive” green diopside from various parcels that totaled about 15 kg. The cobbled rough typically contained abundant inclusions, and the limited quantities of clean transparent pieces mostly weighed <3 grams each. The “chrome” diopside was available in larger quantities (i.e., parcels weighing up to 30–40 kg), and was reportedly cobbled from pods of material measuring up to several centimeters in diameter that were hosted by black mica schist. Extracting the gem-quality pieces was challenging due to the cleavage of the diopside.

Mr. Hashmi had a few stones faceted from each diopside variety, and loaned/donated them to GIA for examination by one of us (EPQ). Gemological testing of three “olive” diopsides (1.33–2.75 ct; figure 11) showed the following properties: color—medium to medium-dark yellow-green; pleochroism—very weak, brownish yellow and gray-green; R.I.— $n_{\alpha}=1.674\text{--}1.675$  and  $n_{\gamma}=1.701\text{--}1.703$ ; birefringence—0.027–0.028; and hydrostatic S.G.—3.29–3.30. These properties are consistent with those reported for diopside by W. A. Deer et al. (*An Introduction to Rock-forming Minerals*, 2nd ed., Longman Scientific and Technical, Essex, England, 1992, pp. 170–176). There was no Chelsea filter reaction, and the stones were inert to both long- and short-wave UV radiation. Absorption features at approximately 450, 505, and 550 nm were visible with the desk-model spectroscope. Microscopic observation revealed moderate doubling of the facet junctions, small transparent low-relief doubly refractive crystals and needles in stringers and planes, and small dark crystals. The stones also contained clouds and stringers of minute particles (which appeared dark in diffused light but white or gray in darkfield illumination); some of the clouds were planar. One of the stones displayed twinning, while another sample had partially healed fractures. EDXRF spectroscopy of two of the samples indicated the presence of



Figure 11. These yellow-green diopside samples (1.33–2.75 ct) reportedly came from Badakhshan, Afghanistan. The stone in the center (GIA Collection no. 36612) is a gift of Intimate Gems. Photo by C. D. Mengason.



Figure 12. Badakhshan, Afghanistan, was also given as the source of these “chrome” diopsides (0.57–0.77 ct). Courtesy of Intimate Gems; photo by C. D. Mengason.

major amounts of Si, Ca, and Mg; minor Fe; traces of Mn and Sr; and possibly Y and Zn.

Gemological testing of four faceted “chrome” diopsides (0.57–0.77 ct; figure 12) showed the following properties: color—medium-dark to dark green; diaphaneity—transparent; pleochroism—moderate, brownish yellow and green; R.I.— $n_o=1.678$  and  $n_e=1.705$ ; birefringence—0.027; S.G.—3.30–3.32; Chelsea filter reaction—none; and fluorescence—inert to both long- and short-wave UV radiation. Again, these properties were consistent with those of diopside reported by Deer et al. (1992). Absorption features at approximately 505, 550, 640, 660, and 690 nm were visible with the desk-model spectroscope; the lines in the red end of the spectrum are consistent with the presence of Cr, while the other features are probably due to iron. Microscopic examination revealed moderate doubling of the facet junctions, small low-relief doubly refractive transparent crystals and needles, and small dark crystals. The stones also contained clouds and stringers of particles and needles (which appeared dark in diffused light but white or gray in darkfield illumination); some of the clouds were planar, and the stringers had a wavy stair-step-like configuration. Two of the stones had partially healed fractures and two contained larger, doubly refractive, low-relief acicular crystals. EDXRF spectroscopy of three of the samples indicated the presence of major amounts of Si, Ca, and Mg; minor Fe; traces of Cr, Ti, Mn, and Sr; and possibly V. The absorption spectra and the detection of Cr in these samples by EDXRF indicate that the intense green color of this diopside is likely due to chromium.

Elizabeth P. Quinn (equinn@gia.edu)  
GIA Laboratory  
BML

**California jadeite with copper inclusions.** The Spring 1996 Lab Notes section (pp. 46–47) reported on jadeite beads from Guatemala with inclusions of native copper. Recently, a slab of mottled gray-green jadeite containing metallic inclusions was brought to our attention by Steve Perry (Steve Perry Gems, Davis, California). The sample was sliced from a boulder that was recovered by Nancy Stinnett and Michael Humenik of Watsonville, California, from the well-known jadeite locality of Clear Creek, San Benito County, California.

The optical and physical properties of the sample were consistent with jadeite, as was the Raman spectrum obtained in the GIA Laboratory. A few “copper”-colored metallic flakes (e.g., figure 13) were the only inclusions visible at 10× magnification. Using a four-probe high-impedance conductance test on the largest inclusion (employing an ohm meter with separate probes to measure the voltage drop and current across the inclusion, and incorporating its measurements into a simple calculation), one of us (RM) determined that the electrical properties were consistent with native copper. A review of the literature found that copper was previously documented in Clear Creek jadeite by R. C. Coleman (“Jadeite deposits of the Clear Creek area, New Idria District, San Benito County,” *Journal of Petrology*, Vol. 2, 1961, pp. 209–247). His description, “Native copper is present as small isolated blebs (less than 1 mm) within the jadeite . . .,” is consistent with the appearance of the inclusions in the slab we examined.

Roger Merk (merksjade@cox.net)  
Merk’s Jade, San Diego, California  
BML

Figure 13. The metallic inclusions in this jadeite from Clear Creek, California, consist of native copper. The largest copper inclusion measures approximately 2 mm in longest dimension. Courtesy of S. Perry; photomicrograph by R. Merk, magnified 10×.





Figure 14. Large quantities of transparent pale yellow labradorite have been mined from this remote area near Casas Grandes, Chihuahua State, in north-central Mexico. Courtesy of Barker & Co.

**Labradorite from Chihuahua, Mexico.** Gem-quality colorless to pale brownish yellow labradorite is known from several localities in western North America, including those in Oregon, Utah, and New Mexico (in the U.S.), as well as Mexico, among others (see J. D. Lindberg, "The source of the facet quality feldspar crystals from Rincon, New Mexico," *Lapidary Journal*, Vol. 38, No. 8, 1984, pp. 1070–1073; J. D. Lindberg, "Golden labradorite," *Lapidary Journal*, Vol. 44, No. 3, 1990, pp. 20, 22, 24; and M. O'Donoghue, *Gems*, 6th ed., Butterworth-Heinemann, Oxford, England, 2006, pp. 263–267). Particularly large and transparent material has come from Mexico's Sierra Madre Occidental mountain range in western Chihuahua State; Lindberg (1990) reported that the largest faceted stone weighed 92 ct and that even larger ones could be cut. In early publications, such feldspar may have been erroneously referred to as orthoclase (e.g., E. M. Barron, "The gem minerals of Mexico," *Lapidary Journal*, Vol. 12, No. 1, 1958, pp. 4–16 passim). Similar labradorite has been found in the bordering state of Sonora (J. T. Gutmann, "Crystal chemistry, unit cell dimensions and structural state of labradorite megacrysts from Sonora, Mexico," *Schweizerische Mineralogische und Petrographische Mitteilungen*, Vol. 56, No. 1, 1976, pp. 55–64).

Recently, large quantities of the pale yellow labradorite from the Casas Grandes area of Chihuahua State have entered the gem market. According to a major supplier of this material, Bill Barker of Barker & Co., Scottsdale, Arizona, the feldspar is mined from weathered volcanic rock using a simple hand screening apparatus. The deposit is located in a remote area on a gentle hillside (figure 14), and the extent of the labradorite-bearing region is not yet known. Mr. Barker reported that his factory has faceted several hundred thousand carats of the material, which is notable for its uniform color, high transparency, and ability to take a good polish. A variety of shapes have been cut, including oval, cushion, radiant, trilliant, and Portuguese

round. The faceted goods are typically 5–10 ct, with larger stones in the 30–60 ct range.

The gemological properties of Mexican labradorite are not well documented in the literature, so we characterized several stones that were donated by Mr. Barker and obtained from the GIA Collection. These included one sample known to be from Casas Grandes, two stones stated to be from Chihuahua State, and two labeled simply as "Mexico" (figure 15). The following properties were determined by one of us (KR): color—light brownish yellow, with weak pleochroism; R.I.—1.560–1.571; birefringence 0.009–0.010; S.G.—2.71–2.72; fluorescence—inert to long-wave and very weak orange to short-wave UV radiation; and no absorption lines visible with the desk-model spectroscope. These properties are comparable to those reported for labradorite by M. O'Donoghue (*Gems*, 6th ed., Butterworth-Heinemann, Oxford, England, 2006, pp. 263–267), except for slightly lower S.G. values in that publication (2.68–2.71). Microscopic examination revealed pinpoint stringers in small discreet parallel planes, some very fine wispy clouds, small dark opaque crystals with thin-film halos, twinning, and series of very thin reflective platelets at an angle to the clouds and stringers.

All five of the faceted stones, as well as four pieces of rough Casas Grandes labradorite that were donated by Mr. Barker, were chemically analyzed by LA-ICP-MS by one of us (CMB). The use of NIST glass standards allowed for semiquantitative (rather than quantitative) analyses, but extensive LA-ICP-MS analyses of plagioclase samples of known composition from a variety of sources showed that normalizing the major-element data provides a reliable way of determining plagioclase composition with this technique. All nine samples of the Mexican feldspar showed a rather narrow compositional range that identified them as labradorite. Expressed in terms of the albite (Ab), orthoclase (Or), and anorthite (An) feldspar end-members (corresponding to Na, K, and Ca, respectively), the



Figure 15. At 1.91–18.56 ct, these samples of labradorite from Mexico were characterized for this report. The 16.15 ct oval is a gift of Barker & Co., GIA Collection no. 36692; the other samples are GIA Collection nos. 32878, 32879 (both heart and triangle), and 34467 (pear shape, gift of H. Obodda, Short Hills, New Jersey). Photo by Robert Weldon.

Mexican labradorite samples had compositions in the range of  $\sim\text{Ab}_{35-42}\text{Or}_{1-3}\text{An}_{56-64}$ . Each stone was analyzed in two or three spots, revealing only minor variations in composition; the largest variation in anorthite content in a single stone was  $\text{An}_{56-61}$ . In addition to Si, Al, Ca, and Na, all the stones contained traces of K, Fe, Sr, Mg, Ti, Ba, Mn, P, Ga. It should be noted that electron-microprobe analysis of a Chihuahua labradorite at the University of Oklahoma measured a composition of  $\sim\text{Ab}_{40}\text{Or}_2\text{An}_{58}$  along with traces of Fe, K, Mg, Sr, and Ba (Dr. George Morgan, pers. comm., 2006). Trace amounts of  $\text{Fe}^{3+}$  in the tetrahedral site of the plagioclase causes the pale yellow color (see [http://minerals.caltech.edu/COLOR\\_Causes/Metal\\_Ion/index.htm](http://minerals.caltech.edu/COLOR_Causes/Metal_Ion/index.htm)).

Although Mexican plagioclase was reported by O'Donoghue (2006) as ranging from labradorite to bytownite (a feldspar in the compositional range of  $\text{An}_{70-90}$ ), all the samples analyzed in this study were labradorite.

BML

Kimberly Rockwell and  
Christopher M. Breeding  
GIA Laboratory, Carlsbad

**Gem news from Mogok, Myanmar.** In April 2006, this contributor participated in a field excursion to the Mogok area with geology students and staff from Panglong University. The information for this report was also gained from additional contacts and students in Myanmar.

- The tailings at the Kadottak ruby mine were being processed by a crushing, washing, and sorting operation for small rubies (<0.5 ct). The material is sold in bags weighing 50–100 kg that are sent to Thailand for heat treatment. The treated ruby is then sold to Thai and Indian jewelers.
- The Pein Pyit area was experiencing a boom in gem prospecting for ruby, sapphire, red spinel, zircon, and moonstone.
- Prospecting for sapphire was taking place in the Napheik and Pazunzeik areas north of Sinkwa village.
- The Kadaykada mining area (for ruby, sapphire, spinel, zircon, moonstone, and topaz) has been exhausted, and work has shifted to the nearby Lone-Cho area for ruby and spinel.
- The workings at the Bawbadan primary ruby deposit have attained a depth of 1,000 feet (328 m), and groundwater is a problem for mining. The high price of diesel fuel has restricted use of pumps, so mining has ceased at lower levels. Only small areas of corundum-mineralized marble in the upper portion of the deposit were being worked.
- Primary and secondary deposits in the Dat Taw Valley were being worked for pink sapphire, ruby, and other gems by a new influx of miners, mostly at higher levels of the deposits.
- Only small amounts of sapphire were coming from the Shwepyiaye Plot, and secondary deposits in the area have been exhausted. Permission to work a new plot in the area has been applied for, and it could yield good results in the future.
- Kwetsaung Taung in Thabeikkyin township was producing pink sapphires and pale red rubies that are opaque to translucent due to abundant parting planes. Translucent pale-to-moderate blue sapphires were also found in this area.
- Claims owned by UMEHL (Union of Myanmar Economic Holdings Limited) in the Pyaunggaung area were still producing peridot.
- Quartz and topaz were being mined in the Sakangyi area. The quartz crystals are sold in China.
- Painite production from Wetloo (a skarn deposit) and Thurein-taung (a secondary deposit) has declined, and good crystals fetch high prices.
- Prices were also high for rubellite from the Momeik area.

In conclusion, formerly insignificant gem materials in Myanmar are becoming more important and commanding

good prices. Small shops selling crystals have appeared along the roads and also in some homes. The Mogok area is full of miners, houses, and new asphalt roads, and gem prices are quite high.

*U Tin Hlaing  
Dept. of Geology (retired)  
Panglong University, Myanmar*

**Moonstone from Madagascar.** In mid-2005, we were informed about a new find of moonstone in Madagascar by Fabrice Danet (Style Gems, Antsirabe, Madagascar). According to Mr. Danet, there has been confusion among local gem dealers between moonstone and labradorite (spectrolite); the latter is abundant on the market and inexpensive. He also noted that some early reports on Madagascar's minerals by French geologists had confused the labradorescence in plagioclase with the adularescence in K-feldspar (moonstone).

Mr. Danet indicated that the new moonstone is mined from a granitic pegmatite that is located between Sahambano and Manivola, about 20 km east-northeast of Ihoay in the southern part of the island. Although the mining rights were obtained by a small French company (Tany Hafa Co.), the mine also occasionally has been worked by local people. A few kilograms of rough have been produced, mostly in small sizes, yielding cabochons that exceptionally range up to 11 ct. The cutting yield is rather low due to the orientation of the adularescence within cleavage fragments of the material.

Mr. Danet donated a parcel of the rough moonstone, along with a rectangular modified brilliant and an oval cabochon, to GIA for examination (see, e.g., figure 16). Gemological testing of the two polished stones by one of us (EPQ) yielded the following properties (those for the faceted stone are listed first; the cabochon had a flat polished back): color—very light yellow-gray and light grayish yellow, with a moderate bluish adularescence; diaphaneity—transparent to semitransparent; R.I.—1.526–1.531 and 1.525–1.530; birefringence—0.005; hydrostatic S.G.—2.57 and 2.58; Chelsea filter reac-

*Figure 16. These moonstones (0.82 and 2.20 ct) are from southern Madagascar. Gift of Fabrice Danet; GIA Collection nos. 36695 (cabochon) and 36696 (faceted stone). Photo by C. D. Mengason.*

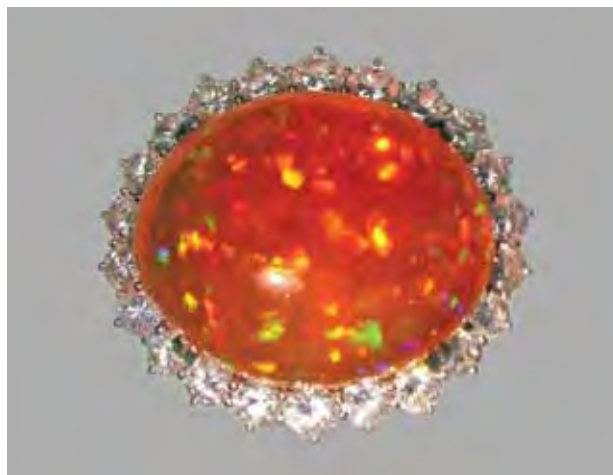


*Figure 17. The 70 ct fire opal in this ring was determined to be of natural origin. Photo by T. Hainschwang.*

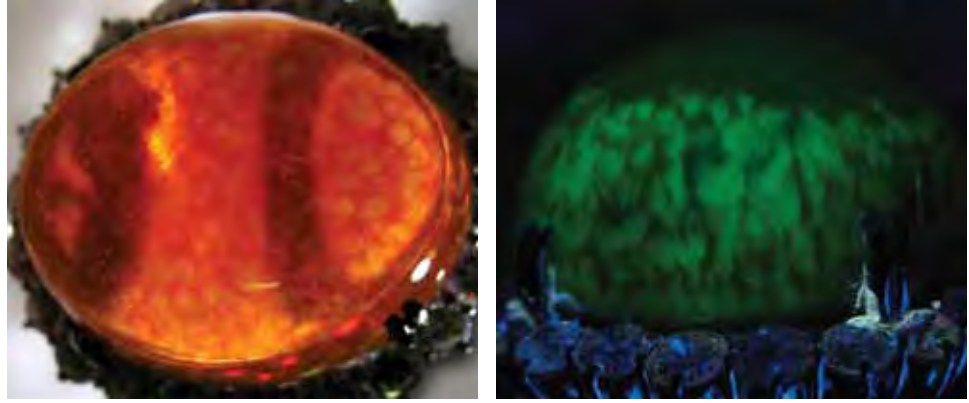
tion—none; and fluorescence—very weak violet-blue to long-wave and weak-to-moderate orangy red to short-wave UV radiation. No absorption features were visible with the desk-model spectroscope. Most of these properties are comparable to those reported for the moonstone variety of K-feldspar by M. O'Donoghue (*Gems*, 6th ed., Butterworth-Heinemann, Oxford, England, 2006, p. 270). Although the R.I. values of the Madagascar samples are higher than those provided for moonstone by this reference (1.518–1.526), they are consistent with the refractive indices given for K-feldspar in mineralogy textbooks. Microscopic examination revealed clusters of very small transparent (sometimes whitish) doubly refractive crystals and very small dark crystals, along with stringers and clouds comprised of clusters of similar but much smaller crystals. EDXRF spectroscopy showed a composition that was consistent with K-feldspar.

*Elizabeth P. Quinn and BML*

**A large phenomenal fire opal with possible uranium-related luminescence.** This contributor recently examined a high-quality 70 ct fire opal with very strong play-of-color (figure 17). The transparent bright orange opal was mounted in a ring, and was analyzed to verify its natural origin for a recent auction at Sotheby's.

The stone was identified as opal by specular reflectance FTIR spectroscopy. Although the spectra of natural and synthetic opal are similar, minor details sometimes allow them to be distinguished by this method. In this case, the spectrum matched perfectly with that of natural opal. The lack of a "snake-skin" structure during microscopic observation of the play-of-color also indicated natural origin. The opal exhibited very distinct orange net-like color zoning (figure 18, left). This zoning was also observed when the stone was exposed to short-wave UV radiation: The pale-colored zones fluoresced weak-to-moderate green, while the strongly colored "net" was almost inert (figure 18, right).

Figure 18. The color zoning of the fire opal in figure 17 (left) was mirrored in its unusual pattern of green luminescence to UV radiation (right). The luminescence was stronger in the pale-colored zones than in the intense orange “net.” Photos by T. Hainschwang.



With long-wave UV, the fluorescence was much weaker but still discernable.

Green luminescence in opal has been attributed to uranium impurities in the form of the uranyl ion  $UO_2^{2+}$  (E. Fritsch et al., “Luminescence of oxidized porous silicon: Surface-induced emissions from disordered silica micro- to nano-structures,” *Journal of Applied Physics*, Vol. 90, No. 9, 2001, pp. 4777–4782). Such uranium impurities can be present in very low concentrations and therefore may not be detected by EDXRF spectroscopy (E. Fritsch, pers. comm., 2006).

Indeed, EDXRF chemical analysis of this opal did not show the presence of uranium, but it did reveal trace amounts of iron. The appreciable iron concentration possibly explains why the more intensely colored zones were nearly inert to UV radiation, since yellow-to-orange color in fire opal has been attributed to nanoinclusions of an iron-containing mineral (E. Fritsch et al., “Mexican gem opals: Nano- and micro-structure, origin of color and comparison with other common opals of gemological significance,” *Australian Gemmologist*, Vol. 21, No. 6, 2002, pp. 230–233). Iron is known to efficiently quench luminescence in minerals; thus, if present in sufficient quantity, it can suppress uranium-related luminescence of opal (again, see Fritsch et al., 2001), even when present within nanoinclusions (E. Fritsch, pers. comm., 2006).

Some opals contain rather large quantities of uranium. For example, a nonphenomenal yellow opal from Madagascar showing very strong green fluorescence was previously analyzed by this contributor. The presence of uranium was easily detected by EDXRF, while Fe was very low. Radioactivity was clearly measurable with a Geiger-Müller counter, and had an intensity 20 times greater than the natural background level with the detector held 9 mm from the sample.

No radioactivity was detected in this 70 ct fire opal, so the presence of uranium could not be verified by the Geiger-Müller counter. The content of uranium in this noticeably fluorescent opal is apparently less than 10 ppm, which was the EDXRF detection limit of this element for the instrument.

Thomas Hainschwang ([thainschwang@yahoo.com](mailto:thainschwang@yahoo.com))  
Geneva, Switzerland

**“Sunset” quartz: A new gem material from Brazil.** In July 2006, a new deposit of yellow-to-orange quartz was discovered in northern Minas Gerais State, Brazil. The material was found by Jean-Claude Nydegger, when he noted some quartz veins containing transparent-to-opaque areas that varied from white to yellow-orange (e.g., figure 19). Closer examination revealed a few thin bands with an attractive yellow-orange color.

Approximately 1,500 kg of quartz were extracted from the veins, but only 5 kg of this was gem quality. The first parcel of stones faceted from the material is shown in figure 20. The cut gems typically weigh 1–10 carats; the largest known to these contributors is 19.5 ct (figure 21). Due to the resemblance of the colors to those of a setting sun, these contributors suggest that the material be called “Sunset” quartz.

Initial examination with a 10× loupe revealed a number of yellow-to-orange needles in the quartz. Depending on the abundance and color of the needles, the quartz varied from pale yellow (in very slightly included samples), to yellow or orange (in samples that were more heavily included). Heating experiments done by Mr. Nydegger

Figure 19. A yellow-orange variety of quartz has been found within milky white quartz veins in northern Minas Gerais, Brazil. The orange areas of the veins, referred to as “Sunset” quartz, are relatively rare. This sample is 10.5 cm wide; photo by M. Macri.



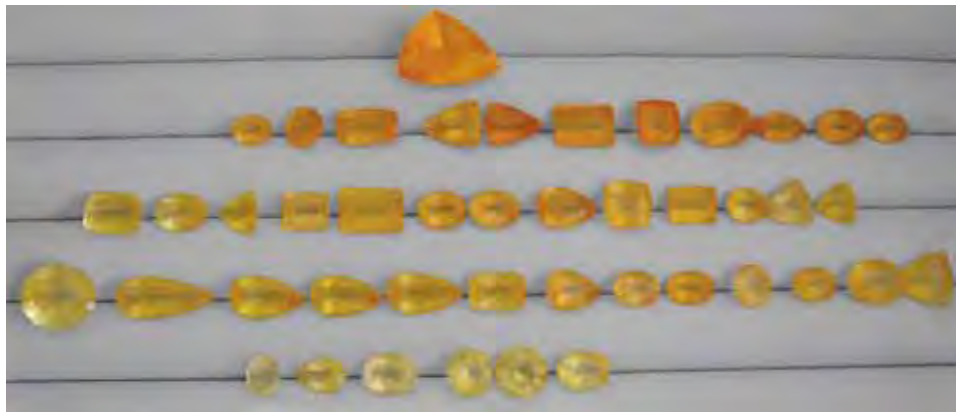


Figure 20. The stones in this first parcel of faceted Sunset quartz ranged from approximately 1 to 19.5 ct. Photo by M. Macri.

showed that the yellow-to-orange quartz can be permanently changed to deep orange at 350°C. However, heating of the colorless and light yellow quartz resulted in no change of color. The heated and unheated quartz may show the same range of color; it is impossible to reliably distinguish them from one another by visual appearance or standard gemological testing. Some, but not all, of the heated samples contained fractures that apparently formed due to the heating process.

Standard gemological testing was performed on three faceted samples that had been heated. In addition, two samples were prepared (a doubly polished slab of unheated material and a thin section of the heated quartz) for observation using an optical microscope in both reflected and transmitted light, as well as with a scanning electron microscope (SEM). The inclusions in these two samples were chemically analyzed using a Cameca SX-50 electron microprobe (accelerating voltage of 15 kV and sample current of 15 nA) at the IGAG-CNR (L'Istituto di Geologia Ambientale e Geoingegneria—Consiglio Nazionale Delle Ricerche) in Rome.

The faceted stones yielded the following gemological properties: color—yellow, yellow-orange, orange;

diaphaneity—transparent to translucent; R.I.— $n_o=1.543$ ,  $n_e=1.552$ ; birefringence—0.009; and S.G.—2.65. Microscopic observations revealed a large number of randomly oriented needle-shaped inclusions in all samples (e.g., figure 22). The needles ranged up to a few millimeters long, with diameters of 1–3  $\mu\text{m}$ . Their strong yellow-orange hue was responsible for the overall color of the quartz, and their abundance also resulted in the slightly milky appearance. When viewed with crossed polarizers, the inclusions showed birefringence.

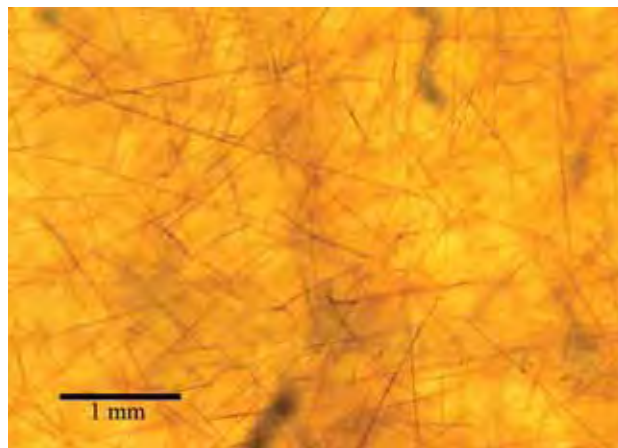
Backscattered electron images of the polished slab and the thin section obtained with the SEM showed that the needles' surfaces had an irregular outline (figure 23). Suitable inclusions for chemical analysis could not be found in the unheated sample, but the needles in the heated quartz were shown by the SEM to be Al- and Fe-rich, with a lower Si content than the quartz host. Electron-microprobe analysis of the needles in this sample confirmed that they contain major amounts of Si, Al, and Fe, along with traces of K. The high iron content is probably responsible for the color of the inclusions.

While only a small quantity of Sunset quartz has been faceted, a significant amount of opaque orange material

Figure 21. This 19.5 ct Sunset quartz is the largest sample known to the authors. Photo by Federico Caprilli.



Figure 22. The Sunset quartz is colored by abundant yellow-orange needle-shaped inclusions. Photomicrograph by M. Macri; transmitted light.



suitable for cabochons and carvings is expected to become available.

*Acknowledgments:* Mario Solini, Elisa Melis, Alfredo Mancini, and Paolo Ballirano are thanked for their generous assistance.

*Michele Macri (michele.macri@uniroma1.it),  
Adriana Maras, and Pier Francesco Moretti  
Università di Roma "La Sapienza," Italy  
Marcello Serracino  
IGAG-CNR of Rome, P. A. Moro, Italy*

**Swedish Blue (slag) and Swedish Iron Ore.** David Olson (Ingeborgs Stenar AB, Stockholm, Sweden) recently informed us about two unconventional gem products from Sweden. He reported that a blue-patterned material called Swedish Blue is cut from slag (a byproduct of smelting ore to extract metals) that was produced from the Middle Ages until about 1865, when the Bessemer process of smelting iron ore was invented. This slag comes from central Sweden, where there was once an abundance of small smelters in operation. The slag was produced when the silica-rich portions of the ore floated to the surface and were poured off as a waste product. The other material, banded iron ore, comes from a small mine near Nora, which is located 26 km north of Örebro in south-central Sweden. This mine is one of the few sources that produces a banded iron ore solid enough to cut and polish; it is sold as Swedish Iron Ore.

Mr. Olson gave GIA three cabochons of Swedish Blue and two of Swedish Iron Ore (figure 24), and these were examined by one of us (KR). The Swedish Blue had the following properties: color—finely banded, semitranslu-

*Figure 23. In this backscattered electron image, the dark spots represent the surface expression of the needle-like inclusions in the Sunset quartz. Note the irregular outline of the central needle. Image by M. Serracino.*



*Figure 24. The blue samples are composed of slag (15.17–26.90 ct), and the banded cabochons are iron ore (16.95–34.00 ct), both from Sweden. The green areas shown by the slag correspond to areas of transmitted light. Gift of Ingeborgs Stenar AB; GIA Collection nos. 36700-36704. Photo by Robert Weldon.*

cent very light gray to translucent blue with a strong yellowish green component in transmitted light; R.I.—1.58 (spot reading) or 1.583 (flat surface); hydrostatic S.G.—2.74–2.76; fluorescence—weak blue to long-wave and very weak blue to short-wave UV radiation; and no diagnostic absorption lines were visible with the desk-model spectroscope. Microscopic examination showed randomly distributed gas bubbles of various sizes and very small metallic spheres and particles. EDXRF spectroscopy performed by GIA Laboratory senior research associate Sam Muhlmeister revealed major amounts of Si and Ca; minor Mg, Al, and Fe; and traces of K, Mn, Rb, Sr, Y, Zr, Ba, and the rare-earth elements La and Ce.

The Swedish Iron Ore had the following properties: color—zebra-like, broadly banded translucent black to opaque metallic black; R.I.—1.54 from a translucent band and over-the-limits of the standard refractometer (>1.81) from a metallic band; S.G.—3.91–4.44 (variation due to different ratios of translucent and metallic material); UV fluorescence—inert; and no diagnostic absorption features visible with the desk-model spectroscope. EDXRF spectroscopy performed by Mr. Muhlmeister indicated major amounts of Si and Fe, and traces of Al and Sb. Microscopic examination showed that the black translucent areas were composed of a near-colorless transparent material that was heavily included with opaque black particles; the near-colorless areas were identified as quartz by Raman spectroscopy. The metallic bands are formed by a dense accumulation of black opaque particles that were identified as hematite with Raman analysis. At the interface of each of these layers were a few scattered very dark red particles that were only visible at higher magnification (~25×).

Mr. Olsen indicated that he sold about 1,000 cabochons (of both materials combined) into the market at the 2006 Tucson gem shows.

*Kimberly Rockwell and BML*



Figure 25. This overview of the Nandihizana tourmaline mining area shows some of the workings, as well as the mining camp in the background. Photo by F. Danet.

**Tourmaline mining at Nandihizana, Madagascar.** In mid-October 2005, a new tourmaline deposit was discovered at Nandihizana, a village located 130 km south of Antsirabe (and only 10 km west of National Road 7). This area lies within the region known as Camp Robin, where several

Figure 26. The main pit at Nandihizana measured about 75 m long and 14 m deep. The mined material was removed in buckets using ropes and ladders. Photo by F. Danet.



tourmaline deposits have been worked over the past few years (see, e.g., Fall 2006 *G&G*, pp. 116, 156).

This contributor recorded the frenzy of mining activity that occurred when about 5,000 diggers and gem traders descended on the site (figures 25–27). The government attempted to control the influx, but this proved impossible. It is interesting to note how virtually any new gem discovery in Madagascar is followed by an immediate rush of such large proportions.

The tourmaline was mined from soil and a large underlying granitic pegmatite with a north-south strike and a subvertical dip. The pegmatite was composed of white perthite feldspar, abundant green amazonite, quartz, small amounts of black tourmaline, lepidolite, and yellow danburite (sometimes showing chatoyancy). The tourmaline production consisted of many colors, including yellow, light green, “olive” green, strawberry-like red, and violetish red. Unfortunately, most of the material was heavily included, and well-formed crystals were rare. Nevertheless, the demand for tourmaline of all qualities is quite high in Madagascar, so the production was readily consumed by African and Chinese traders for carving purposes. Only a few stones have been faceted (see, e.g., figure 28).

Tourmaline production from Nandihizana has declined in recent months. In March 2006, at a mine located near Nandihizana, several hundred kilograms of fan-shaped dark green and dark purple tourmaline crystals were recovered in groups measuring up to 20 cm long.

Fabrice Danet ([fabdanet@wanadoo.mg](mailto:fabdanet@wanadoo.mg))  
Style Gems, Antsirabe, Madagascar



Figure 27. Miners at the Nandihizana main pit are shown here working the primary pegmatite deposit for tourmaline. Photo by F. Danet.

**Green uvite from Afghanistan.** In the Winter 2002 GNI section (pp. 357–358), we reported on some samples of brownish orange uvite from Afghanistan that were loaned to GIA by Farooq Hashmi. Mr. Hashmi has also loaned us several fragments and well-formed crystals of green tourmaline (figure 29) that are also reportedly from Afghanistan. The material was obtained in mid-2006 during a buying trip to Peshawar, Pakistan. Mr. Hashmi first noted this tourmaline in the Peshawar market in 2002. Interestingly, a single faceted stone obtained at that time by Mr. Hashmi within a small parcel of the green tourmaline crystal fragments proved to be tsavorite.

The following properties were recorded by one of us (EPQ) on four of the most intensely green crystals: color—medium-dark to dark green with some of the samples appearing darker green toward the pyramidal termination due to angular color banding oriented parallel to those faces; dichroism—moderate-to-strong greenish blue and greenish yellow; diaphaneity—transparent to translucent; hydrostatic S.G.—3.04; Chelsea filter reaction—moderate-to-strong red; and fluorescence—inert to long-wave UV radiation, and weak to moderate mottled chalky orange-yellow to short-wave UV. Although some of the crystal faces were nearly flat and fairly smooth, it was not possible to measure accurate refractive indices due to growth



Figure 28. These tourmalines were cut from material recovered in the Camp Robin area of Madagascar. The pink stone weighs 4.75 ct. Photo by F. Danet.

features on the surfaces. UV-Vis-NIR spectroscopy of two of the crystals revealed broad absorption bands centered at 420 and 605 nm (for the o-ray) and at 440 and 600 nm (for the e-ray) together with subtle absorption features at 679, 687, and 692 nm that are most likely related to chromium. Observation with a desk-model spectroscope showed general absorption to 480 nm and a broad band centered at 600 nm, but no lines were seen in the red region. Microscopic examination revealed numerous fractures, platy low-relief doubly refractive crystals, partially healed fractures, two-phase inclusions containing a doubly refractive crystal and a liquid, two-phase inclusions containing a dark solid and a liquid, and three-phase inclusions. Two of the crystals contained clouds and one sample contained small, low-relief, pale brown inclusions that were possibly singly refractive.

EDXRF spectroscopy of two of the crystals revealed major amounts of Si, Al, and Mg; traces of Ca, Sr, V, Cr, and Ti; and possibly traces of Na, Ga, and Fe. The presence of major amounts of Mg and some Ca is consistent with

Figure 29. These crystals of green tourmaline (6.45–14.25 mm) from Afghanistan are apparently colored by vanadium and subordinate chromium. The crystals located in the center and second from the left were among the samples that were tested for this report. Courtesy of Intimate Gems; photo by C. D. Mengason.



the tourmaline species uvite. The EDXRF (and UV-Vis-NIR) results were comparable to similar-colored samples of “chrome” tourmaline from Tanzania and Kenya (one sample tested from each locality), but our preliminary data suggest that the Afghan material contained less Ti, Cr, V, and Sr. Notably, the tourmalines from all three localities contained more V than Cr, and did not show particularly strong Cr absorption features in the visible spectra. The intense green color of these particular tourmaline samples (typically referred to as “chrome” tourmaline by the trade) appears to be caused more by vanadium than by chromium. An early study of the Tanzanian tourmaline also indicated that vanadium is the main chromophoric element (R. Webster, “Tanganyika tourmaline,” *The Gemmologist*, Vol. 30, No. 356, 1961, pp. 41–45).

*Elizabeth P. Quinn and BML*

## SYNTHETICS AND SIMULANTS

**Synthetic corundum “gem rough” in Tanzania.** While on a gem buying trip to Tanzania, gem dealer Farooq Hashmi was offered some unusually transparent samples that were represented as rough spessartine and sapphire. Although he was suspicious of their authenticity due to their high clarity and the relatively low asking price, he purchased some for further examination.

In one case, a small parcel of bright orange broken fragments was sold to him as spessartine. Straight parallel stepped patterns on some of the surfaces resembled the etch features that may be seen on rough spessartine. Examination of five of these samples (1.0–3.9 g; figure 30) by one of us (EAF) showed the following properties: color—orange; hydrostatic S.G.—4.01; fluorescence—inert to long- and short-wave UV radiation; and general absorption to 500 nm and a line at 690 nm observed with the desk-model spectroscope (proving that they were not spessartine). Microscopic examination revealed no inclusions, while the surface of the samples showed conchoidal fractures as well as the straight parallel stepped areas mentioned above that had the appearance of cleavage/parting planes. Due to the unpolished nature of the samples, it was not possible to obtain R.I. readings, so the material was identified by Raman spectroscopy as corundum. The strong orange color prompted us to check for the presence of Be using LA-ICP-MS. Analysis of one sample by GIA Laboratory research scientist Dr. Andy Hsi-Tien Shen showed that it contained Fe, Cr, and Mg (besides the expected Al). The lack of Ga proved that the material was synthetic corundum.

In another case, Mr. Hashmi was offered a multicolored parcel of waterworn rough that was represented as Umba sapphire. He singled out one purple sample (figure 31) that appeared more waterworn and transparent than the others. The following properties were collected by one of us (EAF): color—reddish purple; pleochroism—purple to light pink; S.G.—3.99; fluorescence—moderate-to-strong red to long-wave UV radiation, and very weak red



*Figure 30. These fragments of synthetic sapphire (1.0–3.9 g) were sold as spessartine in Tanzania. Courtesy of Intimate Gems; photo by Robert Weldon.*

internally and moderate chalky white on the surface to short-wave UV; and absorption lines at 470, 480, and 680 nm were seen with the desk-model spectroscope. Microscopic examination showed a rounded abraded surface with numerous small chips and fractures; no inclusions could be seen in the stone’s interior. Raman analysis provided a spectral match to corundum. LA-ICP-MS analysis by Dr. Shen showed that in addition to Al, this sample contained only Cr and Ti; it had no Ga. Therefore, this sample was also identified as synthetic corundum.

Mr. Hashmi obtained these samples in Dar es Salaam, but he also reported seeing similar orange material in Arusha. According to gem dealers in Tanzania, the synthetics are brought in by Asian merchants who then use local African dealers to sell the material. Mr. Hashmi also reported that in Dar es Salaam, synthetic spinel is being sold as natural red spinel in fragments or abraded octahedral-shaped “crystals.”

*Eric A. Fritz (efritz@gia.edu)  
GIA Laboratory, Carlsbad*

*BML*

*Figure 31. Although it has the appearance of a waterworn piece of gem rough, this 3.2 g sample was fashioned from synthetic sapphire. It was obtained in Tanzania from a multicolored parcel that was represented as Umba sapphire rough. Courtesy of Intimate Gems; photo by Robert Weldon.*





Figure 32. The round brilliants in this ring (average 2.8 mm diameter) proved to be treated-color pink synthetic diamonds. With strong fiber-optic illumination (right), nine of them showed unevenly distributed green luminescence. Photos by S. Singbamroong, © Dubai Gemstone Laboratory.

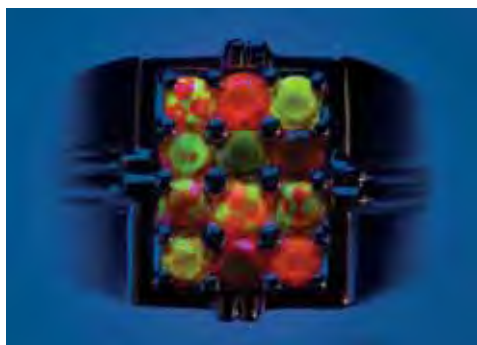
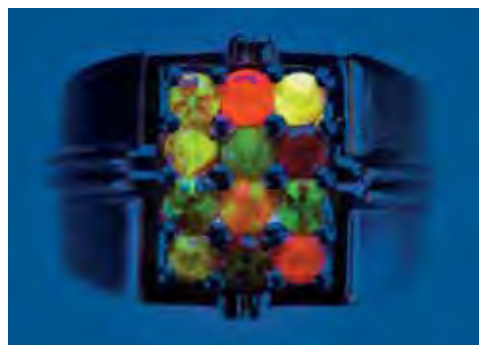


Figure 33. When exposed to long-wave (left) and short-wave (right) UV radiation, most of the treated synthetic pink diamonds revealed zones of greenish yellow to green over a red background, with cross-shaped, hourglass, or three-armed patterns. Photos by S. Singbamroong, © Dubai Gemstone Laboratory.

#### Small treated synthetic pink diamonds set in a ring.

Recently, the Dubai Gemstone Laboratory received a yellow metal ring set with 12 pink round brilliants for identification. The round brilliants averaged 2.8 mm in diameter and exhibited a saturated color that varied from orangy pink to brownish purplish pink (figure 32, left). They gave a positive (diamond) reaction to a thermal conductivity tester.

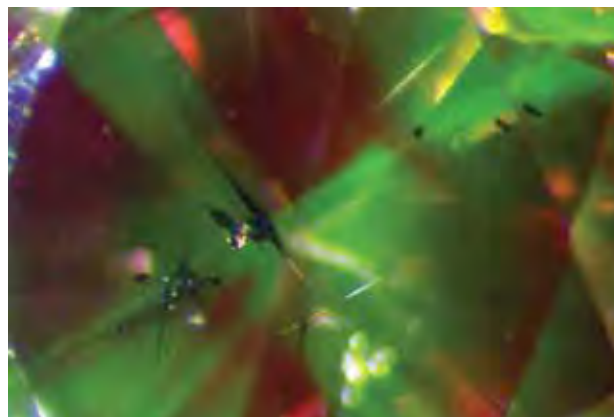
With strong fiber-optic illumination, nine of the 12 samples showed unevenly distributed weak-to-moderate green luminescence (figure 32, right). The reaction to ultraviolet radiation was also striking. When exposed to long-wave UV, all displayed a distinctive weak-to-strong yellowish orange, orange, or orangy red fluorescence, with the same nine samples also showing zones of greenish yellow to green (figure 33, left). The reaction to short-wave UV was similar but stronger, and the zoning was more clearly defined (figure 33, right). In both cases, the green fluorescing areas showed the cross-shaped, hourglass, or three-armed growth sector patterns that are typical of synthetic diamond. There was no phosphorescence reaction in any of the stones. DiamondView luminescence images of the nine samples displayed additional distinctive features characteristic of synthetic diamond.

Microscopic examination revealed metallic inclusions in six of the samples (e.g., figure 34) and a cloud of reflective pinpoint inclusions in one; among these were the three samples that did not show the green luminescence zoning mentioned above. Immersed in water and examined with diffused light, the nine samples that *did* have green zoning showed uneven color distribution, with distinct zones of yellow and pink (figure 35). Such zoning is also a typical feature of synthetic diamond.

Due to the small size of the synthetic diamonds and

the nature of the mounting, it was not possible to perform UV-Vis absorption spectroscopy. However, low-temperature photoluminescence spectra recorded for two samples with a Raman microspectrometer using a 514.5 nm argon laser showed emission peaks at 575 and 637 nm, which are indicative of irradiation and annealing treatment, as well as a 658 nm band due to nickel impurities that is indicative of synthetic origin (see J. E. Shigley et al., "Lab-grown colored diamonds from Chatham Created Gems," Summer 2004 *Gems & Gemology*, pp. 128–145).

Figure 34. Needle-like metallic inclusions were seen in this treated-color synthetic pink diamond. This image also shows a cross-shaped pattern of green luminescence to visible light. Photomicrograph by S. Singbamroong, © Dubai Gemstone Laboratory; magnified 50x.



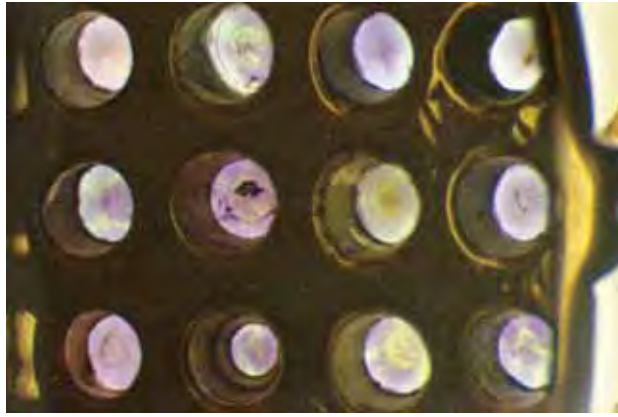


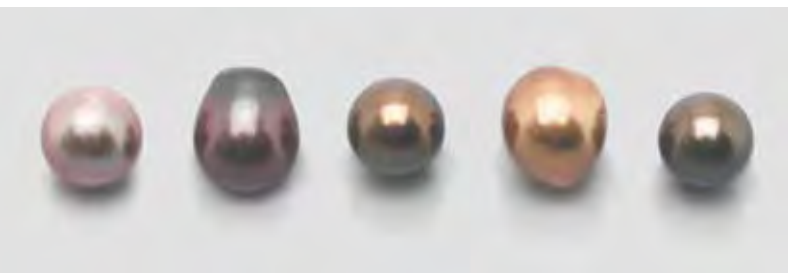
Figure 35. When viewed with diffused light while they were immersed in water, most of the synthetic diamonds in figure 32 showed distinct yellow and pink color zoning, another clue to their synthetic origin. Photomicrograph by S. Singbamroong, © Dubai Gemstone Laboratory; magnified 8x.

The infrared spectra of two samples revealed features that were a mixture of type Ib, IaA, and IaB (with IaA>>IaB, Ia>Ib). They also revealed a peak at 1450  $\text{cm}^{-1}$ , providing additional evidence of irradiation and annealing (W. Wang et al., "Treated-color pink-to-red diamonds from Lucent Diamonds, Inc.," Spring 2005 *Gems & Gemology*, pp. 6–19). EDXRF chemical analysis of two samples revealed the presence of Ni and Fe.

On the basis of the color zoning, luminescence characteristics, and chemical/spectroscopic properties, we identified the 12 small round brilliants as treated-color pink synthetic diamonds.

Sutas Singbamroong (ssutas@dm.gov.ae)  
and Abdalla Abdelqadir Yousif  
Dubai Gemstone Laboratory  
Dubai, United Arab Emirates

Figure 36. Represented as "chocolate pearls," these variously colored samples (up to 12.7 mm) were examined for this report. One of them (second from the left) proved to be silver treated, while no silver was detected in the other cultured pearls. The sample on the far left was bleached but not dyed. Slicing and/or polishing the other samples revealed narrow (~0.05 mm) concentrations of brown color at their surface. Photo by H. A. Hänni, © SSEF.



## TREATMENTS

**Update on "chocolate" Tahitian cultured pearls.** Treated-color brown Tahitian cultured pearls were introduced a few years ago as "chocolate pearls," and there have been a number of conflicting reports about the coloration mechanism (see, e.g., "Trade raises questions about 'chocolate pearls,'" *Jewellery News Asia*, No. 241, September 2004, pp. 160–162; M. Zachovay, "'Chocolate' Tahitian cultured pearls," Summer 2005 *Gem News International*, pp. 183–184; "Better techniques improve brown pearls," *Jewellery News Asia*, No. 262, June 2006, p. 60). Good-quality but overly dark Tahitian cultured pearls are said to be treated to lighten the surface color. This treatment is claimed to be stable and to penetrate deeply into the cultured pearls, sometimes even turning their bead nuclei brown.

According to some of these reports, the treatment somehow affects the melanin (dark pigment) molecules in the nacre. It is not clear, though, how the surface color could be lightened by modification of the melanin, while at the same time the originally white bead in the center could turn brown. Though the color would still be considered "treated," the process is represented as superior to simple dyeing.

The SSEF Swiss Gemmological Institute has been seeking test material for some time to learn more about this mystery, and we recently received five samples represented as "chocolate pearls" from three different dealers (in England, Japan, and Switzerland) for research purposes (see, e.g., figure 36). Each sample was sawn in half, and/or a small flat spot was polished on the surface, to reveal the depth of color penetration.

The results were surprising and confirm that common sense is always helpful when facing such mysteries. One of the samples (far left in figure 36) was bleached but not dyed. The other four cultured pearls showed distinct color concentrations in their outermost layers, the thickness of which was about 0.05 mm (see, e.g., figure 37). The underlying nacre was gray to light brown (figure 38); in none of these samples was the underlying nacre darker than the surface. Furthermore, there was no apparent darkening of the bead in any of our samples. These results are nearly identical to properties exhibited by cultured pearls that have been dyed, such as those treated with silver nitrate or more modern dyes. When the samples were tested for the presence of silver using EDXRF spectroscopy, one revealed this element—indicating that it was treated by the traditional silver nitrate method—but silver was not found in any of the other cultured pearls.

Future research on a broader selection of "chocolate pearls" is necessary before we can make a better determination of the treatment process. In our experience, a non-destructive gemmological test to detect this treatment is not yet available; however, polishing a tiny flat spot (e.g., around a drill hole) would show a color concentration confined to a superficial layer. The SSEF laboratory would welcome additional "chocolate pearls" for further testing.

HAH

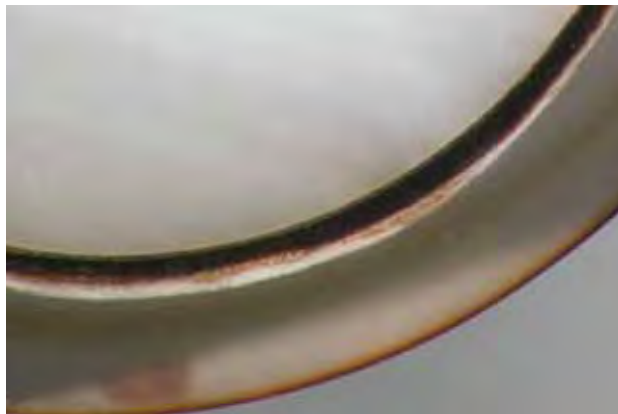


Figure 37. In this cross-section of one of the “chocolate pearls” (middle sample in figure 36), the white bead and a thin ~0.05 mm surface layer of brown coloration is clearly visible, while the nacre underlying the dark surface is lighter and predominantly gray. Photo by H. A. Hänni, © SSEF.

**Treated violetish blue to violet quartz from Brazil.** Blue quartz is quite rare, and the color of almost all such reported natural material is produced by mineral inclusions (see, e.g., K. Schmetzer, “Methods for the distinction of natural and synthetic citrine and prasiolite,” *Journal of Gemmology*, Vol. 21, 1989, pp. 368–391). Such quartz has an orange tint when viewed in transmitted light, due to scattering by the minute particles. Thus far, the only blue quartz not colored by inclusions has been synthetic material that is colored by cobalt or heat-treated and iron-bearing (K. Nassau and B. E. Prescott, “Smoky, blue, greenish-yellow, and other irradiation-related colors in quartz,” *Mineralogical Magazine*, Vol. 41, 1977, pp. 301–312).

Figure 39. The Montezuma area in Minas Gerais, Brazil, is once again being mined for amethyst (such as the 4 cm crystal pictured here). This material can be turned green by heat treatment and violetish blue to violet by subsequent irradiation. The cut stones weigh about 3–4 ct. Photo by R. S. Güttler.

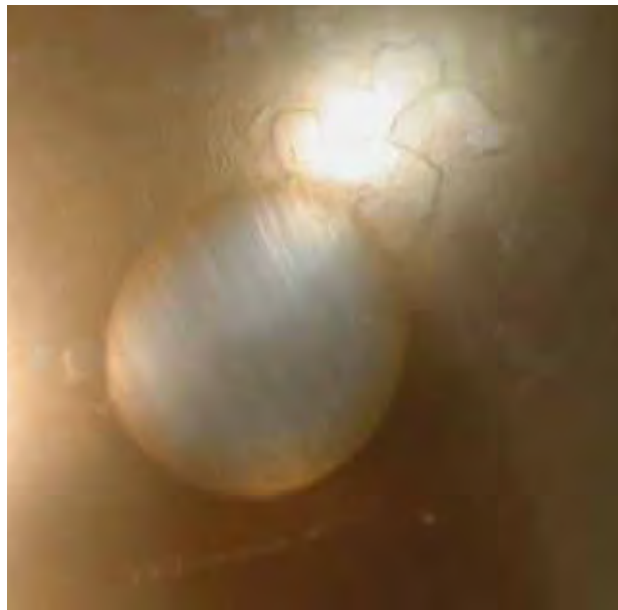


Figure 38. Polishing a small flat area (1.6 mm in diameter) on one of the “chocolate pearls” revealed the shallow depth of the surface-related color concentration. Photomicrograph by H. A. Hänni, © SSEF.

A new variety of violetish blue to violet quartz (figures 39 and 40) has recently been produced through the heating and gamma irradiation of amethyst from a mine near Montezuma, in the Rio Pardo region in northern Minas Gerais. This deposit, often called the Montezuma mine, initially became famous during the 1960s for amethyst that could be turned green by heating, known today as “prasiolite” or “greened amethyst” in the trade (J. P. Cassedanne and J. O. Cassedanne, “Axinite, hydromagnesite, amethyst, and other minerals from near Vitória da Conquista [Brazil],” *Mineralogical Record*, Vol. 8, 1977, pp. 382–387; Summer 2004 Lab Notes, p. 167). One of the

Figure 40. These samples show the coloration of the Montezuma mine quartz as untreated amethyst (left, 2.40 ct), heated green quartz (center, 3.54 ct), and heated and irradiated violet quartz (right, 2.37 ct). Gift of Henrique Fernandes and Gabriel Freitas, Pinkstone International, Governador Valadares, Brazil; GIA Collection nos. 36697–36699. Photo by Robert Weldon.



veins at this deposit is now being mined again, yielding about 500 kg/month of amethyst, of which about 1–2% is gem quality.

It is well known that heat may reduce the oxidation state of iron in amethyst, and at about 300–500°C the purple color will change to colorless or yellow or green (see, e.g., E. Neumann and K. Schmetzer, "Mechanism of thermal conversion of colour and colour centres by heat treatment of amethyst," *Neues Jahrbuch für Mineralogie Monatshefte*, Vol. 6, 1984, pp. 272–282). The resulting green quartz is quite stable to heat, unlike the pale green quartz that has been produced with gamma irradiation (but no heat treatment) from colorless to very slightly green quartz from Rio Grande do Sul State. This latter quartz loses much of its green color when heated to about 150–200°C or exposed to strong sunlight. The two types of treated green quartz may be distinguished by their different responses to the Chelsea filter (see H. Kitawaki, "Green quartz," [www.gaa-jzenhokyo.co.jp/index-e.html](http://www.gaa-jzenhokyo.co.jp/index-e.html)) or the Aquamarine filter (Göttinger Farbfilter, Germany). Viewed with each of these filters using incandescent light, the heated variety (derived from amethyst) appears green due to absorption in the red part of the spectrum at about 750 nm (produced by Fe<sup>2+</sup>), whereas the irradiated material (derived from colorless quartz) appears red due to an as-yet-unexplained weak absorption peak at about 620 nm and efficient transmission in the red spectral region.

Gamma irradiation experiments were undertaken by one of us (HCK) to improve the green color of heated (350–450°C) Montezuma amethyst at Embrarad Ltda., a commercial irradiation facility near São Paulo. The irradiation unexpectedly produced a range of colors from violet to violetish blue to deep blue. According to the Color Atlas 5510 (Mitsumara Suiko, Shoin, Japan, 1986), the colors ranged from 4.25PB2/10 to 8.75PB4/3 (deep blue to deep purplish blue). The optical properties were typical for quartz, but with strong violetish blue and reddish orange pleochroic colors when viewed with a dichroscope perpendicular to the c-axis. Although the coloration appears to be distributed evenly in cut material, detailed microscopic examination showed color concentrations along zones parallel to the rhombohedral sectors. Preliminary experiments by HCK have shown that the stability of the coloration is comparable to that of amethyst when exposed to strong UV radiation or moderate heating (400–500°C).

The color-producing mechanism has not yet been investigated, but it may involve a charge transfer between traces of Fe<sup>2+</sup> and Fe<sup>3+</sup> in interstitial sites of the quartz structure (G. Lehmann, "Farben von Mineralien und ihre Ursachen" *Fortschritte der Mineralogie*, Vol. 56, No. 2, 1978, pp. 172–252), which produces absorption in the red end of the spectrum and enhances transmission in the blue-to-violet range.

About 100 kg of rough gem-quality green quartz have been stockpiled. At the time of this report, only a small amount had been irradiated to violetish blue. Research is

currently being undertaken to improve the process for producing the blue color, and initial contacts are being made with gem suppliers to develop the market for this unique treated gem.

Rainer Schultz Güttler ([rainersg@usp.br](mailto:rainersg@usp.br))  
University of São Paulo, Brazil

Hisahiro Claudio Kohigashi  
São Paulo, Brazil

**Circular ring-like inclusions in a diffusion-treated sapphire.** The Gem Testing Laboratory, Jaipur, India, recently examined an interesting 6.64 ct blue oval mixed cut. The refractive indices of 1.762–1.770, birefringence of 0.008, and hydrostatic specific gravity of 3.98 identified the sample as a natural or synthetic corundum. It was inert to UV radiation (both long- and short-wave) and displayed a weak iron-related band at 450 nm in the desk-model spectroscope.

When viewed face-up, the sample showed uneven coloration (figure 41). The cause of this became evident when it was immersed in methylene iodide: The areas of patchy coloration followed the facet outlines, and the facets around the culet appeared colorless or pale colored (figure 42). This confirmed the material as diffusion treated; the colorless areas likely resulted from repolishing after treatment.

Microscopic examination revealed straight, hexagonal zones that were slightly cloudy and whitish (figure 43, left), which were indicative of natural origin. In addition, the stone contained some irregular cloudy patches. At higher magnification, these milky zones were seen to consist of fine pinpoint inclusions (figure 43, right), as are commonly encountered in heat-treated natural corundum.

The stone displayed an interesting feature when viewed with magnification and illuminated with a fiber-optic light:

Figure 41. This 6.64 ct blue sapphire showing uneven patchy coloration owes its color to diffusion treatment. Photo by G. Choudhary.



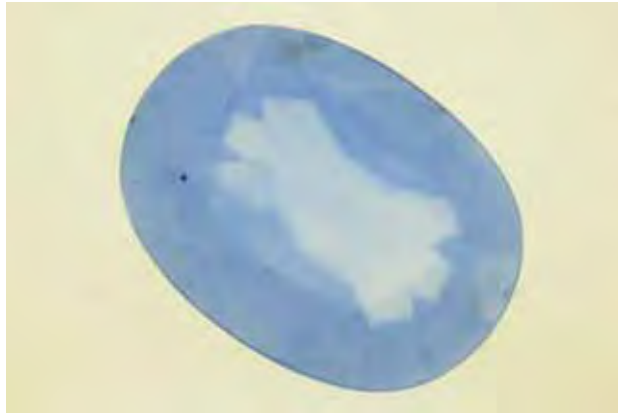


Figure 42. Immersion of the 6.64 ct diffused sapphire in methylene iodide revealed obvious color concentrations, as shown in this view of the pavilion. Photo by G. Choudhary.

groups and rows of circular rings composed of fine white particles (figure 44). Such inclusions have been reported previously in beryllium-treated corundum (Fall 2003 Lab Notes, p. 220; A. Peretti and D. Günther, "The beryllium-treatment of fancy sapphires with a new heat-treatment technique, Part C: Inclusions," *Contributions to Gemology*, No. 4, 2005, p. 54), as well as in traditionally heated sapphires exposed to very high temperatures (AGTA GTC Laboratory Update, [www.agta.org/consumer/news/20060329labupdate.htm](http://www.agta.org/consumer/news/20060329labupdate.htm), March 29, 2006). So far such

inclusions have not been encountered in unheated sapphires; it may therefore be concluded that these inclusions are likely a side effect of exposure to high temperatures, regardless of whether such conditions involved a diffusion process (using beryllium or other elements) and irrespective of the final color.

Due to a lack of sophisticated equipment such as LIBS or LA-ICP-MS, we could not test for the presence of beryllium, so the stone was simply identified as diffusion treated.

Gagan Choudhary and Chaman Golecha  
([gtljpr\\_jp1@sancharnet.in](mailto:gtljpr_jp1@sancharnet.in))  
Gem Testing Laboratory, Jaipur, India

**Diffusion-treated synthetic sapphire with unusual fluorescence.** Recently, the Gem Testing Laboratory, Jaipur, India, received a 5.85 ct blue oval mixed cut for identification (figure 45). Initial testing gave R.I., birefringence, optic sign, and hydrostatic S.G. values consistent with a natural or synthetic sapphire.

The specimen had a blotchy color appearance similar to that often seen in sapphires subjected to diffusion treatment. Furthermore, its hue was typical of the diffusion-treated sapphires that we commonly encounter.

When exposed to short-wave UV radiation, the specimen showed a strong patchy chalky blue fluorescence that followed the facet pattern. However, careful examination revealed that only the star and upper girdle facets showed this reaction, whereas the table and kite facets remained



Figure 43. The 6.64 ct sapphire contained straight, hexagonal, milky zones that suggest a natural origin (left). The milky zones were composed of fine pinpoint inclusions (right), which are commonly associated with heat-treated corundum. Photomicrographs by G. Choudhary; magnified 20× (left) and 40× (right).

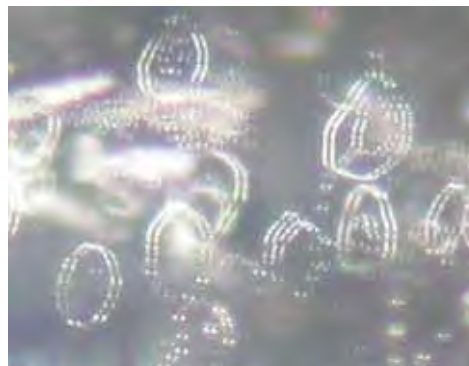


Figure 44. The ring-like inclusions in the sapphire (left) are indicative of high-temperature heat treatment (in this case by a traditional surface-diffusion process). At higher magnification, the circular inclusions were seen to be composed of fine particles. Photomicrographs by G. Choudhary; magnified 25× (left) and 70× (right).



Figure 45. This 5.85 ct blue oval mixed cut was identified as a flame-fusion synthetic sapphire treated by a diffusion process. Photo by C. Golecha.

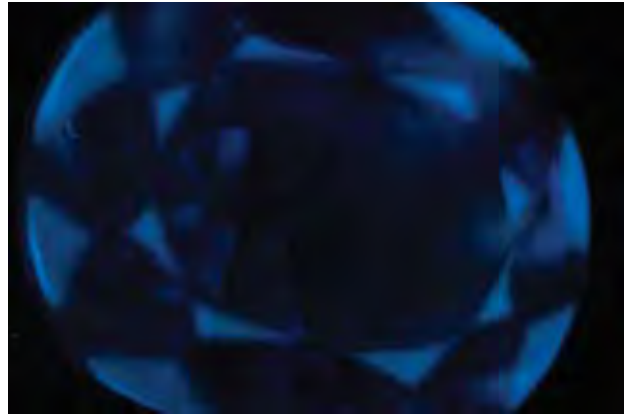


Figure 46. When exposed to short-wave UV radiation, the diffusion-treated synthetic sapphire in figure 45 showed an unusual pattern of symmetrical chalky blue fluorescence: The star and upper girdle facets fluoresced chalky blue, while the table, kite, and pavilion facets were inert. Photo by C. Golecha.

inert (figure 46). The pavilion was also inert, but a weak internal glow—as is commonly associated with synthetic corundum—was observed through this portion of the stone. There was no reaction to long-wave UV radiation.

This fluorescence reaction reminded us of the diffusion-treated synthetic sapphire that one of us (CG) reported previously (see Summer 2006 GNI, pp. 185–186). In that case, however, the patches were random, not following any specific symmetry. No features such as a separation plane were detected that might indicate a composite material.

Microscopic examination with diffuse illumination and immersion in methylene iodide confirmed that the specimen owed its color to a diffusion process (figure 47). However, no color concentrations were seen in the star or upper girdle facets. Also, no curved color banding or angular color zoning was present, which would have been expected if the color was inherent to the specimen. The presence of Plato lines between crossed polarizers is strongly indicative of a flame-fusion synthetic sapphire.

When we compared the color concentrations to the fluorescence reaction (figure 48), it was clear that only the facets lacking color reacted to short-wave UV radiation; those portions showing color concentrations in immersion were inert. This pattern was probably caused by “over polishing” of the star and upper girdle facets after the diffusion treatment, which removed the inert shallow coloration and exposed the untreated, colorless synthetic sapphire portion that fluoresced to short-wave UV. The same thing likely occurred to the sample reported in the Summer 2006 GNI section, although in that case the “over polishing” did not follow any specific pattern.

Chalky blue fluorescence is commonly associated with synthetic and treated sapphires. Typically, synthetic sapphires show fluorescence throughout the volume of the sample, while heat-treated natural sapphires display fluorescence corresponding to the stone’s color zoning, and diffusion-treated natural or synthetic sapphires have chalky blue fluorescence in patches on the surface. Traces of Ti, combined with the high temperatures experienced during the growth of the synthetic corundum or during heat treat-

ment processes, are responsible for the fluorescence, which can be quenched by the simultaneous presence of iron or magnesium (see R. W. Hughes and J. L. Emmett, “Heat seeker: UV fluorescence as a gemological tool,” [www.agta-gtc.org/articles/heat\\_seeker\\_uv\\_fluorescence.html](http://www.agta-gtc.org/articles/heat_seeker_uv_fluorescence.html)). For diffusion-treated sapphires, fluorescence is typically observed in stones with low iron content as patches corresponding to the colored areas of the stone. However, for this synthetic sapphire, that behavior was reversed (again, see figure 48): The fluorescence was present in the colorless regions (i.e., those without a surface diffusion layer).

The fluorescence pattern is consistent with an insufficient concentration of a luminescence quencher (e.g., iron)

Figure 47. Viewed through the pavilion with immersion, the blue color in this 5.85 ct synthetic sapphire was concentrated on specific facets, which indicates diffusion treatment. The pale or near-colorless appearance of the star and upper girdle facets is likely due to “over polishing” after the diffusion process. Photomicrograph by C. Golecha.



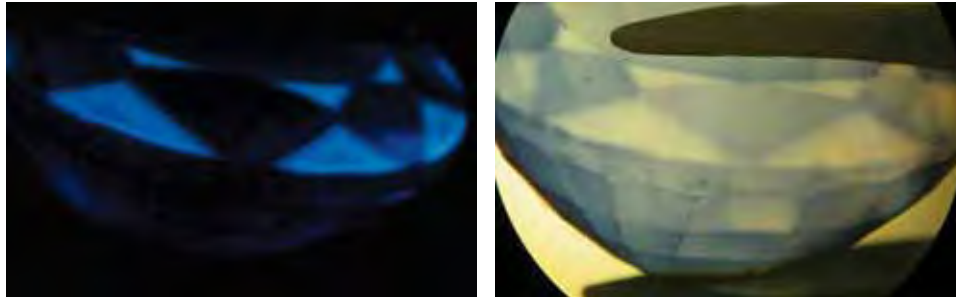


Figure 48. A comparison of the diffusion-treated synthetic sapphire viewed with short-wave UV radiation (left) and in immersion (right) shows that the colored facets are inert. This is likely caused by diffused element(s) quenching the UV fluorescence. Photomicrographs by C. Golecha.

in the synthetic sapphire, and such an element was possibly part of the surface diffusion process. We could not confirm if the quenching element was added purposely in an attempt to negate the tell-tale chalky blue fluorescence, or whether it was a contaminant that was diffused unintentionally. Traditionally, surface diffusion treatments have used titanium oxide, iron oxide, and aluminum oxide. For a detailed review of the diffusion process and chemistry, see R. E. Kane et al., "The identification of blue diffusion-treated sapphires," Summer 1990 *Gems & Gemology*, pp. 115–133.

Gagan Choudhary and Chaman Golecha  
([gtljpr\\_jp1@sancharnet.in](mailto:gtljpr_jp1@sancharnet.in))  
Gem Testing Laboratory, Jaipur, India

## CONFERENCE REPORTS

**32nd Annual GSJ Gemological Conference.** The Gemological Society of Japan was founded in 1973 by Dr. Ichiro Sunagawa and several other gemologists. Since then, annual GSJ conferences have taken place throughout Japan. Although the official language at these meetings is Japanese, international speakers are welcome to give presentations in English. The 2006 GSJ conference was held July 22–23 at Kobe Design University. Nineteen presentations were given on diamonds, colored stone and pearl treatments, LA-ICP-MS and LIBS applications, and other topics. Abstracts from this and some previous GSJ conferences are available at [www.soc.nii.ac.jp/gsa/index-e.html](http://www.soc.nii.ac.jp/gsa/index-e.html).

The 2006 conference also included a field trip to a cultured pearl bead nucleus factory on Awaji Island. The beads are made from several types of freshwater mussels, such as the washboard (*Megalonias gigantea*), mapleleaf (*Quadrula quadrula*), ebonyshell (*Fusconaia ebena*), three-ridge (*Amblyma plicata*), and the pigtoe (*Fusconaia flava*). Approximately 120,000–130,000 momme (1 momme = 3.75 g) of bead nuclei are produced annually.

Next year's GSJ conference will be held at the Tsukuba public library, Tsukuba City on June 2–3, 2007.

Ahmadjan Abduriyim ([ahmadjan@gaaj-zenhokyo.co.jp](mailto:ahmadjan@gaaj-zenhokyo.co.jp))  
Gemological Association of All Japan, Tokyo

**International Mineralogical Association Biennial Meeting.** Over 800 researchers from some 50 countries attended the 19th general meeting of the IMA in Kobe, Japan, July 23–28, 2006. The conference included a session titled "Natural and Artificial Gem Materials." **One of these con-**

**tributors** (EF) discussed the several causes of brown color in diamonds, the most common being associated with brown graining resulting from plastic deformation. Recent work suggests that this brown color can be qualitatively correlated with a series of near-infrared absorption bands known as the "amber center," which possibly consists of a particular arrangement of two nitrogen and two carbon atoms in the diamond lattice. A system to classify several European fossil resins (i.e., amber) on the basis of optical, spectroscopic, and chemical properties was discussed by **Prof. Corina Ionescu** of Babes-Bolyai University in Cluj-Napoca, Romania. Her work indicates that these ambers can be divided into three chemically and structurally different categories. **Dr. Carlo Aurisicchio** of the Institute of Geosciences and Georesources in Rome described a study to establish the country of origin of emeralds using trace-element analysis determined by secondary ion mass spectrometry (SIMS) in combination with inclusion characteristics and oxygen and hydrogen isotope ratios. Unique patterns of trace elements are distinctive of at least some important emerald localities. A theoretical modeling study supported by heat-treatment experiments involving beryllium diffusion in corundum was carried out by **Dr. Jun Kawano** of the Yamanashi Institute of Gemmology and Jewellery Arts in Kofu, Japan. His work suggests that Be diffusion in corundum can occur at lower temperatures (1300 K and possibly lower) than previously thought. Several potential applications for LA-ICP-MS chemical analysis to solve identification problems in gemology were discussed by **Dr. Ahmadjan Abduriyim** of the Gemmological Association of All Japan in Tokyo. Examples included the detection of Be in diffusion-treated sapphires and the determination of the geographic source of blue sapphires and Cu-bearing tourmalines.

This same session also included several poster presentations. **Dr. Hisao Kanda** of the National Institute for Materials Science in Tsukuba, Japan, studied the broad-band luminescence (known as band-A, extending between 400 and 550 nm) in natural diamonds using cathodoluminescence spectroscopy. Two kinds of band-A luminescence were documented: (1) a band with a maximum at about 415 nm in type Ia diamonds that displays a pattern that follows the growth structure and, hence, appears to be produced by defects introduced during growth; and (2) a band with a maximum at about 435 nm in all diamond types, with a pattern that follows slip planes and is therefore produced by defects created by plastic deformation

during post-growth processes. **Prof. Norimasa Shimobayashi** of the Department of Geology and Mineralogy, Kyoto University, described iridescent andradite from Tenkawa, Nara Prefecture, Japan. The iridescence is thought to arise from a fine lamellar structure in which the layers have slightly different Al/Fe ratios.

Several presentations in other sessions were of gemological interest. **Dr. George Harlow** of the Department of Earth and Planetary Sciences, American Museum of Natural History, New York, spoke about the need for all mineralogical museums to standardize the data used to describe mineral samples in their collections in order to make this information more accessible and useful. **Dr. Satoshi Matsubara** of the National Science Museum in Tokyo described a special jade exhibit at the museum that took place in 2004–2005. **Prof. Georges Calas** of the Institut de Minéralogie et de Physique des Milieux Condensés, University of Paris, described various improved spectroscopic techniques for characterizing transition metals, such as Cr in minerals, which are important coloring agents. In a study of four highly included (“cloudy”) diamond crystals from two kimberlites in Siberia, **Dr. Alla Logvinova** of the Institute of Geology and Mineralogy, Russian Academy of Sciences, Novosibirsk, found a variety of mineral and fluid phases in nanometer-sized inclusions. The similarity with the phase assemblages in analogous inclusions in diamonds from Canadian kimberlites indicates a similarity in their diamond forming environments in the mantle. **Dr. Galina Kudrayvtseva** of Moscow State University described the characteristics of gem-quality type I diamonds from the Grib kimberlite in the Arkhangelsk region in northwestern Russia. Many of the diamond crystals were colorless and of good clarity. Among the mineral inclusions identified were chromite, olivine, diopside, orthopyroxene, and Fe/Ni sulfides.

**Dr. Anastasia Shuskanova** of the Institute of Experimental Mineralogy, Russian Academy of Sciences, Chernogolovka, demonstrated that although sulfide melts allow the growth of diamond, they are not consistent with the inclusion suites observed in natural diamonds. Therefore, sulfide melts are at best immiscible droplets in silicate-carbonate melts during diamond growth. **Dr. Dan Schulze** of the Department of Geology, University of Toronto, Canada, studied the chemical composition of eclogitic diamonds from the Quebrada Grande region of Venezuela. These diamonds are thought to result from crystallization of biogenically derived carbon that originated in subducted oceanic crust. **Dr. Nikolai Sobolev** of the Institute of Geology and Mineralogy, Russian Academy of Sciences, Novosibirsk, reported some new trace-element data—for Ni, Mn, Ca, Co, Cr, and Al—in olivine inclusions within diamonds. Olivine is the most typical type of inclusion in peridotitic diamonds. **Dr. Makoto Arima** of the Geological Institute of Yokohama National University, Japan, discussed how various factors, such as local thermal and chemical conditions, influence both the growth and resorption of diamond crystals during their long residence

in the earth’s mantle. **Dr. Ben Harte** of the Grant Institute of Earth Science, University of Edinburgh, Scotland, studied majoritic (high-Si) garnet inclusions in alluvial diamonds from the São Luiz River in Juina Province, Brazil. These single-crystal inclusions appear to indicate that the diamonds formed at depths greater than 400 km.

Discoveries of blue sodalite fashioned for personal adornment as long ago as 1300 BC in the central Andes led to a study by **Dr. Masaaki Shimizu** of the Department of Earth Sciences, University of Toyama, Japan. The source of this material was identified as Cerro Sapo in Bolivia, and its distribution in archeological sites has revealed valuable information on historical trade routes across South America.

Separately from the conference, the Gemological Association of All Japan (GAAJ) organized a short field trip to the Hirayama Co. pearl nucleus factory near Kobe. The company uses 22 tonnes of freshwater mussel (*Anadonta*) shells annually to produce about 700 kg of bead nuclei. The manufacture of these beads consists of 20 steps, and the finished beads range from 1 to 15 mm in diameter. The final polish is obtained with a garnet-based powder. The best-quality beads are used for Japanese Akoya cultured pearls, while the others are sent to China.

James E. Shigley  
GIA Research, Carlsbad

EF

## ANNOUNCEMENTS

**G&G online conference calendar.** A regularly updated list of conferences and museum announcements pertaining to gems is now available on the G&G web site at [www.gia.edu/gemsandgemology](http://www.gia.edu/gemsandgemology).

**GIA’s Russell Shor wins Liddicoat Journalism Award for *Gems & Gemology* article.** GIA senior industry analyst and frequent G&G contributor Russell Shor won the 2006 AGS Richard T. Liddicoat Journalism Award in the category of Industry/Trade Reporting for his Fall 2005 G&G article “A review of the political and economic forces shaping today’s diamond industry” (pp. 202–233). This is the third G&G article so honored since the competition began in 2003.

**Visit *Gems & Gemology* in Tucson.** Meet the editors and take advantage of special offers on subscriptions and back issues at the G&G booth in the publicly accessible Galleria section (middle floor) of the Tucson Convention Center during the AGTA show, January 31–February 5, 2007. GIA Education’s traveling Extension classes will offer hands-on training in Tucson with “Gem Identification” (January 29–February 2), and several free seminars will be offered by GIA staff February 3–4. To enroll, call 800-421-7250, ext. 4001. Outside the U.S. and Canada, call 760-603-4001. The GIA Alumni Association will host a dance party in Tucson on February 2 celebrating the

---

Association's 25th anniversary. To reserve tickets, call 760-603-4204 or e-mail [events@gia.edu](mailto:events@gia.edu).

### Conferences

**NAJA Annual Conference.** The National Association of Jewelry Appraisers is holding its 27th annual Winter Educational Conference January 29–30, 2007, during the Tucson gem shows. Visit [www.najaappraisers.com](http://www.najaappraisers.com).

**Rapaport International Diamond Conference 2007.** Scheduled for February 5 in New York, this conference will focus on the most important issues confronting the diamond industry, including conflict diamonds, the internet, and branding. Call 877-987-3400 or e-mail [conference@diamonds.net](mailto:conference@diamonds.net).

**Hasselt Diamond Workshop.** Held February 28–March 2, 2007, at Hasselt University, Diepenbeek–Hasselt, Belgium, this conference will cover the physics of diamond defects and characterization of CVD synthetic diamond. Visit [www.imo.uhasselt.be/SBDD2007](http://www.imo.uhasselt.be/SBDD2007).

**PDAC 2007.** The Prospectors and Developers Association of Canada convention will take place March 4–7 in Toronto. Diamonds will be featured in a session called "Diamond Facets from Exploration to Environment," and also will be included in other sessions. Visit [www.pdac.ca/pdac/conv](http://www.pdac.ca/pdac/conv).

**WJA in New York.** The Women's Jewelry Association "Women In the Know" business conference will be held on March 16, 2007, at the Fashion Institute of Technology in New York City. Visit [www.womensjewelry.org](http://www.womensjewelry.org).

**Bead Expo.** The 2007 International Bead Expo will be held in Oakland, California, April 11–15. Over 60 workshops and educational lectures on bead jewelry design and manufacture are scheduled. Visit [www.beadexpo.com](http://www.beadexpo.com).

**BASELWORLD 2007.** The BASELWORLD show will be held April 12–19 in Basel, Switzerland. GIA will host GemFest Basel on April 14, 4–6 p.m., at the Basel Convention Center, Hall Montreal. Kenneth Scarratt, director of GIA Research (Thailand), will be speaking on GIA's Pearl Classification System. RSVP by April 5 at [events@gia.edu](mailto:events@gia.edu). During the show, *Gems & Gemology* editor-in-chief Alice Keller will be available at the GIA Booth in Hall 2, Stand W23. Visit [www.baselshow.com](http://www.baselshow.com), call 800-922-7359, or e-mail [visitor@baselworld.com](mailto:visitor@baselworld.com).

**Sinkankas Jade Symposium.** Jade will be featured at this year's John Sinkankas Memorial Symposium, held April 21, 2007, at GIA Carlsbad. A variety of experts will speak on jade localities, inclusions, treatments, appraising, lapidary work, and literature at this all-day educational event. E-mail [merksjade@cox.net](mailto:merksjade@cox.net).

**2007 ICA Congress.** The International Colored Gemstone Association Congress will be held May 5–9 in Dubai, United Arab Emirates. The theme will be "Embracing Global Trends from Mine to Market." Presentations will be given by industry leaders on gem sources, manufacturing centers, marketing, branding, laboratory services, and education/ethics/economics. Visit [www.gemstone.org/gem-news](http://www.gemstone.org/gem-news).

**Granitic Pegmatites: The State of the Art.** Held May 6–12, 2007, at the Universidade do Porto, Portugal, this workshop will focus on the study of granitic pegmatites, and will include a field trip to rare-element pegmatites in northeastern Portugal and central-western Spain. Visit [www.fc.up.pt/peg2007](http://www.fc.up.pt/peg2007).

**2007 GAA-NSW Conference.** The 2007 conference of the New South Wales Division of the Gemmological Association of Australia will be held May 18–20 at Hadley's Hotel in Hobart, Tasmania. Subjects will include the history of gems and lapidary, rare ivories, and Art Deco/Art Nouveau jewelry. Visit [www.gem.org.au/conference.htm](http://www.gem.org.au/conference.htm).

**GAC-MAC 2007.** The 2007 joint meeting of the Geological Association of Canada and the Mineralogical Association of Canada will take place May 23–25 in Yellowknife, Northwest Territories. The conference will include a special session titled "Diamonds: Exploration to Production—A Northern Canada Perspective." A "Geology of Gem Deposits" short course is also scheduled, as well as a field trip to the Ekati and Diavik diamond mines. Visit [www.nwtgeoscience.ca/yellowknife2007](http://www.nwtgeoscience.ca/yellowknife2007).

**Maine Pegmatite Workshop.** The 5th Maine Pegmatite Workshop will be held May 26–June 3, 2007, in Poland, Maine. In addition to the in-depth curriculum, field trips to gem-bearing pegmatites in New England are planned. Visit [homepage.mac.com/rasprague/PegShop](http://homepage.mac.com/rasprague/PegShop).

**New Diamond and Nanocarbons.** Scheduled for May 28–31, 2007, in Osaka, Japan, this conference will address recent developments in the growth and characterization of synthetic diamond. The NDNC is a merger of the International Conference of New Diamond Science and Technology (ICNDST) and the Applied Diamond Conference (ADC). Visit [www2.convention.co.jp/NDNC2007](http://www2.convention.co.jp/NDNC2007).

**First European Gemmological Symposium: "Presence and Future of Gemmology."** Honoring the 75th Anniversary of the German Gemmological Association, this international symposium will take place June 22–24, 2007, in Idar-Oberstein, Germany, and will feature numerous scientists in gemology and well-known business leaders from the gem and jewelry industry. Visit [www.dgemg.com/gemmologen\\_eng/index.php?seite=aktuell](http://www.dgemg.com/gemmologen_eng/index.php?seite=aktuell).

---

**30th International Gemmological Conference.** Scheduled for July 15–19, 2007, in Moscow, Russia, this conference will cover new gem deposits, synthetics, treatments, gem identification methods, and markets. The talks will be given only by IGC delegates, but the conference is open to observers and students. E-mail [balvld@iem.ac.ru](mailto:balvld@iem.ac.ru).

### Exhibits

**Colored diamonds at the Natural History Museum.** On loan from Alan Bronstein and Harry Rodman, the Aurora Collection of 296 naturally colored diamonds is now on display at the Natural History Museum in London. Visit [www.nhm.ac.uk/about-us/news/2006/november/news\\_9996.html](http://www.nhm.ac.uk/about-us/news/2006/november/news_9996.html).

**Jewelry History at the Newark Museum.** “Objects of Desire: 500 Years of Jewelry,” an exhibition of more than 200 jewelry pieces from the collection of the Newark Museum, New Jersey, is on display through February 26, 2007. The collection covers American and European jewelry from the 1500s to the modern era. Visit [www.newarkmuseum.org](http://www.newarkmuseum.org).

**Symbols of Identity—Jewelry of Five Continents.** On display through March 2007 at the Mingei International Museum in San Diego, this exhibit features examples of personal adornment from native cultures in North and South America, Africa, Asia, and Europe. Visit [www.mingei.org/curex.html](http://www.mingei.org/curex.html).

**Gold at AMNH.** “Gold,” an exhibition exploring the historical fascination with this precious metal, is on display at the American Museum of Natural History in New York through August 19, 2007. The exhibit includes both rare natural specimens and significant cultural artifacts. Visit [www.amnh.org/exhibitions/gold](http://www.amnh.org/exhibitions/gold).

**Jewelry of Ben Nighthorse.** Ben Nighthorse Campbell, who was a U.S. senator from Colorado from 1992–2004, has enjoyed a successful second career as an innovative jewelry designer. This collection of his work, which debuted at the Smithsonian Institution’s National Museum of the American Indian in 2004, is on display at the Colorado History Museum in Denver through December 31, 2007. Visit [www.coloradohistory.org](http://www.coloradohistory.org).

**South Sea Pearls at the GIA Museum.** “White Magic,” an exhibit of South Sea cultured pearl jewelry, will be on view at the GIA Headquarters in Carlsbad January 19–May 15, 2007. The exhibit features jewelry suites by 17 of today’s top designers, including Henry Dunay, David Yurman, Stephen Webster, Casa Vhernier, and Orlando Orlandini. Advance reservations are required; to schedule

a tour, call 760-603-4116 or e-mail [museum@gia.edu](mailto:museum@gia.edu).

**French Jewelry at the Legion of Honor.** “Masterpieces of French Jewelry,” an exhibition of notable French jewelry pieces from American collectors, will be on display at the Legion of Honor art museum in San Francisco, February 10–June 7, 2007. Among the pieces included are the Taj Mahal diamond necklace by Cartier, given to Elizabeth Taylor by Richard Burton in the 1970s, and an Art Nouveau brooch owned by Jacqueline Kennedy Onassis. Visit [www.thinker.org/legion/exhibitions](http://www.thinker.org/legion/exhibitions).

**Native American Jewelry.** “Shared Images: The Jewelry of Yazzie Johnson and Gail Bird” will be on display February 17 through June 2007 at the Heard Museum in Phoenix, Arizona. The exhibit includes examples of their belts, earrings, bracelets, rings, and necklaces. Visit [www.heard.org](http://www.heard.org).

### ERRATA

1. In the Spring 2006 GNI entry on pyrope-spessartine from Tanzania (pp. 66–67), the second sentence should have indicated that the garnets came from Tanzania, rather than Madagascar.
2. In table 3 (p. 106) of the Summer 2006 LA-ICP-MS article by A. Abduriyim et al., next to the parameter “Laser line size,” the GAAJ logo size should have been reported as 80 × 230 mm.
3. The Summer 2006 GNI section included a note on jerejevite from Myanmar and Sri Lanka (pp. 175–176). The jerejevite reported to be from Sri Lanka actually came from Madagascar (see Winter 2004 GNI, pp. 340–341). The rough came to Sri Lanka via dealers who purchased the material in Madagascar. We thank E. Gamini Zoysa (Mincraft Co., Mount Lavinia, Sri Lanka) for bringing this to our attention, and Dudley Blauwet (Dudley Blauwet Gems, Louisville, Colorado) for confirming this with the dealer who purchased the rough in Sri Lanka.
4. In the Fall 2006 Gemological Research Conference poster session abstract on demantoid from Iran (by G. Du Toit et al., p. 131), the banded opaque material consisting of layers of apatite and calcite actually comes from a different part of Iran, rather than being associated with the demantoid deposits.
5. The Fall 2006 International Gemological Symposium poster session abstract on the Bahia sculpture (by G. Lehrer and L. Stoller, p. 158) erroneously described its source material as a rutile crystal. Bahia was carved from a rutiled quartz crystal.

# Challenge WINNERS

This year, hundreds of readers participated in the 2006 GEMS & GEMOLOGY Challenge. Entries arrived from around the world, as readers tested their gemological knowledge by answering questions listed in the Spring 2006 issue. Those who earned a score of 75% or better received a GIA Continuing Education Certificate recognizing their achievement. The participants who scored a perfect 100% are listed here.

Congratulations!

## ANSWERS

See pages 81–82 of the Spring 2006 issue for the questions: 1 (b), 2 (a), 3 (b), 4 (b), 5 (c), 6 (b), 7 (d), 8 (a), 9 (a), 10 (a), 11 (c), 12 (d), 13 (d), 14 (b), 15 (d), 16 (d), 17 (c), 18 (b), 19 (d), 20 (d), 21 (d), 22 (b), 23 (a), 24 (d), 25 (a)

**AUSTRALIA** *Coogee, Western Australia*: Helen Judith Haddy. *Cronulla, NSW*: Ava Quibranza Livne • **BELGIUM** *Brussels*: Sheila Sylvester. *Diksmuide*: Honoré Loeters. *Ghent*: J. G. J. Loyens. *Ruiselede*: Lucette Nols • **CANADA** *Vancouver, British Columbia*: John R. J. Scott. *St. Catharines, Ontario*: Alice J. Christianson. *Bobcaygeon, Ontario*: David R. Lindsay. *Kingston, Ontario*: Brian Randolph Smith • **ENGLAND** *London*: Despina Nicole Sideras • **GERMANY** *Leipzig*: Noomi Levinsson • **HONG KONG** *Causeway Bay*: Cristina O. Pierley-O'Brien • **ITALY** *Aosta*: Fabrizio Troilo. *Civitavecchi*: Luigi Ceretti. *Padova*: Marco Maso • **THE NETHERLANDS** *Rotterdam*: E. Van Velzen • **RUSSIA** *Moscow*: Vadim Prygov • **SCOTLAND** *Aberdeen*: Helen L. Plumb. *Edinburgh*: James Heatlie, A. Ewen Taylor • **SPAIN** *Valencia*: Monika Bergel • **SWITZERLAND** *Zollikon*: Adrian Meister • **THAILAND** *Bangkok*: Somapan Asavasanti, Alexander Ross, Pattarat Termpaisit. *Samutprakarn*: Thomas Estervog • **UNITED STATES** **California** *Carlsbad*: Martin Harmon, Brenda Harwick, Michael T. Jakubowski, Mark Johnson, Douglas Kennedy, Abba Steinfeld, Heng H. Taing, Louisa Turner, Lynn Viall, Mike Wobby, Philip York, Marisa Zachovay. *Fremont*: Ying Ying Chow. *Lancaster*: Samuel Denson. *Marina Del Rey*: Veronika Riedel. *Orange*: Alex Tourubaroff. *Rancho Cucamonga*: Sandy MacLeane. **Florida** *Clearwater*: Tim Schuler. **Georgia** *Atlanta*: Ella Golden. **Hawaii** *Ewa Beach*: Jane J. Chen. *Makawao*: Alison Fahland. **Illinois** *Chicago*: Heidi Harders. *DuQuoin*: William Duff. **Indiana** *Carmel*: Mark A. Ferreira. **Maine** *Milbury*: Bernard M. Stachura. *Temple Hills*: Bobby Mann. **Minnesota** *Minneapolis*: Andy Stevens. **Nevada** *Reno*: Allen P. Salgado, Terence Terras. **New Jersey** *Moorestown*: Rosemarie C. Hill. **New York** *New York*: HyeJin Jang-Green, Wendi Mayerson, Anna Schumate, Carolyn van der Bogert. **North Carolina** *Advance*: Blair Tredwell. *Kernersville*: Jean Bonebreak. **Ohio** *Cuyahoga Falls*: Catherine Lee. **Oregon** *Cottage Grove*: Lyndeth Esgar. *Medford*: Julia Ann Horton. **Pennsylvania** *Schuylkill Haven*: Janet Steinmetz. **Rhode Island** *Rumford*: Sarah A. Horst. **South Carolina** *Sumter*: James Markides. **Texas** *Livingston*: Janet S. Mayou. **Virginia** *Hampton*: Edward Goodman. *Herndon*: Lisa A. Marsh-Vetter. *Kilmarnock*: Mary K. Helne. **Washington** *Battle Ground*: Joseph Bloyd. *Bellingham*: Mary L. Harding. *Millcreek*: Nicki Taranto. *Seattle*: Janet Suzanne Holmes.

## EDITORS

Susan B. Johnson  
Jana E. Miyahira-Smith  
Stuart Overlin

**Agates: Treasures of the Earth**

By Roger Pabian with Brian Jackson, Peter Tandy, and John Cromartie, 184 pp., illus., publ. by Firefly Books, Buffalo, NY, 2006. US\$35.00

Written by four recognized authorities in the field, this book fills a long-standing need for a reliable introductory guide to the agates of the world. Though beautifully illustrated, it is not a coffee table book; it is a standard hardcover book size, measuring 8.25 × 6 inches (15.5 × 21 cm). Most of its 184 pages feature stunning agate photos in full color. These are not just "eye candy" but, for the most part, really do fit in with the text. Almost every picture has an informative caption.

The first 47 pages introduce the reader to what an agate is—not an easy task, with 19 pages devoted to definitions of some of the more important types.

The part that should be of the greatest interest and importance to every reader—whether a beginning "rockhound," a seasoned collector, or a geoscientist interested in the mineralogy of quartz—is the 100-page section titled "Sources of Agates."

There is a very brief (four page) section on lapidary. A chapter on imitations and forgeries of agates is disappointingly brief (two pages), just enough to whet the reader's appetite. The authors did not bother to rehash the ancient history of agate scams but concentrated instead on cutting-edge technology. Most of these scams were new to us, and we have long collected such triumphs of warped genius.

The book finishes with 14 pages of historical material that is interesting but too brief to give more than a

small taste of the subject. The index is, happily, quite adequate.

There are a few warts on the toad, however. We found the bibliography to be somewhat lacking, even if perhaps better than the current (often low) standard. The references are divided into journals and books. The journal articles could be a bit more extensive, but at least they are organized alphabetically by author. The books, strangely, are organized alphabetically by the first word in the title. Of the 44 books referenced, seven started with "The" and are alphabetized under the letter *t*. Additionally, five journals (four in English) are listed along with eight websites. Considering the prospective audience for this book, it would have been kinder to many of the readers to suggest more journals. Also, all three volumes of John Sinkankas' *Gemstones of North America* should have been cited, especially since volume two is probably the best available source for references to agate articles.

We were a bit shocked that none of the authors' own various works were listed in the bibliography. Only the second edition of Webster's *Gems* was included.

There are a number of other rather trivial objections and corrections that could be listed. The description of Mexican "coconuts" (page 17) is very poor. The picture showing "marble-like" patterns (page 25) is actually Mexican lace agate. The magnificent picture of brecciated agate (page 22) is not attributed to any locality, but almost certainly comes from Schlottwitz in Germany. The comment on page 23 that chalcedony is brittle would certainly be disputed by anyone who has spent time trying to

break up a large piece. Perhaps they should have mentioned that heat treatment makes chalcedony more brittle, a fact probably discovered by Neolithic people.

In spite of these few things we would quarrel with, this is a wonderful book, suitable for a wide variety of readers. Every rockhound and jeweler could benefit from having it on their shelves, and it should be made available to educational institutions of all levels.

SI and ANN FRAZIER  
*El Cerrito, California*

**Bling Bling: Hip Hop's Crown Jewels**

By Minya Oh, 208 pp., illus., publ. by Wenner Books, New York, 2005. US\$27.50

Since this book's publication in 2005, the imprint of rap music and its lifestyle successor hip-hop on America's cultural scene has only grown larger. The title phrase, a reference to showy or expensive jewelry, gained further acceptance as part of the lexicon by its inclusion in the latest editions of the Webster's and Oxford dictionaries. Today, the catchy phrase needs no repetition: one "bling" will do.

Despite its inner-city roots and the raw personalities of its more outrageous ambassadors, hip-hop culture has spun off jewelry trends and clothing fashions admired and emulated in unexpected places, from elite shopping boulevards to grade schools in America's small towns to villages around the world. When impresario Russell Simmons embarked on a fact-

finding mission to Africa in late 2006 to research how the diamond industry might work with his jewelry company to help empower Africans' lives, the jewelry world and major media outlets took notice.

In her first book, pop-culture reporter and radio show host Minya Oh presents a range of iconic figures from the world of hip-hop—rappers, producers, and the jewelers who answered the call to adorn them. A series of interviews, interspersed with photographs culled from news features, wire services, and personal snapshots, include some of hip-hop's biggest names from the 1970s to the present, nearly all of them proponents of bling. Most have a story to tell about jewelry, if not a detailed remembrance of their first piece or the significance they place on being "iced."

Oh's interviews exemplify how, in many ways, hip-hop's pervasive influence catapulted some of jewelry's hottest trends of the last 20 years to the far reaches of pop and mainstream culture, and often did so more effectively than any organized marketing campaign. Examples include the resurgence of extravagant and pavé diamond jewelry; the revitalization of the entire men's jewelry category; the flashy appeal of oversized or outrageous watch styles; the appeal of ethnic jewelry, beads, and medallions; the craving for colored diamonds; the ghetto-fabulous fashion of huge hoops and "doorknocker" earrings; and the revival of rose gold.

As Grammy Award-winning rap artist and actor Ludacris explains in his foreword, *bling* (which he uses to refer to anything with many diamonds) has the power to completely transform one's image and imbue one's persona with star quality, if not a sense of immortality. In the history of wealth's accoutrements and mystique, such insights are hardly novel. To no one's surprise, he and other rappers also spell out one of bling's biggest benefits: getting women.

The book's pages are filled with

the pictures, profiles, and patois of LL Cool J, Slick Rick, Missy Elliott, Lil' Kim, 50 Cent, Public Enemy's Chuck D, and others, sporting "dookie ropes" (heavy gold chains), massive earrings, Jesus-head pendants, monster watches, and custom pieces that—though seen—may still not be believed. Well-known Hollywood actors and rappers alike are photographed baring mouth jewelry from braces-like diamond grills to gold teeth.

The influences of individual jewelers are prominently featured in the book, which also includes a buyer's guide with contact information. Most often cited is Yakov Arabov who, as Jacob the Jeweler, has outfitted some of hip-hop's biggest stars. (Arabov made a different kind of news in mid-2006 after his indictment on drug-related money laundering charges, to which he has pleaded not guilty.)

This is not a book for the faint-hearted or those seeking a scholarly socio-cultural treatise. The heavy lingo and profanity-laced language begins on page one of the foreword and doesn't let up. Oh's questions are often more styled to music television chatter, or just plain street talk, than a focused or probing read. Ironically, the most articulate and complete-sentence responses, though appearing more e-mailed than spoken, come from West African-born jewelry designer Chris Aire, one of the few subjects to raise the issue of conflict diamonds as he urges his clientele to bling the right way.

Anyone interested in understanding the formative jewelry mindset of today's pop culture, Generation Next, and men's fashion may want to flip through this book's pages. Its jarring photographs, with heavy grain and often-poor focus, are not for everyone, but they tell a story that jewelers, designers, and others will find hard to ignore as long as America's celebrity limelight shines on hip-hop and its bling.

MATILDE PARENTE  
*Libertine*  
*Indian Wells, CA*

## Masterpieces of French Jewelry from American Collections

By Judith Price, 144 pp., illus., publ. by Running Press, Philadelphia, PA, 2006. US\$29.95

In France, as author Judith Price points out in this companion book to the similarly titled exhibit, the office of the Minister of Culture carries clout that is unparalleled anywhere else in the developed world. While such influence is testimony to respect for that country's traditions, it also underscores a boundless creativity in cuisine, cinema, couture, and other areas that, no matter how far-reaching, remains at its core unmistakably, fabulously French.

As a newly moneyed elite emerged in 19th century America and quickly claimed a place at the global table of prosperity, they too looked to France for all things *haute*, including jewelry.

Those elite, this exhibit's curators, and the author all chose well. The exhibit's 150 pieces, culled from museums, galleries, and private collections, represent jewelry artists whose works typify major periods from Art Nouveau to the contemporary styling of Paris-based New Yorker Joel Arthur Rosenthal, more familiar as JAR.

Exhibit sponsors include titans from the worlds of jewelry and finance in partnership with the National Jewelry Institute, a nonprofit organization founded in 2002 that Price serves as president and whose mission is to preserve and educate the public about fine jewelry as art.

Striking pieces from anonymous private collectors include a Boucheron brooch ca. 1894 with engraved diamond butterfly wings and a ruby body; a 1913 garland-style Cartier bow brooch; a 1925 Art Deco jazz-band charm bracelet and a sun ray handbag in gold and diamonds by Sterlé ca. the 1950s; and one of the book's many exquisitely detailed *minaudières*.

Featured designs by Van Cleef & Arpels, innovators of the invisible setting and an exhibit sponsor, include a

1980s platinum “mystery-set” emerald and diamond bracelet with earrings as well as a ruby, diamond, and sapphire flower brooch created for the U.S. bicentennial, both from the collection of Iris Cantor.

Elizabeth Taylor’s 40th birthday present from Richard Burton embodies the eternal history of love’s tragedy and triumph. Set with ruby in gold ca. 1970 by Cartier Paris, the pendant’s cornerstone diamond—heart-shaped and inscribed—dates to the 17th century, when it was given by Mogul emperor Shah Jahan to his second wife, in whose memory the Taj Mahal was built.

Magnificent pieces by Lalique, Fouquet, and other well-known artists are as sensitively rendered as those by unknown (presumably French) artists, as in the artful gold earrings and sculpture bracelet ca. 1948 that flaunt spiky citrine briolettes with rubies.

Gentle editing might have improved the book’s editorial content, which occasionally reads like an effusive, albeit earnest, term paper. Collectors’ commentaries, billed as back stories, are not especially illuminating given the creative and historical gravity of the pieces that grace each page. Their behind-the-scenes remarks might have been better placed together at the back of the book to avoid jarring segues from Art Nouveau on one page to *Caddyshack II* references on the next.

At 11 inches (27.5 cm) square, the book is an ideal coffee-table size. The typesetting is clear and well-spaced for easy scanning or reading. Although the various photography credits fill the entire last page, the images demonstrate consistently high quality and harmony across styles, eras, and collectors. Readers keen for detail will appreciate their large sizes.

While the exhibit’s debut at The Forbes Galleries in New York ended in

late December 2006, lovers of fine jewelry and period pieces have yet another reason to visit San Francisco in springtime. There, inside the Beaux-Arts confines of The Legion of Honor, the exhibit can be enjoyed February 10–June 10, 2007, after which its companion book will bring pleasure for years to come to Francophiles, jewelry historians, designers, and all who appreciate timeless artistry.

MATILDE PARENTE

### The Jeweler’s Directory of Gemstones

*By Judith Crowe, 176 pp., illus., publ. by Firefly Books, Buffalo, NY, 2006. US\$29.95*

This book is a practical guide to both common and exotic gems for jewelry designers, hobbyists, and consumers. Its goal, stated upfront, is to provide information on the nature of gems—their sources, markets, and quality factors—and to show how they can be used creatively and appropriately in jewelry. This is achieved through clear, concise writing, careful organization, and beautifully photographed jewels.

Three sections take the reader through (1) the basics of gemology and the gem trade, (2) a variety of gem materials, and (3) the principles of design and jewelry manufacturing (with an emphasis on handcrafted jewels). The first section also covers information on gem properties, inclusions, formation, mining methods, and cutting techniques, with a good overview of the mining and cutting of diamonds.

The second section, which covers 35 gems such as diamond, corundum, lapis, and the organic materials, begins with a look at color and clarity treatments in general. Each gem is given

one or more well-illustrated pages covering sources, quality factors, pricing, and (where pertinent) information about synthetics and treatments. Authoritative sections on pearls, coral, amber, and shell (and their imitations) will be especially useful for consumers baffled by the range of products available in these categories. In this section, though, there are several stones whose inclusion made me wonder what the author had chosen to omit: Did hemimorphite and tugtupite edge out pectolite and azurmalachite? And an otherwise-strong entry on diamond would, I think, have benefited from a paragraph or two on the importance of cut and its relationship to appearance in modern-cut stones. As it is, the choice of a yellowish old mine cut for the Grading Factors page is an odd one.

The third section will be of help to anyone interested in jewelry design or in working with a jeweler to complete custom work. Its discussion of settings, finishes, and the care and feeding of delicate stones, rough gems, and beads benefits tremendously from a firm grounding in color and design theory and the basic principles of jewelry engineering. The images chosen to illustrate these topics are extraordinary: beautifully cut gems, graceful and wearable studio jewels, and clear and precise drawings, all of which make the book a visually striking and useful reference.

*The Jeweler’s Directory of Gemstones* ends with an index and several useful appendices: a list of trade groups and laboratories in North America and Europe, a glossary, a short bibliography of books, and a list of useful websites. Well-known gemology and geology writer Cally Hall is credited as a contributing author.

LISA SCHOENING

*Gemological Institute of America  
Los Angeles, California*

'06

gemological  
ABSTRACTS

## EDITORS

**Brendan M. Laurs**  
**Thomas W. Overton**  
 GIA, Carlsbad

## REVIEW BOARD

**Christopher M. Breeding**  
 GIA Laboratory, Carlsbad

**Jo Ellen Cole**  
 Vista, California

**Eric A. Fritz**  
 GIA Laboratory, Carlsbad

**R. A. Howie**  
 Royal Holloway, University of London

**Alethea Inns**  
 GIA Laboratory, Carlsbad

**Hyejin Jang-Green**  
 GIA Laboratory, New York

**Paul Johnson**  
 GIA Laboratory, New York

**David M. Kondo**  
 GIA Laboratory, New York

**Taijin Lu**  
 GIA Research, Carlsbad

**Wendi M. Mayerson**  
 GIA Laboratory, New York

**Kyaw Soe Moe**  
 GIA Laboratory, New York

**Keith A. Mychaluk**  
 Calgary, Alberta, Canada

**James E. Shigley**  
 GIA Research, Carlsbad

**Boris M. Shmakin**  
 Russian Academy of Sciences, Irkutsk, Russia

**Russell Shor**  
 GIA, Carlsbad

**Jennifer Stone-Sundberg**  
 Portland, Oregon

**Rolf Tatje**  
 Duisburg University, Germany

**Sharon Wakefield**  
 Northwest Gem Lab, Boise, Idaho

COLORED STONES AND  
ORGANIC MATERIALS

**Application of geochemical ratios for delineating gem-bearing areas in high grade metamorphic terrains.** P. N. Rana-singhe [nalakaranasinghe@hotmail.com], C. B. Dissana-yake, and M. S. Rupasinghe, *Applied Geochemistry*, Vol. 20, 2005, pp. 1489–1495.

Gems account for 80% of the annual mineral foreign-based income of Sri Lanka, and roughly 25% of the island's landmass is gem bearing. Traditionally, luck has played a large role in the discovery of new Sri Lankan gem deposits, and developing an effective, scientifically based approach to prospecting would greatly benefit the expansion and overall economic health of the country.

Trace-element data for stream sediment samples collected from six river basins in different regions of Sri Lanka were analyzed to identify geochemical ratios indicative of the gem-bearing potential of these alluvial deposits. Previous studies have indicated that the Rb/Sr ratio has potential for delineating gem-bearing localities. However, there are only small differences in the ratios that point to gem potential (>1) vs. no gem potential (<0.4), creating a high possibility of error. Trends among various elements were studied using Spearman rank correlation, and those showing high correlations were selected to calculate ratios. The elements Rb, Ba, Sr, Ti, Nb, and Zr were highly correlative, and  $Rb \times Ba/Sr^2$  gave the best representation for locating gem-bearing areas. Ratios >4 appear to indicate locations with high gem potential, and ratios <1 point toward areas with no-to-low gem potential. However, field testing by pilot exploration programs must be carried out before this method is applied to large gem exploration surveys. *EAF*

*This section is designed to provide as complete a record as practical of the recent literature on gems and gemology. Articles are selected for abstracting solely at the discretion of the section editors and their reviewers, and space limitations may require that we include only those articles that we feel will be of greatest interest to our readership.*

*Requests for reprints of articles abstracted must be addressed to the author or publisher of the original material.*

*The reviewer of each article is identified by his or her initials at the end of each abstract. Guest reviewers are identified by their full names. Opinions expressed in an abstract belong to the abstractor and in no way reflect the position of Gems & Gemology or GIA.*

*© 2006 Gemological Institute of America*

**The content and distribution of microelements in *Pinctada martensii* and its manual nucleus inserted pearl layer.** F. Huang, C. Deng, W. Song, and H. Huang, *Guangdong Weiliang Yuansu Kexue [Science of Trace Elements, Guangdong]*, Vol. 12, No. 10, 2005, pp. 38–41 [in Chinese with English abstract].

The Japanese pearl oyster *Pinctada martensii* is one of the major mollusks used for culturing saltwater pearls in China, particularly in waters of the Guangxi, Guangdong, and Hainan Provinces. Although trace elements have been studied previously in mollusks and cultured pearls, the research has mainly concentrated on the “pearl layer” tissue (where the nucleus would be inserted) of the mussels used for producing freshwater cultured pearls. In this article, the authors used inductively coupled plasma-atomic emission spectrometry (ICP-AES) to investigate the trace elements in various portions of a *P. martensii* oyster aged 26 months (76 × 63 × 31 mm shell size) from Guangdong.

Eleven trace elements were detected in the tissue of the oyster: Se, Si, V, Zn, P, B, Cd, Co, Cu, Fe, and Mn. There were clear variations in the concentration and distribution of these elements between different portions of the oyster. The pearl layer showed enrichment in Se, Si, and Zn, while B, Co, Fe, and Mn were higher in the cuticle of the oyster. P was greatest in the visceral sac portion, and Cu and Cd were highest in the adductor muscle. V contents were greatest in the pearl layer, cuticle, and adductor muscle. The pearl layer contained the smallest weight-percent ratio of Cu/Zn. The contents of these trace elements (in ppm by weight) in the pearl layer were 0.09 Se, 9.32 Si, 0.13 V, 45.9 Zn, 77.7 P, 1.73 B, 0.46 Cd, 22.8 Cu, 158 Fe, and 18.9 Mn; no Co was detected. TL

**Influence of supergene conditions upon quality of fossil ivory.** A. N. Smirnov, *Proceedings of the Russian Mineralogical Society*, Vol. 135, No. 1, 2006, pp. 130–139 [in Russian with English abstract].

Fossil ivory (from tusks of the extinct Siberian mammoth) is a natural composite that consists of organic components (i.e., collagen, up to 55%), water (10–11%), and hydroxylapatite (up to 34–50%). Electron-microprobe data show a composition of 18.3–25.9 wt.% CaO, 14.9–21.6 wt.% P<sub>2</sub>O<sub>5</sub>, and 0.2–1.8 wt.% MgO.

The tusks remain well preserved while embedded in permafrost, but they are unstable when exposed on the surface (and especially in placers) since they lack an outer enamel layer. They may become discolored due to the formation of vivianite (blue) in fractures, or the presence of “azovskite” (a brown-red iron phosphate) as a surface film. Although such colors can be decorative, they are a negative result of weathering.

Reserves of mammoth ivory are significant, but there are some limitations on the sale of this material under regulations imposed by the Sakha (Yakutia) government.

BMS

**A miscellany of organics.** G. Brown [austgem@gem.org.au], *Australian Gemmologist*, Vol. 22, No. 6, 2005, pp. 264–268.

The identification of amber may involve one or more potentially destructive tests in addition to the nondestructive ones. Careful examination with a loupe may reveal flow structures and their two-phase inclusions; a sink/float test may be performed in an aqueous supersaturated salt solution (amber, copal resin, and polystyrene will float, whereas other polymer imitations of amber will sink); the sectility may be tested using magnification and a sharp scalpel; and, finally, an estimate of solubility in an appropriate volatile organic solvent may be made, applying a small drop to an inconspicuous area. The author suggests the hot point test is too destructive and less exact than sometimes assumed. Notes are also included on paua (abalone) shell objects (i.e., checking for color enhancement), “rattlers” (bead-nucleated cultured pearls that have missing internal layers), and imitation lacquer ware.

RAH

**A new geochemical tool to separate basaltic from metamorphic blue sapphires: The Ga/Mg ratio.** J.-J. Peucat [peucat@univ-rennes1.fr], P. Ruffault, E. Fritsch, C. Simonet, M. Bouhnik-Le Coz, and B. Lasnier, *Revue de Gemmologie a.f.g.*, No. 153, 2005, pp. 8–12 [in French with English abstract].

While the separation of “metamorphic” from “basaltic” sapphires has typically been made by evaluating a combination of Fe, Ti, Cr, V, and Ga contents, this article proposes the use of Fe, Mg, and Ga. Numerous sapphires were analyzed by LA-ICP-MS from known sources originating in alkali basalts (e.g., Pailin, Cambodia), syenites (Garba Tula, Kenya), metamorphic rocks (Ilakaka, Madagascar), metasomatic/plumasitic rocks (Kashmir, India), and rocks with as-yet-disputed origins (Yogo Gulch, Montana). Reasons for the systematic variations in trace-element content of sapphires from different geologic settings are discussed. The authors show that the determination of the Ga/Mg ratio in combination with Fe and Mg contents provides an easy separation of “metamorphic” from “basaltic” sapphires.

RT

**The origin of asterism in almandine-pyrope garnets from Idaho.** M. J.-F. Guinel and M. G. Norton, *Journal of Materials Science*, Vol. 41, No. 3, 2006, pp. 719–725.

As is well known, the presence of star-like reflected patterns in certain gem materials is due to oriented inclusions. In star corundum, these inclusions are needle-like and often referred to as “silk”; they scatter light at right angles to their length. In this study, oriented rutile needles were also determined to be the cause of weak four- and six-ray stars in almandine-pyrope from Emerald Creek, Latah Country, Idaho. Garnet thin-sections were subjected

to optical microscopy, electron-microprobe analysis, transmission electron microscopy, and electron diffraction. In particular, electron diffraction of the acicular inclusions showed overlapping patterns for rutile and the host garnet. This technique also was used to measure the orientation between the host garnet (*g*) and the rutile inclusions (*r*):  $[011]_g // [0\bar{1}0]_r$ ,  $(022)_g // (100)_r$ ,  $(400)_g // (001)_r$ . Four-rayed stars had needles oriented in the  $\langle 111 \rangle$  directions, while six-rayed stars also had needles along  $\langle 011 \rangle$ ; cat's-eyes had silk only along  $\langle 011 \rangle$ . The authors suggest that these findings may be extended to asteriated garnets from other sources.

DMK

**A spectroscopic index for estimating the age of amber.** H. Kimura, Y. Tsukada, H. Mita, Y. Yamamoto, R. Chujo, and T. Yukawa, *Bulletin of the Chemical Society of Japan*, Vol. 79, No. 3, 2006, pp. 451–453.

Two samples of copal and four of amber were studied by  $^{13}\text{C}$  cross-polarization magic-angle sample-spinning nuclear magnetic resonance spectrometry. In this nondestructive method, the sample is spun at an angle of  $54.7^\circ$  relative to the magnetic field direction of  $^{13}\text{C}$ . This allows individual atoms to be identified and located, and represented by a spectrum showing “chemical shift” in ppm. Four peaks were observed in the olefinic carbon region of the spectrum (160–100 ppm), at approximately 148, 141, 127, and 108 ppm. The 148 and 108 ppm peaks represent exocyclic methylene carbons of  $\text{C}_8$  and  $\text{C}_{17}$ , respectively. The intensities of these two peaks decreased as the age increased, while the other two peaks broadened. The “R value,” a spectroscopic index, was calculated by dividing the sum of the intensities of the 148 and 108 ppm peaks by the sum of the 141 and 127 ppm peaks. The highest R values of 1.38 and 1.44 were obtained for Madagascan copal (50–60 years) and Colombian copal (400–600 years), respectively. The R values decreased as the age increased—0.32 for Dominican amber (12–20 million years [Ma]) and 0.15 for Baltic amber (35–55 Ma). The lowest R values (zero) were obtained for ambers from two localities in Japan: Kuji (83–89 Ma) and Choshi (112–125 Ma).

The inversely proportional relationship between R value and amber age suggests that the rate of amber formation (i.e., cross-linkage between the exocyclic methylene groups of labdane polymers) is extremely slow, with a half-life of ~13 million years. It further indicates that climatic temperature fluctuations do not affect the rate of amber formation.

KSM

**Tsavorite: Une pierre africaine [Tsavorite: An African gem].** V. Pardieu, *Revue de Gemmologie a.f.g.*, No. 154, 2005, pp. 8–11 [in French].

This article reviews tsavorite's history as a gem and its current status, particularly in comparison to emerald. The author suggests that tsavorite has better qualities than emerald: although slightly softer, it is not brittle; it is more

brilliant (higher R.I. and dispersion, and thus not so “sleepy”); and it is much rarer, with only eight sources known (in Kenya, Tanzania, and Madagascar). However, while emeralds have been appreciated since antiquity and are readily available in almost all sizes and qualities, tsavorite was discovered only a few decades ago, and is still little known and too rare to become a public favorite.

RT

## DIAMONDS

**The “amber centres” and their relation to the brown colour in diamond.** L. Massi [laurent.massi@cnrs-imn.fr], E. Fritsch, A. T. Collins, T. Hainschwang, and F. Notari, *Diamond and Related Materials*, Vol. 14, 2005, pp. 1623–1629.

Understanding the cause of brown color in diamond has become more important in recent years with the use of high pressure, high temperature (HPHT) treatment to change brown diamonds to more attractive colors. Brown graining, produced by plastic deformation and infrared-active defects known as *amber centers*, is common in brown diamonds. However, the origin of these features and their relation to one another is poorly understood, so the authors studied 100 faceted samples (0.2–2.0 ct) of these brown diamonds using UV-Vis-NIR and FTIR absorption spectroscopy at room temperature and at 77 K.

Most of the diamonds fluoresced yellow to short-wave and blue to long-wave UV radiation. The UV-Vis-NIR absorption spectra (250–850 nm range) revealed a progressive increase in absorption toward lower wavelengths, resulting in the brown color. The infrared absorption spectra (~10,000–1000  $\text{cm}^{-1}$  range) indicated that all the diamonds with amber centers also contained A-aggregates of nitrogen. Four distinct amber center groups (AC1–4) were identified, with major peaks at approximately 4676, 4170, 4137, 4113, 4098, and 4067  $\text{cm}^{-1}$ . Further investigation of the most common amber center (AC1, at 4168  $\text{cm}^{-1}$ ) revealed an increase in its intensity with greater concentration of A-aggregates and depth of brown color. The authors interpreted AC1 as a defective A-aggregate (N-C-C-N<sup>+</sup>) that has been plastically deformed perpendicular to a {111} glide plane. This explains the association of type IaA nitrogen, brown graining, and the amber center, and is thought to correlate with the previously reported W7 defect in these types of diamonds.

CMB

**Diamonds from the desert.** M. Forrest, *Materials World*, March 2006, pp. 27–29.

Namibia's diamonds are mined from alluvial and marine deposits. Although many of the diamonds retrieved from Namibia's Atlantic Coast have been traced to the Orange River, which drains the Kimberley area of South Africa, diamonds have also been found at the mouth of the Ugab

River in the northern part of the country. No primary source has been located for the diamonds found in this northerly coastal region, but an Australian venture now has some promising leads in eastern Namibia.

Mount Burgess Mining has been prospecting for this primary source by following the upper headwaters of the Ugab at Tsumkwe, near Namibia's borders with Botswana and Angola. Although only non-diamondiferous kimberlites have been found in this area, their presence indicates that this is in fact a kimberlitic province.

Prospecting for kimberlites and diamondiferous gravels is challenging in this arid, inhospitable region. Most of the prospective area is deeply buried beneath sands of the Kalahari Desert, requiring a great deal of drilling along with geomagnetic surveys. Sediment sampling of the Aha Hills to the east of this region, speculated to be part of the paleo-watershed draining into the Ugab, revealed G10 garnets and eight macrodiamonds. If the Tsumkwe region is indeed the source of the far-off marine terrace diamonds of Namibia's Atlantic shore, it would represent a significant gain for this country's mineral assets.

DMK

**Geodynamic controls on diamond deposits: Implications for Australian occurrences.** C. J. O'Neill [cjoneill@rice.edu], L. Moresi, and A. L. Jaques, *Tectonophysics*, Vol. 404, 2005, pp. 217–236.

Conventional diamond exploration guidelines predict that economic diamond occurrences are restricted to Archean cratons (i.e., Clifford's Rule). In the lower portions of such cratons, the lithosphere is thick and cool, and diamond is the stable form of carbon. However, Australia's economic diamond deposits do not fit well within these Archean cratonic guidelines. Seismic tomography shows that the deposits lie at step-changes in lithospheric thickness within Proterozoic craton-like provinces of thick ( $\geq 200$  km) lithosphere. The central Proterozoic regions of the Australian continent contain the thickest portions of lithosphere, not the predicted Archean areas. The step-like changes in lithospheric thickness focus stress gradients and affect melt migration paths. Economic diamond pipes originate where conditions favorable to diamond stability and alkaline volcanism occur simultaneously. The confluence of these factors at abrupt changes in lithospheric thickness marks them as potential exploration targets.

EAF

**Paragenesis of inclusions in diamonds from the Botoubinskaya kimberlite pipe, Nakyn field, Yakutia.** Z. V. Spetsius [spetsius@yna.alrosa-mir.ru], S. I. Mityukhin, A. S. Ivanov, and S. V. Banzeruk, *Doklady Earth Sciences*, Vol. 403, 2005, pp. 808–811.

Inclusions in diamonds from kimberlite pipes are important because they contain detailed information on the temperature and pressure of the diamond's formation, and they also provide a window into the chemical makeup of

the upper mantle. Representative diamonds from the Botoubinskaya pipe were studied to investigate the diamonds' source region. The sulfide minerals pyrrhotite and pentlandite, as well as monosulfide solid solutions, together constituted more than 50% of the inclusions. The abundance of sulfide minerals is typical of the majority of the Yakutian kimberlites. The remaining inclusions were formed by common olivine, garnet, spinel, pyroxene, and rutile. Based on these data, a reconstructed initial composition of sulfide melts suggests that more than half of the diamonds were associated with eclogitic source rocks.

EAF

**The re-engineering of the ground handling system at Cullinan diamond mine.** A. W. Bester, *Journal of the South African Institute of Mining and Metallurgy*, Vol. 105, No. 3, 2005, pp. 149–162.

The kimberlite pipe at South Africa's Cullinan diamond mine is currently exploited using a technique known as "mechanized panel retreat block caving." The ore body is first undercut by drilling and blasting, which is followed by caving. The ground handling system ensures the removal of the broken ground at the same rate it is produced. The mining array includes inclined ore passages, box fronts (where ore is loaded into train cars), a crushing system, a conveyor system, and the hoisting infrastructure. Two blocks (BA5 and BB1 East), are currently active; a new block (BA West) is scheduled to be mined in 2011. Improvements to the current ground handling system will be needed for efficient operation when BA West becomes active.

To reach the goal of handling 3.8 million tons annually from the current 3.2, the author proposes a two-fold solution: (1) increase the number of shifts for each workday from two to three, and (2) upgrade the machinery using a larger train system, trucks, or a conveyor belt system. The train option would be familiar to employees, and would have lower operating costs since it uses electricity (compared to trucks, which use diesel fuel). However, a high initial expense would be incurred to upgrade the train infrastructure. The diesel truck option includes two choices: conventional trucks or Combi trucks with removable ore containers. The operating and maintenance costs for the conventional trucks would be higher than the train option. Combi trucks have advantages over conventional trucks (e.g., they require fewer vehicles and therefore a smaller capital investment) but higher operating costs. The author did not discuss the conveyor belt system in detail but concluded that coordination among the different blocks is essential for an efficient ground handling system.

KSM

**A venture into the interior of natural diamond: Genetic information and implications for the gem industry (Part I: The main types of internal growth structures).** G. P. Bulanova, A. V. Varshavsky, and V. A.

Kotegov, *Journal of Gemmology*, Vol. 29, No. 7/8, 2005, pp. 377–386.

The growth history and internal structure of diamond has been studied with a variety of techniques, such as anomalous birefringence (ABR), X-ray topography, photoluminescence (PL) and cathodoluminescence (CL) imaging, and Fourier-transform infrared (FTIR) spectroscopy. The authors studied diamond plates using CL and FTIR, and discussed the effects of different types of internal structures on cutting and polishing. The plates were polished from octahedral diamond crystals (2–5 mm) from Yakutian kimberlites.

CL images are two dimensional and can reveal detailed features of diamonds to a depth of 1–5  $\mu\text{m}$ . To study a diamond's growth history effectively, it is important to polish a plate that incorporates the genetic center from which the diamond grew (not necessarily the geometric center). The authors suggest that the best direction for polishing the central plate is a dodecahedral {110} plane, which can be located by the combined application of CL, ABR, and PL imaging, since these techniques together can show three-dimensional internal structure.

Examination with an optical polarizing microscope can detect a variety of defects, including twinning, crystal aggregates, and plastic and brittle deformation—these can cause local “hard” directions for cutting and polishing (“soft” directions, such as the cubic and dodecahedral planes, are so-called because they are easier to cut and polish). ABR and PL imaging can be used to locate single or multiple growth centers. If a diamond has two growth centers, the authors suggest that it is best to cut between the centers or keep both centers contained in the largest section. Cutting through a growth center or directly through inclusions is not recommended since it can create cracks. *KSM*

**Water-related IR characteristics in natural fibrous diamonds.** D. A. Zedgenizov, A. A. Shiryaev [shiryaev@ns.crys.ras.ru], V. S. Shatsky, and H. Kagi, *Mineralogical Magazine*, Vol. 70, No. 2, 2006, pp. 219–229.

Water molecules can be trapped inside diamond as hydrous components (e.g., HOH or OH) during diamond formation in the upper mantle. Infrared spectroscopy can detect the bending vibration of HOH and stretching vibration of OH. Studying these hydrous species can give more understanding about mantle-derived fluids that are critical in mantle metasomatism and diamond formation. In this study, 35 cuboid diamonds with fibrous structures from Russia (Yakutia), Democratic Republic of the Congo, and Canada were polished into 100–200  $\mu\text{m}$  thick plates. Most of them were type IaA and a few were type IIa; B aggregates and platelets were also observed in some diamonds.

At room temperature, the HOH-bending vibration was detected as a broad band at around 1650  $\text{cm}^{-1}$  and the

OH-stretching (both symmetric and asymmetric) as a broad band between 3600 and 2800  $\text{cm}^{-1}$ . These broad bands were decomposed into components (Gaussian peaks) using computer software. The broad bands of HOH-bending consisted of at least two components, whereas those of OH-stretching had at least three components. The observation of both symmetric and asymmetric OH-stretching indicated that water molecules were formed in different aggregate states or species among the samples. At higher temperatures, the broad bands of HOH-bending shifted toward higher wavenumbers. The broad bands of OH-stretching did not shift upon heating, but their shape and intensity changed. At low temperatures (–150°C), the spectra were the same as at room temperature, suggesting that water molecules may exist as supercooled fluids inside the diamonds. At high pressure and room temperature, water undergoes a phase transition to various polymorphs of ice. The HOH-bending vibration band for liquid water, ~1650  $\text{cm}^{-1}$ , shifted to 1690  $\text{cm}^{-1}$  at ~0.6 GPa and 1620  $\text{cm}^{-1}$  at ~1.8 GPa. These bands are associated with ice VI and ice VII, respectively. In this study, the authors concluded that water molecules were formed as a residual fluid inside micro-inclusions and in the diamond lattice. Various water species were also detected within some samples, suggesting that fibrous diamonds may form during several growth events. *KSM*

## GEM LOCALITIES

**Emerald mining in Afghanistan.** A. Kalukiewicz, *Mining Engineering*, Vol. 57, No. 9, 2005, pp. 17–21.

This article describes the improvements being made to safety, viability, and recovery through mechanization of emerald mining in Afghanistan. At roughly 3,000–4,000 m above sea level, the remote mountainous region where the emeralds are found has very little in the way of transport or support infrastructure. With irregular fuel supplies and no electricity, previous mining operations used hand tools to drill holes for blasting with TNT salvaged from leftover military ordnance. There was no ventilation for noxious blasting residues, illumination was provided by kerosene lamps, and the high shattering characteristics of TNT damaged or destroyed otherwise recoverable emeralds.

Between 1997 and 2000, a Polish team of experts improved mining methods and equipment at one of the Khenj deposits in the Panjshir Valley. The team set forth several objectives: to enhance the safety of the miners, promote better techniques to recover the emeralds, and ensure longer-term profitability. They considered the hardness of the rocks to determine the optimal types of hydraulic drills and hammers, installed electrical generators, and made appropriate modifications to the equipment to account for the high altitude. They also stockpiled 1–2 years' worth of spare parts to support the initial

delivery of five full sets of drills, hammers, and other tools. Dynamite was used instead of TNT, due to its lower brisance (i.e., explosive velocity); it shattered fewer emeralds and was safer for workers. Mining lamps were instituted, as was proper ventilation. Although no roof support (other than for portals) was planned, anchors with wire net lagging would help safeguard the tunnels against collapse.

With these changes and a two-week training session for about 20 miners and mechanics, the recovery of gem-quality material increased as fewer crystals were shattered by blasting and the workers were able to reach eight times deeper (400 m) than was previously possible.

DMK

**Discovery of corundum and its mineralogical properties in north Jiangsu.** Y. Sun and F. Yan, *Jiangsu Geology*, Vol. 30, No. 2, 2006, pp. 87–88 [in Chinese with English abstract].

Gem-quality ruby and sapphire are known from many localities in China, such as Shandong, Yunnan, Hainan, Heilongjiang, Qinghai, and Jiangsu Provinces. This article reports on a new source of ruby from northern Jiangsu.

Field geologic surveys found that the ruby is hosted by an ultrabasic serpentine-garnet rock body measuring approximately  $1000 \times 180 \times 250$  m. Pyrope, ruby, augite, and some nickel-containing minerals are the major constituents. The ruby crystals (typically up to 3 mm) are purplish red and semitranslucent to transparent. The smaller their size, the more saturated the color. The ruby contains abundant fractures, has refractive indices of  $n_o=1.766$  and  $n_e=1.757$ , and contains 0.37–0.56 wt.%  $\text{Cr}_2\text{O}_3$ .

The authors indicate that the ruby formed due to hydrothermal alteration of the ultrabasic rock, and they suggest that additional ruby deposits might be found in northern Jiangsu and southern Shandong Provinces.

TL

**Exploration et exploitation des gemmes en Australie [Exploration and mining of gems in Australia].** F. L. Sutherland, *Revue de Gemmologie a.f.g.*, No. 155, 2006, pp. 13–19 [in French].

This article focuses on Australian opal, diamond, corundum (mainly sapphire), and cultured pearls, which make up the majority of the country's gem production. A variety of other gems are summarized, including beryl, topaz, nephrite, quartz, and other silicates. Australia is still the source of over 90% of the global supply of opal. It produces about 50% of South Sea cultured pearls, and the culturing operations are expanding. Australia continues to be an important source of sapphire, although new treatments and competition from other sources have caused difficulties in this market. Meanwhile, the Argyle diamond mine will continue operating until at least 2012.

RT

**Kosmochlor and chromian jadeite aggregates from the Myanmar jadeite area.** G. H. Shi [shiguanghai@263.net.cn], B. Stöckhert, and W. Y. Cui, *Mineralogical Magazine*, Vol. 69, No. 6, 2005, pp. 1059–1075.

Four distinct textures and related compositions of kosmochlor and Cr-bearing jadeite from rocks in the Myanmar jadeite area are described. One of these four textures involved recrystallized fine-grained aggregates in deformed jadeite. The concomitant redistribution of Cr from chromite into kosmochlor, Cr-bearing jadeite, and finally jadeite with <1 wt.%  $\text{Cr}_2\text{O}_3$ , together with the high transparency related to the fine-grained microstructure, produced the gemologically important Imperial jadeite.

RAH

**New discovery in Sri Lanka—Green, semi-translucent to opaque, opal.** S. I. Glaser, *Midlands Focus*, No. 8, 2006, pp. 25–26.

The author describes a trip to Rawana Falls near Ella in Sri Lanka, where she found semitranslucent to opaque green opal scattered among the material that was being sold as agate by local miners. This opal came from a small village not far from Wellawaya. The colors included yellow-green, "apple" green, and dark green to blackish green. The R.I. was 1.45, S.G. was 2.00, and absorption features for a large dark green sample were seen across the green-blue, blue, and violet regions of the spectrum. Smaller samples had absorption features in the far end of the blue and red regions. Some of the opal was noted as being fragile and porous (emitting bubbles when immersed in water).

HJ-G

**Oxygen isotope studies on placer sapphire and ruby in the Chanthaburi-Trat alkali basaltic gemfield, Thailand.** T.-F. Yui [tfyui@earth.sinica.edu.tw], C.-M. Wu, P. Limtrakun, W. Sricharn, and A. Boonsoong, *Lithos*, Vol. 86, 2006, pp. 197–211.

Ruby and sapphire are found in secondary deposits related to the weathering of alkali basalts in southeastern Thailand. However, the question remains as to whether the gems crystallized directly from the basalt as phenocrysts or were simply transported by the basalt as xenocrysts. The authors studied the oxygen isotope values of gem corundum from the Chanthaburi-Trat region to clarify their origin.

The three mining areas around Chanthaburi-Trat (labeled western, central, and eastern zones) displayed markedly different  $\delta^{18}\text{O}$  values for rubies versus sapphires. Sapphires from the western zone (at Khao Phloi Waen) yielded values of +5.1 to +6.2‰.  $\delta^{18}\text{O}$  values for rubies from the central (at Tok Phrom and Bo Na Wong) and eastern (at Nong Bong and Bo Rai) zones were much lower (and more varied): +2.4 to +3.9‰ at Tok Phrom; +2.1 to +3.1‰ at Bo Na Wong; +1.6 to +4.2‰ at Nong Bong; and +1.3 to +3.7‰ at Bo Rai. Furthermore, the  $\delta^{18}\text{O}$

values for olivine phenocrysts within the basalt were found to be within a limited range of +4.8 to +5.0‰.

The authors conclude that the corundum and olivine could have been in oxygen isotopic equilibrium with one another. Thus, ruby and sapphire could not have grown as phenocrysts alongside olivine in the alkali basalt. The authors theorized that the sapphires, with their more homogeneous  $\delta^{18}\text{O}$  values, crystallized from evolved mantle alkali magmas in the lower crust/upper mantle. Ruby, with its lower and more variable  $\delta^{18}\text{O}$  values, crystallized from mafic metamorphic rocks in the upper mantle. Both gems were brought to the surface by later alkali basalt magmatism. The authors tentatively propose garnet pyroxenite as the primary source of the corundum. KAM

**The sapphire and spinel deposit of An Phu, Luc Yen mining district, Yenbai Province, Vietnam.** D. Blauwet, *Mineralogical Record*, Vol. 37, No. 3, 2006, pp. 225–238.

The An Phu mine, near An Phu village in the Luc Yen mining district about 100 km from Hanoi, Vietnam, has been the source of attractive specimens of ruby and large red spinel crystals, as well as phlogopite, pyrite, dravite, and green edenite crystals embedded in a white marble matrix. Mining methods are primitive, and much of the extraction is by hand tools. The mine is reportedly 90% worked out, and activity may cease in the next few years; however, high-quality material is still being recovered. Some rounded gem rough is also found in alluvial deposits in the same area. It is reported, however, that pegmatitic tourmaline and beryl labeled as An Phu are actually from the nearby Minh Tien pegmatite. RAH

**A SIMS study of the transition elemental distribution between bands in banded Australian sedimentary opal from the Lightning Ridge locality.** P. S. Thomas [paulthomas@uts.edu.au], L. D. Brown, A. S. Ray, and K. E. Prince, *Neues Jahrbuch für Mineralogie, Abhandlungen*, Vol. 182, No. 2, 2006, pp. 193–199.

The distribution of trace elements in banded Australian sedimentary opal from the Lightning Ridge region was investigated with secondary ion mass spectrometry (SIMS) using both spot and spatial analysis (i.e., stepping incrementally across the sample).

The opal was found to be fairly homogeneous within bands, but it showed a relatively sharp change in composition at the interface between bands for trace elements such as Ti, V, Co, Cu, Zn, and Y. However, numerous elements did not vary significantly between bands (i.e., Na, Mg, Al, K, Ca, Mn, and Fe), which may suggest that the adjacent bands in the opals formed simultaneously. These observations are consistent with earlier reported LA-ICP-MS results, and they support the solution-depletion sedimentation model proposed as the mechanism for band formation in this opal. RAH

## INSTRUMENTS AND TECHNIQUES

**Attenuated total reflection Fourier transform infrared spectra of faceted diamonds.** P. Thongnopkun and S. Ekgasit [sanong.e@chula.ac.th], *Analytica Chimica Acta*, Vol. 576, 2006, pp. 130–135.

Attenuated total reflection (ATR) Fourier-transform infrared (FTIR) spectroscopy is a highly sensitive surface-characterization technique. An infrared beam is reflected off the interface between the sample being analyzed and another crystal with a higher refractive index (in this case, germanium), and a wave that decays rapidly with distance is generated at this interface due to the total internal reflection (TIR) phenomenon. The incident angle must be greater than the critical angle for TIR to occur. One drawback of the ATR measurement is that an air gap or a thin film of foreign material on the sample surface will prohibit acquisition of good-quality spectra. However, ATR FTIR spectroscopy can be applied to large or small, opaque or transparent, colored, or highly fractured gems with a flat surface. The molecular information obtained from an ATR spectrum is directly correlated to the structure and composition at the surface, and can be used for gem identification, classification, and detection of treatments.

The authors demonstrated the utility of ATR FTIR spectroscopy by comparing the ATR spectra of three ~0.1 ct round brilliant-cut diamonds (table size ~3 mm; types IaB, IaA, and IaAB; before and after cleaning in an alkali solution) with corresponding diffuse reflectance and transmittance spectra. The ATR spectra of the diamonds with low nitrogen agreed well with the diffuse reflectance and transmittance spectra, while the stone with high nitrogen showed more detail in the one-phonon region.

Kimberly Rockwell

**Transmittance spectra of faceted diamonds acquired by infrared microscopy.** S. Ekgasit [sanong.e@chula.ac.th] and P. Thongnopkun, *Applied Spectroscopy*, Vol. 59, No. 9, 2005, pp. 1160–1165.

Most methods of measuring IR absorption are not feasible or accurate for mounted diamonds. The authors connected an infrared microscope (with a 15× Cassegrain objective) to an FTIR spectrometer to collect infrared spectra of loose and mounted round brilliant-cut diamonds. These “transmittance” spectra were then compared to diffuse reflectance spectra taken from the same diamonds. Although the shapes of the spectral features appeared somewhat different (e.g., many large peaks were broader at their bases), the spectral positions were similar, and diamond type and treatment-related features could be detected.

This method works on round brilliant-cut diamonds because they are faceted to reflect light off the pavilion facets back through the crown; the infrared beam is assumed to follow similar paths. Nitrogen- and hydrogen-bearing impurities, color centers, and the like absorb specific wavelengths as the beam travels through the diamond,

creating spectral absorbance features. Compared to diffuse reflection, transreflectance allows resolution of much more detailed absorption features in the one-phonon region for diamonds with high nitrogen content.

Mary L. Johnson

**Diffraction enhanced imaging: A new X-ray method for detecting internal pearl structures.** J. Schlüter [jochen.schlueter@uni-hamburg.de], M. Lohmann, J. Metge, and B. Reime, *Journal of Gemmology*, Vol. 29, No. 7/8, 2005, pp. 401–406.

Despite its limitations, X-radiography has traditionally been one of the most important methods of pearl identification. An alternate method developed by these authors, diffraction enhanced imaging (DEI), was found to show internal growth features and structures more clearly than conventional X-radiographs. DEI employs a monochromatic X-ray beam generated from synchrotron radiation, and is based on the separation of scattered and nonscattered X-rays behind the sample. Two kinds of images can be generated, based on either extinction or refraction contrast. Although DEI is currently too expensive for routine pearl testing, it is useful for scientific purposes.

AI

**Filtres colorés Hanneman pour pierres gemmes [Hanneman color filters for gemstones].** L. Gautron [3genvt@wanadoo.fr], *Revue de Gemmologie a.f.g.*, No. 153, 2005, pp. 20–24 [in French].

Color filters have proven to be useful and inexpensive tools for the quick separation of various gems. This article reviews filters developed over the past 25 years by gemologists William Hanneman and Alan Hodgkinson. Generally, incandescent light must be used and the stones observed in front of a white background (such as a sheet of paper). The following filters, designed to distinguish certain groups of stones, are discussed: the “Aqua filter” for blue stones, the “Ruby filter” for red stones, two filters for natural and synthetic emeralds (in combination with the Chelsea filter), a filter for natural and dyed lavender jade, a filter for tanzanite and its simulants, and a “Bead buyer’s & parcel picker’s filter set.” Transmission spectra of all filters are shown, as well as photos of sample stones seen through them.

RT

**Possibilities of X-ray non-destructive diagnostics of turquoise in jewellery.** M. V. Cherednik and E. A. Goilo, *Abstracts of the International Symposium on Mineralogical Museums, St. Petersburg*, V. G. Krivovichev, Ed., St. Petersburg State University, 2005, p. 356 [in Russian].

Due to the differences in orientation of microcrystals in turquoise and its imitations, standard powder X-ray diffractometry can be used for identification. A Russian-made diffractometer DRON-2 with a Co anode was used, with a  $2\theta$  angle interval of 10–50°. The most intense reflections

were recorded in a narrow  $2\theta$  interval of 27–37°, so only 5–10 minutes were needed for identification.

Of the 15 samples tested, 12 were identified as turquoise; the other three proved to be colored calcite, gibbsite, and plastic. Studies also were undertaken of some specific minerals of the turquoise group (chalcociderite, coeruleolactite, and planerite) containing Fe, Ca, and trace-element impurities. From differences in unit-cell parameters, it was possible to identify the presence of certain elements and determine geographic origin.

BMS

**Synchrotron micro-X-ray fluorescence analysis of natural diamonds: First steps in identification of mineral inclusions in situ.** H. Sitepu, M. G. Kopylova [mkopylov@eos.ubc.ca], D. H. Quirt, J. N. Cutler, and T. G. Kotzer, *American Mineralogist*, Vol. 90, No. 11–12, 2005, pp. 1740–1747.

Diamond inclusions record information about the chemical composition of the earth’s mantle that is useful for mantle petrology research and diamond exploration. Using quantitative *in situ* spectroscopic techniques known as  $\mu$ SXRF (synchrotron micro-X-ray fluorescence) and  $\mu$ XANES (micro-X-ray absorption near edge structure), mineral inclusions were nondestructively identified in three diamonds (up to 3 mm in size) from the Jericho kimberlite in Canada.  $\mu$ SXRF was also used to analyze the compositions of several kimberlite indicator minerals (e.g., chromite, clinopyroxene, and garnet). Unlike time-consuming destructive methods of inclusion analysis, these techniques take only minutes and can be used on samples as small as 5–10  $\mu$ m. High-resolution maps for Ti, Cr, Fe, Ni, Cu, and Zn distributions within the diamonds were also collected, with detection limits of 5–10 ppm. The  $\mu$ SXRF analyses indicated that elemental distributions within the diamonds were heterogeneous (with the signal confined to the outer ~0.5 mm surface of the stones). All visible inclusions, as well as several that were not visible with an optical microscope (~10  $\mu$ m), were clearly observed in the element maps. Inclusions identified using  $\mu$ SXRF consisted of green eclogitic clinopyroxene, light orange eclogitic garnet, colorless peridotitic olivine, purple peridotitic garnet, and opaque sulfides. Analysis of the inclusions by  $\mu$ XANES showed absorption lines at 6010, 6008.5, and 6006 eV, suggesting that Cr<sup>3+</sup> in the inclusions occurred as regular or distorted octahedra. These data were consistent with the identified minerals.

CMB

## SYNTHETICS AND SIMULANTS

**As-grown, green synthetic diamonds.** C. M. Breeding, J. E. Shigley, and A. H. Shen, *Journal of Gemmology*, Vol. 29, No. 7/8, 2005, pp. 387–394.

Synthetic diamonds showing a green bodycolor face-up with no evidence of post-growth irradiation are described.

The eight samples studied were from a set of 129 synthetic diamonds supplied by Chatham Created Gems. The authors ruled out irradiation as the cause of the green body-color based on the lack of general radiation (GR) peaks in the UV-Vis-NIR absorption spectra that are normally associated with irradiated diamonds. Instead, they found that the green color resulted from blue (boron-rich) and yellow (nitrogen-rich) color zones corresponding to specific internal growth sectors. This conclusion was supported by an investigation of synthetic diamonds with bodycolors ranging from dark blue to grayish greenish blue to light yellowish green to brownish orangy yellow, via face-down immersion in water and absorption spectroscopy. Immersion in water revealed distinct blue, yellow, and colorless zones, and the spectroscopic data showed a correlation between the simultaneous decrease of the 2457  $\text{cm}^{-1}$  peak (corresponding to the presence of boron) and increase of the 270 nm and 1344  $\text{cm}^{-1}$  peaks (corresponding to the presence of nitrogen) from the dark blue to the brownish orangy yellow sample. The authors suggest that the boron and nitrogen ratios were deliberately controlled during growth of the synthetic diamonds to manipulate the face-up bodycolors from blue to green to yellow. [Editors' note: Yellow, blue, green, and pink synthetic diamonds from Chatham Created Gems were described in the Summer 2004 *Gems & Gemology*, pp. 128–145.] JS-S

**Development of high-quality large-size synthetic diamond crystals.** H. Sumiya, N. Toda, and S. Satoh, *SEI Technical Review*, No. 60, 2005, pp. 10–15.

Researchers at Sumitomo Electric Industries in Itami, Japan, have been leaders in the production of large synthetic diamonds for various industrial and scientific applications (e.g., optical parts, radiation detectors, high-pressure anvils, and monochromators for X-rays). This article reports on colorless type IIa synthetic diamond crystals weighing 7–8 ct (~10 mm diameter) produced at a growth rate of 6–7 mg/hr by the temperature-gradient method at high pressure and temperature. The use of a high-purity carbon source material, a high-quality seed, and an Fe-Co solvent with Ti added as a nitrogen getter reduced the concentration of chemical impurities (such as N, B, and Ni) in these crystals to levels below 0.1 ppm. The use of Cu in the solvent inhibited the formation of TiC inclusions in the synthetic diamonds. The high crystalline quality of these crystals resulted from optimizing the metals and additives used in the solvent and precisely controlling the temperature throughout the growth process.

JES

**Distinguishing natural from synthetic amethyst: The presence and shape of the 3595  $\text{cm}^{-1}$  peak.** S. Karampelas [steka@physics.auth.gr], E. Fritsch, T. Zorba, S. M. Parakevopoulos, and S. Sklavanounos, *Mineralogy and Petrology*, Vol. 85, 2005, pp. 45–52.

This study examines the conditions under which the 3595

$\text{cm}^{-1}$  IR absorption band can be used to separate natural from synthetic amethyst. The band is present in most natural amethyst but is also rarely found in some synthetic amethyst, thus limiting its use as an identification criterion. In this study, the intensity and shape of the 3595  $\text{cm}^{-1}$  band was measured as a function of crystallographic orientation in four natural and two synthetic samples from various sources. Resolution was increased to 0.5  $\text{cm}^{-1}$ , and the full width at half maximum (FWHM) of the 3595  $\text{cm}^{-1}$  peak was then measured. In the synthetic amethyst the FWHM was about 7  $\text{cm}^{-1}$ , which is about twice that measured for the natural amethysts (3  $\text{cm}^{-1}$ ). The authors propose using this criterion to separate natural from synthetic amethyst. AI

**Grow[th of] large high-quality diamonds with different seed surfaces.** C.-Y. Zang, X.-P. Jia [jiaxp@jlu.edu.cn], H.-A. Ma, S.-S. Li, Y. Tian, and H.-Y. Xiao, *Chinese Physics Letters*, Vol. 23, No. 1, 2006, pp. 214–216.

The authors documented the crystal morphology and quality of type Ib synthetic diamonds grown by the temperature-gradient method at high temperatures (~1250–1350°C) and pressures (5.5 GPa), with a Ni-Mn-Co alloy used as the metal solvent. Seeds consisting of 0.5 mm industrial diamonds with well-developed {111} or {100} faces were chosen to initiate crystallization. The best conditions for growing large, high-quality synthetic diamond crystals occurred at temperatures approximately 50°C higher with the {111} seeds as compared to the {100} seeds. For growth from {100} seeds, more tabular crystals formed at relatively lower temperatures for the conditions selected, while more-equant crystals formed at higher temperatures. In contrast, growth from {111} seeds produced the opposite morphologies. Regardless of the seed selected, metal inclusions were less common within the tabular as compared to the equant synthetic diamond crystals. The authors suggest that the optimum growth rates were approximately 2.5 mg/h for the tabular synthetic diamond crystals and 1.5 mg/h for the equant crystals. JES

**High pressure–high temperature growth of diamond crystals using split sphere apparatus.** R. Abbaschian [rabba@eng.ucr.edu], H. Zhu, and C. Clarke, *Diamond and Related Materials*, Vol. 14, No. 11–12, 2005, pp. 1916–1919.

Diamond growth under conditions of high temperatures (~1300–1700°C) and high pressures (~5–6.5 GPa) takes place by the “temperature gradient” method. In this process, a molten catalyst dissolves carbon from a source (graphite or diamond powder), and transports it to a growth site where the carbon precipitates on a diamond seed. Various types of machinery are used for this process, with synthetic diamond crystals up to several carats grown in time periods of approximately 100 hours or less. Introduction of the split-sphere (or BARS) apparatus has lowered the capital and operational costs for diamond synthesis.

In this article, the authors, who were associated with

the Gemesis Corp., Sarasota, Florida, review the use of the split-sphere apparatus for producing gem-quality type Ib yellow synthetic diamonds. According to their experience, higher growth temperatures (above ~1350°C) yield better-quality crystals with more intense colors. Type IIa (colorless) and type IIb (blue) crystals can also be grown by this process, but at appreciably slower growth rates and within a more restricted range of temperature and pressure conditions. [Editors' note: Gemesis synthetic diamonds were described in the Winter 2002 *Gems & Gemology*, pp. 301–309.] JES

**Prospects for large single crystal CVD diamonds.** S. S. Ho, C. S. Van, Z. Liu, H. K. Mao, and R. J. Hemley, *Industrial Diamond Review*, Vol. 66, No. 1, 2006, pp. 28–32.

Chemical vapor deposition (CVD) has been optimized for fabricating single-crystal synthetic diamond at very high growth rates (up to ~100 µm/h). Single-crystal material >1 cm in thickness and weighing more than 10 ct can now be produced with a range of optical and mechanical properties for various applications. High-pressure, high-temperature annealing can significantly increase the hardness. The process can produce synthetic diamond with improved optical properties in the ultraviolet-to-infrared range, opening prospects for new technological and scientific applications. Illustrations are given of a 5 ct (12 × 6 mm) single-crystal CVD synthetic diamond (without the seed portion) cut from a 10 ct block, and of a 0.2 ct brilliant-cut synthetic diamond produced from a 1 ct block. RAH

**Silica and alumina transfer in supercritical aqueous fluids and growing of topaz monocrystals in them.** V. S. Balitsky, D. V. Balitsky, S. D. Balitsky, C. Aurisicchio, and M. A. Roma, *Geochemistry International*, Vol. 44, No. 2, 2006, pp. 175–181.

To date, large crystals of topaz have not been grown synthetically. However, it is known that topaz (as well as quartz) can grow and dissolve under temperature gradients in granitic pegmatites. This prompted experiments to determine the growth conditions for topaz single crystals. The authors hydrothermally grew synthetic topaz crystals measuring 2.5–5.0 mm thick, 8–15 mm wide, and 20–40 mm long in times ranging from 20 to 60 days. They used natural topaz seed plates (2 × 8 × 40 mm) in an autoclave containing acidic to near-neutral fluoride-bearing aqueous fluids and topaz and quartz fragments. The temperature ranged from 550 to 780°C and the pressure was 20–180 MPa. These growth conditions were based on the authors' investigations of the transfer of silica and alumina during the growth and dissolution of quartz, corundum, and topaz in supercritical aqueous fluids using a defined temperature gradient. The synthetic topaz crystals were compared to natural topaz using electron-microprobe analysis for chemical composition, high-precision XRD patterns for unit-cell parameters, IR spectroscopy for characteristic

absorptions, and standard gemological techniques for refractive index and density. In all cases, there was a match between the natural and synthetic crystals, verifying the identity of the hydrothermally grown topaz. JS-S

**Synthesis of precious opal in a hydrothermal solution.** V. Potapov and D. V. Kamashev, *Glass Physics and Chemistry*, Vol. 32, No. 1, 2006, pp. 89–98.

The authors explored the growth of colloidal silica particles and of ordered supramolecular structures in hydrothermal solutions to understand the formation of play-of-color opal. They correlated the temperature and pH of the silicate mineral-containing hydrothermal solution to the rate of nucleation of orthosilicic acid molecules and the formation, size, and concentration of colloidal silica particles via polycondensation. The silica particles had diameters mainly in the 1–50 nm range. However, play-of-color opal is a supramolecular structure composed of particles with diameters in the range of hundreds of nanometers. The authors propose that the supramolecular structure of play-of-color opal forms either at higher temperatures where the nucleation rate for new particles is decreased and larger particles are produced, or from complexes of smaller particles (i.e., aggregates). Based on their observations of colloidal silica particle sizes in hydrothermal solutions, they judged that play-of-color opal forms from aggregates of the colloidal silica particles. They determined that the best nucleation rate for these particles occurs between 120 and 150°C and that the optimum settling velocity for the supramolecular structure is at rates of less than 10 mm/day. The specific cubic packing orientation of the spheres is pH and particle-size dependent, with the closest cubic packing (characteristic of play-of-color opal) occurring at pH values greater than 9. JS-S

## TREATMENTS

**Change in cathodoluminescence spectra and images of type II high-pressure synthetic diamond produced with high pressure and temperature treatment.** H. Kanda [kanda.hisao@nims.go.jp], A. Abduriyim, and H. Kitawaki, *Diamond and Related Materials*, Vol. 14, No. 11–12, 2005, pp. 1928–1931.

Natural diamonds showing evidence of plastic deformation often exhibit mosaic patterns that may be observed by cathodoluminescence (CL) imaging and the presence of 2BD peaks (at ~260, 270, and 285 nm) in CL spectra. However, no direct correlation between these characteristics and plastic deformation in diamond has previously been demonstrated. The authors used colorless high pressure, high temperature (HPHT)-grown synthetic diamonds showing little evidence of plastic deformation and subjected them to HPHT treatment that induced plastic deformation through non-hydrostatic stress (i.e., by applying non-

uniform pressure, such as along one axis direction). Although brown coloration in natural diamond (generally ascribed to plastic deformation) can be altered by HPHT treatment, no color alteration was seen in these synthetic diamonds in response to the treatment. Comparison of the CL images and spectra of the synthetic diamonds before and after the HPHT treatment showed development of both the mosaic pattern and the 2BD bands, which supports the relationship between plastic deformation and these CL features. The authors suggest that HPHT treatment may have two effects: annealing and plastic deformation. If the diamond is treated under hydrostatic conditions, then the annealing affect would likely be dominant, whereas treatment under non-hydrostatic conditions will cause plastic deformation. *Sally Eaton-Magaña*

**Proton irradiation of natural and synthetic diamonds.** M. A. Viktorov and M. B. Kopchikov, *Moscow University Geology Bulletin*, Vol. 60, No. 5, 2005, pp. 62–75.

Proton irradiation could have commercial potential as a diamond treatment, similar to neutron and electron irradiation. Both neutrons and electrons are capable of deep penetration into diamond, creating uniformly distributed color. In this study, natural and synthetic diamonds were irradiated with 30–100 MeV protons in a Model I-100 linear accelerator, producing a uniform green coloration. The diamonds showed reduced or inert UV-activated fluorescence and reduced cathodoluminescence. The visible absorption spectra of the natural diamonds showed the development of weak peaks at 503 nm (associated with the H3 defect), 637 nm  $[(N-V)^+]$ , and 741 nm (GR1) following proton irradiation. In the synthetic diamonds, the authors observed the development of a CL peak (at liquid nitrogen temperature) at 575 nm  $[(N-V)^0]$ , and a weak peak at 637 nm in the visible absorption spectra. Nickel-related defects in the synthetic diamonds remained stable. Residual radioactivity in both the natural and synthetic diamonds was negligible and short-lived. The authors conclude that diamond treatment by proton irradiation is similar to electron and neutron irradiation, and could perhaps be used on a commercial scale. *Sally Eaton-Magaña*

## MISCELLANEOUS

**Deadly dust: The silicosis epidemic among Guangdong jewelry workers and the defects of China's occupational illnesses prevention and compensation system.** China Labor Bulletin, CLB Research Series No. 1, December 2005, 47 pp., [www.clb.org.hk/fs/view/downloadables/Deadly\\_Dust\\_Dec2005.pdf](http://www.clb.org.hk/fs/view/downloadables/Deadly_Dust_Dec2005.pdf).

Silicosis is an incurable disease of the lungs caused by chronic inhalation of crystalline silica dust. Over several years' exposure, the disease will progressively debilitate normal lung functions, possibly resulting in death. Long a bane of the mining, foundry, glass-making, and stone-

working industries, silicosis has recently been recognized as a risk for lapidary workers.

The general dangers of silicosis have been known for decades, and Western countries such as the U.S. have enacted strict workplace safety regulations. Although China has similar regulations, this report alleges that widespread failures in enforcement on the part of local governmental and judicial authorities have resulted in an epidemic of silicosis among Chinese jewelry workers. Further, deliberate efforts by jewelry companies to conceal the problems from investigators and cumbersome procedures for obtaining compensation for workplace injuries have hampered efforts to aid at-risk workers.

After a background discussion of these issues, the report presents seven case studies examining efforts by workers afflicted with silicosis to obtain compensation and medical care from their employers. Although in most cases the afflicted workers were ultimately able to obtain some compensation, this came only after sustained efforts by the lapidary companies to evade responsibility. The report alleges that the problems can be traced to employers placing profits ahead of worker safety, overly complicated regulations and compensation procedures, and endemic corruption in the Chinese judicial system and local governments. Recommendations for improvement include a thorough government investigation of workplace conditions and worker health; greater enforcement of existing workplace safety laws; and streamlining the compensation process to make it easier for lapidary workers, many of whom are unsophisticated migrants from the Chinese countryside. *TWO*

**Green dreams.** C. Zarin, *New Yorker*, Nov. 21, 2005, pp. 76–83.

This article traces the mysterious history of a magnificent suite of gold and emerald jewelry belonging to New York jeweler Fred Leighton. Leighton acquired the suite from a man who claimed to have salvaged it from the wreck of the great Spanish treasure fleet of 1715, which sank during a hurricane off the coast of Florida. The fleet was carrying a fortune in gold, silver, and gems for the Spanish royal court, including emeralds from the Muzo and Chivor mines in Colombia.

The author follows the stories of various treasure hunters who have searched the wrecks of this fleet and other treasure ships that foundered in the area, including the *Maravilla*, which was lost in 1656. Although multiple appraisers believed that the suite consists of genuine artifacts, and salvagers have been working the area since the 1970s, the author discovered that neither local divers nor the state had any record of this emerald jewelry being recovered from the 1715 fleet. The author postulates the jewels may have come from the *Maravilla* or from another Spanish wreck off the coast of Panama. Further research found that the diver who had owned them before Leighton gave conflicting stories about their origins.

Leighton tells the author, "with [antique] jewelry, sometimes you never know what the hell it is." RS

**How community institutions create economic advantage: Jewish diamond merchants in New York.** B. Richman, *Law & Social Inquiry*, Vol. 31, No. 2, 2006, pp. 383–420.

Richman explores how tight-knit communities can foster economic activity by placing enormous pressure for honesty and trust on all members, as well as providing a ready trading network, particularly with similar groups around the world. The author divides New York's diamond trade into two groups: the long-term players who have built businesses and are dependent on ethical behavior to maintain their connections; and the "independent contractors," who are usually from the ultra-Orthodox community. These latter dealers are generally brokers, often working on very small commissions sufficient to maintain their religious studies. Community pressure and family-based-reputation values mean they can be entrusted with many thousands of dollars worth of diamonds, which allows the industry to support an extensive network of credit sales with minimal fear of loss.

The diamond industry can extend this network through other parts of the world by dealing with a similar community in Antwerp, and through the Jains and Angadias in India, who maintain comparable traditions in their country. The institutions of this community also provide dispute resolution and sanctions so members do not have to resort to the courts. RS

**It's a deal.** O. Galibert, *Luxe Jewellery*, 2006-2007, pp. 136–140.

Practical questions for customers wishing to purchase gemstones include: Is it a good idea to purchase gems from their place of origin, and is it worth the trouble? Are the Internet and auction houses good alternative sources to traditional jewelers?

Knowledge and trust are vital when selecting and purchasing gems. Considerations such as the reputation, education, and reliability of the seller may be questioned. Accurate and up-to-date information is a key component to making wise purchases. Several websites are recommended, as well as technical journals (e.g., *Gems & Gemology* and *Journal of Gemmology*). Major purchases should always be accompanied by a grading or identification report from a reputable laboratory.

Buying from an internationally known jeweler tends to be expensive, but the authenticity and artistry of the jewelry are, consequently, of a high standard. Nevertheless, many smaller stores around the world have outstanding merchandise and do business in an ethical way. Such artisan-fueled jewelry stores (i.e., JAR, Taffin, etc.) are recommended for their selection of rare pieces and fine-quality design. Purchasing over the Internet is also an alternative, but since the buyer does not see the actual merchandise at the time of purchase, a more "hands-on" approach is suggested.

Auction houses offer the advantage of viewing several pieces at once, which can be advantageous when considering a purchase of jadeite, for example. Auction houses also offer services like phone bidding, secured payments, and international shipping. Private viewings are sometimes available for the serious bidder and provide an extra opportunity for examination of the pieces. JEC

**Microhardness, toughness, and modulus of Mohs scale minerals.** M. E. Broz [broz@cems.umn.edu], R. F. Cook, and D. L. Whitney, *American Mineralogist*, Vol. 91, 2006, pp. 135–142.

Most involved in the geosciences are familiar with the Mohs scale. First published in 1825, the scale can be used as an aid in mineral identification. Although commonly referred to as a "hardness" scale, these authors correctly point out that it is more appropriately labeled a *relative scratch-resistance* guide, which is influenced not only by hardness, but also by fracture toughness and elastic modulus (resistance to elastic deformation). This qualitative scale ranks 10 minerals in order of increasing scratch resistance: talc, gypsum, calcite, fluorite, apatite, orthoclase feldspar, quartz, topaz, corundum, and diamond. The authors performed modern hardness tests (microindentation and depth-sensing indentation) on all of the minerals except diamond, and compared them to the Mohs scale scratch-resistance test in an effort to quantify the material properties of the scale.

The data collected showed that the Mohs scale is not linear with any of the three parameters measured: hardness, toughness, or modulus. As an example, fluorite (Mohs 4) actually had higher modulus than orthoclase feldspar (Mohs 6). Thus, the authors concluded that there is no quantitative method to predict the relationship of Mohs number and material properties. Earth science instructors should consider this conclusion when teaching the use of the Mohs scale as an aid to mineral identification. KAM

**The path of stones.** B. Bilger, *New Yorker*, Oct. 2, 2006, pp. 66–79.

The gem mining and trading situations in Madagascar are described through the eyes of American dealer Tom Cushman. Mr. Cushman has been active in Madagascar for nearly 15 years, before many others, and is currently working to help educate the local Malagasy in gemology and stone cutting so they can become less dependent on foreign dealers.

The article describes the rough-and-tumble situation in Ilakaka, the area in which large sapphire deposits were discovered in 1998, with the colorful characters involved. This includes several miners—such as Jean Noel, the local businessman who sought (and found) his fortune in gem mining—and the local gangster, La Bombe, who thrived by intimidation and murder. The article also describes how Thai, Sri Lankan, and later African dealers moved in to take control of gem trading in the area. RS

VOLUME 42  
**INDEX** 2006  
 NUMBERS 1–4

## SUBJECT INDEX

This index gives the first author (in parentheses), issue, and inclusive pages of the article in which the subject occurs for all articles that appeared in Volume 42 of *Gems & Gemology*. For the Gem News International (GNI), Lab Notes (LN), Letters (Let), and Last Page (LP) sections, inclusive pages are given for the item. The Author Index (pp. 319–322) provides the full title and coauthors (if any) of the articles cited.

Note: The Fall 2006 Symposium and Gemological Research Conference Proceedings issue was paginated separately from the other issues in this volume year. This subject index covers the valedictory addresses, feature presentation abstracts, panel and debate center summaries, and poster session abstracts from that volume.

### A

#### Adularescence

- in quartz triplet imitating moonstone (LN)Su06:167–168
- simulated, in labradorite-glass doublet (GNI)Sp06:76

#### Afghanistan

- diopside from Badakhshan (GNI)W06:272–273
- gem sources and exploration in (Snee)F06:116–117
- sphene from Badakhshan (GNI)Su06:180–182
- uvite from (GNI)W06:281–282
- väyrynenite from Laghman Province (GNI)Su06:184–185

AGS, see American Gem Society

Alaska, see United States

#### Amber

- from Alaska, with bug inclusions (GNI)Su06:169–170
- simulants, with lizard “inclusions” (LN)W06:260–261

#### American Gem Society

- diamond cut grading system (Yantzer)F06:160

#### Amethyst

- treated, green and violetish blue (GNI)W06:285–286
- from Zambia (Anckar)F06:112–113

#### Amethyst, synthetic

- separation from natural using IR spectroscopy (Karampelas)F06:155

#### Analytical techniques [general]

- automating IR and Raman analysis (Lowry)F06:91

- characterizing nanofeatures (Rossman)F06:92
- forecast of (Fritsch)F06:90
- to identify colored stone treatments (Rossman)F06:32
- to identify diamond treatments (Collins)F06:33

#### Andradite

- demantoid—5.82 ct, with interesting inclusions (LN)W06:261–262; from Iran (Du Toit)F06:131 [erratum (GNI)W06:292]; from Russia (Kouznetsov)F06:157
- iridescent—“Rainbow,” from Japan (Hainschwang)W06:248–258; from Mexico (GNI)Su06:170–171

#### Appraisals

- ethical issues related to (Symposium Debate Center)F06:76–77
- for insurance documentation (Hendry)F06:169
- software for (Drucker)F06:130–131

#### Aquamarine

- from Canada (Linnen)F06:114
- from India, with cuneiform inclusions (GNI)Sp06:70
- possibly the Bragança “diamond” (Galopim de Carvalho)F06:132
- from Sri Lanka (GNI)Sp06:63–64

#### Assembled gem materials

- copal and plastic containing a lizard (LN)W06:260–261
- emerald matrix specimen with internal inscriptions (LN)Sp06:59–60
- labradorite-glass doublet (GNI)Sp06:76
- quartz triplet imitating moonstone (LN)Su06:167–168
- rutilated quartz—transparent quartz

- doublet (GNI)Sp06:76–77
- synthetic ruby/quartz/spinel composite (LN)Sp06:54
- ulexite—synthetic sapphire triplet imitating cat’s-eye chrysoberyl (GNI)Sp06:77–78

#### Asterism

- in coated quartz imitation of sapphire (LN)Sp06:60
- in emerald (GNI)Su06:171–172

#### Auctions

- sale of luxury jewelry at (Wickstrom)F06:52

#### Augelite

- green, from Peru (GNI)W06:271

#### Australia

- faceting rhodonite from New South Wales (Millstead)Su06:151–158
- prehnite from Northern Territories (GNI)Su06:177–178

### B

#### Baddeleyite

- as inclusion in heat-treated sapphire (Wang)Su06:134–150

#### Basalt

- as matrix of Leopard opal (Coenraads)W06:236–246

#### Beryl

- bicolored, from Namibia (GNI)W06:271–272
- color circle and varieties (Kleiman-tas)F06:137
- fingerprinting using LIBS and XRF (McMillan)F06:126

see also Aquamarine; Emerald

**Beryllium diffusion**, see Diffusion treatment

**Bleaching**, see Treatment

**Bone**  
bovine, dyed yellow, in pendant (LN)Su06:160–161

**Book reviews**  
*Agates: Treasures of the Earth* (Pabian)W06:294  
*Bedazzled: 5,000 Years of Jewelry* (Albersmeier)Su06:191  
*Bling Bling: Hip Hop's Crown Jewels* (Oh)W06:294–295  
*Charming: The Magic of Charm Jewelry* (Alun-Jones and Ayton)Su06:190–191  
*The Heartless Stone: A Journey Through the World of Diamonds, Deceit and Desire* (Zoellner)Su06:189–190  
*The Jeweler's Directory of Gemstones* (Crowe)W06:296  
*Making the Most of Your Flex-Shaft* (Christians)Su06:190  
*Masterpieces of French Jewelry from American Collections* (Price)W06:295–296  
*Modernist Jewelry, 1930–1960: The Wearable Art Movement* (Schon)Su06:191  
*Photoatlas of Inclusions in Gemstones, Volume 2* (Gübelin and Koivula)Sp06:83  
*Schmuck Jewellery 1840–1940: Highlights Schmuckmuseum Pforzheim* (Falk)Sp06:83–84  
*Working with Gemstones: A Bench Jeweler's Guide* (Skuratowicz and Nash)Sp06:84

**Bosnia-Herzegovina**  
hyalophane from Busovaca (Kniewald)F06:137–138

**Branding**  
of colored stones (Braunwart)F06:31  
of cultured pearls (Hoffman)F06:41  
of diamonds (Rothman)F06:26  
of jewelry—(Berg)F06:45, (Yurman)F06:44; Italian and European (Poli)F06:59–60  
of Robbins Bros. (Robbins)F06:47  
of Swarovski (Swarovski)F06:46

**Brazil**  
Bragança “diamond” from (Galopim de Carvalho)F06:132  
colored stones from, in historic Portuguese jewelry (Galopim de Carvalho)F06:167  
Cu-bearing tourmaline from (Abduriyim)Sp06:4–21  
emerald mining and trading in (Lucas)F06:158  
muscovite from Minas Gerais (GNI)Sp06:65–66

quartz—with colored fluid inclusions, from Bahia (GNI)Sp06:71–72; doublet (GNI)Sp06:76–77; Platinum variety, with star inclusion from Minas Gerais (GNI)Sp06:72; rutilated, from Bahia (Cook)F06:130; Sunset variety from Minas Gerais (GNI)W06:277–279; treated green and violetish blue, from Minas Gerais (GNI)W06:285–286

**Brilliantcutting**, see Diamond, cuts and cutting of

**Burma**, see Myanmar

## C

### Calcareous concretions

Melo pearls—and dyed shell imitation of (LN)Su06:166–167; from Myanmar (Htun)F06:135–136  
pen shell and clam (LN)W06:264–265

**California**, see United States

### Canada

aquamarine from Yukon Territory (Linnen)F06:114  
diamond sources and industry outlook (Irving)F06:24  
emerald from Ontario (Brand)F06:113  
sapphire from Baffin Island (Lepage)F06:155–156

### Cathodoluminescence

to identify diamond type (Kanda)F06:125

### Chalcedony

chrysocolla-colored, separation from dyed (Shen)F06:140  
Cr-bearing, from Turkey (Lule-Whipp)F06:115

“**Challenge**,” see *Gems & Gemology*

**Chemical composition**, see Electron-microprobe analysis; Scanning electron microscopy [SEM]; Spectrometry [various]; Spectroscopy [various]; specific gem materials

### Chemical fingerprinting

of beryl (McMillan)F06:126  
of emerald and Cu-bearing tourmaline (Abduriyim)Sp06:4–21 [erratum (GNI)W06:292]  
of opal (Gailou)F06:107–108

**Chemical vapor deposition [CVD]**, see Diamond, synthetic

### China

diamond industry outlook (Ma)F06:25  
freshwater cultured pearls from (Schechter)F06:40  
nephrite from Hetian (He)F06:134  
silicosis among lapidary workers in (Overton)F06:165  
triploidite from (GNI)Su06:183–184  
“**Chocolate pearls**,” see Pearl, cultured

### Chrysoberyl

cat's-eye, imitated by ulexite—synthetic sapphire triplet (GNI)Sp06:77–78

**Chrysocolla**, see Chalcedony

**Clam pearl**, see Calcareous concretions; Pearl

**Clarity grading**, see Grading

### Coating

of diamond to produce pink color (LN)Su06:163–164  
of quartz to imitate star sapphire (LN)Sp06:60  
of topaz (Befi)F06:128–129

### Colombia

assembled emerald matrix specimen from (LN)Sp06:59–60  
copal from (GNI)Sp06:70  
emerald mining and trading in (Lucas)F06:158  
euclase from the Chivor mine (GNI)Su06:173

### Color, cause of

in chameleon diamonds (Massi)F06:101–102  
due to nanofeatures (Rossman)F06:92

### Color change

in fluorite (GNI)Su06:173–174  
reverse, in zircon from Myanmar (Bosshart)F06:94

### Color, description of

using Gemwizard software—(Sevdermish)F06:102–103, (Underwood)F06:143  
using spectrographic imaging (Beaton)F06:93–94  
see also Color grading

### Color grading

definition of key color in (Grozman)F06:96–97  
of D-to-Z diamonds (Tashey)F06:142–143  
of treated-color pink to red diamonds (Smimov)F06:126–127  
“universal” system for (Liu)F06:101

### Color zoning

of facets on diffusion-treated sapphire (GNI)W06:287–289  
in sapphire, unusual colorless-blue (GNI)Sp06:74–75  
in small treated pink synthetic diamonds (GNI)W06:283–284  
in tortoise shell and its imitations (Hainschwang)Sp06:36–52

### Computer software

for appraisals (Drucker)F06:130–131  
Gemwizard, for color communication (Sevdermish)F06:102–103, (Underwood)F06:143  
for modeling diamond crystallography (Botha)F06:129  
OctoNus, for optimizing cut of fancy-color diamonds (Sivovolenko)

F06:104–105

#### Conference reports

Gemological Society of Japan conference (GNI)W06:289

International Mineralogical Association meeting (GNI)W06:289  
Madagascar mining laws, at Tucson show (GNI)Sp06:73

#### “Conflict” diamonds

and the movie *Blood Diamond* (Rapaport)F06:27, (Symposium panel)F06:63–64  
return to legitimate trading in Sierra Leone (GNI)W06:268–270

#### Copal

as amber imitation, containing a lizard (LN)W06:260–261  
from Colombia, with “blood trail” inclusions (GNI)Sp06:70

**Corundum**, see Ruby, Sapphire

**Crowningshield, G. Robert**  
obituary (Keller)W06:205

#### Crystallography

of diamond—(Rondeau)F06:109–110;  
3-D modeling of (Botha)F06:129  
of rhodonite (Millsted)Su06:151–158

#### Cullinan diamonds, I and II

history and gemological characterization of (Scarratt)Su06:120–132

#### Cullinan (formerly Premier) mine

history of (Scarratt)Su06:120–132

**Cultured pearl**, see Pearl, cultured

**Cutting**, see Diamond, cuts and cutting of; Lapidary arts

**CVD [chemical vapor deposition]-grown synthetic diamonds**, see Diamond, synthetic

## D

#### De Beers

Supplier of Choice transition (Tempelman)F06:7–12

**Demantoid**, see Andradite

#### Diamond

with blue sapphire inclusions (LN)Su06:165–166  
Bragança, possible identification of (Galopim de Carvalho)F06:132  
from Canada (Irving)F06:24  
cape, color measurement of rough (Ceulemans)F06:130  
cathodoluminescence to identify type (Kanda)F06:125  
color nomenclature on the D-to-Z scale (Tashey)F06:142–143  
Cross-referencing Identification System (CIS) for (Deljanin)F06:163–164  
Cullinans I and II (Scarratt)Su06:120–132

damaged by laser (GNI)W06:270–271  
dislocation networks in type IIa (De Corte)F06:122–123  
geologic origin of (Harris)F06:107–108  
graining, impact on clarity grading of (King)W06:206–220  
in India, history of (Zucker)F06:160–161  
in Liberia (Hoal)F06:134–135  
marketing and economics of—(Irving)F06:24, (Ma)F06:25, (Rapaport)F06:28, (Rothman)F06:26, (Tannenbaum)F06:23, (Tempelman)F06:7–12; in Sierra Leone (GNI)W06:268–270  
mines and mining (Hoal)F06:134–135  
modeling crystallography of (Botha)F06:129  
morphology of—(Fedortchouk)F06:146, (Rondeau)F06:109–110  
production—from 1870 to 2005 (Janse)F06:136; and distribution (Suwa)F06:58–59  
from Russia—Komsomolskaya mine (Sobolev)F06:117; Siberia (Solodova)F06:141–142; white to gray, from Siberia (Titkov)F06:127–128  
sources—(Janse)F06:148–149  
trace elements in type I (Khamrayeva)F06:90–91  
see also Grading; other Diamond entries

#### Diamond, colored

black, with unusual growth structures (GNI)Sp06:73–74  
blue—phosphorescence of (Eaton-Magaña)F06:95–96; light blue, with clarity determined by graining (LN)Su06:162–163  
with brown and green radiation stains (LN)Su06:161–162  
brown-orange, translucent (LN)Sp06:57–59  
chameleon coloration model (Massi)F06:101–102  
chronology of (LP)Su06:204  
CO<sub>2</sub>-rich (Hainschwang)F06:97  
cutting to optimize color (Sivovolenko)F06:104–105, 140–141  
fluorescence of (Eaton-Magaña)F06:131–132  
Hope diamond, phosphorescence of (Eaton-Magaña)F06:95–96  
pink—with etch channels and glide planes (LN)Sp06:56; with prolonged change of color (LN)W06:263–264  
white, 30.87 ct (LN)W06:262–263  
white to gray, from Siberia, inclusions in (Titkov)F06:127–128  
X-ray topography of (Yuan)F06:93  
see also Diamond, inclusions in; Diamond, synthetic; Diamond treatment

#### Diamond, cuts and cutting of

Cullinans I and II (Scarratt)Su06:120–132  
evolution of the American round brilliant (Gilbertson)F06:133  
Koh-i-Noor diamond, replica of (Hatleberg)F06:158–159  
manufacturing (Hasenfeld)F06:48  
to optimize fancy-color appearance—(Sivovolenko)F06:104–105, 140–141  
two stones from the same crystal (LN)Sp06:56–57  
use of 3-D modeling in (Botha)F06:129  
see also Grading; other Diamond entries

#### Diamond, inclusions in

dissolution features (Lu)F06:138  
etch channel (LN)Su06:165  
fingerprint-like, in natural-color and HPHT-treated (LN)Sp06:54–55  
graining, impact on clarity grading—(King)W06:206–220; in light blue (LN)Su06:162–163  
micro-inclusions in translucent brown-orange (LN)Sp06:57–59  
in white to gray diamonds from Siberia (Titkov)F06:127–128  
whitish banding in Fancy white (LN)W06:262–263

#### Diamond, synthetic

consumer confidence issues (Symposium panel)F06:63–64  
CVD-grown—(Welbourn)F06:34–35; from LIMHP-CNRS, France (Anthonis)F06:152–153; growth and use of (Butler)F06:111–112; and HPHT-grown (Welbourn)F06:34–35; luminescence spectra of defects in (Charles)F06:121–122  
HPHT-grown—from Advanced Optical Technology Co., Canada (Deljanin)F06:154–155; and CVD-grown (Welbourn)F06:34–35  
nomenclature issues (Symposium Debate Center)F06:66–67  
patent applications for incorporating biological remains into (GNI)Sp06:78–79  
treated pink (GNI)W06:283–284  
X-ray topography of (Yuan)F06:93

#### Diamond treatment

coated pink (LN)Su06:163–164  
color grading system for treated-color pink to red (Smirnov)F06:126–127  
and defect deformation, imaged with X-ray topography (Yuan)F06:93  
HPHT—in annealing of CVD synthetic diamonds (Anthonis)F06:152–153; of brown diamonds (Vins)F06:120–121; defects created and destroyed by (Newton)F06:84–85; DiamondView imaging of type IIb diamonds (Breeding)F06:88; impact on color (Collins)F06:33, (Pope)F06:120; producing finger-

- print-like inclusions (LN)Sp06:54–55; of type IaB brown diamonds (Van Royen)F06:86
- jewelry potential of (Perret)F06:159–160
- laser drilling using KM (*Kiduah Meyuhad*) treatment (Collins)F06:33
- DiamondView imaging**
- of CVD synthetic diamond (Welbourn)F06:34–35
  - of diamond with unusual etch channel (LN)Su06:165
  - of dislocation networks in type IIa diamonds (De Corte)F06:122–123
  - and gem identification (Breeding)F06:88
  - of translucent brown-orange diamond (LN)Sp06:57–59
  - of two diamonds from the same crystal (LN)Sp06:56–57
- Diffraction**
- as cause of iridescence in Rainbow andradite (Hainschwang)W06:248–258
- Diffusion treatment**
- of corundum, with beryllium—(McClure)F06:29–30, (Wathanakul)F06:87; detection using EPR (Rossman)F06:32; detection using LA-ICP-MS, LIBS, and SIMS (Abduriyim)Su06:98–118 [erratum (GNI)W06:292], F06:87–88
  - of sapphire, with circular inclusions (GNI)W06:286–287
  - of synthetic corundum—(GNI)Su06:185–186, (Pisutha-Armond)F06:85; showing unusual fluorescence (GNI)W06:287–289
- Diopside**
- from Afghanistan (GNI)W06:272–273
- Disclosure**
- of treated gems—(Symposium Debate Center)F06:68–69; corundum (Scarratt)F06:85–86; and synthetic gems (Kane)F06:36–37
- Dravite**, see Tourmaline
- Dubai**
- retailing and trading in (Dhamani)F06:61
- Durability**
- of lead-glass filling in rubies (McClure)Sp06:22–34 [erratum (GNI)Su06:188]
- Dyeing**
- of bovine bone (LN)Su06:160–161
  - of chalcedony to imitate chrysocolla chalcedony (Shen)F06:140
  - of “chocolate pearls” (GNI)W06:284–285
  - identification of silver-dyed cultured pearls (Wang)W06:222–235
  - of shell to imitate Melo pearls (LN)Su06:166–167
- E**
- Editorials**
- “Business and Science Converge at the 2006 Symposium and Gemological Research Conference” (Kimmel and Keller)F06:1
  - “GIA Celebrates 75 Years. . .” (Keller)Su06:95–96
  - “Remembering G. Robert Crowningshield” (Keller)W06:205
  - “Symposium 2006: Navigating the Challenges Ahead” (Keller)Sp06:1
- Education**
- at GIA—course development (Pay)F06:162; public outreach (Vagner)F06:162–163
  - in Madagascar (Cushman)F06:161
- EDXRF**, see Spectroscopy, energy-dispersive X-ray fluorescence
- Elbaite**, see Tourmaline
- Electron-microprobe analysis**
- of emerald from Ontario, Canada (Brand)F06:113
  - of hiddenite from North Carolina (Wise)F06:152
  - of massive pink muscovite from Brazil (GNI)Sp06:65–66
  - and the RRUFF project database (Downs)F06:89–90
- Emerald**
- assembled, with internal inscriptions (LN)Sp06:59–60
  - from Canada (Brand)F06:113
  - chemical fingerprinting of (Abduriyim)Sp06:4–21
  - production of (Yager)F06:144–145
  - from Sandawana, Zimbabwe (Zwaan)F06:111
  - with six-rayed star (GNI)Su06:171–172
  - in South America (Lucas)F06:158
  - see also Beryl
- Endangered species**
- trade in gem materials of (Carmona)F06:166–167
- Energy-dispersive spectroscopy [EDS]**, see Scanning electron microscopy [SEM]
- England**
- Cullinan diamonds in the Crown Jewels of (Scarratt)Su06:120–132
- Enhancement**, see Coating; Diamond treatment; Dyeing; Treatment; specific gem materials
- EPR**, see Spectroscopy, electron paramagnetic resonance
- Errata**
- to “*Bahia* sculpture” (Lehrer)F06:158—description of source material (GNI)W06:292
  - to “Demantoid from Iran” (Du Toit)F06:131—origin of banded opaque material (GNI)W06:292
  - to “Dr. Edward J. Gübelin Most Valuable Article Award” (Editorial)Sp06:2–3—author bio (GNI)Su06:188
  - to “Identification and durability of lead glass-filled rubies” (McClure)Sp06:22–34—carat weight of sample (GNI)Su06:188
  - to “Jeremejevitte from Myanmar and Sri Lanka” (GNI)Su06:175–176—geographic origin (GNI)W06:292
  - to “LA-ICP-MS” (Abduriyim)Su06:98–118—table 3, logo size (GNI)W06:292
  - to “Pyrope-spessartine from Tanzania” (GNI)Sp06:66–67—geographic origin (GNI)W06:292
- Ethics**
- and appraisal issues (Symposium Debate Center)F06:76–77
  - Council for Responsible Jewellery Practices (GNI)Sp06:78
  - in the jewelry industry (Symposium Debate Center)F06:70–71
  - and maintaining consumer confidence (Symposium panel)F06:63–64
- Euclase**
- from Colombia (GNI)Su06:173
- Europe**
- freshwater pearls from (Strack)F06:105
- F**
- Faceting**
- of rhodonite from Australia (Millstead)Su06:151–158
  - see also Diamond, cuts and cutting of; Lapidary arts
- Fair Trade practices**
- in Africa (Rapaport)F06:27
  - see also Ethics
- Fakes**, see specific gem materials simulated
- Feldspar**
- albitic moonstone, imitation of (LN)Su06:167–168
  - moonstone K-feldspar from Madagascar (GNI)W06:276
  - sillimanite resembling moonstone (GNI)Su06:180–181
  - see also Hyalophane; Labradorite
- Filling, fracture or cavity**
- of ruby with lead glass (McClure)Sp06:22–34 [erratum (GNI)Su06:188]
  - see also Inclusions
- Filters**, see Instruments
- Fluorescence, ultraviolet [UV]**

of assembled emerald matrix specimen (LN)Sp06:59–60  
of diamond—colored (Eaton-Magaña)F06:131–132; Cullinan II diamond (Scarratt)Su06:120–132  
of diffusion-treated sapphire (GNI)W06:287–289  
of haiüyne-sodalite from Myanmar (GNI)Sp06:64–65  
of opal—fire, with play-of-color (GNI)W06:276–277; Leopard (Coenraads)W06:236–246  
of small, treated pink synthetic diamonds (GNI)W06:283–284  
of tortoise shell and its imitations (Hainschwang)Sp06:36–52  
of tourmaline from Tanzania (GNI)Su06:182–183

**Fluorescence, X-ray**, see Spectroscopy, energy-dispersive X-ray fluorescence [EDXRF]

**Fluorite**  
color-change (GNI)Su06:173–174

**Fracture filling**, see Filling, fracture or cavity

## G

**Garnet**  
marketing of (Boehm)F06:28  
see also Andradite; Grossular; Pyrope-spessartine

**Gemewizard**  
color communication software (Sevdermish)F06:102–103, (Underwood)F06:143

**Gemological Research Conference, GIA [2006]**  
proceedings of (Kimmel)F06:1

**Gems & Gemology**  
“Challenge”—Sp06:81–82; winners and answers W06:293  
Edward J. Gübelin Most Valuable Article Award Sp06:2–3 [erratum (GNI)Su06:188]  
Twenty-Five Year Index (LP)Sp06:94

**Geographic origin**  
and colored stone value factors (Symposium Debate Center)F06:74–75

**Geology**  
of placer gem deposits (Prudden)F06:149

**Geopolitics**  
and world affairs (Albright)F06:2–6

**GIA (Gemological Institute of America)**  
75th anniversary of (Keller)Su06:95–96  
2006 International Gemological Symposium and Gemological Research Conference (Keller)Sp06:1,

(Kimmel)F06:1  
see also Education

**Glass**  
in doublet with labradorite (GNI)Sp06:76  
see also Filling, fracture or cavity

**Grading**  
of diamond—(Keenan)F06:100; by AGS (Yantzer)F06:160; by GIA, role of brilliantteering in (Reinitz)F06:138–139; impact of grading on (King)W06:206–220; peer review (Holloway)F06:159  
importance of (Kane)F06:36–37  
issues related to consumer confidence (Symposium panel)F06:63–64  
of ruby and sapphire (Atichat)F06:128  
see also Color grading

**Graining**  
in diamond—Fancy Light blue (LN)Su06:162–163; internal whitish and reflective, impact on clarity grading (King)W06:206–220; translucent brown-orange (LN)Sp06:57–59; whitish banding in Fancy white (LN)W06:262–263

**Greenland**  
ruby and pink sapphire from Fiskensæset (Rohtert)F06:149–150

**Grossular**  
62.81 ct tsavorite, from Tanzania (GNI)Sp06:62

**Growth structure**  
unusual, in black diamond (GNI)Sp06:73–74

**Guatemala**  
jadeite from the Motagua fault zone (Harlow)F06:146–147

**Gulf region**  
jewelry retailing and trading in (Dhamani)F06:61

## H

**Haiüyne**  
mixture with sodalite, from Myanmar (GNI)Sp06:64–65

**Heat treatment**  
of corundum—(Kitawaki)F06:84; indications of (Sutthirat)F06:86; infrared spectroscopy of (Smith)F06:92–93  
of Cu-bearing tourmaline from Mozambique (Abduriyim)Sp06:4–21  
effect on zircon inclusions in Madagascar sapphires (Wang)Su06:134–150  
see also specific gem materials

**Herderite**  
from Pakistan (GNI)Su06:174–175

**Hiddenite**  
from North Carolina, geology of

(Wise)F06:152

**High-pressure, high-temperature [HPHT] synthesis**, see Diamond, synthetic

**High-pressure, high-temperature [HPHT] treatment**, see Diamond treatment

### History

of the American round brilliant (Gilbertson)F06:133  
of the Cullinan diamonds and Cullinan/Premier mine (Scarratt)Su06:120–132  
of diamond trading in India (Zucker)F06:160–161  
of the Koh-i-Noor diamond (Hatleberg)F06:158–159  
of Portuguese jewelry—(Galopim de Carvalho)F06:168–169; with Brazilian colored stones (Galopim de Carvalho)F06:167

### Hope diamond

phosphorescence of (Eaton-Magaña)F06:95–96

### Horn

as a tortoise shell imitation (Hainschwang)Sp06:36–52

**HPHT (high pressure, high temperature)**, see Diamond, synthetic; Diamond, treatment

### Hyalophane

from Bosnia-Herzegovina (Kniewald)F06:137–138

## I

**ICA**, see International Colored Gemstone Association

**Imaging spectroscopy**, see Spectroscopy, imaging

**Imitations**, see specific gem materials imitated

**INAA**, see Instrumental neutron activation analysis

### Inclusions

in adulescent sillimanite (GNI)Su06:180–181  
in amber from Alaska (GNI)Su06:169–170  
in aquamarine—from Canada, fluid (Linnen)F06:114; from India, cuneiform (GNI)Sp06:70  
in copal from Colombia (GNI)Sp06:70  
in demantoid, curved fibers (LN)W06:261–262  
in emerald, star (GNI)Su06:171–172  
in imitation amber, lizard (LN)W06:260–261  
in jadeite from California, copper (GNI)W06:273  
in jerejeveite (GNI)Su06:175–176  
in quartz—(Hyrs)F06:97–98; from Brazil, colored fluid;

- (GNI)Sp06:71–72; needles in Sunset quartz from Brazil; (GNI)W06:277–279; rutile star in Platinum quartz from Brazil (GNI)Sp06:72
- in rubies, lead glass-filled—(McClure)Sp06:22–34 [erratum (GNI)Su06:188]; bead necklace (GNI)Su06:186–187
- in sapphire—cloud-like, with Be traces, in untreated sapphire (McClure)F06:29–30; diffusion-treated (GNI)W06:286–287; heat-treated (Wang)Su06:134–150; from Laos, monazite (Singamroong)F06:103–104; unusual (GNI)Su06:179–180; from Yogo, Montana (Cade)F06:106; of zircon, in heat-treated sapphire (Wang)Su06:134–150
- in synthetic sapphire, diffusion-treated (GNI)Su06:185–186
- in tourmaline from Nigeria, Cu-bearing (Abdurayim)Sp06:4–21
- see also Diamond, inclusions in
- India**
- aquamarine with cuneiform inclusions from (GNI)Sp06:70
- gem sources in (Mohideen)F06:115–116
- history of diamond trading in (Zucker)F06:160–161
- jewelry retailing in (Mehta)F06:62
- sillimanite from—resembling moonstone (GNI)Su06:180–181; transparent, from Andhra Pradesh (GNI)Sp06:67–68
- Infrared spectroscopy**, see Spectroscopy, infrared
- Instrumental neutron activation analysis [INAA]**
- of trace elements in diamond (Khamrayeva)F06:90–91
- Instruments**
- for color measurement of rough cape diamonds (Ceulemans)F06:130
- filters, use in separating gems (Gumpesberger)F06:124
- magnets, use in separating gems (Gumpesberger)F06:124
- refractometer, for identifying biaxial gemstones (Sturman)F06:127
- see also Analytical techniques; Cathodoluminescence; DiamondView imaging; Electron-microprobe analysis; Refractometer; Scanning electron microscopy; Spectrometry [various]; Spectroscopy [various]; X-ray diffraction analysis; X-ray topography
- Interference (optical effect)**
- in iridescent andradite (Hainschwang)W06:248–258
- International Colored Gemstone Association [ICA]**
- world mining report (Boehm)F06:157
- International Gemological Symposium, 4th [2006]**
- proceedings of (Kimmel)F06:1
- Internet**
- distribution of jewelry—(Azrielant)F06:56–57, (Fant)F06:55, (Raff)F06:55–56, (Symposium Debate Center)F06:72–73
- Iran**
- demitoid from Kerman Province (Du Toit)F06:131 [erratum (GNI)W06:292]
- Iridescence**
- in andradite—from Japan (Hainschwang)W06:248–258; from Mexico (GNI)Su06:170–171
- in labradorite-glass doublet (GNI)Sp06:76
- Iron ore**
- banded, from Sweden (GNI)W06:279
- J**
- Jade**, see Jadeite; Nephrite
- Jadeite**
- colorless translucent, resembling moonstone (LN)Su06:167–168
- with copper inclusions, from California (GNI)W06:273
- from Guatemala (Harlow)F06:146–147
- from Myanmar—formation of (Shi)F06:150–151; Hkamti area (Kane)F06:98–99
- Japan**
- jewelry market, analysis of (Suwa)F06:58–59
- Rainbow andradite from Nara Prefecture (Hainschwang)W06:248–258
- Jeremejevit**
- from Myanmar and Sri Lanka (GNI)Su06:175–176 [erratum (GNI)W06:292]
- Jewelry**
- brooches, Madeleine Albright collection of (Albright)F06:2–6
- design—(Bondanza)F06:42, (Esmerian)F06:53, (Perret)F06:159–160, (Perrin)F06:48, (Poli)F06:59, (Singer)F06:43, (Yurman)F06:44
- Italian and European goldsmiths (Poli)F06:59–60
- luxury—(Esmerian)F06:53, (Katz)F06:51, (Perrin)F06:48, (Wickstrom)F06:53
- quality factors (Singer)F06:43
- retailing—(Berg)F06:45; in the Gulf region (Dhamani)F06:61; in India (Mehta)F06:62; via the Internet (Azrielant)F06:56–57, (Fant)F06:55, (Raff)F06:55–56, (Symposium Debate Center)F06:72–73; issues related to consumer confidence (Symposium panel)F06:63–64; via television (Coquillard)F06:54
- technical innovations in manufacturing (Bondanza)F06:42
- Jewelry repair**
- diamond damaged by laser (GNI)W06:270–271
- K**
- “Keshi” pearl, see Pearl, cultured
- Koh-i-Noor diamond**
- replica of (Hatleberg)F06:158–159
- L**
- Labradorite**
- in doublet with glass, imitating moonstone (GNI)Sp06:76
- pale yellow, from Mexico (GNI)W06:274–275
- LA-ICP-MS**, see Spectrometry, laser ablation-inductively coupled plasma-mass
- Laos**
- sapphires from Ban Huai Sai (Singamroong)F06:103–104
- Lapidary arts**
- cutting the *Bahia* quartz sculpture (Lehrer)F06:158 [erratum (GNI)W06:292]
- faceting rhodonite from New South Wales (Millstead)Su06:151–158
- silicosis risks in (Overton)F06:165
- see also Diamond, cuts and cutting of
- Laser drilling**, see Diamond treatment
- LED [Light-emitting diode]**, see Lighting methods
- Legal issues**
- Madagascar mining laws, revisions to (GNI)Sp06:73
- and trade in tortoise shell (Hainschwang)Sp06:36–52
- see also Endangered species; Ethics; Patents
- Letters**
- Chelsea filters and synthetic emeralds (Let)Su06:97
- more about “Medusa” quartz (Let)Su06:97
- Liberia**
- diamond industry development in

- (Hoal)F06:134–135
- LIBS**, see Spectroscopy, laser-induced breakdown
- LifeGem**, see Diamond, synthetic; Patents
- Lighting**  
and fancy-color diamond appearance (Sivovolenko)F06:140–141  
for photography of phenomenal gems (Weldon)F06:144  
using LED and crossed filters to identify gems (Gumpesberger)F06:124  
see also Grading; Instruments
- Luminescence**, see  
Cathodoluminescence; DiamondView imaging; Fluorescence, ultraviolet [UV]; Phosphorescence; Photoluminescence
- M**
- Madagascar**  
gemological education in (Cushman)F06:161  
mining laws in (GNI)Sp06:73  
moonstone from Ihosy (GNI)W06:276  
sapphire from—(Pezzotta)F06:116–117; heat treatment of (Wang)Su06:134–150  
tourmaline from—(Superchi)F06:156; mining at Nandihizana (GNI)W06:280–281; and sapphire (Pezzotta)F06:116–117
- Magnetism**, see Instruments
- Mali**  
prehnite from Kayes region (GNI)Su06:178–179
- Marketing and distribution**  
of colored gemstones in Portugal (Galopim de Carvalho)F06:167–168  
of cultured pearls—(Hoffman)F06:41; Chinese freshwater (Schechter)F06:40; South Sea (Paspaley)F06:38; Tahitian (Galenon)F06:170, (Wan)F06:39  
of diamonds in Japan (Suwa)F06:58–59  
of jewelry—(Berg)F06:45, (Welborn)F06:166; in the Gulf region (Dhamani)F06:61; in India (Mehta)F06:62; via the Internet (Azrielant)F06:56–57, (Fant)F06:55, (Raff)F06:55–56, (Symposium Debate Center)F06:72–73; issues related to consumer confidence (Symposium panel)F06:63–64; luxury (Esmerian)F06:53, (Katz)F06:51, (Perrin)F06:48, (Wickstrom)F06:53; via television (Coquillard)F06:54  
through philanthropy (Buckley)F06:166  
Robbins Bros. strategy (Robbins)F06:47  
of Swarovski products (Swarovski)F06:46  
of untreated and underappreciated gems (Boehm)F06:28  
see also Diamonds; Internet
- Maw-sit-sit**  
from Myanmar (Shi)F06:150–151
- Melo pearl**, see Calcareous concretions
- Metals**  
and consumer confidence (Symposium panel)F06:63–64  
in Italian and European jewelry (Poli)F06:59–60
- Mexico**  
iridescent andradite from Sonora (GNI)Su06:170–171, W06:248–258  
labradorite from Chihuahua (GNI)W06:274–275  
Leopard opal from Hidalgo (Coenraads)W06:236–246
- Microprobe**, see Electron-microprobe analysis
- Microscopic techniques**, see Inclusions; Scanning electron microscopy [SEM]
- Middle East**, see Gulf region
- Mining and exploration**  
of pegmatite-related primary deposits (Clanin)F06:145  
of sapphire from Baffin Island, Canada (Lepage)F06:155–156  
see also specific countries and specific gem materials
- Mogok**, see Myanmar
- Montana**, see United States
- Moonstone**, see Feldspar; Labradorite
- Most Valuable Article award**, see *Gems & Gemology*
- Mozambique**  
Cu-bearing tourmaline from—chemical composition of (Abduriyim)Sp06:4–21; 42.38 ct (GNI)Sp06:62
- Muscovite**  
massive pink, from Brazil (GNI)Sp06:65–66
- Museums and gem collections**  
Gem & Mineral Council of the Natural History Museum of Los Angeles County (Kampf)F06:161–162
- Myanmar**  
jadeite—formation of (Shi)F06:150–151; from Hkamti (Kane)F06:98–99  
Melo pearls from Mergui Archipelago (Htun)F06:135–136  
Mogok—formation of ruby from (Harlow)F06:147; gem production from (GNI)W06:275–276; jeremejevite from (GNI)Su06:175–176; massive haüyne-sodalite from (GNI)Sp06:64–65; zircon with reverse color change from (Bosshart)F06:94
- N**
- Namibia**  
beryl from Erongo Mountains (GNI)W06:271–272
- Nephrite**  
from Hetian, China (He)F06:134
- New Zealand**  
sapphires from Dunedin area (Kiefert)F06:113–114
- Nigeria**  
Cu-bearing tourmaline from (Abduriyim)Sp06:4–21
- Nomenclature**  
of “Keshi” pearls (Sturman)F06:142  
of “padparadscha” sapphire (Beaton)F06:93–94  
of “Paraíba” tourmaline (Symposium Debate Center)F06:74–75  
of synthetic diamond (Symposium Debate Center)F06:66–67
- North Carolina**, see United States
- O**
- Obituary**  
G. Robert Crowningshield (Keller)W06:205
- Opal**  
fire, 70 ct, with play-of-color (GNI)W06:276–277  
geographic origin of (Gaillou)F06:107  
Leopard variety, from Mexico (Coenraads)W06:236–246  
pink, from Peru (GNI)Su06:176–177
- P**
- Pakistan**  
herderite from Northern Areas Province (GNI)Su06:174–175  
sphene from North West Frontier Province (GNI)Sp06:67–68  
vāyrynenite from Braldu Valley (GNI)Sp06:75
- “Paraíba” tourmaline**, see Tourmaline
- Patents**  
applications, for methods of incorporating biological remains into gem materials (GNI)Sp06:78–79
- Pearl**  
formation (Bell)F06:169–170  
freshwater, from Europe (Strack)F06:105  
pen shell, clam, and nacreous, in a

strand (LN)W06:264–265

**Pearl, cultured**  
branding of (Hoffman)F06:41  
Chinese freshwater (Schechter)F06:40  
“chocolate pearls”—examined by the SSEF laboratory (GNI)W06:284–285; identification of (Wang)W06:222–235  
freshwater, identification of pigments in (Kampelas)F06:99–100  
“Keshi,” characterization of (Sturman)F06:142  
nuclei identification using LA-ICP-MS (Abduriyim)F06:87–88  
South Sea (Paspaley)F06:38  
Tahitian—(Wan)F06:39; identification of untreated, “chocolate,” and dyed (Wang)W06:222–235; marketing of (Galenon)F06:170  
treatments (Scarratt)F06:40–41  
UV-Vis spectra of natural- and treated-color yellow (Elen)F06:123

**Pegmatites**  
crystallization of (Taylor)F06:110–111  
formation of gems in (London)F06:108–109, F06:109  
geology of, in Southern California (Snee)F06:151–152  
mining primary deposits (Clanin)F06:145

**Pen shell pearl**, see Pearl

**Peru**  
augelite from Ancash Department (GNI)W06:271  
opal from Monte Rosa (GNI)Su06:176–177

**Pezzottaite**  
X-ray topography of (Liu)F06:100–101

**Philanthropy**  
as investment for retail jewelers (Buckley)F06:166

**Phosphorescence**  
of type IIb diamond—(Eaton-Magaña)F06:95–96, (Breeding)F06:88

**Photography**  
digital asset management system (Colbert)F06:163  
luminescence, reflected-IR and reflected-UV (Elen)F06:123  
of phenomenal gems (Weldon)F06:144

**Photoluminescence**  
of CVD synthetic diamond, before and after HPHT annealing (Anthonis)F06:152–153  
to separate natural and synthetic spinel (Maini)F06:125

**Plastic**  
as an amber imitation, with lizard “inclusion” (LN)W06:260–261  
as a tortoise shell imitation (Hainschwang)Sp06:36–52

**Plato lines**, see Sapphire, synthetic

**Polishing**  
using PolishPlus technique (Richardson)F06:139–140

**Portugal**  
Bragança “diamond” (aquamarine?) in the Portuguese Royal Treasuries (Galopim de Carvalho)F06:132  
historical jewelry—(Galopim de Carvalho)F06:168–169; with Brazilian colored stones (Galopim de Carvalho)F06:167  
marketing colored gemstones in (Galopim de Carvalho)F06:167–168  
see also Diamond, cuts and cutting of; Faceting; Lapidary arts

**Poudretteite**  
3.90 ct pink (LN)W06:265–266

**Prehnite**  
from Australia (GNI)Su06:177–178  
from Mali (GNI)Su06:178–179

**Premier mine**, see Cullinan mine

**Pricing**  
of gems—social, political, economic, and gemological impacts on (Drucker)F06:95  
see also Appraisals

**Pyrope-spessartine**  
from Tanzania (GNI)Sp06:66–67 [erratum (GNI)W06:292]

**Pyroxmangite**  
separation from rhodonite (LN)W06:266–267

**Q**

**Quartz**  
coated, to imitate star sapphire (LN)Sp06:60  
with colored fluid inclusions, from Brazil (GNI)Sp06:71–72  
genetic classification based on inclusions (Hyrsl)F06:97–98  
“Platinum” variety with large rutile star inclusion, from Brazil (GNI)Sp06:72  
rose, massive pink muscovite as imitation of (GNI)Sp06:65–66  
rutilated—from Bahia, Brazil (Cook)F06:130; cutting the *Bahia* sculpture (Lehrer)F06:158 [erratum (GNI)W06:292]; with transparent quartz in doublet (GNI)Sp06:76–77  
“Sunset” variety, from Brazil (GNI)W06:277–279  
treated green and violetish blue, from Brazil (GNI)W06:285–286  
triplet imitating moonstone (LN)Su06:167–168  
see also Amethyst

**Quartz, synthetic**, see Assembled gem materials

## R

**Rainbow andradite**, see Andradite

**Refractometer**, see Instruments

**Religious artifacts**  
and gem identification (Burianek)F06:121  
from Portugal (Galopim de Carvalho)F06:168–169

**Research**  
funding of (Groat)F06:133–134

**Rhodonite**  
faceting of, from New South Wales, Australia (Millsted)Su06:151–158  
separation from pyroxmangite (LN)W06:266–267

**RRUFF project**, see Spectroscopy, Raman

**Ruby**  
from Greenland (Rohtert)F06:149–150  
infrared spectra of (Smith)F06:92–93  
lead glass-filled—bead necklace of (GNI)Su06:186–187; identification and durability of (McClure)Sp06:22–34 [erratum (GNI)Su06:188]  
from Mogok, Myanmar—formation of (Harlow)F06:147; production of (GNI)W06:275–276  
production of (Yager)F06:144–145  
quality grading of (Atichat)F06:128  
source type classification of (McClure)F06:102  
standards for LA-ICP-MS analysis (Wang)F06:105–106  
treatment of—(Scarratt)F06:85–86; identification of heat treatment (Kitawaki)F06:84, (Sutthirat)F06:86

**Ruby, synthetic**  
separation from natural (Bidny)F06:153  
treatment of—beryllium diffusion (Pisutha-Amond)F06:85; identification of heat treatment (Kitawaki)F06:84  
see also Assembled gem materials

**Russia**  
demantoid—from Ural Mountains (Kouznetsov)F06:157; 5.82 ct, purchased in (LN)W06:261–262  
diamond—from Komsomolskaya mine (Sobolev)F06:117; inclusions in white-to-gray diamonds from Siberia (Titkov)F06:127–128; from Siberia (Solodova)F06:141–142

**Rutilated quartz**, see Quartz

## S

**Sapphire**  
from Canada (Lepage)F06:155–156  
with color zoning (GNI)Sp06:74–75

- grading of (Atichat)F06:128  
from Greenland, pink  
(Rohtert)F06:149–150  
imitated by synthetic sapphire  
(GNI)W06:282  
inclusions in (GNI)Su06:179–180  
as inclusions in diamond  
(LN)Su06:165–166  
infrared spectra of (Smith)F06:92–93  
from Laos  
(Singbamroong)F06:103–104  
from Madagascar—heat treatment of  
(Wang)Su06:134–150; from  
Marosely (Pezzotta)F06:116–117  
marketing of (Boehm)F06:28  
from Montana—Gem Mountain/Rock  
Creek (Berg)F06:145; Yogo  
(Cade)F06:106, F06:129–130  
from Myanmar, production from  
Mogok (GNI)W06:275–276  
from New Zealand  
(Kiefert)F06:113–114  
production of (Yager)F06:144–145  
source type classification of  
(McClure)F06:102  
from Sri Lanka, *in situ* deposits  
(Tennakoon)F06:117–118  
standards for LA-ICP-MS analysis  
(Wang)F06:105–106  
star, coated quartz imitation of  
(LN)Sp06:60  
treatment of—(Scarratt)F06:85–86;  
diffusion, with beryllium  
(Wathanakul)F06:87; diffusion, with  
circular inclusions  
(GNI)W06:286–287; indications of  
heating (Kitawaki)F06:84,  
(Sutthirat)F06:86
- Sapphire, synthetic**  
diffusion-treated—with beryllium  
(Pisutha-Armond)F06:85; showing  
Plato lines (GNI)Su06:185–186;  
showing unusual fluorescence  
(GNI)W06:287–289  
forming triplet with ulexite  
(GNI)Sp06:77–78  
imitating gem rough (GNI)W06:282  
separation from natural  
(Bidny)F06:153
- Scanning electron microscopy [SEM]**  
of diamond damaged by laser  
(GNI)W06:270–271  
of lamellae in Rainbow andradite from  
Japan (Hainschwang)W06:248–258  
of lead glass-filled rubies  
(McClure)Sp06:22–34 [erratum  
(GNI)Su06:188]  
of needle-like inclusions in Sunset  
quartz from Brazil  
(GNI)W06:277–279  
of rhodonite cleavage  
(Millsted)Su06:151–158  
of zircon inclusions in heat-treated  
sapphire (Wang)Su06:134–150
- Shell**  
dyed yellow, as Melo pearl imitation  
(LN)Su06:166–167
- Sierra Leone**  
diamond mining and trading in  
(GNI)W06:268–270
- Silicosis**  
in lapidary workers (Overton)F06:165
- Sillimanite**  
from India—resembling moonstone  
(GNI)Su06:180–181; transparent  
(GNI)Sp06:67–68
- SIMS**, see Spectrometry, secondary ion  
mass
- Slag**  
blue, from Sweden (GNI)W06:279
- Sodalite**  
with haüyne, from Myanmar  
(GNI)Sp06:64–65
- South Sea cultured pearl**, see Pearl, cultured
- Spectrometry, laser ablation–inductively  
coupled plasma–mass [LA-ICP-MS]**  
applications (Abduriyim)Su06:98–118  
[erratum (GNI)W06:292], F06:87–88  
of cultured pearls (Wang)W06:222–235  
developing corundum standards for  
(Wang)F06:105–106  
of opal (Gaillou)F06:107–108  
of tourmaline (Abduriyim)Sp06:4–21
- Spectrometry, secondary ion mass [SIMS]**  
of corundum, and comparison to LA-  
ICP-MS (Abduriyim)Su06:98–118  
[erratum (GNI)W06:292]
- Spectrometry, electron paramagnetic  
resonance [EPR]**  
of Be-diffused corundum  
(Rossman)F06:32
- Spectroscopy, energy-dispersive X-ray flu-  
orescence [EDXRF]**  
of beryl (McMillan)F06:126
- Spectroscopy, imaging**  
and gem identification (Del  
Re)F06:88–89
- Spectroscopy, infrared**  
of amethyst and synthetic amethyst  
(Karampelas)F06:155  
of andradite from Japan  
(Hainschwang)W06:248–258  
automation of analysis (Lowry)F06:91  
of corundum (Smith)F06:92–93  
of cultured pearls  
(Wang)W06:222–235  
of diamond—CO<sub>2</sub>-rich colored  
(Hainschwang)F06:97; Cullinan I  
and II (Scarratt)Su06:120–132;  
translucent brown-orange  
(LN)Sp06:57–59  
of haüyne-sodalite from Myanmar  
(GNI)Sp06:64–65
- of tortoise shell and its imitations  
(Hainschwang)Sp06:36–52
- Spectroscopy, laser-induced breakdown  
[LIBS]**  
of beryl (McMillan)F06:126  
of corundum, and comparison to LA-  
ICP-MS (Abduriyim)Su06:98–118
- Spectroscopy, photoluminescence**  
of cultured pearls (Wang)W06:222–235  
of natural and synthetic corundum  
(Bidny)F06:153  
of tortoise shell and its imitations  
(Hainschwang)Sp06:36–52
- Spectroscopy, Raman**  
of amber and its simulants  
(LN)W06:260–261  
automation of analysis (Lowry)F06:91  
of bovine bone (LN)Su06:160–161  
of cultured pearls (Wang)W06:222–235  
of diamond with brown and green  
radiation stains (LN)Su06:161–162  
of gems and minerals—  
(Denton)F06:89; (Downs)F06:89–90  
of pigments in freshwater cultured  
pearls (Karampelas)F06:99–100  
of zircon inclusions in heat-treated  
sapphire (Wang)Su06:134–150
- Spectroscopy, UV-Vis**  
of diamond—coated pink  
(LN)Su06:163–164; Cullinan I and II  
(Scarratt)Su06:120–132; pink with  
prolonged change of color  
(LN)W06:263–264  
of fluorite, color-change  
(GNI)Su06:173–174  
of natural and synthetic corundum  
(Bidny)F06:153  
of natural- and treated-color yellow  
cultured pearls (Elen)F06:123  
of triploidite from China  
(GNI)Su06:183–184
- Spectroscopy, UV-Vis-NIR**  
of andradite from Japan  
(Hainschwang)W06:248–258  
Challenger spectrometer  
(Michailidis)F06:164–165  
of chameleon diamonds  
(Massi)F06:101–102  
of cultured pearls—(Elen)F06:123,  
(Wang)W06:222–235  
of haüyne-sodalite from Myanmar  
(GNI)Sp06:64–65  
of tortoise shell and its imitations  
(Hainschwang)Sp06:36–52  
of tourmaline from Mozambique  
(Abduriyim)Sp06:4–21
- Spessartine**  
synthetic sapphire fashioned to imi-  
tate gem rough (GNI)W06:282
- Sphene**  
from Afghanistan (GNI)Su06:180–182  
from Pakistan (GNI)Sp06:68–69

## Spinel

from Mahenge, Tanzania (GNI)Sp06:69  
marketing of (Boehm)F06:28  
photoluminescence to separate from synthetic (Maini)F06:125

## Spinel, synthetic

photoluminescence to separate from natural (Maini)F06:125  
see also Assembled gem materials

## Spodumene, see Hiddenite

## Sri Lanka

aquamarine from Akkerella (GNI)Sp06:63–64  
*in situ* corundum deposits in (Tennakoon)F06:117–118  
jeremejevit from (GNI)Su06:175–176 [erratum (GNI)W06:292]

## SSEF (Swiss Gemmological Laboratory), see Pearl, cultured

## Subjectivity

in gemology (Ringsrud)F06:165–166

## Supplier of Choice

future of (Tempelman)F06:7–12

## Surface coating, see Coating

## Sweden

blue slag and banded iron ore from (GNI)W06:279

## Synthetics

differentiating from natural counterparts (Sunagawa)F06:112  
see also specific gem materials

## T

## Tahitian cultured pearl, see Pearl, cultured

## Tanzania

geology and mining of Tunduru deposits (Clanin)F06:107  
Merelani—geology of Block D' tanzanite mine (Scheepers)F06:150; tanzanite, recent production of (Yager)F06:144–145; tsavorite, 62.81 ct from (GNI)Sp06:62  
pyrope-spessartine from Lindi Province (GNI)Sp06:66–67 [erratum (GNI)W06:292]  
spinel from Mahenge (GNI)Sp06:69  
synthetic corundum sold as gem rough in (GNI)W06:282  
uvite-dravite from Morogoro (GNI)Su06:182–183

## Tanzanite

geology of, at Merelani Block D' (Scheepers)F06:150

production of (Yager)F06:144–145

## Topaz

coated (Befi)F06:128–129

## Tortoise shell

characterization of, and imitations (Hainschwang)Sp06:36–52

## Tourmaline

from California (Ertl)F06:96  
Cu-bearing—42.38 ct from Mozambique (GNI)Sp06:62; chemical composition of, from Brazil, Nigeria, and Mozambique (Abduriyim)Sp06:4–21; nomenclature of (Symposium Debate Center)F06:74–75  
from Madagascar—(GNI)W06:280–281, (Pezzotta)F06:116–117, (Superchi)F06:156  
uvite from Afghanistan (GNI)W06:281–282  
uvite-dravite, from Tanzania (GNI)Su06:182–183

## Treatment

of amethyst from Brazil (GNI)W06:285–286  
of colored stones—(McClure)F06:29–30; and effect on marketing (Menzie)F06:30–31  
of cultured pearls—(Scarratt)F06:40–41; “chocolate” (Wang)W06:222–235, (GNI)W06:284–285; dyed Tahitian (Wang)W06:222–235  
disclosure of (Symposium Debate Center)F06:68–69  
effect on gem pricing (Drucker)F06:95  
lead-glass filling of ruby—(McClure)Sp06:22–34 [erratum (GNI)Su06:188]; in bead necklace (GNI)Su06:186–187  
safeguards when dealing with (Kane)F06:36–37  
see also Coating; Diamond treatment; Diffusion treatment; Dyeing; specific gem materials

## Triploidite

from China (GNI)Su06:183–184

## Tsavorite, see Grossular

## Tucson Gem and Mineral shows

highlights of (GNI)Sp06:62–73

## Turkey

chalcedony from Central Anatolia (Lule-Whipp)F06:115

## Turquoise

variscite resembling (LN)Sp06:61

## U

## Ulexite

forming triplet with synthetic sapphire (GNI)Sp06:77–78

## United States

amber from Alaska (GNI)Su06:169–170  
hiddenite from North Carolina (Wise)F06:152  
jadeite with copper inclusions from San Benito County, California (GNI)W06:273  
pegmatites in Southern California (Snee)F06:151–152  
sapphire from Montana (Cade)F06:106, F06:129–130; (Berg)F06:145  
tourmaline from the Himalaya mine, California (Ertl)F06:96

## Uvite, see Tourmaline

## V

## Variscite

resembling turquoise (LN)Sp06:61

## Värynenite

from Afghanistan (GNI)Su06:184–185  
from Pakistan (GNI)Sp06:75

## X

## X-radiography

of lead-glass filler in ruby (McClure)Sp06:22–34 [erratum (GNI)Su06:188]

## X-ray diffraction analysis

and the RRUFF project database (Downs)F06:89–90  
using area CCD detectors (Post)F06:91–92

## X-ray topography

using synchrotron beam—of colored diamonds (Yuan)F06:93; of pezzottaite (Liu)F06:100–101

## XRF, see Spectroscopy, energy-dispersive X-ray fluorescence

## Z

## Zimbabwe

emeralds from Sandawana (Zwaan)F06:111

## AUTHOR INDEX

This index lists, in alphabetical order, the authors of all articles that appeared in the four issues of Volume 42 of *GEMS & GEMOLOGY*, together with the full title and inclusive page numbers of each article and the issue (in parentheses). Full citation is given under the first author only, with reference made from joint authors.

Note: The Fall 2006 Symposium and Gemological Research Conference Proceedings issue was paginated separately from the other issues of this volume year, and also contains its own index of presenters. The present index lists authors of Symposium speaker session abstracts and senior authors of Gemological Research Conference (GRC) oral presentation abstracts and all poster session abstracts. For all other authors of GRC and poster session abstracts, as well as for Symposium panelists and debate center participants, please refer to the Fall 2006 issue.

### A

- Abduriyim A.: Applications of LA-ICP-MS (laser ablation–inductively coupled plasma–mass spectrometry) to the gemological field, 87–88 (Fall)
- Abduriyim A., Kitawaki H.: Applications of laser ablation–inductively coupled plasma–mass spectrometry (LA-ICP-MS) to gemology, 98–118 (Summer)
- Abduriyim A., Kitawaki H., Furuya M., Schwarz D.: Paraíba-type copper-bearing tourmaline from Brazil, Nigeria, and Mozambique: Chemical fingerprinting by LA-ICP-MS, 4–21 (Spring)
- Albright M.K.: Opportunities and danger: The world in 2006, 2–6 (Fall)
- Anckar B.: Amethyst mining in Zambia, 112–113 (Fall)
- Antonhis A.: Optical characterization of CVD synthetic diamond plates grown at LIMHP-CNRS, France, 152–153 (Fall)
- Atichat W.: Ruby-sapphire quality grading for the gem trade, 128 (Fall)
- Azrielant O.: Online vs. offline: Are they really in opposite corners of the ring? 56–57 (Fall)

### B

- Beaton D.: Color quantification: A spectrographic imaging approach, 93–94 (Fall)
- Befi R.: Coated topaz, 128–129 (Fall)
- Bell K.C.: Natural pearl formation as seen through macro photography, 169–170 (Fall)
- Berg L.M.: The power of branding and brand-partnering at retail, 45 (Fall)
- Berg R.B.: The importance of surface features and adhering material in deciphering the geologic history of alluvial sapphires—an example from western Montana, 145 (Fall)

- Bidny A.S.: New data for distinguishing between hydrothermal synthetic, flux synthetic, and natural corundum, 153–154 (Fall)
- Boehm E.: ICA colored gemstone worldwide mining report, 157 (Fall)
- Untreated and underappreciated gems, 28 (Fall)
- Bondanza M.: Technical innovations, 42 (Fall)
- Bosshart G.: Rare reverse color change in a blue zircon from Myanmar (Burma), 94–95 (Fall)
- Botha M.: Three-dimensional solid modeling in applied diamond crystallography, 129 (Fall)
- Brand A.A.: Emerald mineralization in northwestern Ontario, Canada, 113 (Fall)
- Braunwart E.: Branding techniques and the fashion industry, 31 (Fall)
- Breeding C.M.: High-energy ultraviolet luminescence imaging: Applications of the DTC DiamondView for gem identification, 88 (Fall)
- see also Wang W.
- Buckley J.: Giving back wisely: Philanthropy as an investment for retail jewelers, 166 (Fall)
- Burianek M.: The gemstones of the Shrine of the Three Magi (ca. 1200 AD) in Cologne Cathedral, Germany, 121 (Fall)
- Butler J.E.: Growth of CVD synthetic diamond, 111–112 (Fall)

### C

- Cade A.: Characterization of sapphires from Yogo, Montana, 129–130 (Fall)
- Garnet inclusions in Yogo sapphires, 106 (Fall)
- Carmona C.I.: Products of endangered

- species used in jewelry, 166–167 (Fall)
- Ceulemans T.: Statistical study of the performance and predictive value of color measurement instruments for cape-colored rough diamonds, 130 (Fall)
- Charles D.: Defects in single-crystal CVD synthetic diamond studied by optical spectroscopy with the application of uniaxial stress, 121–122 (Fall)
- Clanin J.: Geology and mining of southern Tanzanian alluvial gem deposits, 107 (Fall)
- Mining of pegmatite-related primary gem deposits, 145 (Fall)
- Coenraads R.R., Zenil A.R.: Leopard opal: Play-of-color opal in vesicular basalt from Zimapán, Hidalgo State, Mexico, 236–246 (Winter)
- Colbert J.: Digital asset management for gem and jewelry photography, 163 (Fall)
- Collins A.T.: Identification technologies for diamond treatments, 33–34 (Fall)
- Cook B.: “Bahia Gold” golden rutiled quartz, Serra da Mangabeira, Novo Horizonte, Bahia, Brazil, 130 (Fall)
- Coquillard C.: The multichannel retailer, 54 (Fall)
- Cushman T.: Case study Madagascar: Progress and development through education, 161 (Fall)

### D

- De Corte K.: Overview of dislocation networks in natural type IIa diamonds, 122–123 (Fall)
- Del Re N.: Imaging spectroscopy: A developing frontier for gem analysis, 88–89 (Fall)
- Deljanin B.: Study of fancy-color and near-colorless HPHT-grown synthetic diamonds from Advanced Optical

- Technology Co., Canada, 154–155 (Fall)
- Cross-referencing Identification System (CIS): Database and tool for diamond research, 163–164 (Fall)
- Denton M.B.: The present and future potential of Raman spectroscopy in the characterization of gems and minerals, 89 (Fall)
- Dhamani A.: The Gulf perspective, 61 (Fall)
- Douthit T.R., see Wang W.
- Downs R.T.: Report on the progress of the RRUFF project: An integrated database of Raman spectra, X-ray diffraction, and chemical data for minerals, 89–90 (Fall)
- Drucker R.B.:  
Social, political, economic, and gemological impacts on pricing trends, 95 (Fall)  
Software for gemstone grading and appraisal valuation, 130–131 (Fall)
- Du Toit G.: Demantoid from Iran, 131 (Fall)

## E

- Eaton-Magaña S.:  
Fluorescence of fancy-color natural diamonds, 131–132 (Fall)  
Luminescence of the Hope diamond and other blue diamonds, 95–96 (Fall)
- Elen S.: Luminescence, reflected-infrared, and reflected-ultraviolet digital photography: Gemological applications, 123 (Fall)
- Emmett J.L., see Wang W.
- Ertl A.: Elbaite from the Himalaya mine, Mesa Grande, California, 96 (Fall)
- Esmerian R.: In pursuit of elusive luxury, 53 (Fall)

## F

- Fant G.: The Internet as a complementary distribution channel, 55 (Fall)
- Fedortchouk Y.: What determines the morphology of a resorbed diamond? 146 (Fall)
- Fritsch E.: Gem characterization: A forecast of important techniques in the coming decade, 90 (Fall)
- Furuya M., see Abduriyim A.

## G

- Gaillou E.: Geologic origin of opals deduced from geochemistry, 107 (Fall)
- Galenon R.T.: Marketing of the Tahitian

- cultured pearl, 170 (Fall)
- Galopim de Carvalho R.:  
The Bragança “diamond” discovered? 132–133 (Fall)  
Brazilian colored gemstones in Portuguese 18th–19th century jewelry, 167 (Fall)  
Colored gemstone promotion in small scale markets: The Portuguese case, 167–168 (Fall)  
Magnificent jewels in Portugal, 168–169 (Fall)
- Gilbertson A.: The evolution of the American Round Brilliant Diamond (aka American Cut), 1860–1955, 133 (Fall)
- Groat L.A.: Funding for gemological research: Ideas and case studies, 133–134 (Fall)
- Grozman Y.: A close look at gemstone color grading: Definition of the key color, 96–97 (Fall)
- Gumpesberger S.M.:  
Magnetic separation of gemstones, 124 (Fall)  
A variation on the crossed filters approach using pocket LED light sources, 124 (Fall)

## H

- Hainschwang T.: Natural “CO<sub>2</sub>-rich” colored diamonds, 97 (Fall)
- Hainschwang T., Leggio L.: The characterization of tortoise shell and its imitations, 36–52 (Spring)
- Hainschwang T., Notari F.: The cause of iridescence in Rainbow andradite from Nara, Japan, 248–258 (Winter)
- Hall M., see McClure S.F., Wang W.
- Harlow G.E.:  
Jadeite jade from Guatemala: Distinctions among multiple deposits, 146 (Fall)  
Mineral assemblages and the origin of ruby in the Mogok Stone Tract, Myanmar, 147 (Fall)
- Harris J.: Diamond occurrence and evolution in the mantle, 107–108 (Fall)
- Hasenfeld H.: The diamond dealer’s perspective, 48 (Fall)
- Hatleberg J.N.: An exact replica of the original Mogul cut Koh-i-noor diamond, 158–159 (Fall)
- He M.: Relationship between texture and crystallization degree in nephrite jade from Hetian, Xinjiang, China, 134 (Fall)
- Hendry Jr., D.W.: Gemological needs in insurance documentation, 169 (Fall)
- Hoal K.O.: Integrating the diamond project development process, 134–135 (Fall)

- Hoffman M.: Branding cultured pearls: From a retail perspective, 41 (Fall)
- Holloway G.: Diamond grading laboratory peer review, 159 (Fall)
- Htun H.: Melo “pearls” from Myanmar, 135–136 (Fall)
- Hyatt A., see Wang W.
- Hyrsl J.: Genetic classification of mineral inclusions in quartz, 97–98 (Fall)

## I

- Irving M.: The Canadian diamond industry: Where to now? 24 (Fall)

## J

- Janse A.J.A. (Bram):  
Global rough diamond production from 1870 to 2005, 136 (Fall)  
Major diamond mines of the world: Tectonic location, production, and value, 148–149 (Fall)

## K

- Kampf A.R.: The Gem & Mineral Council of the Natural History Museum of Los Angeles County, 161–162 (Fall)
- Kanda H.: Cathodoluminescence spectroscopy to identify types of natural diamond, 125 (Fall)
- Kane R.E.:  
The Hkamti jadeite mines area, Sagaing Division, Myanmar (Burma), 98–99 (Fall)  
Identifying treated and synthetic gems: The dealer’s perspective, 36–37 (Fall)
- Karampelas S.:  
Identification of pigments in freshwater cultured pearls with Raman scattering, 99–100 (Fall)  
A refined infrared-based criterion for successfully separating natural from synthetic amethyst, 155 (Fall)
- Katz M.: Building a luxury clientele, 51 (Fall)
- Keenan C.: Quantifiable cut grade system within an educational setting, 100 (Fall)
- Keller A.S.:  
GIA celebrates 75 years..., 95–96 (Summer)  
Remembering G. Robert Crowningshield, 205 (Winter)  
Symposium 2006: Join us as we navigate the challenges ahead, 1 (Spring)  
see also Kimmel K.

Khamrayeva D.: Autoradiographic investigations of impurity distributions in diamond, 90 (Fall)  
 Kiefert L.: Sapphires from New Zealand, 113–114 (Fall)  
 Kimmel K., Keller A.: Business and science converge at the 2006 Symposium and Gemological Research Conference, 1 (Fall)  
 King J.M., Moses T.M., Wang W.: The impact of internal whitish and reflective graining on the clarity grading of D-to-Z color diamonds at the GIA Laboratory, 206–220 (Winter)  
 Kitawaki H.:  
 Identification of heat-treated corundum, 84 (Fall)  
 see also Abduriyim A.  
 Kleišmantas A.: Identification of beryl varieties: “Beryl Color Circle,” “Color Memory,” and a proposed new variety—chromaquamarine, 137 (Fall)  
 Kniewald G.: Gemological properties of colorless hyalophane from Busovaca, Bosnia-Herzegovina, 137–138 (Fall)  
 Kouznetsov N.B.: The past, present, and future of demantoid green garnet from Russia, 157 (Fall)

## L

Leggio L., see Hainschwang T.  
 Lehrer G.: The techniques and art of cutting “the world’s largest gemstone pendant,” Bahia: A natural, transparent, rutile quartz sculpture, 158 (Fall)  
 Lepage L.: Ultraviolet mineral prospecting for sapphire on Baffin Island, Nunavut, Canada, 155–156 (Fall)  
 Linnen R.L.: A fluid inclusion study of the syenite-hosted “True Blue” aquamarine occurrence, Yukon Territory, Canada, 114 (Fall)  
 Liu S.: Monochromatic X-ray topographic characterization of pezzottaite with synchrotron radiation, 100–101 (Fall)  
 Liu Y.: Universal color grading system, 101 (Fall)  
 London D.:  
 Geochemical cycles of gem-forming elements: What it takes to make tourmaline, beryl, topaz, spodumene, and other pegmatitic gems, 108–109 (Fall)  
 The miarolitic stage in granitic pegmatites: How Mother Nature makes big, clear crystals, 109 (Fall)  
 Lowry S.: Automating the infrared and Raman spectral analysis of gemstones, 91 (Fall)  
 Lu T.: Some dissolution features observed in natural diamonds, 138 (Fall)

Lucas A.: The emerald business in South America, 158 (Fall)  
 Lule-Whipp C.: Chromium chalcedony from Turkey and its possible archeological connections, 115 (Fall)

## M

Ma L.: Developments and challenges of the China diamond market, 25 (Fall)  
 Maini L.: The identification of gemstones by photoluminescence: Synthetic and natural Mg-Al spinels, 125 (Fall)  
 Massi L.: Chameleon diamonds: A proposed model to explain thermochromic and photochromic behaviors, 101–102 (Fall)  
 McClure S.F.:  
 New colored stone treatments, 29–30 (Fall)  
 Source type classification of gem corundum, 102 (Fall)  
 McClure S.F., Smith C.P., Wang W., Hall M.: Identification and durability of lead glass-filled rubies, 22–34 (Spring)  
 McMillan N.J.: Fingerprinting gem beryl samples using laser-induced breakdown spectroscopy (LIBS) and portable X-ray fluorescence (PXRF), 126 (Fall)  
 Mehta R.: India: The jewel in the crown, 62 (Fall)  
 Menzie J.: The impact of treatments on selling colored stones, 30–31 (Fall)  
 Michailidis N.: Challenger gemological spectrometer, 164–165 (Fall)  
 Millstead P.: Faceting transparent rhodonite from Broken Hill, New South Wales, Australia, 151–158 (Summer)  
 Mohideen H.M. Sultan: India—Old sources and new finds, 115–116 (Fall)  
 Moses T.M., see King J.M.

## N

Newton M.: Treated diamond: A physicist’s perspective, 84–85 (Fall)  
 Notari F., see Hainschwang T.

## O

Overton T.W.: Silicosis risks for lapidary workers in developing countries, 165 (Fall)

## P

Paspaley N.: The challenges and opportunities of growing and marketing South

Sea cultured pearls, 38 (Fall)  
 Pay D.: Course development at the Gemological Institute of America, 162 (Fall)  
 Perret E.: Color treatment of diamonds and their potential in designer jewelry, 159–160 (Fall)  
 Perrin E.: Defeating the bling, 49–50 (Fall)  
 Pezzotta F.: New gem localities in Madagascar, 116 (Fall)  
 Pisutha-Armond V.: Role of beryllium in the coloration of Fe- and Cr-doped synthetic corundum, 85 (Fall)  
 Poli L.: The Italian and European goldsmith industry: Current status and possible future scenarios, 59–60 (Fall)  
 Pope S.: High-pressure, high-temperature (HPHT) diamond processing: What is this technology and how does it affect color? 120 (Fall)  
 Post J.: X-ray diffraction using area detectors for mineral and gem characterization, 91–92 (Fall)  
 Prudden J.M.: Geology of placer gem deposits, 149 (Fall)

## R

Raff B.: The multichannel approach, 55–56 (Fall)  
 Rapaport M.: Diamond industry of the future, 27 (Fall)  
 Reinitz I.: The role of brilliantteering variations in the GIA Cut Grading System, 138–139 (Fall)  
 Richardson P.: Preliminary observations of a new polishing process for colored gems, 139–140 (Fall)  
 Ringsrud R.: Subjectivity in gemology, 165–166 (Fall)  
 Robbins S.: Reinventing = Transformation, 47–48 (Fall)  
 Rohtert W.: Three parageneses of ruby and pink sapphire discovered at Fiskensæset, Greenland, 149–150 (Fall)  
 Rondeau B.: Some open questions on diamond morphology, 109–110 (Fall)  
 Rossman G.R.:  
 Characterization of nanofeatures in gem materials, 92 (Fall)  
 New technologies used to identify colored stone treatments, 32 (Fall)  
 Rothman G.: Battle of the minds, 26 (Fall)

## S

Scarratt K.:  
 Focusing on cultured pearl treatments, 40–41 (Fall)  
 The treatment of ruby and sapphire, with implications for gem identifi-

- cation and the integrity of the product, 85–86 (Fall)  
see also Wang W.
- Scarratt K., Shor R.: The Cullinan diamond centennial: A history and gemological analysis of Cullinans I and II, 120–132 (Summer)
- Schechter J.: Chinese freshwater cultured pearl ~~revolution~~ evolution, 40 (Fall)
- Scheepers R.: Controls on mineralization in Block D' of the Merelani tanzanite deposit, Tanzania, 150 (Fall)
- Schwarz D., see Abduriyim A.
- Sevdermish M.: Color communication: The analysis of color in gem materials, 102–103 (Fall)
- Shen A.:  
Identification of dyed chrysocolla chalcedony, 140 (Fall)  
see also Wang W.
- Shi G.-H.: Texture and composition of kosmochlor and chromian jadeite aggregates from Myanmar: Implications for the formation of green jadeite, 150–151 (Fall)
- Shor R., see Scarratt K.
- Singbamroong S.: Sapphires from Ban Huai Sai, Laos, 103 (Fall)
- Singer D.: The mark of excellence in jewelry, 43 (Fall)
- Sivovolenko S.:  
Fancy-color diamonds: Better color appearance by optimizing cut, 104–105 (Fall)  
Study of interdependence: Fancy-color diamond appearance, cut, and lighting conditions, 140 (Fall)
- Smirnov S.: Color grading of color-enhanced natural diamonds: A case study of Imperial Red diamonds, 126–127 (Fall)
- Smith C.P.:  
Infrared spectra of gem corundum, 92–93 (Fall)  
see also McClure S.F.
- Snee L.W.:  
Afghanistan gem deposits: Studying newly reopened classics and looking for new deposits, 116–117 (Fall)  
Pegmatite genesis—Complex or simple emplacement? Revisiting southern California pegmatites, 151–152 (Fall)
- Sobolev N.V.: The new Komsomolskaya mine in Yakutia, Russia: Unique features of its diamonds, 117 (Fall)
- Solodova Y.: Comparative investigation of diamonds from various pipes in the Malaya-Botuobiya and Daldyn-Alakit areas (Siberia), 141–142 (Fall)
- Strack E.: European freshwater pearls: Origin, distribution, and characteristics, 105 (Fall)
- Sturman D.B.: Study of the biaxial gemstones on the refractometer, 127 (Fall)
- Sturman N.: The “keshi” pearl issue, 142 (Fall)
- Sunagawa I.: Growth, morphology, and perfection of single crystals: Concepts in discriminating natural from synthetic gemstones, 112 (Fall)
- Superchi M.: Gemological investigation of multicolored tourmalines from new localities in Madagascar, 156 (Fall)
- Sutthirath C.: Indications of heating in corundum from experimental results, 86 (Fall)
- Suwa Y.: The jewelry market in Japan in 2020, 58–59 (Fall)
- Swarovski N.: Reinventing Swarovski, 46 (Fall)
- T**
- Tannenbaum E.: Magellan's guide to the diamond universe, 23 (Fall)
- Tashey T.E.: A system to describe the face-up color appearance of white and off-white polished diamonds, 142–143 (Fall)
- Taylor M.C.: The gel model for the formation of gem-bearing pockets within granitic pegmatites, and implications for gem synthesis, 110–111 (Fall)
- Tempelman M.: Transitions and traditions, 7–12 (Fall)
- Tennakoon S.: In-situ corundum localities in Sri Lanka: New occurrences, 117–118 (Fall)
- Titkov S.V.: Inclusions in white-gray diamonds of cubic habit from Siberia, 127–128 (Fall)
- U**
- Underwood T.: Digital color communication for gemstones, with an exploration of applications within our industry, 143 (Fall)
- V**
- Vagner K.: Gemological Institute of America's public outreach programs, 162–163 (Fall)
- Van Royen J.: HPHT treatment of type IaB brown diamonds, 86–87 (Fall)
- Vins V.: Natural diamond enhancement: The transformation of intrinsic and impurity defects in the diamond lattice, 120–121 (Fall)
- W**
- Wan R.: The Tahitian cultured pearl, 39 (Fall)
- Wang W.:  
Developing corundum standards for LA-ICP-MS trace-element analysis, 105–106 (Fall)  
see also King J.M., McClure S.F.
- Wang W., Scarratt K., Emmett J.L., Breeding C.M., Douthit T.R.: The effects of heat treatment on zircon inclusions in Madagascar sapphires, 134–150 (Summer)
- Wang W., Scarratt K., Hyatt A., Shen A.H., Hall M.: Identification of “chocolate pearls” treated by Ballerina Pearl Co., 222–235 (Winter)
- Wathanakul P.: Beryllium-assisted heat treatment experiments on blue sapphires, 87 (Fall)
- Welborn P.: Marketing in the 21st century, 166 (Fall)
- Welbourn C.: Identification of synthetic diamonds: Present status and future developments, 34–35 (Fall)
- Weldon R.: Photographing phenomenal gemstones, 144 (Fall)
- Wickstrom D.: The auction house as a purveyor of high-end jewelry, 52 (Fall)
- Wise M.A.: Geology of “true” hiddenite deposits, 152 (Fall)
- Y**
- Yager T.R.: Recent trends in world gem production, 144–145 (Fall)
- Yantzer P.: The AGS performance cut grading system, 160 (Fall)
- Yuan J.C.C.: Investigation by synchrotron X-ray diffraction topography of the crystal structure defects in colored diamonds (natural, synthetic, and treated), 93 (Fall)
- Yurman D.: Jewelry design and brand creation: Designing over the years, 44 (Fall)
- Z**
- Zenil A.R., see Coenraads R.R.
- Zucker B.: From Alexander the Great to Elihu Yale: A study of India and the diamond trade, 160–161 (Fall)
- Zwaan J.C. (Hanco): The Sandawana model of emerald formation, 111 (Fall)

